NOTICE

The quality of this microform is heavily dependent upon the quality of the original thesis submitted for microfilming. Every effort has been made to ensure the highest quality of reproduction possible.

If pages are missing, contact the university which granted the degree.

Some pages may have indistinct print especially if the original pages were typed with a poor typewriter ribbon or if the university sent us an inferior photocopy.

Reproduction in full or in part of this microform is governed by the Canadian Copyright Act, R.S.C. 1970, c. C-30, and subsequent amendments.

AVIS

La qualité de cette microforme dépend grandement de la qualité de la thèse soumise au microfilmage. Nous avons tout fait pour assurer une qualité supérieure de reproduction.

S'il manque des pages, veuillez communiquer avec l'université qui a conféré le grade.

La qualité d'impression de certaines pages peut laisser à désirer, surtout si les pages originales ont été dactylographiées à l'aide d'un ruban usé ou si l'université nous a fait parvenir une photocopie de qualité inférieure.

La reproduction, même partielle, de cette microforme est soumise à la Loi canadienne sur le droit d'auteur, SRC 1970, c. C-30, et ses amendements subséquents.

AN ANALYTICAL AND EXPERIMENTAL STUDY OF DRIVER-SEAT-SUSPENSION SYSTEMS

YOHANNES AFEWORK

A Thesis

in

The Department

of

Mechanical Engineering

Presented in Partial Fulfillment of the Requirements
for the Degree of Master of Applied Science
in Mechanical Engineering at
Concordia University
Montreal, Quebec, Canada

March 1991

ISBN 0-315-64631-4

ABSTRACT

AN ANALYTICAL AND EXPERIMENTAL STUDY OF DRIVER-SEAT-SUSPENSION SYSTEMS

Yohannes Afework

The human body is most sensitive to low frequency whole-body vibrations (WBV). Ride vibrations of off-road vehicles, caused primarily by irregular terrains, predominate in the 0.5 - 5 Hz frequency range. The effects of such vehicle vibrations on driver's discomfort, fatigue and health are reviewed, and performance benefits and limitations of various approaches to vehicle ride improvement are discussed. Developments in seat-suspension designs for off-road vehicles are thoroughly reviewed with special emphasis on vibration requirements and ergonomic considerations. Experimental methodologies to identify suspension parameters and to evaluate the low frequency ride vibration attenuation performance of seat-suspension systems are described.

Analytical models of the selected vertical seat-suspensions are developed and validated using the laboratory test results. These models include nonlinearities due to damping characteristics of shock absorbers, Coulomb friction and bump stops. The dynamic interactions of the human body are also investigated by integrating dynamic models of varying complexities of a driver to the nonlinear two-degrees-of-freedom seat-suspension models.

The vibration attenuation performance characteristic of the seat-suspension and seat-driver system models are investigated for deterministic and random cab floor excitations. The steady-state acceleration

response at the driver-seat interface is evaluated for deterministic excitations, via direct integration of the nonlinear differential equations of motion. The nonlinear suspension models are expressed by their linear equivalent using local equivalent linearization based on energy similarity. The linearized system of equations are solved in the frequency-domain to determine the vibration transmission performance of the seat-suspension and seat-driver system models subjected to deterministic and stochastic cab floor excitations.

Comprehensive parametric sensitivity analysis is carried out to investigate the influence of various suspension parameters on the vibration transmission performance of the seat-suspension models. The vibration performance of the seat-suspension models is assessed based on ISO fatigue decreased proficiency limits.

ACKNOWLEDGEMENTS

I wish to express my sincere appreciation and gratitude to Dr. S. Rakheja, and Dr. S. Sankar, my research supervisors for the constant encouragement and support extended during the preparation of this thesis.

The financial and technical supports provided by CONCAVE Research Center and Institut de Recherche en Santé et en Sécurité du Travail du Québec (IRSST) are gratefully acknowledged.

Many thanks are due to all CONCAVE research personnel, fellow graduate students, and members of the Department of Mechanical Engineering for their help and valuable discussions.

Finally, I like to extend my appreciation to my family and friends for their unyielding love, companionship, and understanding.

Montreal, Canada

March, 1991 Yohannes Afework

TABLE OF CONTENTS

TABLE OF CONTENTS (Continued)

TABLE OF CONTENTS (Continued)

TABLE OF CONTENTS (Continued)

LIST OF FIGURES

LIST OF FIGURES (Continued)

LIST OF FIGURES (Continued)

LIST OF FIGURES (Continued)

LIST OF FIGURES (Continued)

LIST OF FIGURES (Continued)

LIST OF FIGURES (Continued)

LIST OF FIGURES (Continued)

LIST OF FIGURES (Continued)

LIST OF TABLES

LIST OF TABLES (Continued)

NOMENCLATURE

Symbol		Description
$A(\omega_k)$	:	amplitude of base excitation (acceleration) corresponding to excitation frequency, ω_k, m/s^2
a_x, a_y, a_z	:	horizontal, lateral, and vertical accelerations at the seat, respectively, m/s^2
a_{rms}	:	root mean squared acceleration, m/s^2
B	:	constant for frequency band, Hz
C_1, C_2, C_c, C_s	:	damping coefficients of sprung masses, N.s/m
C_{CD}, C_{sh}	:	equivalent damping coefficients of seat cushion and shock absorber, respectively, N.s/m
C_{eq}, C^1_{eq}, C^0_{eq}	:	local equivalent damping coefficients, at excitation frequency band, ω_k, N.s/m
C_{1A}, C_{1B}	:	bleed- and blow-off damping coefficients of shock absorber, N.s/m
CF	:	crest factor
CSD	:	cross spectral density
[D], [D_f]	:	damping and forcing damping matrices, n x 1
D.O.F	:	degree-of-freedom
F_c, F_d, F_f, F_K, F_s	:	total suspension forces due to seat cushion, shock absorber, linkage friction, suspension spring, and bump stops, N
F_{CS}, F_{CD}	:	magnitude of Static and Dynamic friction, respectively, N
F_D	:	damping force across the shock absorber axis, N
F_{DC}	:	seat cushion dissipative force, N
F_c, F_d, F_f, F_K, F_s	:	suspension force vectors, N
FDP	:	fatigue decreased proficiency

NOMENCLATURE (Continued)

Symbol		Description
$f(x,\dot{x},t)$	:	nonlinear suspension force function, N
f	:	temporal frequency, Hz
f_m	:	frequency corresponding to the peak acceleration PSD at the seat attachment point of class I and Class II tractors, Hz
HD	:	horizontal projection of shock absorber end points, m
$[H(j\omega)]$	:	complex frequency response matrix, n x n
$H(j\omega_k, X(\omega_k))$	:	complex frequency response matrix corresponding to excitation frequency ω_k and amplitude response $X(\omega_k)$, n x n
$H^*(j\omega_k, X(\omega_k))$	:	complex conjugate of $H(j\omega_k, X(\omega_k))$
$h(j\omega)$	:	complex frequency response function for single input and single output system
$h^*(j\omega)$	:	complex conjugate function of $h(j\omega)$
ISO	:	International Standards Organization
$[K]$, $[K_f]$	:	stiffness matrices, n x n and n x 1, respectively
K_{eq}	:	equivalent suspension stiffness coefficient at excitation frequency ω_k, N/m
K^I_{eq}, K^0_{eq}	:	equivalent stiffness coefficient at excitation frequency ω_k corresponding to I^{th} iteration and initially assumed, respectively, N/m
K_{1A}, K_{1B}	:	suspension stiffness when deflection is within and exceeding permissible travel, respectively, N/m
K_c	:	cushion stiffness coefficient, N/m
K_S, K^c_S, K^e_S	:	suspension stiffness coefficients within permissible travel at compression and extension, N/m

NOMENCLATURE (Continued)

Symbol		Description
K_{st}, K^c_{st}, K^e_{st}	:	bump stop stiffness coefficients at compression and extension, N/m
LVDT	:	linear variable displacement transducer
[M], [M]	:	mass matrices, n x n
MH	:	static mid-ride height of suspension, m
m_s, m_o, m_1, m_2	:	lumped mass values, kg
N	:	number of discrete frequencies
NIOSH	:	National Institute for Occupational Safety and Health
n, n	:	number of degrees-of-freedom
PSD	:	power spectral density
pp	:	peak to peak
ROPS	:	rollover protection structure
rms	:	root mean squared acceleration
S	:	nonlinear function describing stiffness of bump stops
$S_1(j\omega)$, $S_1(j\omega_k)$	:	vector of input acceleration PSD
$S_o(j\omega)$, $S_o(j\omega_k)$	:	vector of response acceleration PSD
$S_{rd}(j\omega_k)$	:	vector of response relative displacement PSD
$\Delta_1(j\omega)$	:	input acceleration PSD corresponding to frequency ω, $(m/s)^2/Hz$
$\Delta_o(j\omega)$	:	response acceleration PSD corresponding to frequency ω, $(m/s)^2/Hz$
t_1	:	time at which piston velocity approaches V_s, s
t_2	:	time at which suspension deflection approaches permissible deflection (β), s
t	:	time, s

NOMENCLATURE (Continued)

Symbol		Description
V_b	:	value of velocity around zero to represent the viscous band, m/s
V_r	:	velocity across the shock absorber axis, m/s
V_s	:	preset velocity of transition from high to low damping constant of the shock absorber, m/s
WBV	:	whole-body vibration
$X_1, X_2, \ldots, X_n$	:	amplitudes of response relative displacements, m
$\mathbf{x}$	:	vector of relative displacement, n x 1
$x_1, x_2, \ldots, x_n$	:	response relative displacement variables, m
$Z_1, Z_2, \ldots, Z_n$	:	response displacement amplitude of lumped mass, m
$\{Z(j\omega)\}, \{Z_0(j\omega)\}$	:	Fourier transform of vectors containing response and excitation variables, respectively, n x 1
Z_0	:	amplitude of displacement excitation, m
$\mathbf{z}$	:	displacement vector of lumped masses, n x 1
$z_1, z_2, \ldots, z_n$	:	response displacement variable of lumped masses, m
z_0	:	excitation displacement variable, m
β	:	maximum permissible travel from mid-ride position, m
ΔE	:	energy function, N.m
$\Delta(.), \partial(.)$	:	change of or differential of (.), respectively
δ_{1A}, δ_{1B}	:	shock absorber damping factors
$\mathcal{E}, \varepsilon$	:	error parameters
Φ_{max}	:	denotes constants for maximum values of acceleration PSD's at the seat attachment point for various Classes of tractors, $(m/s^2)^2/Hz$
g, g_{rms}	:	gravitational constants equivalent to (9.81 m/s^2)

NOMENCLATURE (Continued)

Symbol		Description
Ψ	:	multiplying constant
μ	:	suspension mass ratio, m_s/m_o
θ	:	shock absorber inclination angle with respect to seat base, rad
τ	:	period of one vibration cycle, s
φ_k	:	randomly distributed phase angle, rad
ω, ω_k	:	excitation frequencies, rad/s
$\oint(.)$	:	cyclic integral of (.)
exp(.)	:	exponential function defined as $e^{(.)}$ or $2.71828^{(.)}$
$(\dot{})$, $(\ddot{})$	:	first and second derivatives with respect to time
$[.]^{-1}$	:	inverse matrix of [.]
$\lvert(.)\rvert$	:	magnitude of (.)
$[.]^T$	:	transpose of a matrix, [.]

CHAPTER 1

INTRODUCTION AND LITERATURE REVIEW

1.1 BACKGROUND

Comfort and safety of off-road vehicle drivers depend highly on the driver environment: visibility, space, placement of controls, noise and ride vibrations. The ride vibration environment of an off-road vehicle is strongly dependent upon vehicle-terrain interactions and dynamics of the vehicle. Wheeled off-road vehicles are often unsuspended, and large-diameter soft tires offer very light damping. Consequently, the ride vibration of such vehicles can be characterized by lightly damped system resonance occurring at low frequencies. The shock and vibration, primarily originating from irregular terrains, is directly transmitted to the seat-pan through unsprung chassis and cab.

Modern off-road vehicles, such as those used in forestry, mining, agricultural, construction, are designed for high power to achieve improved mobility over unprepared terrains. The operators are thus exposed to large amplitude whole-body ride vibration predominant at low frequencies. Exposure to such ride vibrations reduces performance rate of the driver and poses increased risks to driver's health and safety. The vehicle manufacturers are thus increasing their efforts to develop efficient driver's enclosure and suspension systems to improve driver's comfort, safety and productivity.

A number of approaches to improve off-road vehicle ride have been proposed, namely: suitable tires, primary-suspension at front and rear axles, cab-suspension, and seat-suspension. The ride improvement via tires and primary-suspension, however, have been considered infeasible due to limitations on tire size and requirements of high stability limits. A need to

develop effective secondary, seat- and cab-suspension systems has thus been emphasized to accomplish improved ride quality.

In this investigation, passive seat-suspension systems are analytically modeled to determine their vibration isolation performance. Commercially available seat-suspensions are tested in the laboratory to identify the static and dynamic characteristics of the components, and to determine their vibration attenuation performance. The nonlinear analytical models are validated for sinusoidal excitations, and their performance potential are investigated via stochastic response analyses.

1.2 REVIEW OF PREVIOUS INVESTIGATIONS

Subjective and objective studies conducted on off-road vehicle vibration encompass a diversity of subjects concerning development of ride criteria, human body models, suspension designs, and impact of ride vibrations. The studies in this area have progressed from subjective basis to advanced laboratory test methods, modeling and computer simulation techniques. The relevant investigations are reviewed and grouped in a sequence to develop the scope of this dissertation.

1.2.1 Effects of Off-road Vehicle Vibrations

Off-road vehicle vibrations transmitted to the driver are of whole-body nature impinging on virtually the entire body. The human body possesses a set of physical properties responding to input vibrations in a highly complex manner. The human body comprising of several principal masses linked by visco-elastic elements exhibits several resonances in the frequency range of 5 to 20 Hz. A number of subjective and objective studies have concluded that human body, seated or standing, is most fatigue sensitive to whole-body

vibrations in the frequency range 4 to 8 Hz [1]. Prolonged exposure to low frequency, large amplitude whole-body vibrations (WBV) either aggravates or causes degenerative physical symptoms and degrades driver response to certain stimuli prominent to driver safety and efficiency [2].

The physiological effects of long term exposure to WBV are not yet quite clear. Most of the evidence come from epidemiological investigations of heavy equipment operators. These workers have disproportional incidence of spinal disorders, hemorrhoids, hernias, and digestive and urinary problems [3]. Prompted by worker and union complaints, NIOSH performed four morbidity (health) record studies on various U.S. worker populations: inter city bus drivers [4]; long distance truck drivers [5]; and two studies on heavy equipment operators [6,7].

The study on the bus drivers showed a significant incidence of venous, bowel, respiratory, muscular and back disorders in a population of 1,448 interstate bus drivers as compared to two control groups: office workers and general population. This study concluded that the combined effects of body posture, postural fatigue, dietary habits, and whole-body vibration would appear to contribute to the occurrence of these disorders.

The long distance truck driver study looked at 3,205 drivers and a control group of air traffic controllers who experience stress but no vibration. The study showed that the combined effects of forced body posture, cargo handling, improper eating habits and whole-body vibration were factors contributing to significant vertebragenic pain, spinal deformities, sprains, strains and hemorrhoid disorders among truck drivers.

Guignard and King [8] summarized the physiological effects of whole-body vibrations in the following manner:

Muscular Activity and Maintenance of Posture: During exposure to vibrations in the 1-30 Hz range human body subjects have difficulty in maintaining posture and experience increased postural swing.

Cardiovascular System Effects: During exposure to vibration below 20 Hz, an increase in heart rate has been observed.

Cardiopulmonary Effects: Whole-body vibration of human body appeared to cause increase in oxygen uptake, pulmonary ventilation and respiratory rate and hyperventilation, particularly in the 0.5 *g*, 1-10 Hz range.

Central Nervous System Effects: European researchers claim vibration causes a general debilitating and malaise effect which is called "vibration sickness." The first stage of vibration sickness is marked by epigastralgia, distension, nausea, loss of weight, drop in visual acuity, insomnia, disorders of the labyrinth, colonic cramps, etc. [9]. The second stage is marked by more intense pain concentrated in the muscular and osteoarticular systems.

Gastrointestinal System Effects: A series of laboratory studies, using primates subjected to whole-body vibration of 1.5 *g* peak vertical amplitude at a frequency of 12 Hz for 5 hours/day, 5 days/week for a total of 130 hours, indicated a general stress response, namely, extensive gastrointestinal bleeding and lesions for 10 exposed animals.

Motion Sickness Effects: Motion sickness, vomiting and general malaise occurs during exposure to vibration in the 0.1-1 Hz frequency band with the patient recovering after the removal of the vibration stimulus and/or medication.

Increased muscular tension is an aspect of special importance for seated operators exposed to WBV of random nature, over a prolonged duration. Clarsoo [10] concluded that exposure to WBV increases muscle tension, due to human reaction to dampen the vibration. Since the initial aneurysm caused by

an increase of vibration dose is followed by increased muscular tension stiffness of muscles, and contraction of vein walls, the inadequate circulation hinders regeneration of the tiny damages suffered by the vertebrae.

A number of studies have been carried out on the performance effects of whole-body vibrations. Results of these studies are often confusing and contradictory, however, the studies show some common denominators. Nearly all of the human performance studies thus far performed are for short term exposure to vibrations, often using physically fit, young male (military) personnel as subjects. Many studies use sinusoidal vibrations at a single frequency in the vertical direction. The acceleration is maintained at low to moderate levels (less than 0.5 g_{rms}) due to the possibility of inflicting injury on the subjects. Unfortunately, with few exceptions, these studies do not necessarily resemble the off-road vehicle situations which contain multiple vibration frequencies and accelerations appearing simultaneously (e.g., from vehicle dynamics, road conditions, etc.); and whose drivers are not necessarily young and physically fit personnel in optimum condition.

Some of the studies performed were concerned with perception of vibration magnitude (acceleration), frequency dependence, exposure time [11,12], and the effects of seat belts and other body restraint systems [13]. These led in part to the conclusion that human's perceived endurance was both frequency and magnitude dependent, with the lowest tolerance being in the 4-8 Hz whole-body resonance range for vertical sinusoidal vibration with seated subjects.

Studies conducted for short term exposure of agricultural tractor drivers have established that the performance ability of drivers is highly impaired in an environment of discomfort [14]. The reduced working efficiency has been attributed to several factors influenced by tractor vibrations. Schimitz *et*

al. [5] and Hornick [15] presented experimental evidences to establish deterioration of performance ability of drivers subjected to vibrations, which are also supported by the experimental investigations of Matthews [16] and Müller [17]. Their findings concluded the following:

(i) Detrimental effects of vertical sinusoidal vibration generally occur in the 4 to 20 Hz range with acceleration exceeding 0.2 *g*. These conditions can produce tracking errors up to 40% greater than that under non-vibratory control conditions. Results of an experimental study are presented in Figure 1.1.

(ii) Visual Performance is generally impaired by vibration and generally is greatest in the range of 10 to 24 Hz and is a function of vibration intensity. Results of an experimental study are presented as shown in Figure 1.2.

(iii) Performance of tasks that require steadiness or precision of muscular control is likely to show decrements due to vibration. Experimental studies have established that drivers, exposed to low frequency WBV vibration, experience difficulty in maintaining constant foot pressure, as shown in Figure 1.3.

(iv) Human's reaction time decreases considerably, when exposed to low frequency WBV, as shown in Figure 1.4.

1.2.2 Ride Vibration : Perception, Standards and Tolerance Criteria

The ride quality is a subjective perception, associated with the level of comfort experienced when travelling in a vehicle. Perceived ride quality is a cumulative function of vibration transmitted to the operator body, vibration transmitted to the hands and feet, seat design and its capability to provide postural support, temperature, ventilation, interior space, hand holds and many other factors. However, the tactile vibration transmitted to the driver's body through the seat is the primary factor most commonly associated with the ride.

Tolerance to vibration: Studies in human sensitivity to ride vibration in general focus on tolerance as it relates to discomfort in a seated position [1,18,19,20]. These subjective studies have revealed that human

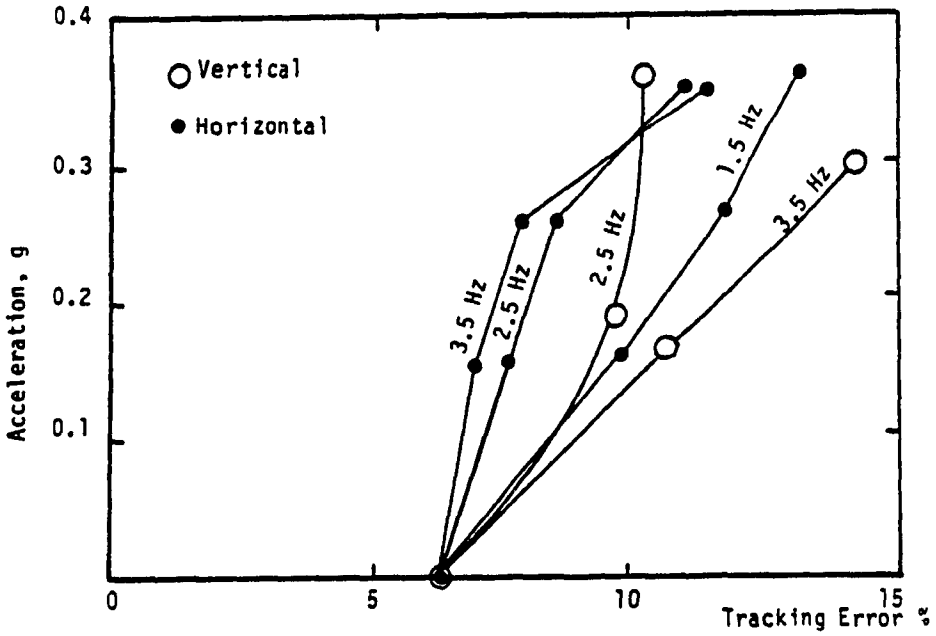

Figure 1.1. Compensatory Tracking Error Caused by Vertical and Horizontal Vibrations [16].

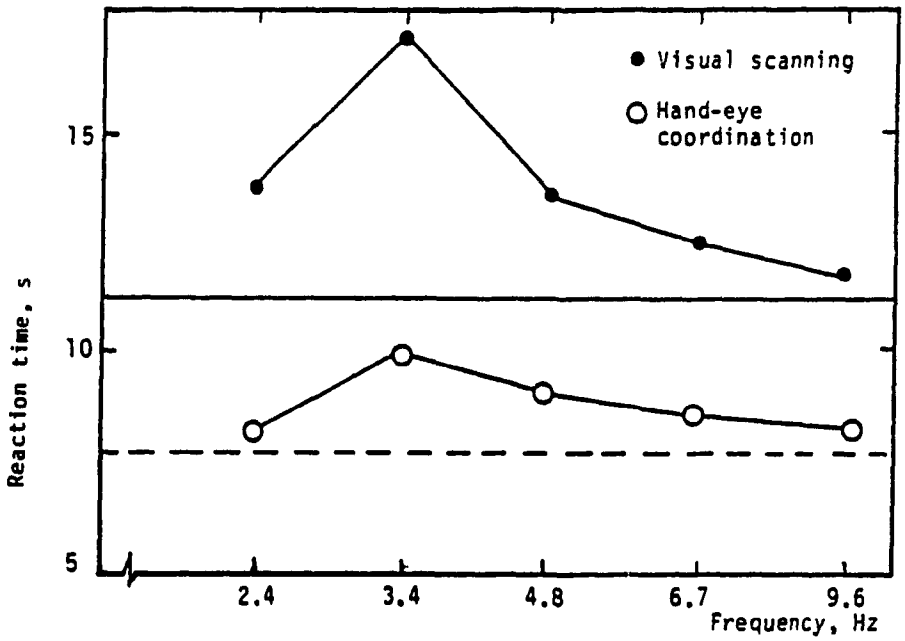

Figure 1.2. Effects of Vertical Vibration on Visual Acuity [17].

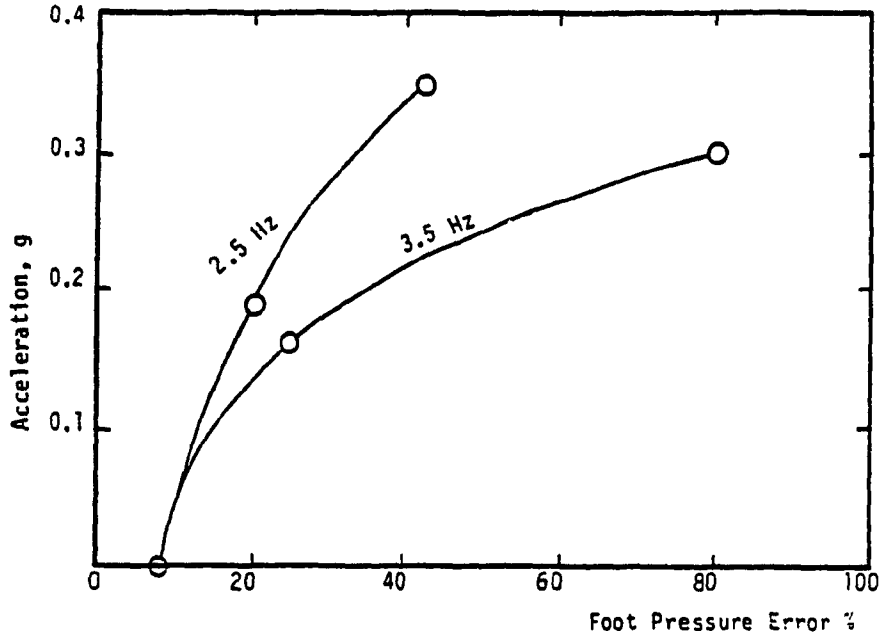

Figure 1.3. Error in Maintaining Constant Foot Pressure due to Exposure to Vertical Vibrations [16].

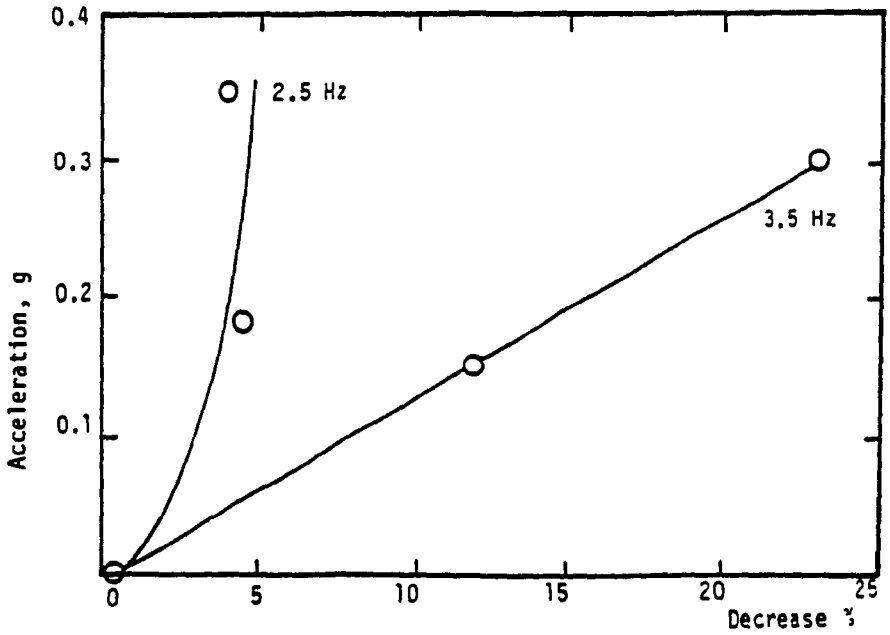

Figure 1.4. Effects of Vibration on Performance Rate [15].

sensitivity to an imposed vibration is not only dependent on the physiological and biomechanical response of the body but also on a number of psychological and environment ' factors. It is also concluded that human response to vibration is a function of several factors such as: vibration magnitude and frequency; character (rotational,linear) and direction of vibration; and duration of vibration.

These investigations carried out on various aspects of human response to vibration have provided the data base to establish ride criteria for preservation of health, comfort and performance. A number of vibration performance criteria have been established based on: subjective response, relative ride quality ranking of a group of vehicles, tolerance related to machine productivity, vibration interference with normal operator control tasks, health aspects due to vocational exposure, competitive significance and cost/benefit ratio of potential ride-improvement [21]. Although reasonable similarity in the proposed comfort criteria has been shown with respect to input frequency, the subjective response data has been insufficient and inconsistent to derive a generally acceptable comfort criterion with respect to intensity of vibration. The inconsistencies inherent to the proposed criteria have a multitude of explanations, namely semantic problems, age and moods of subjects at the time of experiments, and the like.

Alternatively, objective methods propose direct measure of physical quantities such as velocity, acceleration, and jerk as ride evaluation criteria. At the present time, although many objective methods have been suggested, a generally acceptable measure is yet to be established. However, objective measures of mean square jerk and acceleration have shown good correlation with subjective human response [22]. In general, a considerable similarity exists among the ride evaluation criteria, regardless of the types

of subjective or objective measures. Some of the ride criteria are summarized in the following sections.

Ride Vibration Standards: A number of objective methods have been proposed to assess the ride vibrations of off-road vehicles. However, after forty or more years of rather intense research around the world, a single acceptable criteria is still being sought by vehicle designers. Many factors including the following contribute to the general complexity of ride vibration criteria:

1. Complex nature of human response to vibration and difficulty to achieve precise measurement using linear accelerometers.
2. Use of pure sinusoidal rather than random excitations in the laboratory.
3. Differences in various investigations due to varying objectives, experimental methods, data analysis and data reporting techniques.
4. Lack of standardized test procedures.
5. Approaches to the ride question (subjective, relative, health aspects, activity disturbance, etc.).
6. Seating position.
7. Duration of exposure.

Despite the controversy, certain common denominators can be seen in the results from the recent studies [18]. Majority of these studies show that the human body is most sensitive to vertical vibrations in the frequency range 4 to 8 Hz, due to vertical resonances of the abdominal cavity and to horizontal vibrations in the frequency range 1 to 2 Hz due to the resonances of the upper torso. Figures 1.5 and 1.6 present the lines of constant fatigue decreased proficiency limits for vertical and longitudinal vibrations, respectively, related to preservation of working proficiency, established by the International Standards Organization (ISO) [23].

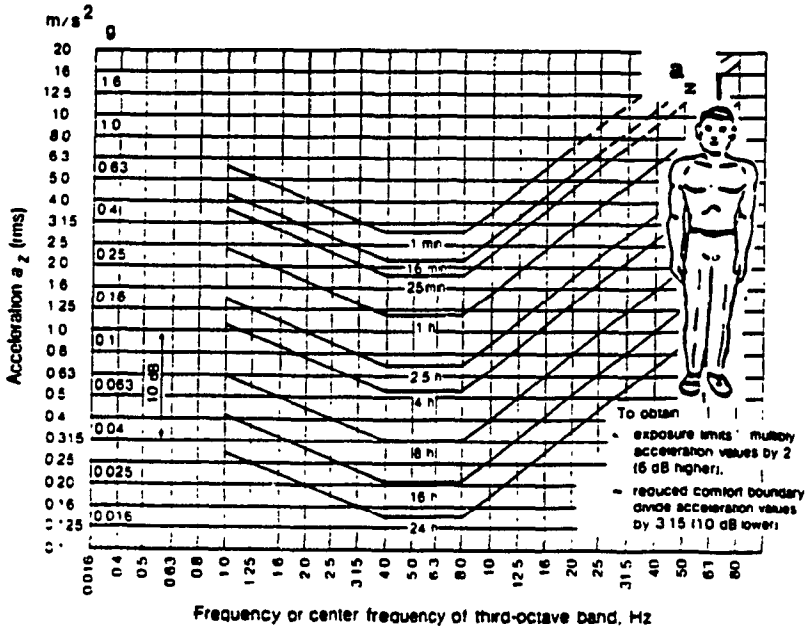

Figure 1.5. Fatigue Decreased Proficiency Limits for Exposure to Vertical Vibrations as Defined by ISO 2631 [23].

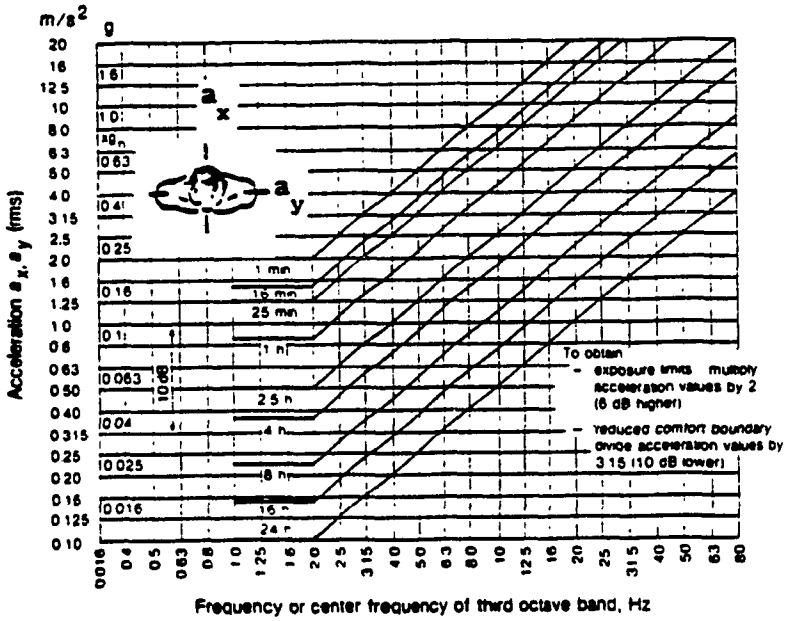

Figure 1.6. Fatigue Decreased Proficiency Limits for Exposure to Transverse Vibrations as Defined by ISO 2631 [23].

The ISO has set forth three exposure criteria as a function of exposure time in the frequency range 1-80 Hz under horizontal and vertical vibrations. The proposed exposure limits are *health and safety* limits for occupational exposure, *fatigue decreased proficiency* (FDP) limits associated with preservation of working efficiency, and *comfort* limits. The main thrust of the standard can be summarized as follows:

(i) For seated vehicle operators, the seat-human interface acceleration in the vertical, transverse and longitudinal directions are the parameters of importance.

(ii) The acceleration signals are analyzed to determine the rms acceleration levels in 1/3 octave frequency bands up to 80 Hz.

(iii) The 1/3 octave intensities are plotted vs frequency and the specified tolerance curves are then superimposed to determine the ride quality for a given exposure time.

ISO has also proposed weighting factors in the frequency range 1 to 80 Hz in order to quantify the ride quality by a single number. In this method, the measured ride vibration is frequency weighted using the filters to compute an overall root mean square (rms) acceleration value. This method of assessing the ride has been gaining popularity due to its simplicity. However, there has been a growing controversy associated with the measurement procedure and the vibration limits proposed in ISO-2631. Studies conducted by Boileau [24] have clearly demonstrated the limitations of ISO-2631 for assessment of off-road vehicle vibrations with high crest factors. In this study, he has summarized the main controversial aspects of the current ISO-2631 with respect to its frequency weighting, time-dependence relationship, and applicability for motions with large crest factor.

The Fourth power criteria has been proposed to assess the off-road vehicle vibration with high crest factors. The draft standard [24] defines

frequency weighting curves for exposure to vertical, longitudinal and lateral vibrations affecting health, comfort, human activities and motion sickness. The weighting curves, defined in the frequency range 0.5-80 Hz, differ from those proposed by ISO 2631 as shown in Figure 1.7.

A more fundamental method for assessing the influence of combining vertical and longitudinal vibrations emerged from the work of Lee and Pradko [25]. The level of discomfort was related to the level of vibration power being dissipated in the subject's body due to vertical, lateral or longitudinal inputs. The measured rms acceleration is weighted along each axis of vibration, to compute the average absorbed power for each direction. The total absorbed power quantity is then obtained by summing the absorbed power quantities for three orthogonal axes. The primary limitations of this method have been outlined by Murphy [26] as:

1. The weighting curves are based on a single biomechanical criterion, where as, human response to vibration is far more complex, since various parts of the body respond to vibration of different frequencies in different ways.

2. Absorbed power values do not directly relate to subjective response. Absorbed power effectively corresponds to acceleration squared where as most evidence point to response being directly proportional to acceleration magnitude.

A number of other criteria have been proposed to assess the ride vibration environment of vehicles. k- factor, as a measure of vibration intensity, function of frequency and rms acceleration, velocity or displacement amplitude has been proposed in Germany [27]. Suspension seats characterizing a k-factor of 25 or less, which is equivalent to rms acceleration 1.25 m/s^2 or approximately 1 hour exposure time with reference to ISO fatigue decreased proficiency criteria, have been proposed to be acceptable. The Dieckman constant and Janeway limits [28], based on

experimental subjective response, imply that human is most sensitive to vertical vibrations below 20 Hz, and were proposed as comfort criteria for automotive passengers. Goldman [29] also established three vibration limits in the vertical mode, viz, perceptible, unpleasant and intolerable, as a function of frequency and peak acceleration response.

Of all these, only ISO-2361 standard specifies rms acceleration limits as a function of exposure time under vertical as well as horizontal vibration, and is most widely accepted. The standard is applicable to WBV as percepted by the drivers of off-road vehicles. However, the standard fails to quantify ride criteria under rotational modes of vibration.

1.2.3 Seat-Suspension Systems

One of the last links in the chain by which vibration get through to the drivers of off-road vehicles is the seat. The seats used in modern tractors range from simple fixed seats to air-suspended versions with automatic compensation for driver weight. Considerable research has been done in seat-suspension design over the past few decades. Comprehensive information to date relative to driver seats for off-road and road vehicles has been reported [30,31,32,33]. The majority of research on ride improvement is related to the vertical seat-suspensions since the vertical vibration is very severe.

For simple fixed seat the frame of the seat is attached directly to the cab floor with foam cushioning between the seat frame and the passenger as a primary element for vibration isolation. The seat cushions are often selected to support driver's weight with the static deflection limited to 60mm, thus from simple mechanical considerations, the fixed seat is limited to providing isolation only in the range above 2 Hz.

The vertical vibration of off-road wheeled vehicles predominate in the frequency range 0.5-5 Hz due to the resonance of the pneumatic-tired vehicle. Since human body is most fatigue sensitive to such low frequency vibration, modern off-road vehicles are often equipped with seat-suspension systems to minimize the transmission of these vibrations arising from tire-terrain interactions and jolting.

Seat-suspension systems, invariably, comprise either an air spring or mechanical spring interposed between the seat structure and base, and a double acting hydraulic damper to absorb vibration energy. Either rubber or metal bump stops are incorporated to prevent excessive relative motion of the low natural frequency suspension. A total stroke of 100 to 160 mm can be accommodated, although at the cost of having to provide adjustments for variations in driver's weight. The commercially available seat-suspensions exhibit natural frequencies in the 1-2 Hz range. These low natural frequency suspension designs are also equipped with a weight adjustment mechanism in order to provide either a mid-ride or a selected ride height to drivers in the weight range 50-110 kg.

Several investigations have emphasized that the off-road vehicles specifically with implements exhibit predominant pitching motions which cause excessive fore-aft motion at the seat due to high location of the driver. A fore-aft isolator, in the form of a track mechanism, is thus attached to the vehicle seat to absorb vibration arising from pitching motions.

In an attempt to further improve the vibration isolation performance and to limit the static and dynamic travel of soft passive suspensions, a number of active and semi-active seat-suspension concepts have been investigated [34,35,36]. Active seat-suspensions employ active elements which have the capability of providing or dissipating energy using an additional

power source and control devices. Active suspensions provide high load bearing capacity at low dynamic stiffness. The relative displacement, therefore, is no longer directly related to the natural frequency of the suspension.

Stikeleather *et al.* [34] developed an active seat-suspension to isolate the operator from low frequency vibrations. Their investigation concluded that the input acceleration can be attenuated by 65-75% in the 1.5 - 8 Hz frequency range. Young and Suggs [35] developed an active seat-suspension to isolate the low frequency roll and pitch vibrations, using angular acceleration and displacement feedbacks. The active rotational seat-suspension system provided 70-80% attenuation of vibration displacement in the 1-2 Hz frequency range. Although, active seat-suspension systems provide superior vibration attenuation performance, their application to off-road vehicles have been severely limited due to excessive cost and complexities.

1.2.4 Mathematical Modeling of Human Body

Development of standardized methods for testing vehicle seats has facilitated the relative assessment of performance benefits and limitations of various seat designs. While the field tests are conducted with human drivers, the laboratory evaluation of seats are often carried out using a rigid mass.

Quantitative information on human body dynamics have been obtained from impedance and transmissibility characteristics of human body. Coermann *et al.* [37] established impedance characteristics of standing and seated subjects as shown in Figure 1.8. The impedance measurements revealed that the frequency impedance characteristics of a human body can be approximated by a rigid mass model only in the low frequency range below 2.0 Hz. Since the

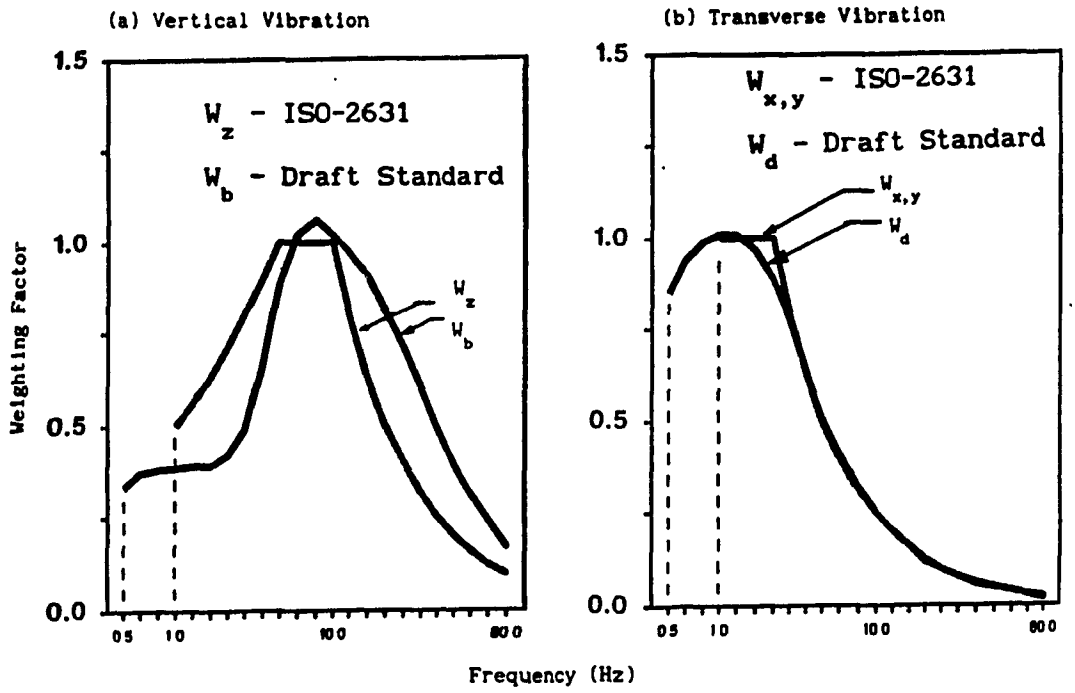

Figure 1.7. Comparison of Weighting Curves Defined by Draft Standard to that of ISO 2631 [24].

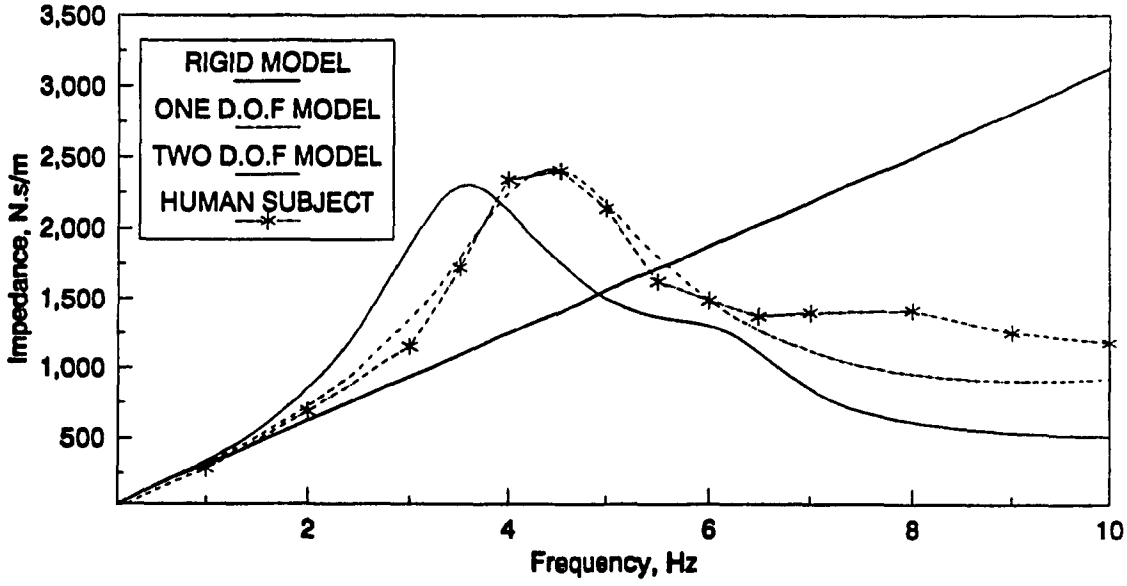

Figure 1.8. Mechanical Impedance of a Seated Human Subject, Rigid Mass, and One- and Two-Degrees-of-Freedom Human Models [38].

off-road vehicle vibration dominate up to 6 Hz, a rigid mass representation of the driver may lead to considerable errors when evaluating relative performance of seat-suspensions. Studies conducted by Stikeleather [38] have illustrated that a seat-suspension system loaded with a rigid mass yields considerably higher acceleration response, when compared to that with human driver. A need to develop a human body simulator has thus been emphasized to carry out laboratory assessment of driver seats.

The human body possess a set of physical properties responding to input vibration in a highly complex manner. The impedance characteristics of seated subjects, measured by Coermann *et al.* [37], revealed two resonant peaks corresponding to 5 Hz and 11 Hz, suggesting that the seated human body dynamic can be characterized by a two degrees-of-freedom system. Their studies were further supported by various other experimental investigations, as summarized in Table 1.1 [39]. Consequently, a human body simulator of two damped sprung masses suspended from a common frame has been proposed by Suggs *et al.* [40] and Park *et al.* [41]. This model approximates the mechanical impedance of the seated 50th percentile male in the frequency range 1 to 10 Hz. Although the proposed simulator duplicated the low frequency characteristics accurately, the models have been questioned due to the lack of resemblance of the human anatomy.

The majority of these human body models, developed assuming linear characteristics, yield unreliable response characteristics when subjected to oscillatory excitations of varying character (random, shock) and level. Nonlinear multi degrees-of-freedom human body models developed by Demic [42] and Patil [43] have demonstrated a better approximation of experimental data obtained for various types of excitations.

Table 1.1

Comparison of Human Body Models [39]

DEVELOPER	POSTURE	FIRST TWO RESONANCE FREQENCIES	DEGREES OF FREEDOM
Coerman *et al.*	Sitting	5 Hz - Upper Torso 11 Hz - Pelvis	2
Suggs *et al.*	Sitting	4.5 Hz - Lower body 8.0 Hz - Upper body	2
Payne *et al.*	Sitting	4-6 Hz - Torso 30 Hz	4
Muksian and Nash	Sitting	3 Hz 6-7 Hz	7

1.2.5 Analytical Methods, Computer Applications, and Laboratory Techniques in Seat Design.

Considerable efforts have been expended in an attempt to reduce the discomfort experienced by off-road vehicle drivers, by improving postural support and vibration attenuation performance of the seats. Much of the development work, however, has been carried out using repetitive field tests and subjective evaluation. In view of the severe effects of exposure (short and long term) to vibration, and driver's awareness; the ride vibration environment of a vehicle has become one of the major factors related to acceptance of the vehicle. Design practices based upon expensive field trials have become obsolete. Modeling and simulation approaches are being explored to derive preliminary designs and design modifications. Such an approach permits, performance analysis prior to hardware realization, and provides a flexible design tool to carry out extensive parameter sensitivity analyses.

Only a limited number of field tests are then needed to develop an optimal seat-suspension system.

In recent years computer modeling techniques have been employed to study vehicle ride performance as affected by geometry, mass distribution, and tire and suspension characteristics. Computer simulations permit the user to conduct relative performance analyses to arrive at optimal component designs.

The design and analyses of a seat-suspension system necessitates careful consideration of the following:

(i) Description of a truly representative cab floor excitation.

(ii) Description of the seat and human body as a system of components.

(iii) Determination of dynamic response of the seat-human system.

(iv) Interpretation of vibration response at the driver-seat interface to a human stress parameter.

A better understanding of the qualitative and quantitative behavior of seat-suspension systems can be obtained by including the nonlinear effects. These nonlinearities refer mainly to the characteristics of shock absorber, cushion, suspension springs, linkage geometry, dry friction, bump stops and human reaction.

Rakheja [36] proposed a six degrees-of-freedom rotational seat isolator to attenuate roll pitch and bounce ride vibration of agricultural tractors, and developed a nonlinear analytical model of the seat. The investigation revealed that a seat-suspension can successfully be employed to improve ride performance in the bounce, longitudinal, and pitch modes. Attenuation of lateral and roll vibrations via passive seat-suspension was considered infeasible due to requirements of extremely low natural frequencies.

Kyeong [44] presented a study on vertical ride simulation of passive,

active and semi-active seat-suspension systems for off-road vehicles using linear models. Each suspension model was combined with a three-dof-model of the driver to formulate models of the ride systems of off-road vehicles. The input vibrations for the simulation were obtained by measuring a real time history of accelerations at the base of the seat-suspension of an agricultural tractor during transport and mold board plowing operations.

In general, computer aided analyses free the designer from the repetitive task of manual design analyses and allow him/her to concentrate on the more creative aspects of design. They permit the analysts to experiment and study system performance while changing parameters and operating conditions at will. Another important advantage is that the actual span over which the dynamic simulations are performed can be magnified so that the behavior over short periods may be examined, perhaps permitting a discovery of important phenomena. Further, the systems can be tested beyond the range of normal or safe operation without endangering lives or property.

To ensure validity and reliability of seat-suspension models as representative of the real system, both the behavior of the model and the real system should be studied under the same conditions. This requires the measurement of static and dynamic characteristics of the real seat-suspension systems and their system components.

Static and dynamic performance characteristics of seat-suspension systems have been invariably determined via laboratory and field measurements. The manufacturers have continued to follow the design practice comprising of repetitive field tests to develop effective driver seats. Controlled laboratory test methods, that do not expose the human subjects to vibration, have also been used by many researchers [45,46].

These studies have investigated vibration isolation performance of seats

in terms of vibration transmissibility and vibration intensity at the seat-operator interface. Force-displacement characteristics of seat cushion and suspension subsystems have also been measured in the laboratory to assess their relative performance characteristics. However, no attempts have been made to determine the dissipative properties of air-filled foam cushions and other nonlinear properties of the seats, i.e. friction force, bump stop characteristics, etc. Consequently, the computer modeling of seat-suspension systems has been primarily limited to only linear models.

1.3 SCOPE OF THE THESIS

The overall objective of this investigation is to contribute to improvement of the working environment for the off-road vehicle operators through attenuation of terrain induced vertical vibrations. This is sought via systematic analytical and experimental analyses of passive vertical seat-suspension systems for reasons of simplicity, low cost and ease of adapting to existing vehicles. The specific objectives of the study include the following:

1. Analyze the off-road vehicle vibration data and determine its impact on health and safety of vehicle operators.
2. Develop a general design criteria for seat-suspension systems for a class of off-road vehicles, and conduct a review of design aspects of commercially available seats.
3. Design and fabricate a laboratory seat simulator to assess the vibration isolation performance of vertical seat-suspension systems for sinusoidal and random excitations.
4. Identify the static and dynamic characteristics of candidate vertical seat-suspension, and evaluate their vibration isolation performance via laboratory testing.
5. Develop a general nonlinear analytical model of passive seat-suspension systems, using a rigid body representation of the human driver, and validate the analytical model.

6. Develop and integrate a dynamic model of seated human body to the seat suspension model to investigate the influence of compliant human body.

7. Carry out parametric sensitivity analyses to determine near optimal seat-suspension parameters, and assess the ride quality with reference to the ISO proposed limits.

In chapter 2, designs of various commercial seat-suspension systems are reviewed, and a general design criterion is derived on the basis of off-road vehicle vibrations. A nonlinear mathematical model of vertical seat-suspension systems is developed using rigid body representation of the driver, cushion characteristics, linkage geometry, static and dynamic characteristics of the suspension, and bump stops. Single- and two-degrees-of-freedom human body models are integrated to the seat suspension model to investigate the vibration levels transmitted to the driver.

In chapter 3, static and dynamic laboratory test procedures to identify model parameters are described. Results of the static and dynamic tests performed in the laboratory are presented and discussed. The test data is analyzed to yield the model parameters. The random vibration measured at the cab floor and those proposed by the ISO are characterized for computer simulation and performance evaluation of the analytical models.

In chapter 4, laboratory test methodology and apparatus for seat-suspension systems are described. The vibration transmissibility characteristics of the selected seat-suspension systems are derived from laboratory tests based on sinusoidal excitations. The nonlinear differential equations of motion for the seat-suspension models are solved in the time-domain using numerical integration algorithm, and response characteristics are compared to those attained from the laboratory tests to demonstrate the validity of the analytical model.

In chapter 5, methods of solving the nonlinear differential equations for

the seat-suspension models in the frequency-domain are reviewed. Performance of seat-suspension models using various human body models are compared. Linearized models are developed to represent the nonlinear seat dynamics based on the energy balance concept. The vibration isolation characteristics of the linearized seat-suspension models are compared with that of the nonlinear model to illustrate the effectiveness of the linearization technique.

In chapter 6, sensitivity of the vibration isolation properties of the seat models to changes in suspension parameters are investigated. Ride vibration performance of the seat-suspension systems is assessed with reference to the ISO proposed limits and the influence of various suspension parameters on the driver fatigue is discussed. The conclusions derived from this investigation and recommendations for future work are finally presented in chapter 7.

CHAPTER 2
DEVELOPMENT OF OFF-ROAD VEHICLE SEAT-SUSPENSION MODELS

2.1 GENERAL

The ride vibration of vehicles, whether highway or off-highway, predominate in the frequency range 0.5-5 Hz. The amplitude of vibration encountered by the off-road vehicle drivers, however, is significantly larger than that encountered by the highway vehicle drivers. Although considerable research and development efforts have been made to improve off-road vehicle ride via suitable tires, and primary-suspension, the need for further improvement in ride has been emphasized in view of three factors: large amplitude of ride vibration, specifically in off-road vehicles; prolonged exposure time; and ride frequencies coinciding with the human body resonances. Investigations on the influence of ride vibration on human body have established that prolonged exposure to low frequency, large amplitude, and whole-body vibration causes degenerative physiological symptoms, and degradibility in responding to certain stimuli prominent to human safety and efficiency.

In order to accomplish the off-road vehicle ride performance to meet the ISO proposed FDP limits, the need for developing effective secondary (seat and cab) suspension has long been identified by the concerned industries. Suspension at the cab can provide for the drivers: a stable floor, isolation from forces introduced by implemented loads, and isolation from noise and chassis vibrations. However, the cabs in small size off-road vehicles are often welded to the chassis along with the Rollover Protection Structure (ROPS), and hence the suspension at the cab mount requires complex

alterations. Suspension at the seat is perhaps the simplest option for ride improvement.

In this chapter, design specifications of various commercially available passive vertical seat-suspensions are summarized, and a selection/design criteria is proposed in view of characteristics of off-road vehicle vibrations and ergonomic factors. The seat-suspension systems are analytically modeled incorporating three different driver models. The analytical models formulated incorporate the nonlinearities arising from Coulomb friction, elastic bump stops and shock absorbers.

2.2 DEVELOPMENTS IN SEAT-SUSPENSION

The driver seat is perhaps more closely linked to comfort than any other vehicle component. Addition of an effective suspension system at the seat offers the simplest alternative for potential ride improvement of off-road vehicles. The driver seat is designed to maintain acceptable driver comfort, and driver interaction with various controls. The primary considerations in seat design include the following:

1. Provide the driver with a comfortable and controlled seated posture.
2. Protect the driver from excessive shock and vibration as outlined in the SAE standard J1384 [47].
3. Position the driver to permit adequate vision, and safe and efficient performance of driver's tasks [48].
4. Position the driver to provide easy and non-fatiguing access to machine controls.
5. Restrain the driver within a safety zone in the event of a collision or rollover.
6. Minimize back slap and head snapping, caused by pitch motion of the vehicle or the seat.
7. Attenuate vertical and horizontal vibrations.

8. Minimize leg pumping action, caused by excessive relative vertical motion of the driver with respect to the cab floor.

2.2.1 Seat-Suspension Components

The dynamic comfort offered by the seat is a function of design, construction, kinematics, ease of suspension adjustment, and ride performance of the suspension system. Among these factors, the kinematics of the suspension linkage, stiffness, and the damping mechanisms influence the vibration transmission characteristics of the seat-suspension.

Seat Cushion: Human beings normally sit on their ischial tuberosities which are bony prominences, about 11 cm apart, covered by muscle, fat and skin. They transmit most of the weight of the upper body directly and uniformly from the spinal column to the seat cushion. Vibration forces are directly transmitted to these prominences, and thus to the back. The firmness of the seat cushion thus affects the degree of driver's comfort and fatigue.

Very hard cushions result in discomfort at the tuberosities, which encourage slouched posture to shift weight to more fleshy areas. But if a cushion is too soft or too contoured, the femurs are pushed upward, as shown in Figure 2.1, and carry a major part of the weight causing increased pressure leading to possible pain and discomfort in the hip joint. Seat cushions, neither too hard nor too soft, are thus desirable. Figure 2.2 presents subjective rating of comfort with respect to cushion firmness from studies conducted by Whyte and Stayner [49]. The main support provided by the seat cushion must be at or slightly forward to the ischial tuberosities. Care must be taken that the pressure applied to the thighs close to the knee is not too

high, as that may pinch the femoral artery and nerve leading to numbness of the foot and lower leg.

Back Rest: Adequate back rest designs can improve the driver's comfort considerably by providing lumbar support and controlled seated posture. It is generally recognized that in order to minimize discomfort, fatigue and potential damage to the spinal column, the driver's back should maintain its normal curvature as shown in Figure 2.3. A slouched back creates high and uneven pressure in the vertebral discs, leading to increased tension in various spinal ligaments and stress in individual vertebrae, especially in the lower back [32]. The vibration isolation characteristics of seat-operator system is influenced by the operator posture. An erect posture experiences large vibrations corresponding to frequencies greater than 4 Hz, while a slouched posture experiences slightly larger vibrations at low frequencies [39]. Back rests with adjustable lumbar supports have thus been developed to help the drivers in maintaining an adequate S-shaped spinal curve.

Seat Compliance: The compliance in seat-suspensions is, invariably achieved through include steel springs, rubber or air springs. Leaf springs have been extensively used in former rudimentary seats, but they are unable to meet the present stroke prerequisite. Torsion bars offer a convenient design, but the constraints on overall seat dimensions limit the use of plain conventional torsion bar. However, composite bars made of small wires and thin plates have been proposed. Rubber springs are to be used for systems with large leverage ratio between the bump and the suspension. They are inherently high strength

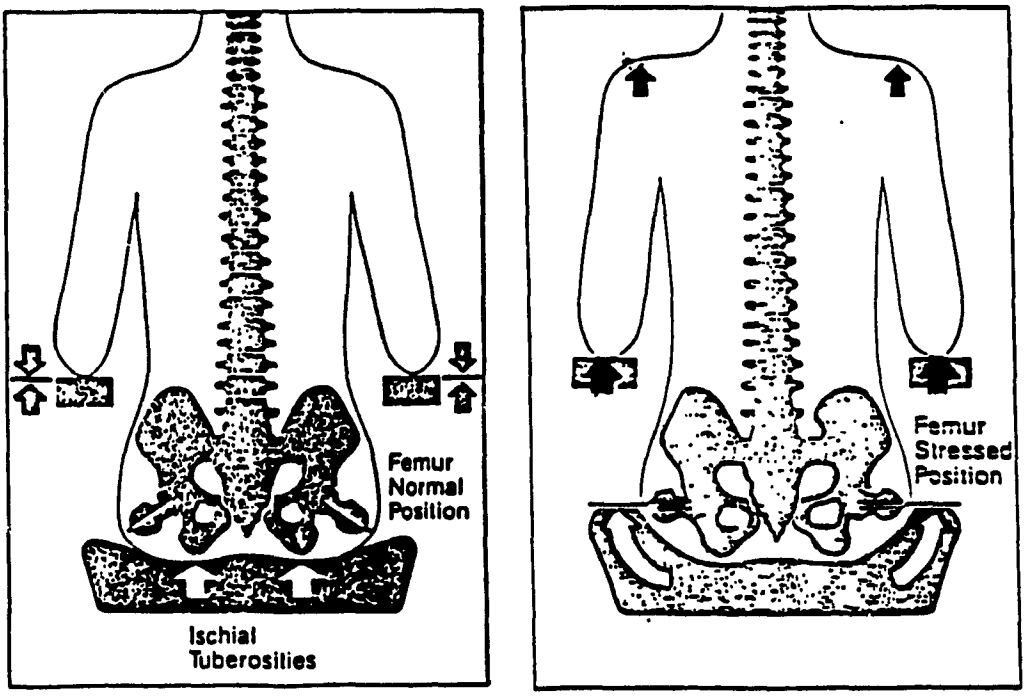

Figure 2.1. Ischial Tuberosities: (a) Femur normal position, (b) Deflection of Femur Bones Due to Soft Cushions [32].

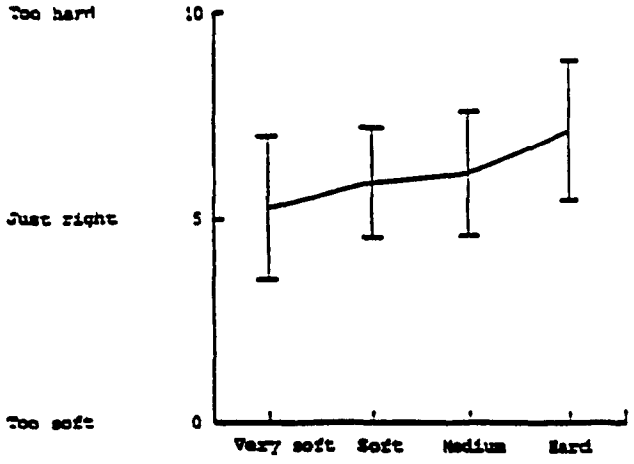

Figure 2.2. Subjective Rating of Comfort with Respect to Cushion Firmness [49].

and small displacement springs. Insufficient internal damping of the rubber material poses the requirement of an auxiliary shock absorber. Pneumatic springs are being used extensively, since they provide the flexibility to adjust for driver's weight and natural frequency.

Seat-Suspension Linkage: The linkage system in a seat-suspension is designed to ensure parallel seat displacement nearly as vertical as possible along the suspension stroke while providing the necessary height adjustment. The limiting factor is usually the available room. Linkage systems can be grouped in two categories: under the seat linkage systems, as shown in Figure 2.4 and behind the seat linkage system, as shown in Figure 2.5. The oldest and simplest parallelogram linkage still remains the popular one for highway vehicle seats, while some configurations of off-road vehicles use the conventional and cam-operated scissors linkage as shown in Figure 2.6.

Prime considerations in linkage design are:

1. To provide a wide range of height adjustment.
2. To ensure almost vertical motion.
3. Minimum joint friction to minimize jerk.
4. Compactness

Damping Mechanism: The suspension seats invariably include a shock absorber to provide adequate damping. However, certain seats offer a mechanism to engage the shock absorber only when a severe shock input is encountered.

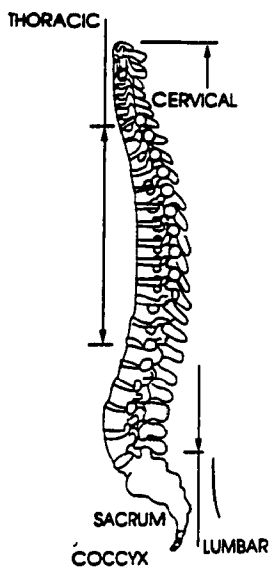

Figure 2.3. Normal Curvature of the Spine Vertebral Column in Relation to Body Outline [32].

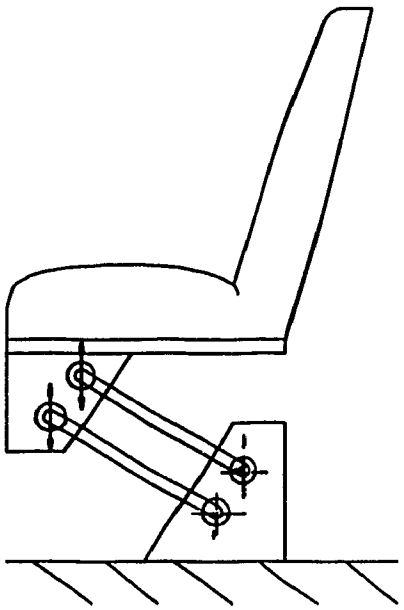

Figure 2.4. Schematic of the Driver Seat with Under-the-Seat Linkage System.

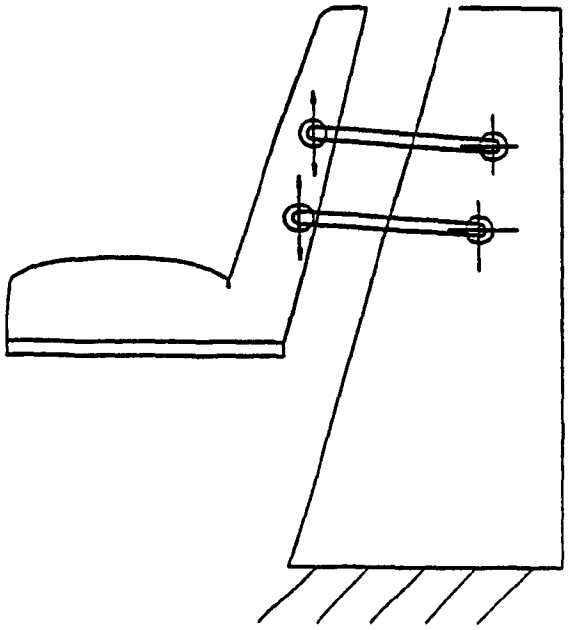

Figure 2.5. Schematic of the Driver Seat with Behind-the-Seat Linkage System.

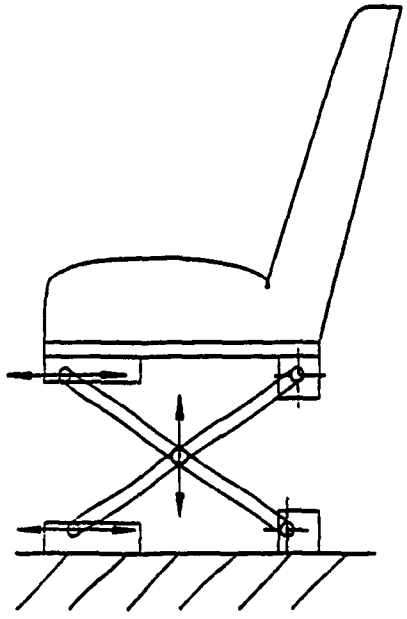

Figure 2.6. Schematic of the Driver Seat with Scissors Linkage System.

2.3 DESIGN CONSIDERATIONS

The human body is most sensitive to low frequency whole-body vibration and thus a suspension seat must be selected to minimize the transmission of these vibrations arising from terrain interactions and jolting. In order to provide the drivers with a controlled comfortable posture, the suspension seat should yield minimal relative displacement of the driver with respect to the controls, and minimize head snapping and back slap. Adjustabilities in view of seat height, seat-pedal distance, lumbar support, cushion angle, etc., must be available to ensure adequate vision and posture. The vibration environment and the enclosure design must be given appropriate consideration in selecting the seat-suspension for a specific vehicle.

2.3.1 Vibration Requirements

The rms acceleration spectrum of a forestry vehicle, measured under typical operating condition, shown in Figure 2.7, reveals that the ride vibration predominate in the low frequency range around 2.6 Hz [50], which is attributed to the resonant frequency of the pneumatic-tire in off-road vehicles. This frequency corresponds to the excitation frequency that should be attenuated through a properly tuned seat suspension. Consequently, the seat must be designed with a resonant frequency less than $1/\sqrt{2}$ times the forcing frequency, or 1.8 Hz, for the seat-to-floor transmissibility ratio to be less than 1.0 at the predominant frequency of 2.5 Hz.

Since the seat's natural frequency, and thus its transmissibility characteristics, are likely to be influenced by the driver's weight, it is important that the seat-suspension be equipped with a control, whether manual or automatic, to permit suspension stiffness variations such that the natural

frequency remains nearly constant independent of the driver's weight. Most mechanical seat suspensions are equipped with a manual dial which permits adjustments for the driver's weight.

In the case of pneumatic suspensions, automatic self-leveling mechanisms exist to automatically adjust the stiffness according to the driver's weight on the seat. In any event, the weight compensation mechanism should be independent of height adjustment for the seat to preserve its optimal attenuation capabilities. Low natural frequency suspension yields excessive static and dynamic relative travel, that affects the driver's interactions with the controls in an adverse manner. The suspension travel should thus be limited either by installing elastic limit stops, adequate suspension linkages, or both. A maximum total travel of 100 mm is generally acceptable for off-road vehicles.

Finally, the damping coefficient associated with the suspension should be such that the amplification of the vibration at the seat's resonant frequency is not excessive. A transmissibility ratio ranging from 1.5 to 2.0 at the resonant frequency is generally considered to be a maximum acceptable value for the seat to be effective. In addition, damping must be sufficient to prevent occasional bottoming of the suspension in the case of shock loading or transient vibration.

2.3.2 Ergonomic Considerations

Except for larger models of off-road vehicles, the cab dimensions are generally very small, especially the height of the cab. This is particularly true for the forestry and mining vehicles. In the case of a skidder cab, the height of the platform from the cab floor on which the seat can be installed

is of the order of 365 mm, whereas the horizontal distance between the pedals and the seat reference point is on the order of 680 mm. The suggested optimal height between the floor and the seat reference point in ISO-4253 [51] and SAE J899 [48] is 525 mm and 510 mm, respectively. Thus, for the seat to be adequate, it has to have a height of 165 mm between the platform base and the seat reference point. However, it is generally estimated that a suspension installed under the seat usually requires a minimum height of 200 mm between the base and the seat reference point, posing a rather difficult problem for such small cab vehicles. Seats equipped with behind the seat suspension, may be considered appropriate for such vehicles.

In addition to the standard referred above which specify the dimensions that must be respected for the driver's work station, several recommendations on desirable characteristics of off-road seat design and adjustabilities have been reported in the literature [48]. The recommendations on the dimensions of the seat cushion and back rest, desirable inclinations, height, travel, accessories, and adjustments are summarized in Table 2.1.

Seating developments have taken anthropomorphic data into consideration to improve static comfort involving size, configuration, adjustments and materials. A number of necessary adjustments have evolved from the anthropomorphic data [48]. Seats are capable of maintaining adequate static position for driver weight in the range 50-110 kg [52]. It has been established that 75% to 82% of the total driver weight is supported by the seat [53]. Thus the seat must be adjustable for weights in the approximate range 45-83 kg. The seats are designed for a minimum vertical adjustment of ± 30 mm from the mid-position and a fore-aft adjustment of ± 75 mm [52].

Table 2.1

Off-Highway Vehicle Seats Recommended Characteristics [51].

SEAT CHARACTERISTICS		RECOMMENDATION
BACK REST		
• Width	(mm)	400 - 500
• Height	(mm)	> 260
• Angle	(degrees)	95 - 110
CUSHION		
• Width	(mm)	> 440
• Length	(mm)	350 - 450
• Angle	(degrees)	3 - 12
• Thickness	(mm)	40 - 100
VERTICAL DISTANCE TO THE SEAT REFERENCE POINT (SRP)	(mm)	140 - 180†
VERTICAL TRAVEL	(mm)	± 50
ADJUSTMENTS		
• Weight	(kg)	-
• Height	(mm)	≤ 100
• Fore-aft displacement	(mm)	± 75 (min)
• Arm-rests		Required
• Head-rest		Optional

† Depending on the horizontal distance between the SRP and the pedals.

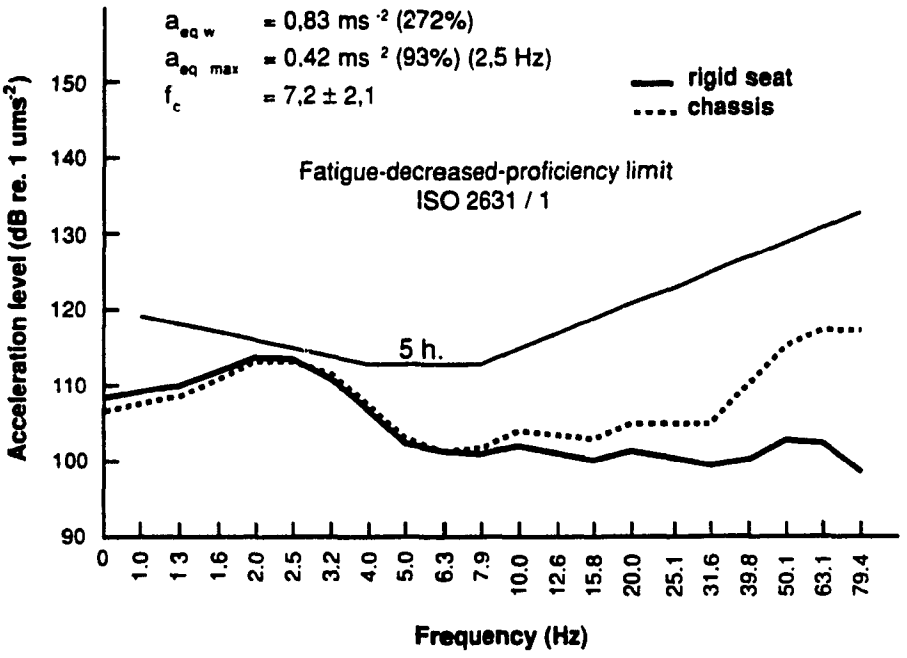

Figure 2.7. Frequency Spectrum of Vertical Vibrations Measured at the Cab Floor of the Skidder [24].

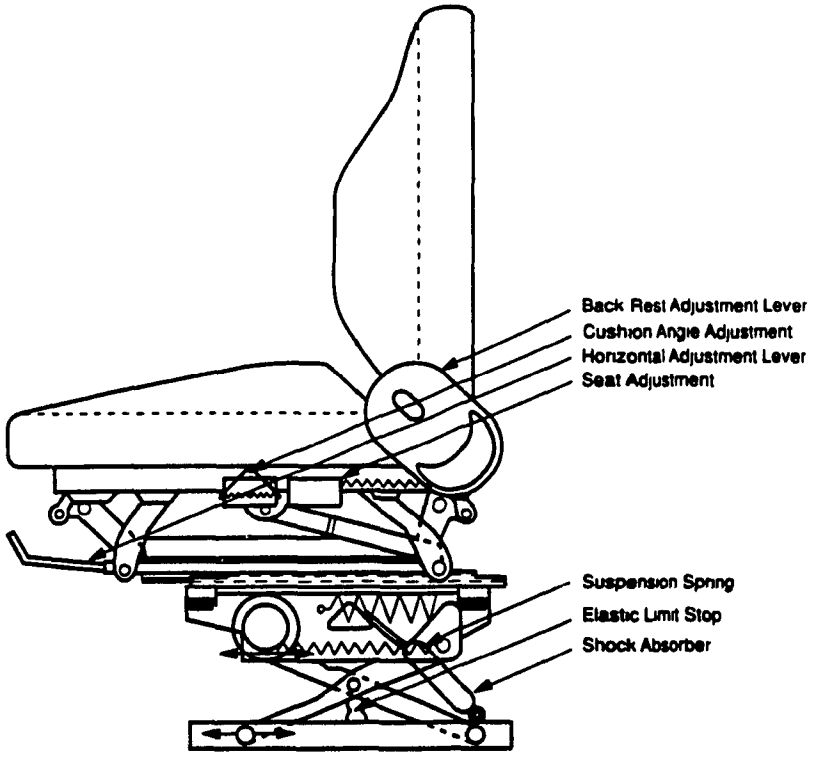

Figure 2.8. Schematic of the ISRI Mechanical Seat-Suspension.

However, in the modern air suspension seats the available vertical travel is as high as ± 75 mm from the mid-ride position.

Apart from the above adjustments, seats are often designed with adjustable back rest, cushions and arm rest to provide adequate postural support.

2.4 DESIGN FEATURES OF SELECTED COMMERCIALLY AVAILABLE SEAT-SUSPENSIONS

A number of seat-suspension systems with low natural frequency have been developed for highway as well as off-highway vehicles. The seats are designed with a range of adjustments, such as ride height, fore-aft, cushion angle, back-rest inclinations, etc. Attenuation of terrain induced ride vibration is primarily achieved through suspension springs and shock absorber. A total of five commercially available seat-suspension systems are selected in this study to evaluate their vibration transmissibility characteristics and to develop a general analytical model. The specification of these seats are briefly reviewed in view of the design criteria presented in section 2.3.

Figures 2.8 and 2.9 illustrate the schematics of mechanical and air-suspension seats, respectively, developed by ISRINGHAUSEN. Both the suspension systems comprise a cross-linkage mechanism, an inclined shock absorber and necessary adjustments. The mechanical suspension employs a horizontally mounted coil spring, while the air-suspension employs an air bag, accumulator and cam-operated control valve to provide automatic leveling and variable spring rate. Both the seats are equipped with a pneumatic lumbar support integrated within the back-rest. The lumbar support consists of two independently inflatable chambers arranged at the level of lumbar vertebral and lower thoracic vertebrae.

Figure 2.10 illustrates the schematic of a behind-the-seat suspension, developed by SIFRA (a division of ISRINGHAUSEN). This suspension configuration offers extremely compact seat design, specifically suitable for small size off-road vehicles with limited height. The seat consists of a sprung seat pan, mounted on vertical rail. The construction of the seat permits only vertical motion of the seat, unlike the cross-linkage and parallelogram linkage seats. The seat pan and the cushion are suspended by an inclined coil spring and a hydraulic shock absorber, mounted behind the seat pan. Rubber mounts are incorporated to limit the maximum vertical travel in compression as well as rebound stroke. Weight compensation is accomplished manually by varying the preload on springs.

Figures 2.11 and 2.12 illustrate the schematics of the GRAMMAR seat-suspension systems with and without a gas shock absorber named as GRAMMAR and GRAMMAR (Gas Shock), respectively. Both the seats comprise of cross-linkage mechanism, torsion bar and coil spring. A ratchet operated cam mechanism is integrated to achieve weight adjustment and variable spring rate. The specifications and construction details of selected and some other commercially available seat-suspensions are summarized in Table 2.2.

2.5 ANALYTICAL MODELING OF SEAT-SUSPENSION SYSTEMS

Vibration attenuation performance of seat-suspension systems, in general, has been evaluated through transmissibility characteristics established either in the laboratory or the field. Alternatively, an analytical model may be developed and computer simulation techniques may be used to assess their performance characteristics. Analytical models of physical systems are developed based on two fundamental approaches: (i) using physical laws characterizing the system; and (ii) using empirical laws derived from

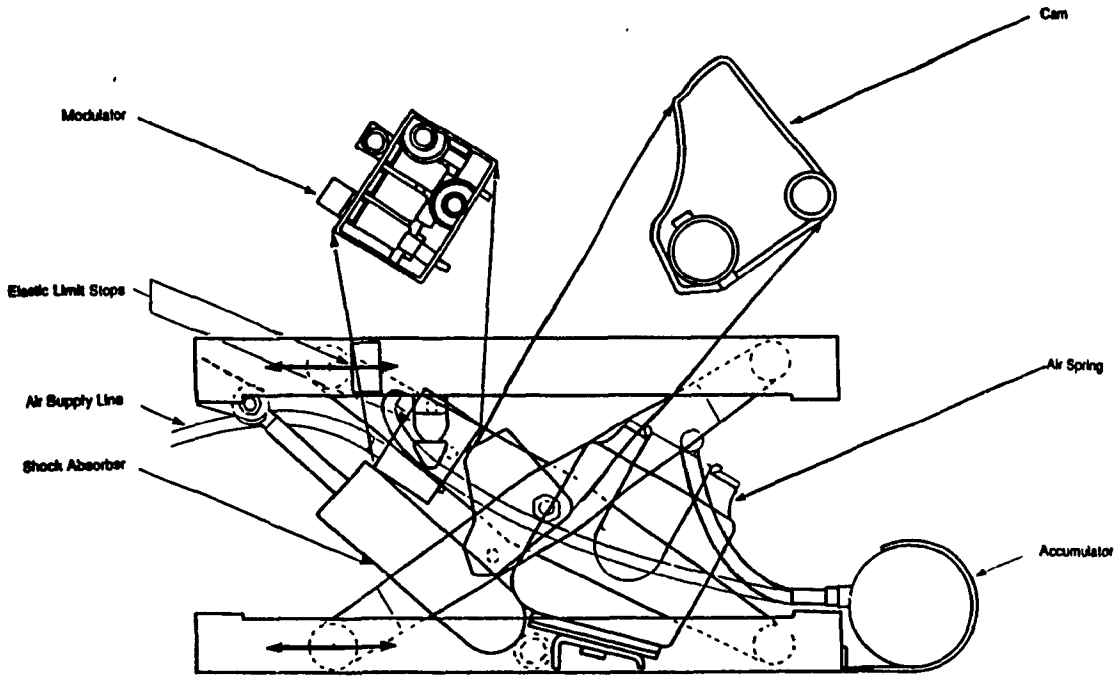

Figure 2.9. Schematic of the ISRI Self Leveling Pneumatic Seat-Suspension.

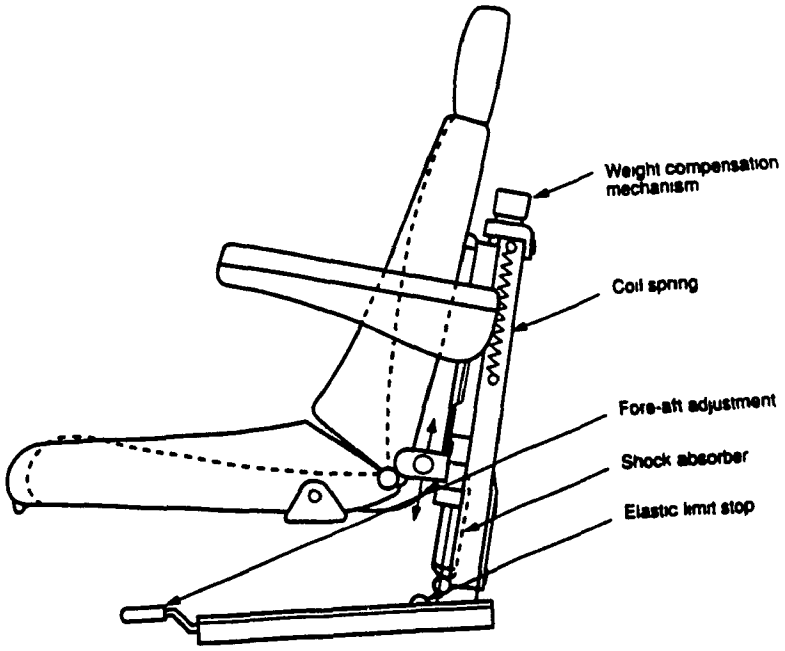

Figure 2.10. Schematic of SIFRA Seat-Suspension.

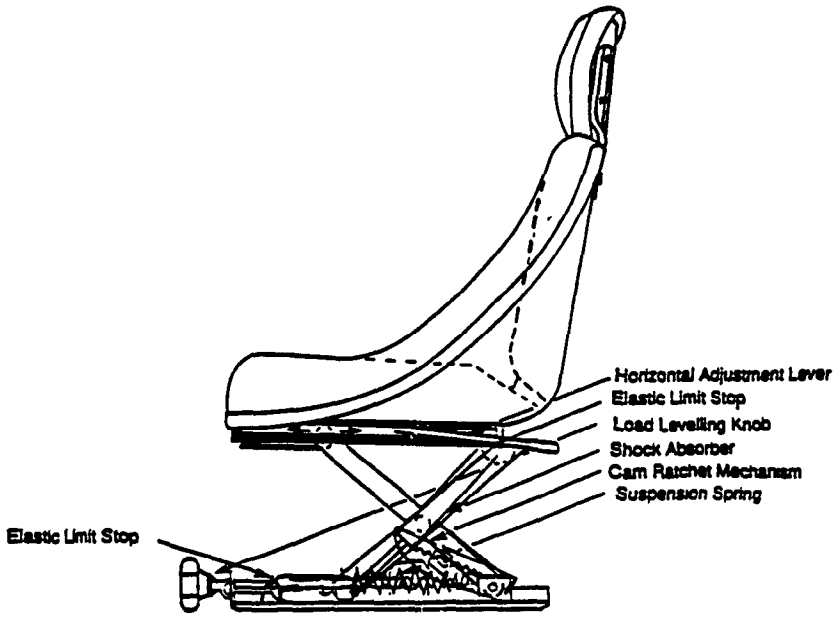

Figure 2.11. Schematic of GRAMMAR (Gas Shock) Seat-Suspension.

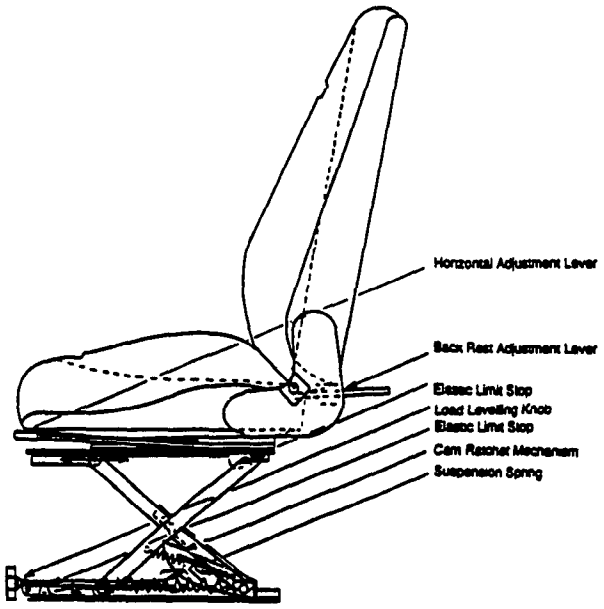

Figure 2.12. Schematic of GRAMMAR Seat-Suspension.

experiments. Analytical models can also be formulated using a combination of both approaches. Such an approach requires identification of static and dynamic characteristics of various components. In the case of seat-suspension systems nonlinearities due to linkage friction, shock absorber, air-springs and bump stops should also be considered. Development of an analytical model thus necessitates adequate representation of the following:

(i) Dynamic characteristics of the human driver.

(ii) Static and dynamic characteristics of the cushion, suspension springs, bump stops and shock absorber.

Static and dynamic characteristics of suspension systems are identified, and a general nonlinear analytical model incorporating various human body models is developed.

2.5.1 Modeling the Driver

The seat-suspension performance is affected not only by the suspension design but also by the dynamics of the suspended mass of the driver. It is thus essential to develop an acceptable human body model in order to investigate the performance characteristics of the total driver-seat-suspension system. Three lumped-parameter driver models are formulated using the quantitative information on seated human body dynamics, obtained from impedance and transmissibility characteristics along the vertical axis. The human body models are described below:

Rigid Mass Model

Impedance characteristics of human body, seated with semi-rigid envelope around the abdomen, reveal that human body subjected to whole-body vibration

behaves similar to a rigid mass up to approximately 2 Hz. Since off-road vehicle vibrations predominate only up to 5 Hz, a simple rigid mass representation of the driver may be used to analyze the seat-suspension system. Such a seat-suspension model, however, may not accurately predict the suspension performance for excitation frequencies above 2 Hz.

Single Degree-of-Freedom Model

The impedance measurements, performed on seated human subjects [39], illustrate that the upper torso and lower body resonate in the 4-6 Hz and 7-11 Hz excitation frequency ranges, respectively. Since off-road vehicle vibration predominate up to 6 Hz, a single-degree-of-freedom model representing the dynamics of upper torso and lower body can be formulated, as shown in Figure 2.13. The buttocks and legs are treated as rigid mass and lumped with the skeletal frame. The model parameters, derived from impedance data, are presented in Table 2.3.

Two Degrees-of-Freedom Model

Suggs [54] proposed a two degrees-of-freedom seated human body model that can simulate the dynamic behavior of upper and lower bodies. A schematic representation of the two degrees-of-freedom model is presented in Figure 2.14, and the corresponding parameters, derived from measured impedance data, are presented in Table 2.3.

Three seat-suspension models are then developed incorporating the three human body models. The seat-suspension model with rigid mass representation of the driver is extensively used for validation using the transmissibility characteristics measured in the laboratory.

Table 2.2

Specifications of Seat-Suspension Systems for Off-Road Vehicles

Manufacturer	Model	Construction	Height Adjustment	Travel	Other Adjustments
ISRINGHAUSEN	Pneumatic	Cross linkage, air spring and inclined shock absorber	Automatic	85 mm	•Fore-aft •Back rest •Seat angle •Lumbar Support
	Mechanical	Cross linkage, coil spring and inclined shock absorber	Manual	80 mm	•Fore aft •Back-rest •Seat angle •Lumbar Support
	SIFRA	Sprung seat pan supported on vertical spring and shock absorber	Manual	110 mm	•Fore-aft •Seat angle •Head-rest •Arm-rest
GRAMMAR	GRAMMAR	Cross linkage, torsion bar & coil spring	Manual	100 mm	•Fore-aft
	GRAMMAR (Gas Shock)	Cross linkage torsion bar, spring and gas shock absorber	Manual	100 mm	•Fore-aft •Back-rest •Seat angle •Arm-rest
BOSTROM	Air	Cross linkage, air spring and inclined shock absorber	Manual	102 mm	•Fore-aft •Back rest •Seat angle
	Viking Air	Cross linkage, torsion bar, coil spring and inclined shock absorber	Manual	5-100mm	•Fore-aft •Back rest

Table 2.3

Mass, Spring, and Damping Parameters of Human Models [38]

MODEL	m_o(kg)	m_1(kg)	m_2(kg)	$C_1(N\frac{s}{m})$	$C_2(N\frac{s}{m})$	$K_1(\frac{N}{m})$	$K_2(\frac{N}{m})$
RIGID	49.72	-	-	-	-	-	-
ONE DEGREE OF FREEDOM	14.62	35.1	-	500.1	-	27951.4	-
TWO DEGREES OF FREEDOM	14.62	29.25	5.85	364.7	145.9	23297.7	14728.4

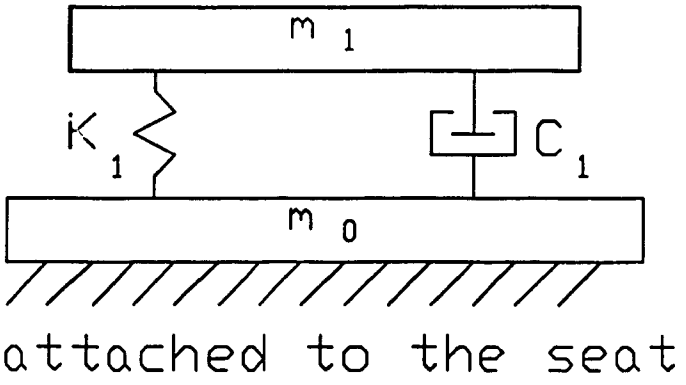

Figure 2.13. One Degree-of-Freedom Model of the Seated Human Body.

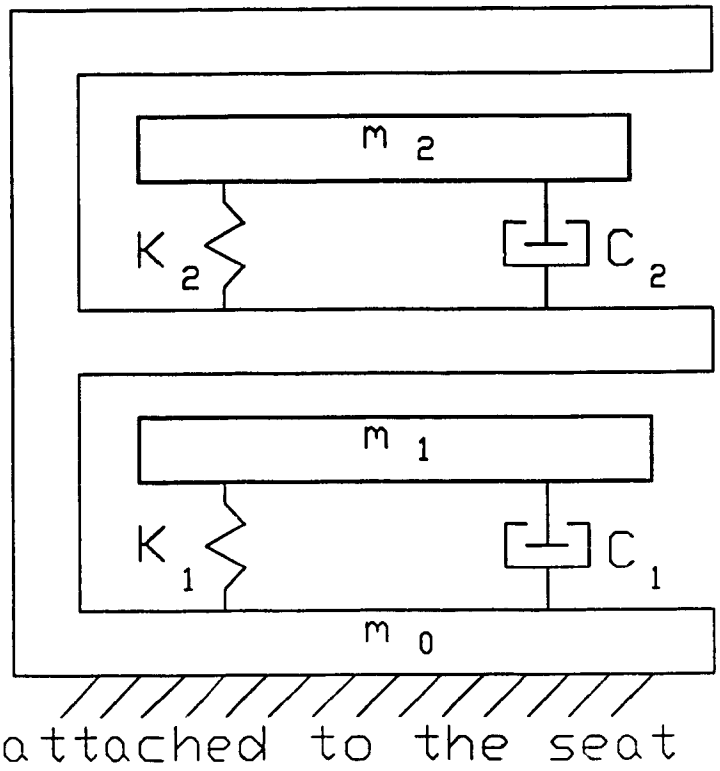

Figure 2.14. Two Degrees-of-Freedom Model of the Seated Human Body [38].

2.5.2 Analytical Modeling of Vertical Seat-Suspension Systems

Development of an analytical model of a seat-suspension system necessitates identification of static and dynamic characteristics of linkage mechanism, suspension spring and damper. The current designs of seat-suspensions can be classified under two configurations: (i) under-the-seat-suspension; and (ii) behind-the-seat-suspension. Under-the-seat-suspensions are designed with either a cross-linkage or a parallelogram linkage mechanism. Seat-suspension systems for off-road vehicles, in general, employ cross-linkages to ensure nearly vertical motion of the operator, when subjected to large displacement excitations. The kinematics and dynamics of the suspension linkage does not play a significant role in the vibration attenuation performance, and hence the kinematics and dynamics of the linkage system can thus be neglected.

Vertical seat-suspension systems, irrespective of the linkage type, can be characterized by a two degrees-of-freedom system, while neglecting the dynamics of the driver. Figures 2.15 and 2.16 illustrate the two-degrees-of-freedom models of under and behind the seat-suspension configurations, respectively. Additional degrees-of-freedom, however, need to be incorporated when dynamics of the driver are considered. Three analytical models of the seat-suspension systems are developed incorporating different human operator models. The primary assumptions implied in the modeling process are as follows:

(i) Transverse stiffness of the cushion is assumed to be very high. The visco-elastic properties of the foam-cushions along the vertical axis are characterized by equivalent linear stiffness and viscous damping coefficients, within the operating range.

(ii) Coulomb friction within the linkage mechanism is assumed to possess ideal characteristics.

(iii) The resilient means, whether air, vertical coil springs, or horizontal coil spring, is modeled as vertical spring with linear coefficient in the operating range.

(iv) The shock absorber is modeled as a nonlinear damper incorporating bleed and blow-off stages, symmetric in compression and extension.

(v) Motions along the generalized coordinate system are small relative to overall dimensions of the seat.

(vi) Seat is considered to move in vertical direction only.

(vii) Influence of horizontal suspension system on the vertical suspension is assumed to be insignificant.

2.5.2.1 Seat-Suspension Model with Rigid Mass Driver Model

The impedance and transmissibility characteristics of a human body seated with a semi-rigid envelop around the abdomen, resemble to those of a rigid mass up to 2 Hz [38]. Representing the driver as a rigid mass, the vertical seat-suspension systems may be modeled as two degrees-of-freedom dynamic systems, as shown in Figures 2.15 and 2.16. In view of the complexities associated in developing a quantitative model of the human body and the fact that vehicle vibration dominate around low frequencies, a rigid body representation of the human driver may be considered appropriate. Based on the experimental studies conducted by Stikeleather [53], it is further assumed that only $\frac{5}{7}$ of the driver mass is supported by the seat. The equations of motion for the suspension models are derived subject to the assumption described in previous subsections.

Equations of Motion

The equations of motion for the seat-suspension models, presented in Figures 2.15 and 2.16, can be expressed in the following manner:

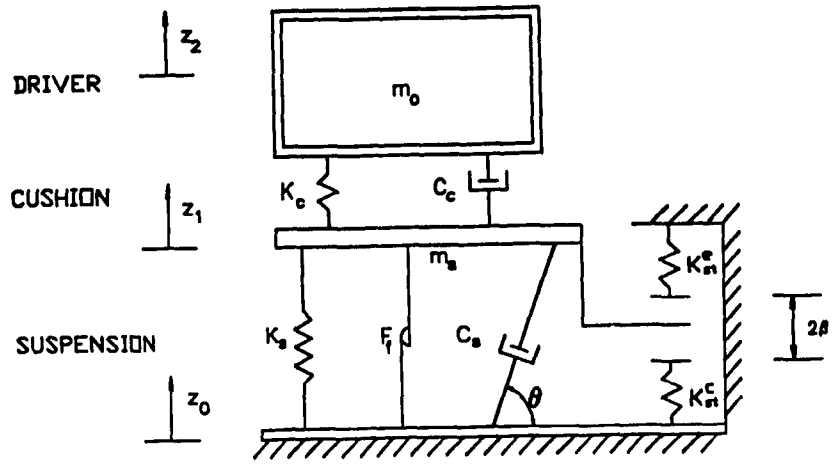

Figure 2.15. A Two Degrees-of-Freedom Model Representation of an Under-the-Seat, Seat-Suspension System.

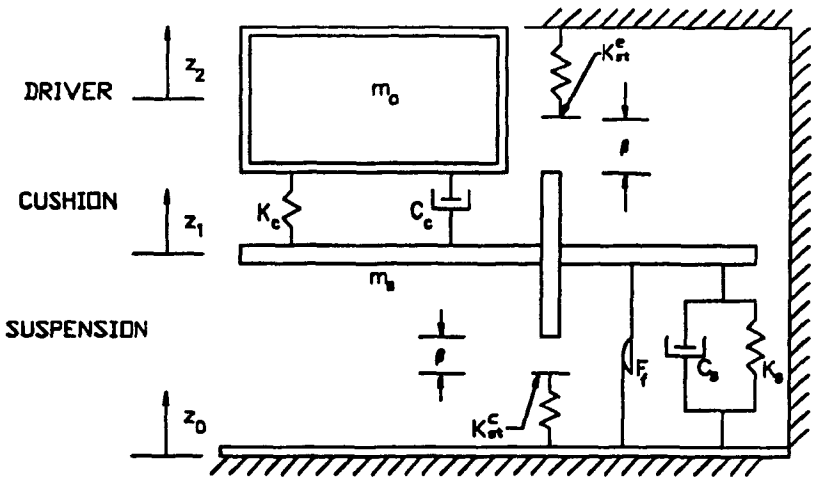

Figure 2.16. A Two Degrees-of-Freedom Model Representation of a Behind-the-Seat, Seat-Suspension System.

$$m_s \ddot{z}_1 + F_s(x_1, \beta) + F_K(x_1) + F_d(\dot{x}_1, \theta) + F_f(\dot{x}_1) - F_c(x_2, \dot{x}_2) = 0 \qquad (2.1)$$

$$m_o \ddot{z}_2 + F_c(x_2, \dot{x}_2) = 0 \qquad (2.2)$$

where m_o is the effective operator mass ($\frac{5}{7}$ of the total mass) and m_s is the sprung mass of the seat-suspension system. z_1 and z_2 are vertical displacements of the suspension and operator masses, respectively, and

$$x_1 = z_1 - z_0$$

$$x_2 = z_2 - z_1$$

$F_c(x_2, \dot{x}_2)$ is the total suspension force developed by the cushion. Assuming constant stiffness, and viscous damping coefficient, the dynamic force due to cushion can be expressed as:

$$F_c(x_2, \dot{x}_2) = K_c (z_2 - z_1) + C_c (\dot{z}_2 - \dot{z}_1) \qquad (2.3)$$

where K_c and C_c are linear stiffness and damping coefficients of the cushion. F_K, F_f, and F_s are the suspension forces due to suspension spring, linkage friction and bump stops, respectively, given by:

$$F_K(x_1) = K_s (z_1 - z_o) \qquad (2.4a)$$

$$F_f = F_{CD} \text{ sgn } (\dot{z}_1 - \dot{z}_o) \qquad (2.4b)$$

$$F_s = K_{st} S [z_1 - z_o - \beta \text{ sgn } (z_1 - z_o)], \qquad (2.4c)$$

where K_s is suspension spring rate, F_{CD} is magnitude of Coulomb friction and K_{st} is the spring rate of the bump stop, which assumes different values

corresponding to compression (K_{st}^{c}) and extension (K_{st}^{e}), as shown in Figure 2.17. K_{st} is given by:

$$K_{st} = \begin{cases} K_{st}^{e} & ; \quad x_1 > \beta \\ K_{st}^{c} & ; \quad x_1 < -\beta \end{cases}$$

S and sgn(...) are nonlinear functions, given by:

$$\text{sgn}(\ldots) = \begin{cases} +1 & ; \quad (\ldots) > 0 \\ -1 & ; \quad (\ldots) < 0 \end{cases}$$

and

$$S = \begin{cases} 1 & ; \quad |z_1 - z_o| > \beta \\ 0 & ; \quad |z_1 - z_o| < \beta \end{cases}$$

The shock absorber generate high damping force corresponding to low piston velocity due to bleed control, and the damping coefficient reduces considerably when piston velocity exceeds certain preset velocity due to blow-off valves. A typical force-velocity characteristics of a shock absorber is presented in Figure 2.18. The damping force, F_D, developed along the shock absorber axis is given by :

$$F_D = \begin{cases} C_{1A} V_r & ; \quad \text{if } |V_r| \le V_s \\ C_{1A} V_s \, \text{sgn}(V_r) + C_{1B}(V_r - V_s \, \text{sgn}(V_r)) & ; \quad \text{if } |V_r| > V_s \end{cases} \qquad (2.5)$$

where V_s is the preset or transition velocity, V_r is the velocity across the shock absorber, and C_{1A} and C_{1B} are damping coefficients corresponding to bleed and blow-off stages. The suspension force, due to shock absorber within the seat-suspension system, $F_d(\dot{x}_1, \theta)$, is derived as a function of its

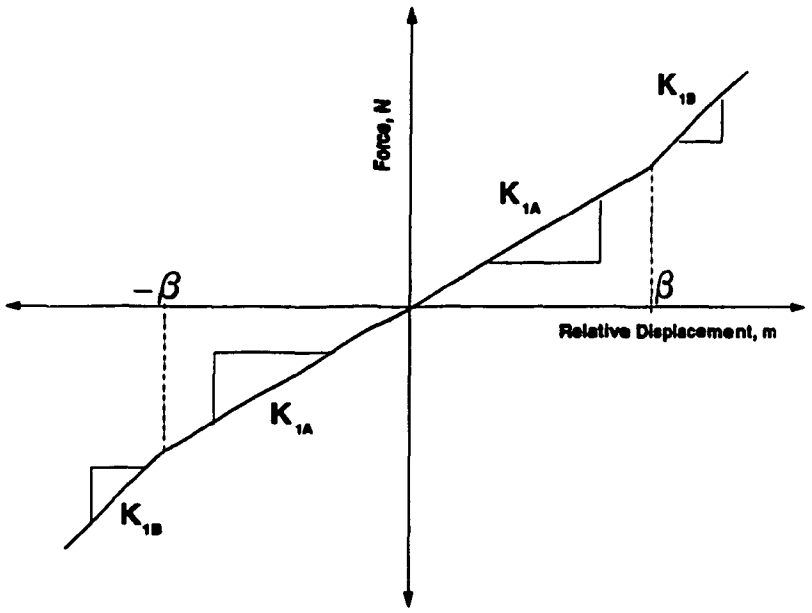

Figure 2.17. Force-Deflection Characteristics of the Suspension Spring.

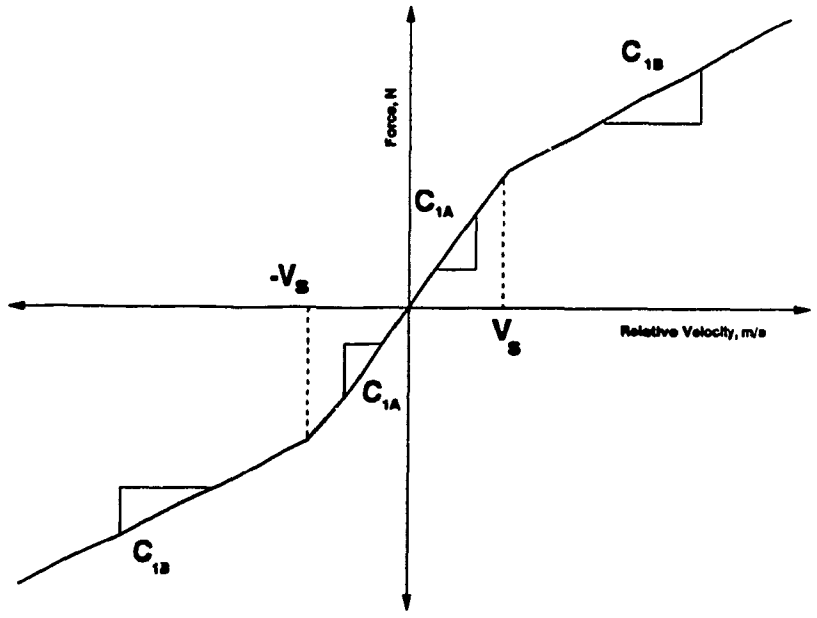

Figure 2.18. Force-Velocity Characteristics of the Shock Absorber.

inclination, θ. The relative velocity across the shock absorber is thus expressed as:

$$V_r = (\dot{z}_1 - \dot{z}_o) \sin \theta \tag{2.6}$$

The angle of inclination θ, in the case of the behind-the-seat seat-suspension system, remains constant. In case of under-the -seat seat-suspension system, the angle θ is dependant on the travel of the suspension mass relative to the floor. Using the representation shown in Figure 2.19, it is derived as:

$$\theta = \tan^{-1} \left(\frac{MH + (z_1 - z_o)}{HD} \right) \tag{2.7}$$

where, MH is the static mid-ride height and, HD is horizontal projection of shock absorber end points. The vertical suspension force due to shock absorber is then derived as :

$$F_d(\dot{x}_1, \theta) = F_D \sin \theta \tag{2.8}$$

Equations (2.1) through (2.8) describe the dynamics of a two degrees-of-freedom seat-suspension model incorporating geometric and suspension nonlinearities. Equation (2.1) describes the nonlinear dynamics of the suspension mass. It is applicable for all the seat-suspension ride models irrespective of the human body models.

2.5.2.2 Seat-Suspension Model with One Degree-of-Freedom Driver Model

A seat-suspension model lumped with a one-degree-of-freedom driver model is illustrated in Figure 2.20. The equations of motion for the three-degrees-of-freedom seat-suspension model presented can be derived in the following manner:

$$m_s \ddot{z}_1 + F_s(x_1, \beta) + F_K(x_1) + F_d(\dot{x}_1, \theta) + F_f(\dot{x}_1) - F_c(x_2, \dot{x}_2) = 0 \quad (2.9)$$

$$m_o \ddot{z}_2 + F_c(x_2, \dot{x}_2) - K_1 x_3 - C_1 \dot{x}_3 = 0 \quad (2.10)$$

$$m_1 \ddot{z}_3 + K_1 x_3 + C_1 \dot{x}_3 = 0 \quad (2.11)$$

In this case, m_o is the mass of human body simulator frame, representing the mass due to seated driver's buttocks and legs supported by the seat. $x_3 = (z_3 - z_2)$, represents the relative displacement of the combined pelvis, abdomen, chest and head mass (m_1) with respect to mass m_o. K_1 and C_1 are stiffness and damping coefficients of the human body model, derived from the impedance data.

2.5.2.3 Seat-Suspension Model with Two Degree-of-Freedom Driver Model

Suggs [54] proposed a two-degrees-of-freedom seated human body model, comprising of two masses suspended from a common frame representing the rigid spinal column. The lower mass (m_1) represents the pelvis and abdomen, while the upper mass (m_2) represent the mass due to head and chest.

A four-degrees-of-freedom seat-suspension model is thus derived by integrating two-degrees-of-freedom driver model to the basic seat-suspension

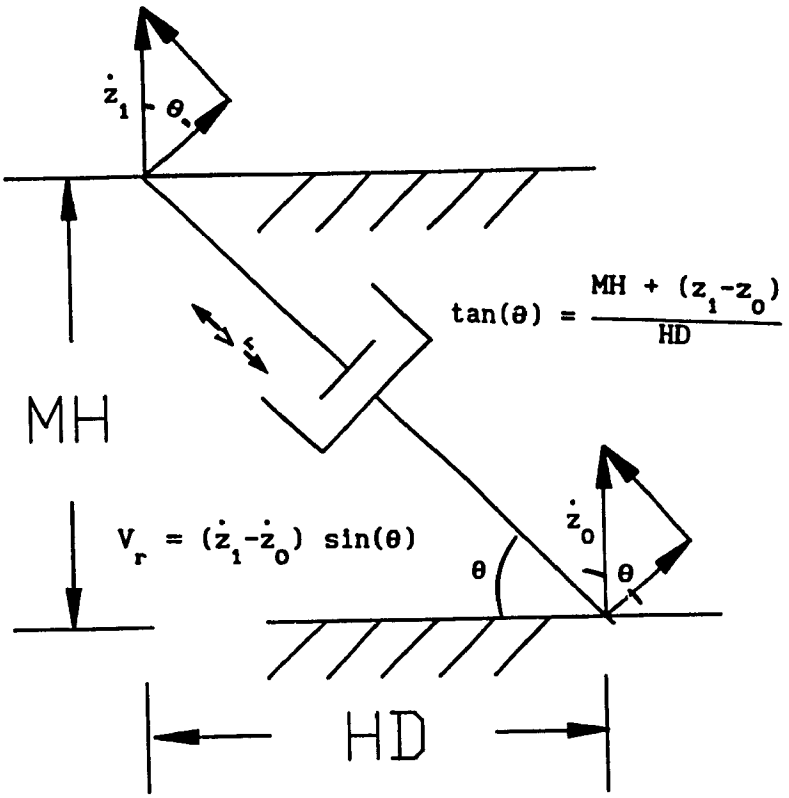

Figure 2.19. Free-body Diagram Representation of an Inclined Shock Absorber Damping Mechanism.

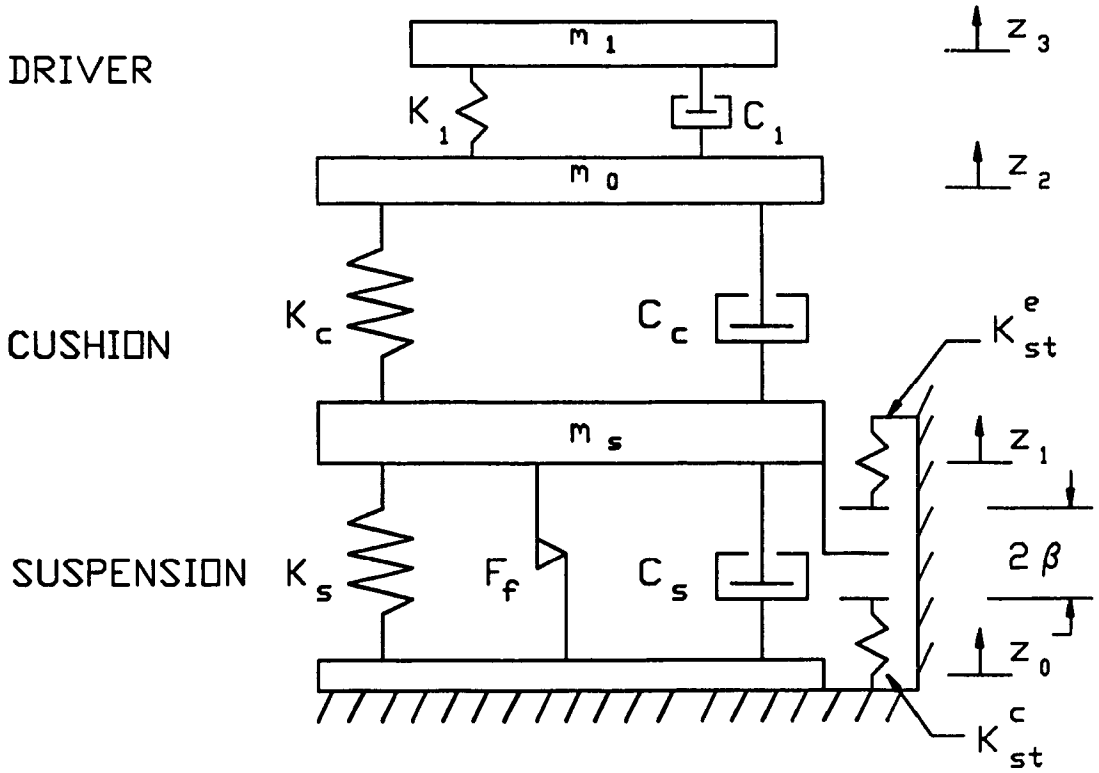

Figure 2.20. Seat-Suspension System Model Using a One Degree-of-Freedom Driver Model.

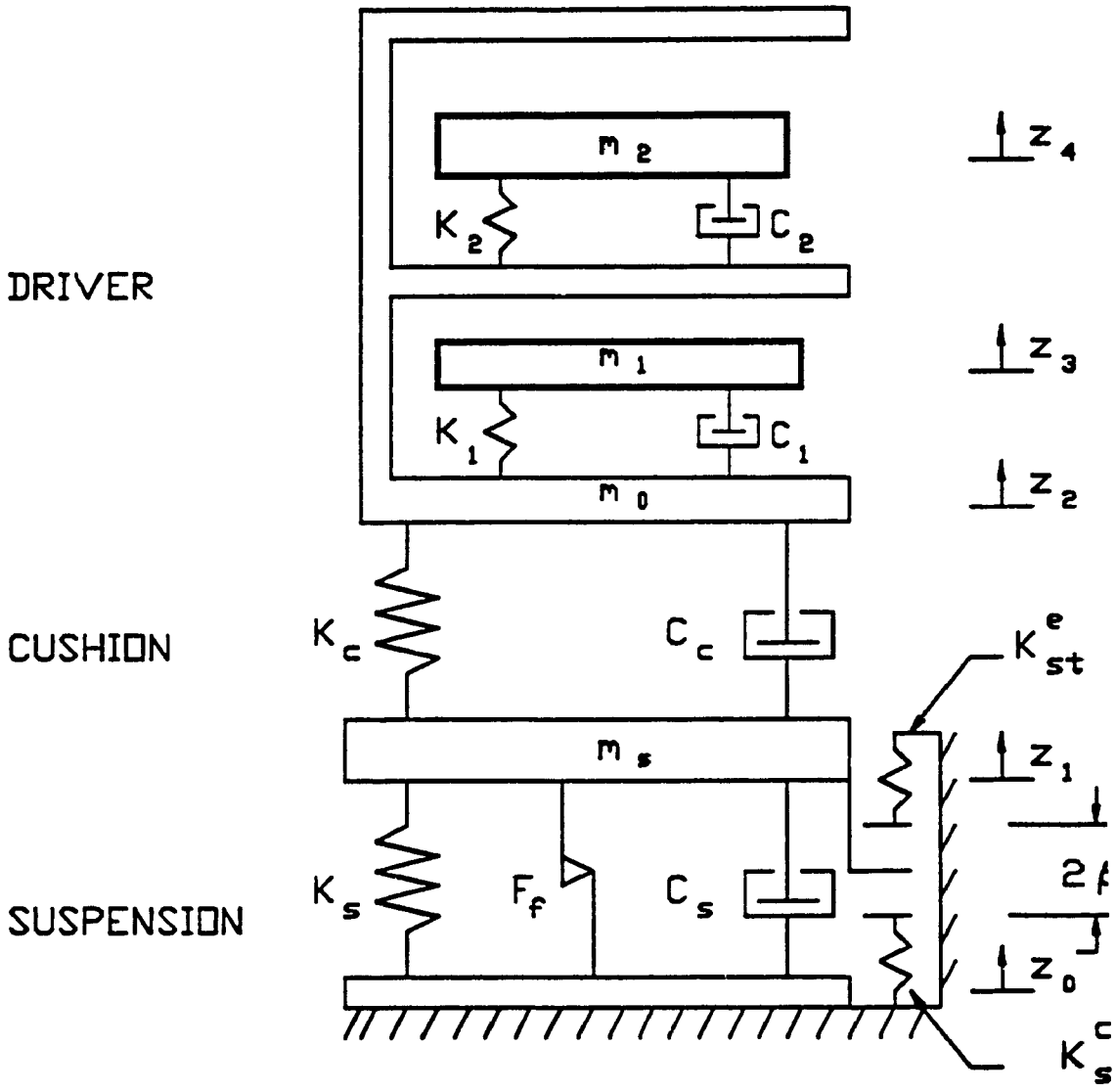

Figure 2.21. Seat-Suspension System Model Using a Two Degrees-of-Freedom Driver Model.

model, illustrated in Figure 2.21. The equations of motion for the four-degrees-of-freedom are derived as follows:

$$m_s \ddot{z}_1 + F_s(x_1, \beta) + F_K(x_1) + F_d(\dot{x}_1, \theta) + F_f(\dot{x}_1) - F_c(x_2, \dot{x}_2) = 0 \quad (2.12)$$

$$m_o \ddot{z}_2 + F_c(x_2, \dot{x}_2) - K_1 x_3 - C_1 \dot{x}_3 - K_2 x_4 - C_2 \dot{x}_4 = 0 \quad (2.13)$$

$$m_1 \ddot{z}_3 + K_1 x_3 + C_1 \dot{x}_3 = 0 \quad (2.14)$$

$$m_2 \ddot{z}_4 + K_2 x_4 + C_2 \dot{x}_4 = 0 \quad (2.15)$$

where, m_o is the mass of the frame, representing the mass due to seated driver's buttocks and legs. $x_3 = (z_3 - z_2)$ and $x_4 = (z_4 - z_2)$ represent the relative displacements of lower mass (m_1) and upper mass (m_2), respectively, with respect to the frame. The mass, spring and damping parameters of the driver models are presented in Table 2.3.

2.6 SUMMARY

In this chapter, current design considerations, and selection criteria for off-road vehicle seat-suspension systems are outlined. The desirable functions of seat-suspension components and their static and dynamic characteristics are described. The seat-suspension systems loaded with a rigid mass are characterized by a general two-degrees-of-freedom dynamic system, and analytically modeled incorporating nonlinearities due to linkage friction, shock absorber damping, bump stops and inclination of the shock absorber. The seated driver is characterized by one- and two-degrees-of-freedom dynamic models.

CHAPTER 3

IDENTIFICATION OF MODEL PARAMETERS AND INPUT EXCITATIONS

3.1 GENERAL

Performance analyses through computer simulation of an analytical model require: (i) identification of model parameters; and (ii) description of excitation forces. Dynamic analysis of seat-suspension models necessitates identification of human body and suspension model parameters, and description of vibration input data. The parameter values, which are not directly measurable, are determined by testing on the system itself. The parameters are derived from the measured input and output using the physical laws that describe the dynamic or static behavior of the components.

The vibration data characterizing the input excitation shall precisely represent the typical tire-terrain interactions and must be concise to minimize the degree of effort and computation costs. Since the ride vibration of wheeled off-road vehicles predominate around its resonant frequencies, the preliminary performance analyses may be carried out using harmonic excitations around these resonant frequencies. Wheeled off-road vehicles exhibit resonant behavior around 2.6 Hz and 3.3 Hz, depending upon the weight and size of the vehicle. The performance analyses of the seat-suspension system can thus be carried out using sinusoidal excitations in the frequency range 0.5-6.0 Hz.

The ride vibrations originating from tire-terrain interaction, however, are random in nature. Performance analyses of seat-suspension systems thus require a description of random excitations at the cab floor and response evaluations to such random vibrations. The random excitations, caused by randomly rough terrains, are often characterized in terms of their power

spectral densities (PSD). The response characteristics of seat-suspension models can be then evaluated using the random input excitation characterized by its PSD.

In this chapter, static and dynamic laboratory test procedures to identify model parameters are briefly described. Both static and dynamic characteristics of seat cushions, and suspension components are obtained in the laboratory, and the data are analyzed to estimate the model parameters. The PSD of input acceleration, proposed by ISO, is presented and discussed in view of the fatigue decreased proficiency limits.

3.2 IDENTIFICATION OF MODEL PARAMETERS

Development of an effective analytical system model necessitates a comprehensive knowledge of both static and dynamic characteristics of various subsystems. Seat-suspension models, presented in Section 2.5, require quantitative description of the properties of the cushion, spring, shock absorber, etc. These model parameters are derived from static and dynamic tests performed on the suspension components.

3.2.1 Static Characteristics of Seat-Suspension Systems

Selected seat-suspension systems were tested in the laboratory to identify the static characteristics of their cushions and suspensions. SAE recommended test procedures were used to measure the static characteristics of the seat components [55]. An MTS testing machine, consisting of a test bed supported on a hydraulic ram was used to generate the appropriate static loads. The test apparatus consisted of a 0.203 m (8 in) diameter flat indenter with a swivel joint, as shown in Figure 3.1. The swivel joint

accounts for the inclination of seat cushions and minimizes the magnitude of side forces acting on the hydraulic ram. The seat cushions were mounted on to the test bed as shown in Figure 3.2. The applied force and static deflection of the cushion were measured using a load cell and a linear variable differential transformer (LVDT) displacement sensor, respectively.

3.2.1.1 Static Characteristics of Seat Cushions

The seat cushion mounted on the MTS test bed was preflexed three times by slowly applying and reducing the force (up to 1334 N) at a rate of 102 mm/min. The test cushion was allowed to relax for a period of 15 minutes after preflexing. The static testing was initiated by applying a force of 220 N (50 lbf) and the corresponding cushion deflection is recorded after a relaxation duration of 1 min. The applied force is gradually increased by an increment of 220 N until the maximum force of approximately 1210 N is reached. The magnitude of maximum force reached was varying from one cushion to another depending upon the maximum cushion deflection that was possible in each type of cushion. The applied force was increased slowly to minimize the shock. The resulting deflection of the cushion was measured using an LVDT. The test process was repeated by gradually reducing the force in the same manner while permitting the cushion to relax for 1 min. after each decrement. The loading and unloading force-deflection curves, thus obtained were analyzed to estimate the static stiffness characteristics of the cushions, K_c:

$$K_c = \frac{\partial F}{\partial x} = \frac{\Delta F}{\Delta x} \tag{3.1}$$

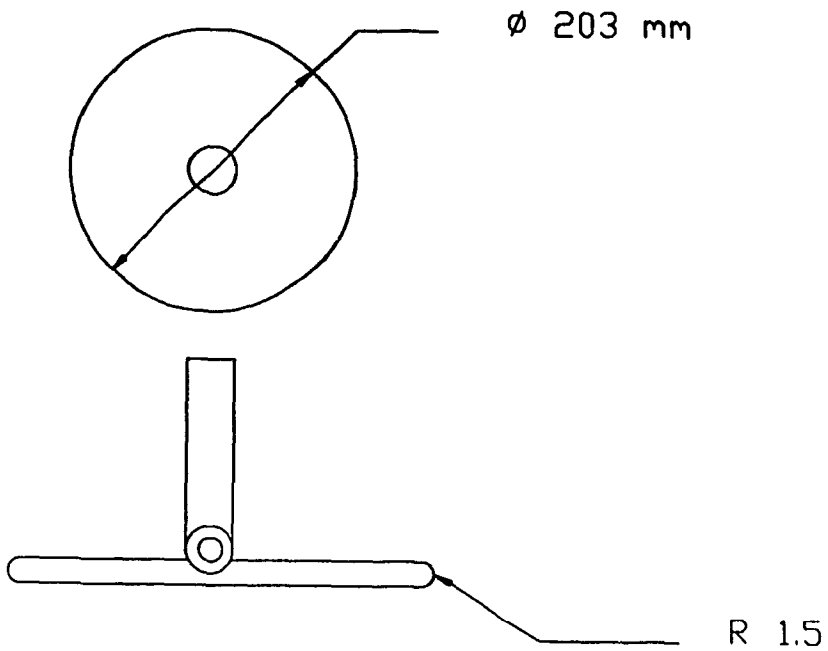

Figure 3.1. Flat Indenter Used for Static and Dynamic Testing of Seat Cushions.

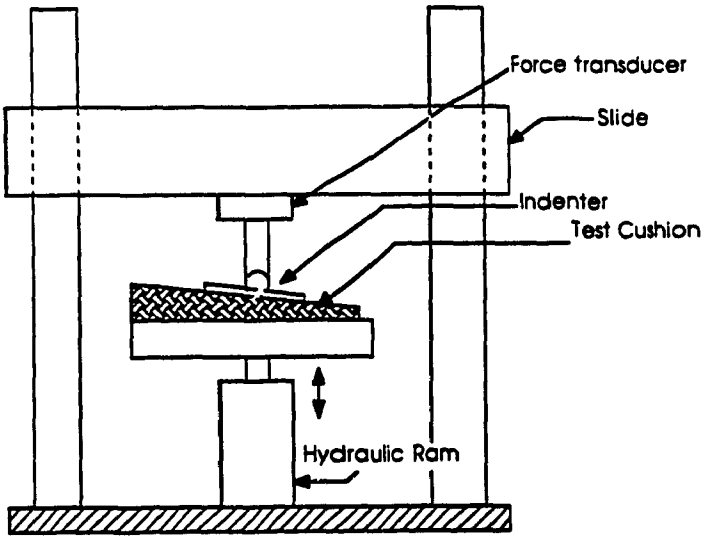

Figure 3.2. Test Apparatus for Static and Dynamic Testing of Seat cushions.

where Δx represents the change in displacement due to change in load ΔF, around an operating point.

Figures 3.3a to 3.3d present the static force-deflection characteristics of cushions employed in selected seats. The following are observed from these figures:

(i) The seat cushions exhibit considerable hysteresis, as indicated by the difference between the loading and unloading curves (Figures 3.3a to 3.3d).

(ii) The force-deflection curves of the seat cushions are highly nonlinear.

(iii) The static stiffness of the cushion, employed in GRAMMAR seat with out shock absorber, reveals an extremely high value at high preloads. This is partly attributed to bending of the seat-pan.

(iv) The cushion employed in SIFRA seat reveals high stiffness compared to those used in GRAMMAR and ISRI seats.

Assuming linear force-deflection of the seat cushions for small variations in load around a known preload, the static stiffness of seat cushions are computed corresponding to three selected values of preloads. The values of preloads were selected as 540 N (120 lbf), 706 N (158 lbf) and 960 N (215 lbf) to represent a range of driver weights supported by the cushion, which are classified as light, medium, and heavy. The static stiffness characteristics of the seat cushions are summarized in Table 3.1.

3.2.1.2 Static Characteristics of Seat Suspension

Static force-deflection characteristics of the selected seat-suspension systems were measured, using the flat force indenter on the MTS testing machine to determine the spring rate, hysteresis due to linkages, seat travel, and elastic properties of travel limit stops. The seat-suspension without the

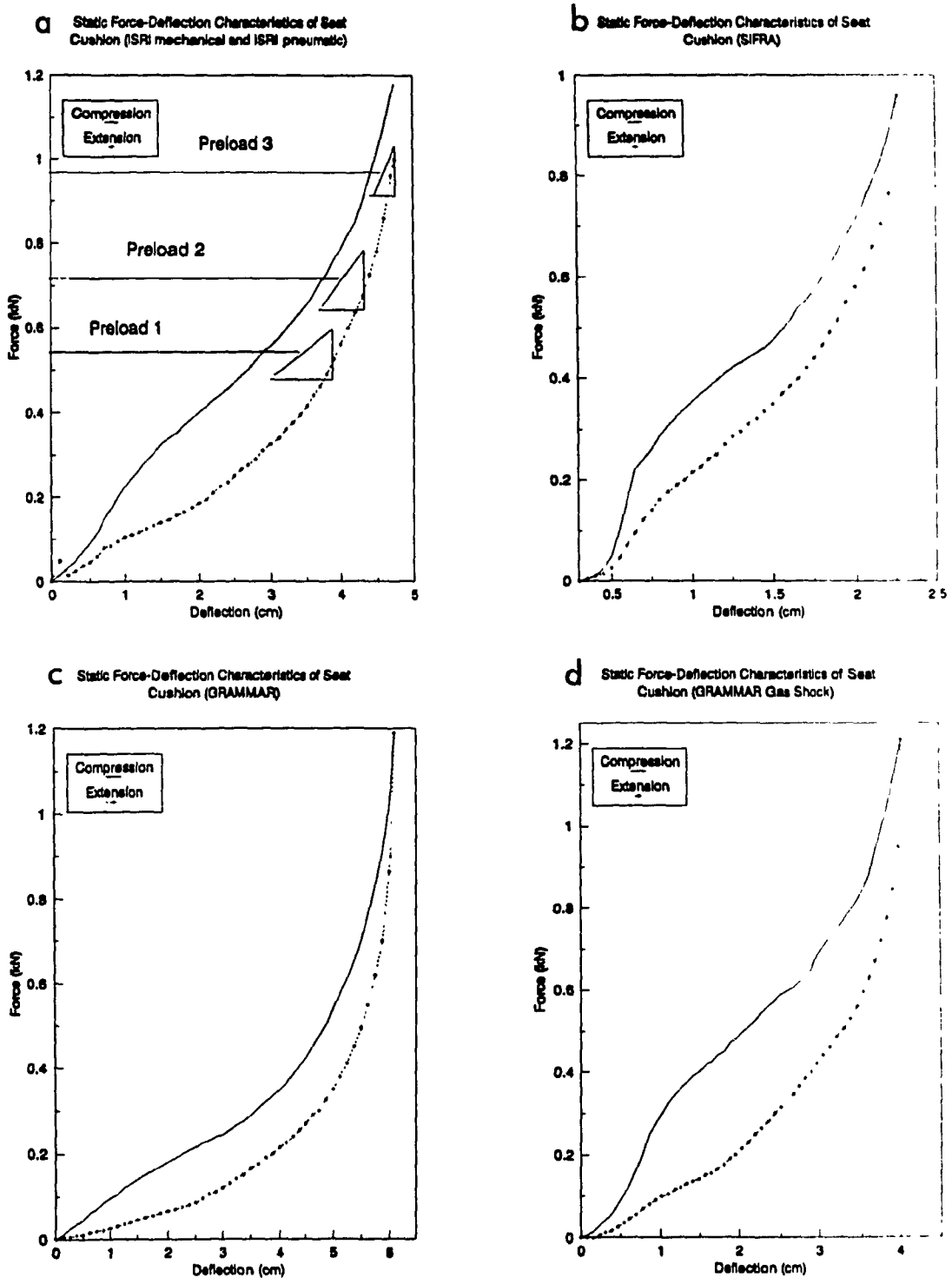

Figure 3.3. Static Force-Deflection Characteristics of Seat Cushions: (a) ISRI Mechanical and Pneumatic, (b) SIFRA, (c) GRAMMAR, and (d) GRAMMAR (Gas Shock).

cushion and the shock absorber was mounted on the test bed of the MTS testing machine. The flat indenter with the swivel joint was placed against the suspension. The seat-suspension was preloaded to a selected value (540 N) of the driver weight supported by the seat and the suspension was adjusted to achieve mid-ride position. The suspension was gradually loaded until the compression bump stop was encountered and the corresponding forces and deflections were recorded. The suspension load was gradually reduced until the extension bump stop was reached. Then it was gradually loaded again until the mid-ride height was reached. The force-deflection data corresponding to loading and unloading cycles were plotted to evaluate magnitude of static friction, and spring rates of the suspension and elastic bump stops. The test was repeated for 706 N and 960 N preloads to compute the suspension properties over a range of driver weights.

Figure 3.4 present the static force-deflection characteristics of the SIFRA seat suspension for 540 N preload. The spring rates in compression, K_s^c and extension, K_s^e were determined from the constant slope of the curve around the mid-ride position:

$$K_s^c = \frac{\Delta F}{\Delta x} \; ; \quad \text{Compression}$$

$$K_s^e = \frac{\Delta F}{\Delta x} \; ; \quad \text{Extension}$$

The force-displacement curves during loading and unloading revealed a steep slope at the extremities of the suspension travel, as shown in Figure 3.4. The slope of the curve around the extremities determines the spring rate of the bump stops in compression and rebound (extension). The magnitude of

static friction force, F_{cs} in the linkages was computed as:

$$F_{cs} = 0.5 \text{ (static force at mid-ride during compression} - \text{static force at mid-ride during extension)} \quad (3.2)$$

The static suspension stiffness, friction force, suspension travel and elastic properties of bump stops of various seat-suspension systems are summarized in Tables 3.2 and 3.3. The static-force deflection characteristics of various seat-suspension systems are discussed in the following sections.

Seat-Suspension Travel:

Seat-suspension systems are often designed with low natural frequency (around 1 Hz), in order to effectively attenuate vehicle vibrations around 0.5-5.0 Hz. Such low natural frequency seat-suspension systems yield excessive dynamic relative motion of the driver with respect to the floor and the controls. Elastic or rigid bump stops used to limit the dynamic travel cause high accelerations at the driver seat. Thus, the ride dynamics of a seat-suspension is strongly dependent upon the elastic properties of the bump stops and the total suspension travel. A large seat travel leads to driver discomfort due to excessive relative movement. However, too small a seat travel will result high amplitude vibrations at the driver's location due to frequent impact with bump stops. The ISRI seats exhibited a suspension travel of 75 mm while the SIFRA seat provided a suspension travel of 100 mm. The suspension travel of GRAMMAR seats ranged from 80 mm to 100 mm.

Stiffness of Bump Stops:

The primary function of the bump stops is to limit the magnitude of

Table 3.1

Static Stiffness Characteristic of the Seat Cushions.

Specification of the seat cushion	Preload		
	540 N	706 N	960 N
	Static Stiffnesss (N/cm)		
ISRI (Pneumatic)	221	358	680
ISRI (Mechanical)	221	358	680
SIFRA	477	823	--†
GRAMMAR	338	590	1,222
GRAMMAR (Gas Shock)	238	390	865

† SIFRA cushion failed when tested under the 960 N preload

Table 3.2

Suspension Travel and Static Stiffness of Bump Stops.

Specification	Preload (N)	Stroke (mm)	Static Stiffness of Limit Stops	
			Compression (N/cm)	Extension (N/cm)
ISRI	540	75	250	660
	706		260	660
	960		305	660
ISRI (Mechanical)	534	75	280	1,400
	714		325	2,100
	960		470	2,880
SIFRA	540	100	1,200	620
	706		1,200	750
	960		1,260	1,080
GRAMMAR Position 1	706	80	1,640	593
	906		1,640	713
Position 2	577	90	---†	877
	706			1,067
	960			1,318
Position 3	775	92.5	1,000	800
	960		1,000	893
GRAMMAR (Gas Shock)				
	785	80	440	720
Position 1	960		500	825
	1,170		490	880
Position 2	960	97.5	---†	840
	1,170			847
Position 3	1,000	100	---†	1,060
	1,170			1,310

† Extremely high stiffness due to cam interference

relative motion of the driver with respect to the controls and the cab floor. The bump stops may be either rigid or elastic. Rigid bump stops yield high acceleration at the driver's seat, when the seat motion exceeds the permissible travel, while the elastic bump stops limit the seat travel in a relatively smooth manner.

ISRI pneumatic and mechanical seat-suspension systems consist of elastic bump stops in both compression and extension. Limiting of compression stroke is achieved by soft rubber bumps mounted on the suspension frame (Figures 2.8 and 2.9), and the extension stroke is limited by the stops mounted within the roller guides. The ISRI pneumatic seat-suspension comprises of soft rubber stops in the guides, while the mechanical seat-suspension utilizes stiff bump stops. The ISRI-mechanical seat thus revealed a high spring rate for the bump stop in extension as indicated in Table 3.2.

SIFRA seat consists of elastic bump stops in compression as well as rebound motion of the seat. The compression bump stops consist of stiff rubber bumps at its base, as shown in Figure 2.10, and revealed high values of static stiffness (1200 N/cm). The extension bump stops, integrated within the slider mechanism, revealed relatively lower values of static stiffness. Force-deflection behavior of bump stops in compression and rebound for different preloads is summarized in Table 3.2.

The static stiffness characteristics of the GRAMMAR seats were quite complex due to interference of the cam in extreme positions. The GRAMMAR seat (without a shock absorber) revealed relatively stiffer bump stops in compression than in extension, as indicated in Table 3.2. However, high values of bump stop stiffness were observed with the cam position 2, independent of the preload. Cam slippage was observed during the test and it

is believed that high values of the limiting stiffness is attributed to the interference of the cam, with the suspension system. The GRAMMAR seat, equipped with a gas shock, reveals elastic bump stops in compression as well as extension. The interference from the cam caused extremely rigid stop in compression, under high preloads.

Static Friction:

The seat-suspension linkages invariably exhibit dry or Coulomb friction due to rollers, pin-joints and mechanical springs. The magnitude of static friction is directly related to the preload and properties of the sliding surfaces. Coulomb friction within the suspension system provides the necessary damping to suppress the resonance peaks. However, too large a value of Coulomb friction deteriorates the suspension performance in the isolation region. Furthermore, high friction tends to limit the effective seat travel due to its lock-up behavior.

ISRI-pneumatic seat-suspension revealed low magnitude of friction force (Table 3.3) due to almost frictionless air spring. The magnitude of friction force increased with the preload and the coefficient of friction (ratio of friction force to the preload) was obtained to be approximately 0.05. ISRI-mechanical seat-suspension revealed slightly larger friction force and an average value of the coefficient of friction was obtained to be 0.09. The coefficient of friction of the SIFRA seat was observed to be around 0.12, while the coefficient of friction of the GRAMMAR (without a shock absorber) seat was observed to range from 0.05 to 0.07. The magnitude of static friction force of the GRAMMAR seat with a gas shock absorber was considerably

larger than that of the seat without shock absorber and the coefficient of friction was observed to be around 0.09-0.10.

Suspension Spring Rate:

Effective attenuation of low frequency off-road vehicle ride vibrations transmitted to the cab floor is achieved via seat-suspension systems with soft springs. Extremely soft springs lead to excessive static and dynamic relative movement of the driver and thus cause discomfort and poor performance rate of the driver. However, a stiff seat-suspension cannot isolate the driver from low frequency vehicle vibration. The spring rate of a seat-suspension system is often selected to achieve a compromise between the vibration attenuation and relative displacement characteristics of the seat. The ISRI-pneumatic seat revealed a constant spring rate over the entire seat travel as shown in Figure 3.5. The spring rate of the air-suspension was quite low and increased with an increase in the charge pressure. An air spring charged with 80 psi air pressure (960 N preload) revealed a spring rate of 20 N/cm, which is quite soft for off-road vehicle applications.

The ISRI-mechanical seat revealed considerably high spring rate when compared to that of the pneumatic suspension, as shown in Figure 3.6 and Table 3.3. The spring rate, however, increased slightly with increase in preload. The spring rate of SIFRA seat-suspension, illustrated in Figure 3.4, is quite similar to that of the ISRI-mechanical seat-suspension.

The spring rate of GRAMMAR seats is strongly related to the cam-position, height adjustment and the preload. The lowest cam position (1) revealed a relatively soft spring and the spring rate decreased when the preload was

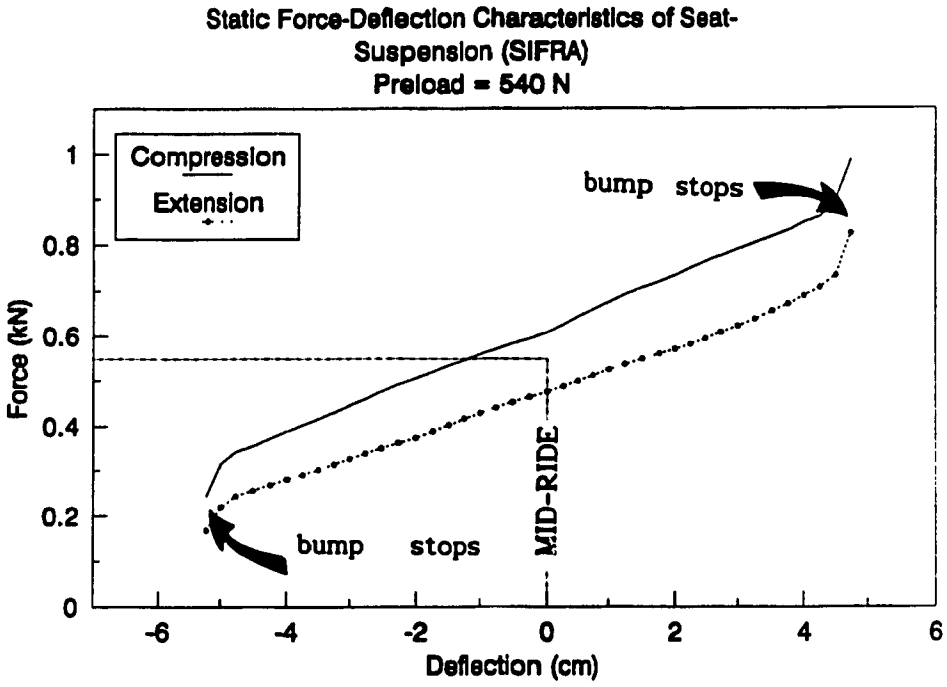

Figure 3.4. Static Force-Deflection characteristics of Suspension Spring (SIFRA).

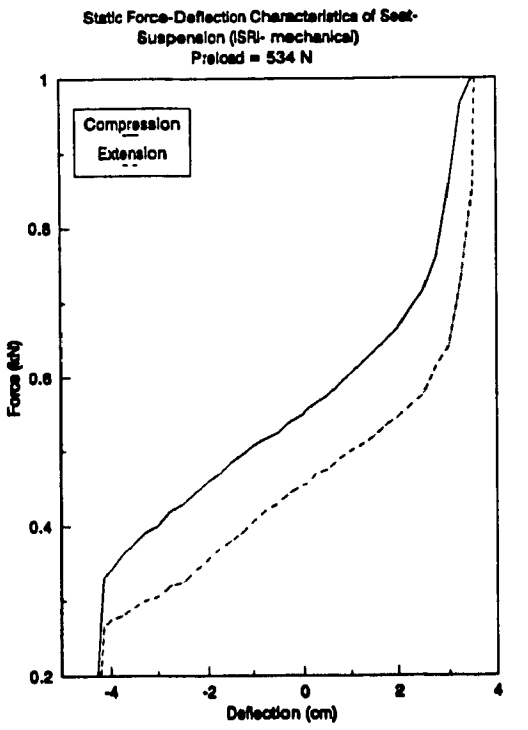

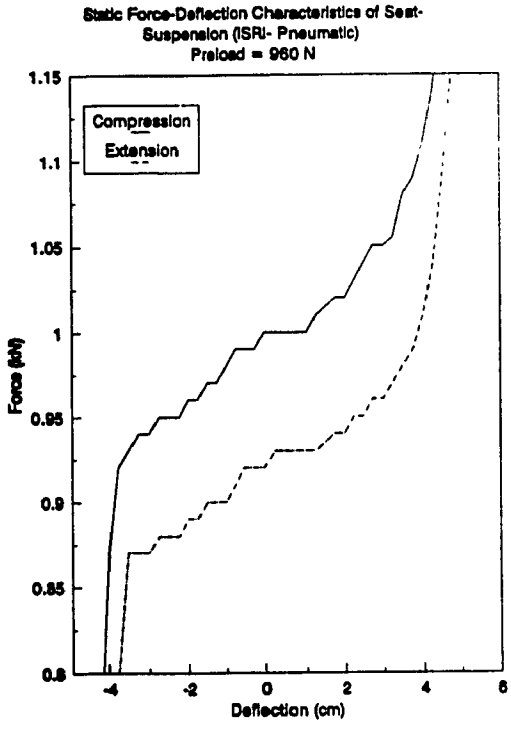

Figure 3.5. (right) Static Force-Deflection characteristics of Suspension Spring (ISRI Pneumatic).

Figure 3.6 (left) Static Force-Deflection characteristics of Suspension Spring (ISRI Mechanical).

increased. The decrease in spring rate was attributed to the slippage of the cam under these test and load conditions. The suspension spring rate corresponding the cam position 2 was relatively high and quite similar to those of the SIFRA and ISRI mechanical seat-suspension systems. However, the effective suspension spring rate in compression increased considerably corresponding to the highest cam position 3. This sharp increase in the spring rate was perhaps attributed to the interference caused by the cam.

3.2.2 Dynamic Characteristics of Seat Cushions

The damping properties of seat cushions were evaluated via dynamic testing of cushions. The seat cushions were tested for sinusoidal displacement excitations in the frequency range 1-8 Hz with peak displacement amplitudes of 0.5 cm and 1 cm. Sample force-displacement characteristics are plotted in the form of Lissajous diagrams in Figures 3.7 through 3.10. The damping associated with a cushion was estimated from the energy dissipated per cycle of vibration by the cushion. The energy dissipated per cycle is given by:

$$\Delta E = \oint F_{DC}\, dx \tag{3.3}$$

where ΔE is the energy lost per cycle and F_{DC} is the dissipative force. Cushion damping can be conveniently approximated by an equivalent damping coefficient by equating the energy dissipated by the cushion to that of a viscous damper. The energy dissipated per cycle by a viscous damper is given by:

$$\Delta E = \pi\, C_c\, \omega\, X^2 \tag{3.4}$$

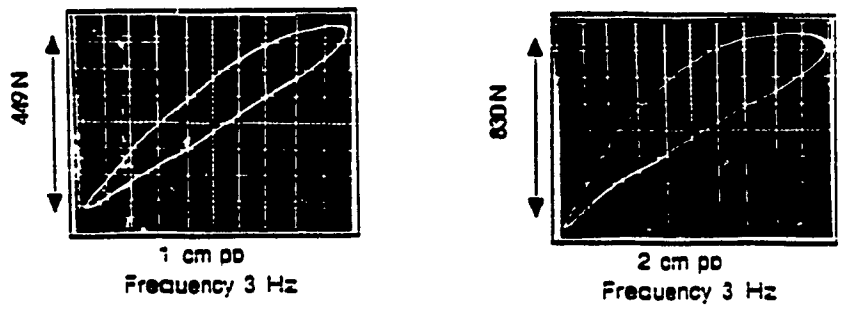

Figure 3.7. Dynamic Force-Displacement Characteristics of Seat Cushion (ISRI Mechanical and Pneumatic).

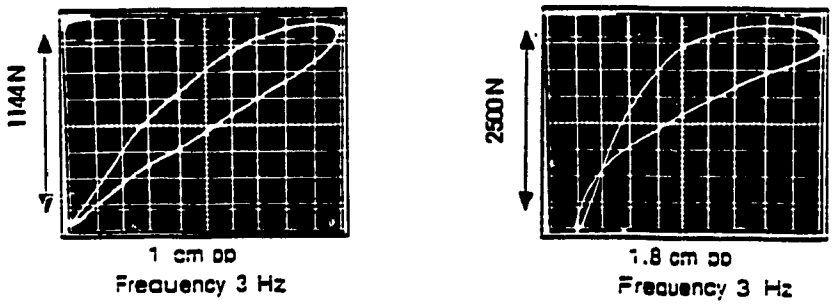

Figure 3.8. Dynamic Force-Displacement Characteristics of Seat Cushion (SIFRA).

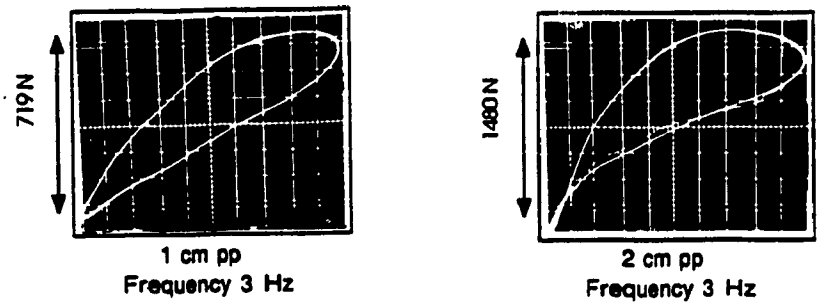

Figure 3.9. Dynamic Force-Displacement Characteristics of Seat Cushion (GRAMMAR).

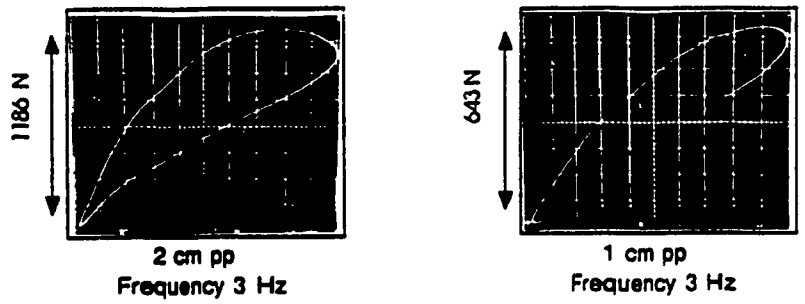

Figure 3.10. Dynamic Force-Displacement Characteristics of Seat Cushion (GRAMMAR-Gas Shock).

where C_c is the equivalent viscous damping coefficient, ω is the circular frequency in rad/s and X is the peak displacement amplitude. The equivalent damping coefficient due to cushion was then obtained by equating Equations (3.3) and (3.4):

$$C_c = \frac{\Delta E}{\pi \omega X^2} \tag{3.5}$$

The seat cushions exhibit dissipative properties due to two phenomena: (i) hysteresis of the foam, and (ii) air flow to and from the pneumatic filled foam. Stiff cushions provide large hysteretic damping, while the soft cushions provide higher damping due to air flow. The equivalent damping coefficients of the seat cushions as a function of velocity and amplitude are presented in Figures 3.11a through 3.11d. The seat cushions revealed high damping at low frequencies and the damping coefficients decreased rapidly with increase in excitation frequency. The cushions, employed in SIFRA exhibit high damping when compared to the damping properties of the ISRI and GRAMMAR seat cushions.

3.2.3 Dynamic Characteristics of Shock Absorbers

The force-velocity characteristics of the shock absorbers are derived from the data, supplied by the manufacturer. Assuming symmetric characteristics, the shock absorber parameters are deduced as: C_{1A}= 710 N.s/m, C_{1B}= 592 N.s/m, and V_s= 0.032 m/s.

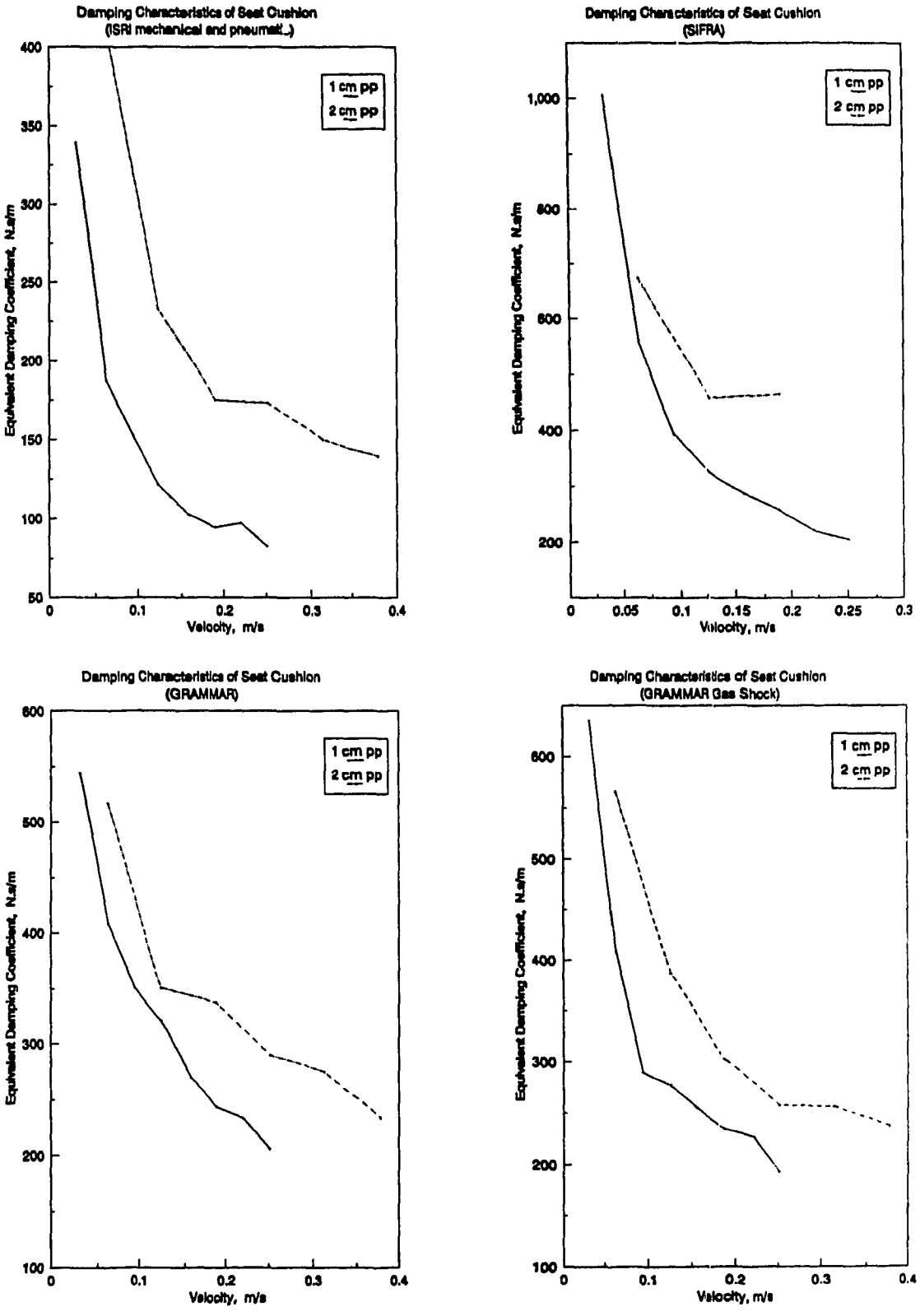

Figure 3.11. Equivalent Damping Coefficients of Seat cushions: (a) ISRI Mechanical and Pneumatic, (b) SIFRA, (c) GRAMMAR, and (d) GRAMMAR (Gas Shock).

3.3 INPUT EXCITATIONS

The ride vibrations encountered at the cab-floor arise from many sources, which can be classified in two broad classes: (i) terrain roughness; and (ii) on-board sources. The on-board sources include the structure and rotating components, such as tire/wheel assemblies, drive line, engine, and the like. The vibration originating from on-board sources often predominates around higher frequencies, while the ride vibration induced by terrain roughness predominates around the low frequencies to which human body is most fatigue sensitive. Furthermore, the amplitude of terrain induced vibration is considerably larger than that induced by the on-board sources. The terrain induced vibrations, encountered at the cab floor, thus need to be quantified in order to evaluate the performance characteristics of the seat-suspension systems.

3.3.1 Deterministic Excitations

Vertical vibrations, measured on the cab floor, of wheeled agricultural tractors and forestry vehicles reveal that these vibrations predominate in a narrow frequency band centered around the resonant frequency of the vehicle in the bounce mode. Wheeled off-road vehicles, suspended on large and soft tires, exhibit resonant behavior in 2.5-3.5 Hz frequency range. Vibration attenuation performance characteristics of seat-suspension systems may thus be evaluated using sinusoidal excitations in this frequency range. Since the seat-suspension systems invariably exhibit resonant behavior in the frequency range 1.0-1.5 Hz, the performance can thus be carried out for sinusoidal excitations in the total frequency range 1.0-3.5 Hz. However, in order to establish the fundamental behavior of nonlinear seat-suspension models,

response evaluations are carried out in the frequency interval 0.6-8.0 Hz. Response evaluation, using sinusoidal excitations, is specifically useful when model validations are carried out via laboratory tests.

3.3.2 Random Excitations

Random vibrations more closely represent the true vibration environment in which the seat-suspension system must operate. Ride vibration data of various off-road vehicles have been reported in the literature [47,50]. The random data gathered during field measurements have been characterized by either acceleration PSD or rms acceleration. Figure 2.7 presents the vertical ride vibrations, measured at the cab floor of a Class II agricultural tractor and a forestry vehicle, in terms of root mean squared acceleration [50]. The measured acceleration levels are assessed in view of the ISO specified fatigue decreased proficiency limits. The rms acceleration levels of the forestry vehicle predominate in the 2.5 Hz frequency band and exceed the 1 hour ISO FDP limit, as shown in Figure 2.7.

The consistency of the measured vibration data has lead to a rather standardized terrain description for performance analyses of vertical seat-suspension systems. The ISO has proposed approximate expressions describing vertical acceleration PSD [47], which has been widely accepted for testing of vertical seat-suspension systems [36]. The off-road vehicles are grouped into two classes based on the vehicle weight, tire pressure and wheel base, namely Class I and Class II. Table 3.4 presents the technical data for the Class I and Class II agricultural tractors.

The PSD of the vertical acceleration $S_1(f)$ at the seat attachment point is described as:

Table 3.3

Static Force - Deflection Characteristics of Seat-Suspension Systems.

Specification	Preload (N)	Magnitude of Static Friction (N)	$\mu_{fr}^{\ddagger}$	Suspension Spring Rate	
				Compression (N/cm)	Extension (N/cm)
ISRI (Pneumatic)	540	30	.06	16	16
	706	35	.05	18	18
	960	40	.04	20	20
ISRI (Mechanical)	534	47.5	.09	49	49
	714	62.5	.09	49	49
	960	80	.08	55	55
SIFRA	540	65	.12	53.3	53.3
	706	87.5	.12	55	55
	960	107.5	.11	58	58
GRAMMAR					
Position 1	706	45	.06	38	38
	906	70	.07	28	28
Position 2	577	40	.07	50	50
	706	45	.06	45	45
	960	55	.06	40	40
Position 3	775	40	.05	130	50
	960	50	.05	130	42
GRAMMAR (Gas Shock)					
	785	70	.09	74	54
Position 1	960	90	.09	74	55
	1,170	100	.09	82	50
Position 2	960	95	.10	---†	63
	1,170	105	.09		58
Position 3	1,000	100	.10	---†	70
	1,170	115	.10		69

‡ Coefficient of friction † Progressively hardening spring

Table 3.4

Technical Data of Reference Tractors [47].

TECHNICAL DATA	CLASS 1	CLASS 2
Unladen mass, kg.	3040	4750
Front axle load, kg.	1300	1830
Rear axle load, kg.	1740	2920
Front tires	7.5 - 18	12.4 / 11 - 28
Rear tires	16.9 / 14 - 34	16.9 / 14 - 38
Front tire pressure, kPa.	200	150
Rear tire pressure, kPa.	110	130
Wheelbase, m	2.125	2.59

Table 3.5

Constant Values Defining the Approximate PSD's.

CONSTANTS	CLASS I	CLASS II
Φ_{max} , $(m/s^2)^2/Hz$	6.	5.5
f_m , Hz	3.25	2.65
B , Hz	0.33	0.3

$$S_1(f) = \Phi_{max} \exp\left[- \frac{(f - f_m)^2}{2B^2} \right] \qquad (3.6)$$

where Φ_{max}, f_m and B are constants, and f is the excitation frequency. Table 3.5 presents the values of constants for the two classes of vehicles.

Figures 3.12a and 3.12b represent the acceleration power spectral densities at the seat attachment point, derived from Equation (3.6) for Class I and Class II vehicles, respectively. The vertical acceleration PSD at the seat attachment point is compared to the fatigue decreased proficiency limits for 1.0 to 8.0 hours of exposure. The figures clearly illustrate that the vibration levels of Class I and Class II vehicles predominate around 3.25 Hz and 2.65 Hz, respectively, and the acceleration levels exceed the fatigue decreased proficiency limit for 1 hour exposure.

3.4 SUMMARY

In this chapter, laboratory methods of identifying seat-suspension model parameters are discussed. Parameter data evaluated from laboratory investigations are presented, and deterministic and random excitations at the seat-attachment point are described.

(a) CLASS I

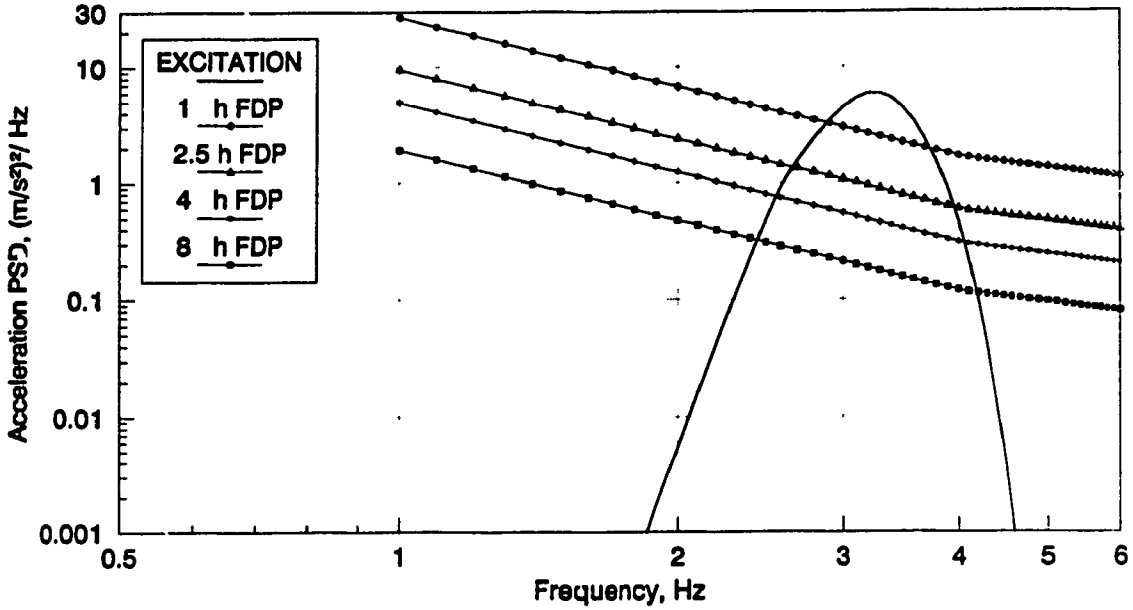

(b) CLASS II

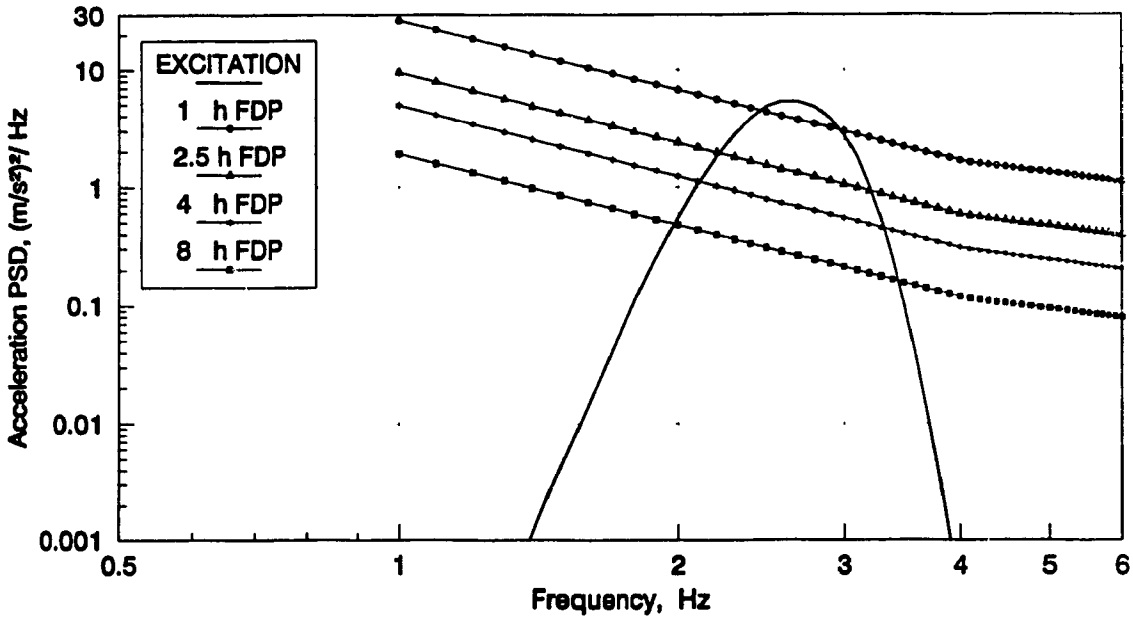

Figure 3.12. The Vibration Spectra for Testing Wheeled Off-Road Vehicle Seats Recommended by SAE [47]: (a) Class I, (b) Class II.

CHAPTER 4

LABORATORY TESTING AND VERIFICATION OF THE ANALYTICAL MODELS

4.1 GENERAL

Analytical models, in general are formulated with a number of simplifying assumptions. The validation of analytical models is thus vital to gain confidence in analytical investigations and to develop reliable computer-assisted design tools. The analytical model of the seat-suspension system, when validated, can be further utilized to derive an optimal design in a highly efficient manner. The analytical models may be verified using either laboratory or field experimentation of the physical system. Since the field tests require a human driver, the results are influenced by the human body dynamics, driver tasks, cab design, etc. The task of identifying the contributions due to the human body dynamics and driver's interactions is often quite complex. Alternatively, laboratory test methods may be conveniently used to determine the vibration attenuation performance of the suspension system using a passive mass.

The nonlinear differential equations of motion of the seat-suspension model, incorporating rigid mass representation of the driver can be solved using direct integration routines to determine the analytical vibration transmissibility of the suspension system. The analytical vibration transmissibility is then compared to the laboratory data to qualify the analytical model.

In this chapter, the test apparatus and the test methodology is briefly described. Vibration transmissibility characteristics of the selected seat-suspension systems are derived from the laboratory tests using sinusoidal excitations. The nonlinear differential equations of motion for the

seat-suspension models are solved using numerical integration algorithm, and the response characteristics are compared to those attained from the laboratory tests.

4.2 TEST METHODOLOGY

The test apparatus consists of a servo-hydraulic vibration exciter, capable of generating deterministic and random excitations along the vertical axis. The servo-hydraulic vibration exciter can provide excitations up to 7.5 cm (3 in) peak in the frequency range 0-300 Hz. A seat vibration test stand, consisting of a seat platform, is fabricated and is supported on the linear bearings and the servo-hydraulic exciter, as shown in Figure 4.1. The test stand is designed such that the structural resonances do not interfere with the dynamics of the seat. A resonance search test is conducted to identify the resonant frequencies of the test stand in the frequency range 1–200 Hz. First resonant frequency of the test stand was observed around 40 Hz. Since the suspension seats are tested in the frequency range 0.5-8 Hz, the structural resonance is thus not expected to affect the vibration characteristics of the seat suspension system.

The suspension seat is mounted on the platform as shown in Figure 4.1. The seat is loaded with two sandbags, where the lower sandbag weighs 35 kg (77 lbf) and the upper sandbag, rested against the back rest, weighs 28.6 kg (63 lbf). The seat suspension test apparatus is instrumented with three single axis B & K delta shear accelerometers and one tri-axial seat accelerometer. Three single axis accelerometers are mounted at the test frame, seat platform and the seat pan. The accelerometer mounted at the frame provides the necessary feedback to measure feedback acceleration ($\ddot{z}_f$) for the servo control, input acceleration to the seat suspension ($\ddot{z}_o$) and the response

acceleration of the seat suspension, ($\ddot{z}_1$), respectively, as shown in Figure 4.2. The tri-axial seat accelerometer is mounted between the sandbag and the cushion and it measures the vertical (a_z), longitudinal (a_x), and lateral (a_y) accelerations of the transmitted vibrations. The measured signals are conditioned, filtered and recorded for further analysis.

Each seat-suspension system is tested for sinusoidal excitations in the frequency range 0.5-8.0 Hz. The vertical vibration transmissibility of the suspension and the seat are evaluated as the ratio of amplitude of response acceleration ($\ddot{z}_1$ and $\ddot{z}_2$, respectively) to the amplitude of input acceleration ($\ddot{z}_0$) at each excitation frequency. The tests are performed for sinusoidal displacement excitations of amplitudes 1.25 cm, 2.5 cm, and 3.75 cm pp.

The influence of suspension stiffness on the vibration transmission performance is investigated by varying the ride height. The vibration transmissibility of suspension seats is measured for nominal stiffness values (mid-ride) and softer stiffness values (reduced ride height). Apart from the objective measurement of vibrations, the following observations are made during the tests:

- Resonant frequency and resonance behavior.
- Suspension lock-up due to Coulomb friction.
- Break-away frequency to determine the magnitude of dynamic friction.
- Seat rotation.
- Interference with the motion limiting stops.
- Separation of sandbags from the seat.
- Sliding of sandbags due to excessive rotational or horizontal motion.

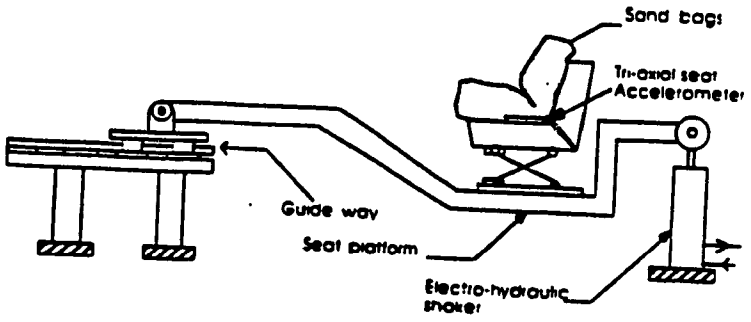

Figure 4.1. Schematic of the Seat Vibration Test Stand.

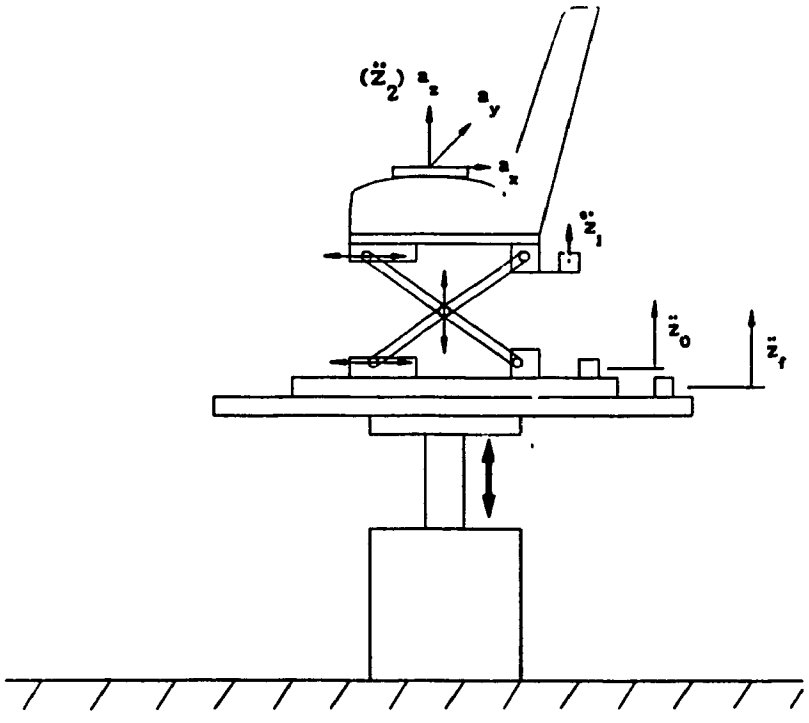

Figure 4.2. Location of Accelerometers on the Seat Vibration Test Stand.

4.3 VIBRATION ATTENUATION PERFORMANCE OF SEAT-SUSPENSION SYSTEMS

Vibration transmissibility of a seat-suspension describes the extent to which vehicle ride vibration is modified or attenuated by the suspension at various frequencies. Laboratory tests are thus performed for constant amplitude sinusoidal displacement excitation to determine the vibration transmissibility of various seats. Owing to the small amplitude of horizontal acceleration measured at the seat, the discussion of horizontal acceleration transmissibility is omitted.

Figures 4.3a and 4.3b present the acceleration transmissibility of ISRI-pneumatic seat-suspension for constant displacement excitations of 1.25 cm, 2.5 cm and 3.75 cm pp amplitudes. The air-spring is charged at 80 psi to attain mid-ride height. The seat suspension system exhibits resonant behavior at 1.2 Hz when subjected to 1.25 cm pp harmonic excitations, however, the resonant frequency reduces to 1 Hz when the excitation amplitude is increased. The resonant transmissibility ratio is approximately 1.27 for low amplitude (1.25 cm) excitation and it increases considerably as the excitation amplitude is increased. This is attributed to the nonlinear nature of the restoring and dissipative forces of the suspension systems. Due to the soft nature of the ISRI-pneumatic seat the suspension exhibits excessive dynamic relative displacement around the resonant frequency when subjected to high amplitude excitations. The excessive relative displacement of the suspension system is also observed around 3.5-4.0 Hz. The suspension system does not exhibit any lock-up behavior due to low friction.

The vibration transmission performance of the ISRI mechanical seat suspension system for various amplitudes of excitations is presented in Figures 4.4a and 4.4b. The suspension system exhibits lock-up behavior due to coulomb friction around the low excitation frequencies. The suspension tends

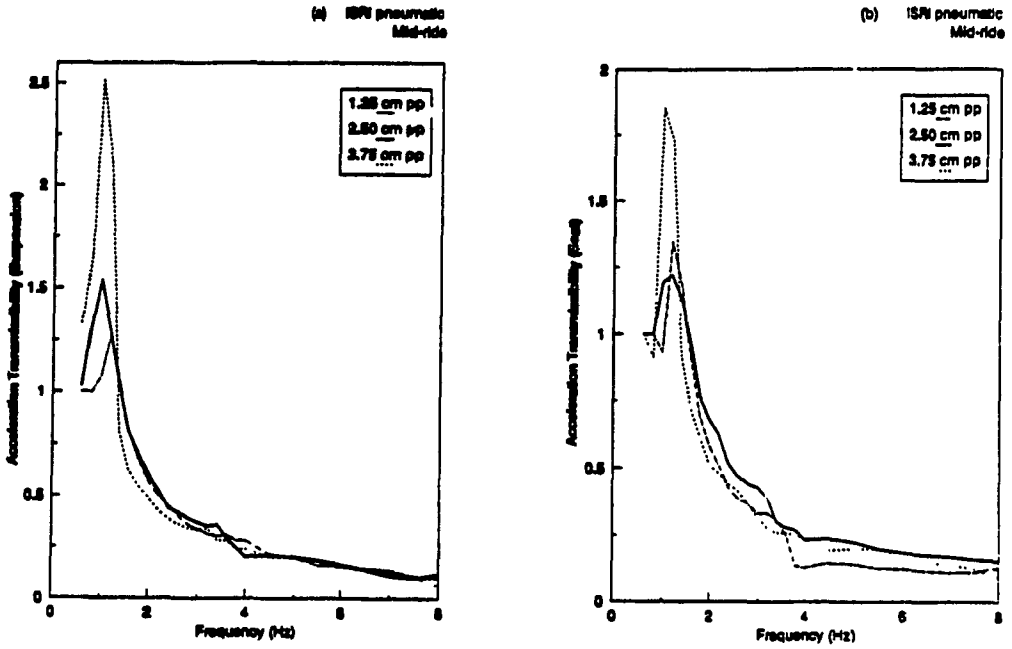

Figure 4.3. Acceleration transmissibility ratio of ISRI Pneumatic seat-suspension (pressure = 80 psi): (a) Suspension ($\ddot{z}_1 / \ddot{z}_0$); (b) Seat ($\ddot{z}_2 / \ddot{z}_0$).

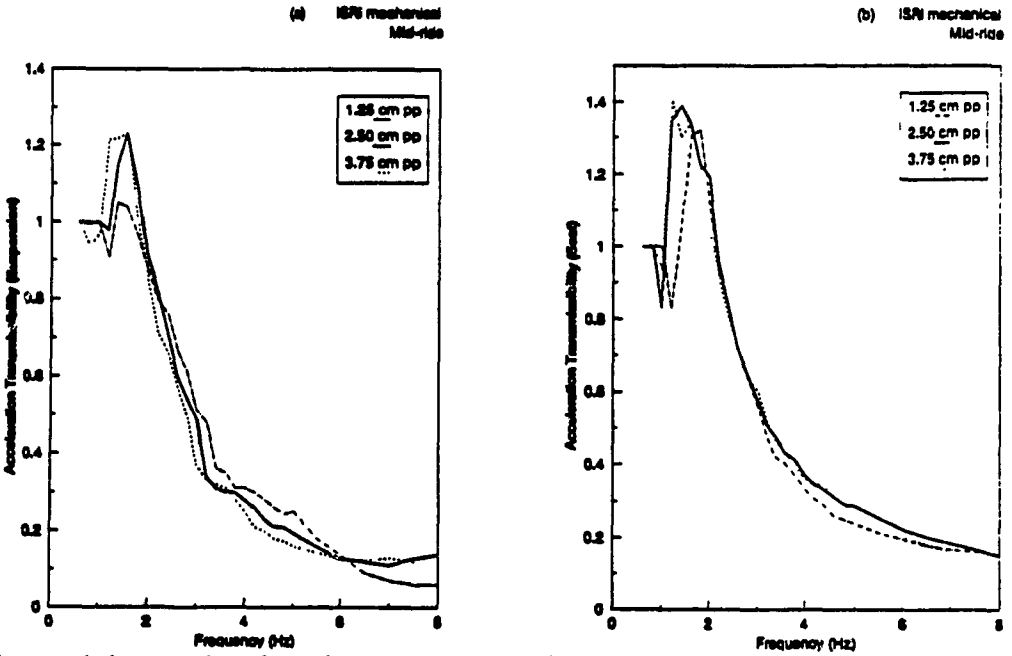

Figure 4.4. Acceleration transmissibility ratio of ISRI Mechanical Seat-Suspension: (a) Suspension ($\ddot{z}_1 / \ddot{z}_0$); (b) Seat ($\ddot{z}_2 / \ddot{z}_0$).

to break away at an excitation frequency of 1 Hz corresponding to 1.25 cm pp excitation. The break frequencies corresponding to 2.5 cm and 3.75 cm pp excitations are observed to be 0.8 Hz and 0.6 Hz, respectively. The acceleration transmissibility of the suspension system, adjusted to mid-ride position, exhibit resonant frequencies around 1.5 Hz, 1.6 Hz and 1.6 Hz, corresponding to 1.25 cm, 2.5 cm and 3.75 cm pp displacement excitations, respectively. The resonant transmissibility ratio increases considerably as the amplitude of excitation is increased, as shown in Figure 4.4a. The soft cushion of the seat tends to increase the resonant transmissibility response of the seat as illustrated in Figure 4.4b.

The vibration transmission performance characteristics of SIFRA seat-suspension system for various amplitudes of excitation are presented in Figures 4.5a and 4.5b. The acceleration transmissibility of the suspension systems, adjusted to mid-ride, reveals resonant frequencies around 1.2-1.3 Hz depending upon the excitation amplitude. A second peak is observed around an excitation frequency of 3.4 Hz. Further laboratory tests were undertaken to identify the cause of this peak and it was concluded that this transmissibility peak is attributed to the clearance between the base plate guides and the suspension base. The peak transmissibility ratio corresponding to the bounce frequency is established as 1.22 for 1.25 cm pp excitation. However, this increases to 1.76 and 1.81, respectively, when the pp excitation amplitude is increased to 2.5 cm and 3.75 cm.

The suspension system exhibits lock-up behavior for excitation frequency up to 0.7 Hz due to coulomb friction. The seat acceleration transmissibility ratio of the SIFRA seat-suspension, adjusted to mid-ride, is considerably lower than the acceleration transmissibility of the suspension alone, for 1.25 cm and 2.5 cm pp excitations, as shown in Figure 4.5b. However, the peak

value of seat transmissibility is considerably larger than the suspension transmissibility for high amplitude excitation (3.75 cm).

The acceleration transmissibility characteristics of the GRAMMAR seat-suspension are presented in Figures 4.6a and 4.6b, for various amplitudes of excitation. The suspension system reveals lock-up until 1 Hz, when subjected to 1.25 cm pp displacement excitation. The break away frequency reduces to 0.8 Hz when the excitation amplitude is increased, as shown in Figure 4.6a. The undamped suspension system exhibits high resonant peaks around 1.4 Hz for 1.25 cm pp excitation. However, as the excitation amplitude is increased, the cam tends to interfere with the suspension mechanism by repetitive slippage and impact during each cycle of vibration. The repetitive impacts due to the cam lead to excessively high transmissibility ratio, 1.88 for 2.5 cm pp excitation, and 2.0 for 3.75 cm pp excitation. The corresponding resonant frequency also increases to 1.8 Hz as compared to 1.4 Hz achieved corresponding to the low amplitude excitation. Furthermore, the cam interference caused during 3.75 cm pp excitation leads to slippage of the load at excitation frequencies above 4 Hz due to excessive vibrations.

The acceleration transmitted by the suspension system is effectively attenuated by the medium hard seat cushion, as shown in Figure 4.6b. A comparison of Figures 4.6a and 4.6b reveals that the cushion tends to reduce the magnitude of transmitted vibration in the entire frequency range.

Figures 4.7a and 4.7b present the acceleration transmissibility characteristics of the GRAMMAR (Gas shock) seat-suspension system. The suspension system, adjusted to mid-ride, exhibits resonant frequency around 1.2 Hz corresponding to 1.25 cm and 2.5 cm pp excitations. However, when the seat is subjected to higher amplitude of excitation (3.75) cm pp, the peak transmissibility occurs at a considerably higher frequency of 2 Hz. This

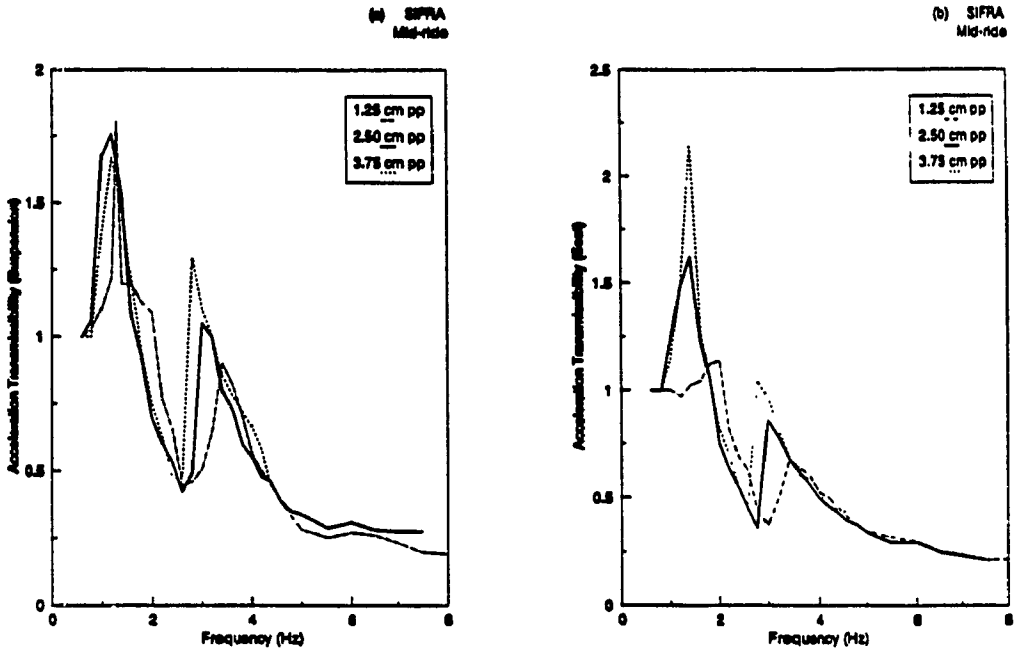

Figure 4.5. Acceleration transmissibility ratio of SIFRA Seat-Suspension: (a) Suspension ($\ddot{z}_1 / \ddot{z}_0$); (b) Seat ($\ddot{z}_2 / \ddot{z}_0$).

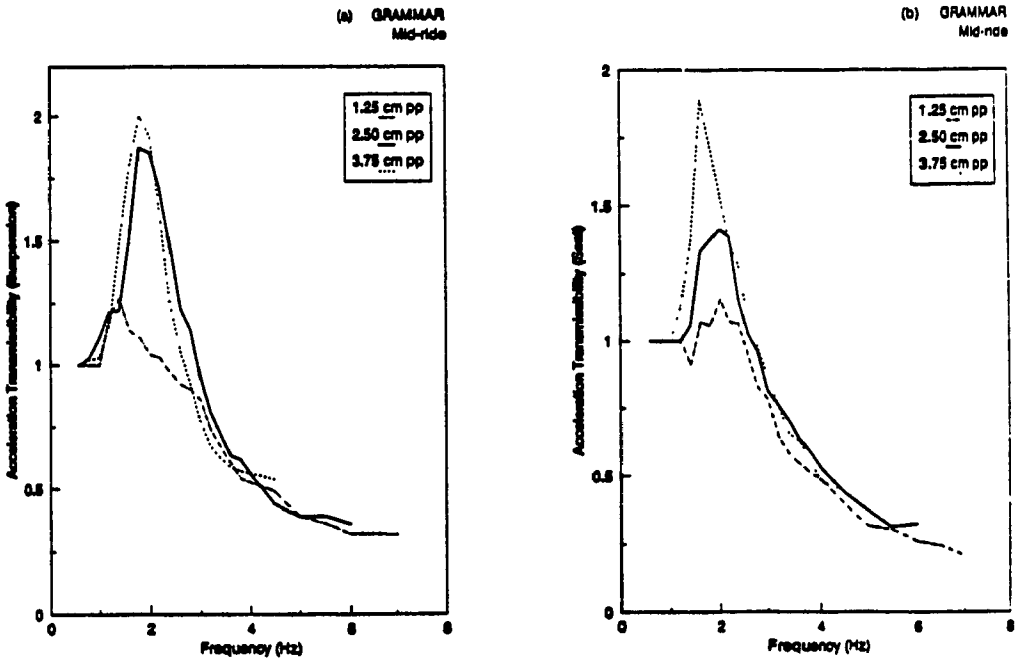

Figure 4.6. Acceleration transmissibility ratio of GRAMMAR Seat-Suspension: (a) Suspension ($\ddot{z}_1 / \ddot{z}_0$); (b) Seat ($\ddot{z}_2 / \ddot{z}_0$).

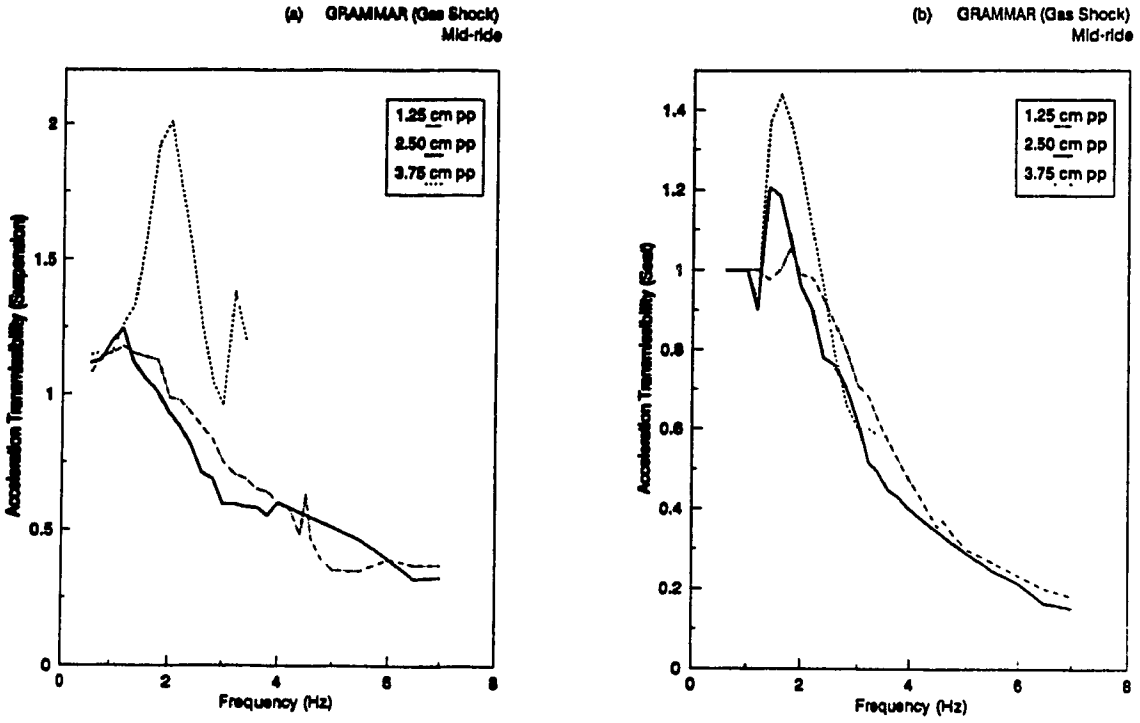

Figure 4.7. Acceleration transmissibility ratio of GRAMMAR (Gas Shock) Seat-Suspension: (a) Suspension ($\ddot{z}_1 / \ddot{z}_0$); (b) Seat ($\ddot{z}_2 / \ddot{z}_0$).

considerable shift in the frequency is caused by the slippage and impacting of the cam mechanism. Consequently, the peak suspension transmissibility ratio at 3.75 cm pp excitation is excessively high, as shown in Figure 4.7a. The effect of cam slippage is also observed for 2.5 cm excitations, specifically at excitation frequencies above 3.2 Hz. A comparison of seat and suspension acceleration transmissibility ratios (Figures 4.7a and 4.7b) reveals that the soft seat cushion reduces the magnitude of transmitted vibrations considerably, independent of the amplitude of excitation.

4.4 COMPARISON OF VIBRATION TRANSMISSION PERFORMANCE OF SEAT-SUSPENSION SYSTEMS

The vibration transmission characteristics of the selected seat-suspension systems are studied to assess their relative performance characteristics. The relative vibration transmission performance of the seat-suspension systems are assessed in terms of peak value of resonant transmissibility ratio, resonant frequency, and the transmissibility ratio corresponding to the off-road vehicle resonant frequencies (around 2.6 Hz). Seat-suspension systems with low resonant peak and low value of transmissibility around the vehicle resonant frequency are highly desirable. However, a seat-suspension design with these desirable characteristics is extremely difficult to realize. Realistic seat-suspension designs offer a compromise between the two desirable characteristics in view of their vibration isolation behavior.

The vibration transmissibility characteristics of the candidate seats corresponding to the resonant frequencies of the seat and the vehicle are summarized in Tables 4.1 and 4.2.

4.5 RESPONSE EVALUATION AND VALIDATION OF THE ANALYTICAL SEAT-SUSPENSION MODEL

The differential equations of motion, describing the dynamics of seat-suspension systems, may be solved either in the time-domain or in the frequency-domain. The frequency-domain approach utilizes Fourier transform of the time-dependent variables transform into frequency-dependent variables and is applicable to either linear or linear equivalent system of equations. The time-domain approach utilizes numerical integration techniques to solve linear

Table 4.1

Resonant Vibration Transmission Characteristics of

Seat-Suspension Systems

SEAT TYPE	MEASUREMENT LOCATION	PEAK TO PEAK EXCITATION AMPLITUDE (cm)		
		1.25	2.50	3.75
		PEAK TRANSMISSIBILITY RATIO (FREQUENCY)		
ISRI (Pneumatic)	Suspension	1.265 (1.2)	1.54 (1.0)	2.52 (1.0)
	Seat	1.35 (1.2)	1.22 (1.2)	1.85 (1.0)
ISRI (Mechanical)	Suspension	1.05 (1.4)	1.23 (1.6)	1.23 (1.6)
	Seat	1.32 (1.8)	1.39 (1.4)	1.41 (1.2)
SIFRA	Suspension	1.22 (1.2)	1.76 (1.2)	1.81 (1.3)
	Seat	1.14 (2.0)	1.62 (1.4)	2.16 (1.4)
GRAMMAR	Suspension	1.27 (1.4)	1.87 (1.8)	2.00 (1.8)
	Seat	1.15 (2.0)	1.42 (2.0)	1.89 (1.6)
GRAMMAR (Gas Shock)	Suspension	1.18 (1.2)	1.24 (1.2)	2.00 (2.0)
	Seat	1.05 (1.8)	1.18 (1.6)	1.44 (1.6)

Table 4.2

Vibration Transmission Characteristics of Seat-Suspension Systems

SEAT TYPE	MEASUREMENT LOCATION	PEAK TO PEAK EXCITATION AMPLITUDE (cm)		
		1.25	2.50	3.75
		TRANSMISSIBILITY RATIO @ 2.6 Hz		
ISRI (Pneumatic)	Suspension	0.40	0.42	0.36
	Seat	0.39	0.47	0.42
ISRI (Mechanical)	Suspension	0.66	0.60	0.57
	Seat	0.71	0.72	0.72
SIFRA	Suspension	0.44	0.42	0.48
	Seat	0.63	0.45	0.55
GRAMMAR	Suspension	0.92	1.23	1.05
	Seat	0.94	1.03	1.07
GRAMMAR (Gas Shock)	Suspension	0.88	0.71	1.25
	Seat	0.86	0.76	0.79

as well as nonlinear differential equations of motion. The frequency-domain analysis involves solution of algebraic equations and is thus extremely convenient for parametric as well as optimization studies, where repetitive simulations are performed. The nonlinear differential equations, however, need to be linearized in order to employ frequency-domain analysis. For the purpose of validation of the analytical models, numerical integration technique is employed to directly solve the nonlinear differential equations of motion.

4.5.1 Solution of Nonlinear Differential Equations of Motion

Since the laboratory tests are performed with passive load, the seat-suspension model employing a rigid mass representation of the driver is analyzed for validation purposes. The nonlinear differential equations, Equations (2.1) and (2.2) are solved for sinusoidal excitations using numerical integration technique in conjunction with the frequency sweep.

The nonlinear second order differential equations of motion describing the dynamics of the seat-suspension with rigid mass operator model, developed in chapter 2, can be presented in the following form:

$$[M]\{\ddot{x}\} + \{F_c\} + \{F_K\} + \{F_d\} + \{F_f\} + \{F_s\} = -[M]\ddot{z}_0 \qquad (4.1)$$

where [M] is the n x n mass or inertia matrix and n is number of degrees-of-freedom. $\{F_c\}$, $\{F_K\}$, $\{F_d\}$, $\{F_f\}$, $\{F_s\}$ are (n x 1) vectors of suspension forces due to cushion, suspension spring, shock absorber, Coulomb damping and bump stop, respectively, and $\{x\}$ is the vector containing relative displacements of the driver and suspension mass. Equation (4.1) can be rewritten as:

$$\{\ddot{x}\} = -[M]^{-1}\left\{\{F_c\} + \{F_K\} + \{F_d\} + \{F_f\} + \{F_s\}\right\} - \ddot{z}_0 \qquad (4.2)$$

The set of n second order differential equations are transformed to 2n first order differential equations using the following substitutions:

$$\dot{x}_i = x_{i+n} \quad , \quad i = 1, 2, \ldots, n \qquad (4.3a)$$

$$\ddot{x}_i = \dot{x}_{i+n} \quad , \quad i = 1, 2, \ldots, n \qquad (4.3b)$$

The resulting 2n first order expressions are integrated to evaluate velocities and displacements using the fourth-order Runge-Kutta algorithm, for a set of successive time instants t_i's. The velocities and displacements, obtained at previous instant t_{i-1} are used as the initial conditions to determine the response values at t_i. The integration process is repeated for successive t_i's and terminated when t_i approaches a certain predetermined final time, t_f. The value of t_f is selected such that dynamic phenomena are fully illustrated.

4.6 VERIFICATION OF THE ANALYTICAL MODEL

The coupled nonlinear differential equations describing the motion of the seat-suspension model with rigid driver mass are solved for sinusoidal excitation using the fourth-order Runge-Kutta algorithm and the results are presented in terms of acceleration transmissibility in the frequency range 0.5 - 8 Hz. The analytical acceleration transmissibilities are then compared to those obtained from the laboratory in order to validate the analytical model.

The model parameters that are used to study the dynamic response of ISRI

and SIFRA, both in the time-domain and frequency-domain are determined from the static and dynamic laboratory measurements discussed in chapter 3. Table 4.3 lists all the base line parameters that are used to investigate the dynamic response of the seat models in this study. Verifications of the ISRI-mechanical and SIFRA seat-suspension models are presented in the following sub-sections.

4.6.1 Verification of ISRI Seat-Suspension Model

Equations (2.1) through (2.2) are solved for sinusoidal excitations in the frequency range 0.5 to 8 Hz, using numerical integration. Validations are initially performed for seat-suspension model without a shock absorber ($F_d = 0$). Figures 4.8a and 4.8b present a comparison of the analytical and experimental vibration transmissibility characteristics of the suspension and driver mass, respectively. The undamped seat suspension system exhibits a high resonant peak around the resonant frequency due to highly stiff extension limit stops, as shown in the vibration transmissibility characteristics of both the suspension and the seat. The analytical vibration transmissibility characteristics of the suspension system are in good agreement with those established via laboratory experimentation, with the exception of the resonant amplitude. This discrepancy is perhaps attributed to the analytical model's inability to simulate the impacts against an almost rigid stop.

The acceleration transmissibility characteristics reveal that the seat-suspension system resonates around 1.4 Hz. The excessive relative motion of the suspension mass around the natural frequency yields repetitive impacts against the bump stops. The steady-state acceleration measured at an excitation frequency of 1.4 Hz, exhibits high peak at the compression and

Table 4.3

Parameters of the ISRI and SIFRA Seat-Suspension Systems.

DESCRIPTION	SYMBOL	SEAT TYPE	
		ISRI	SIFRA
Driver Mass (kg)	m_o	56.2	56.2
Suspension mass (kg)	m_1	15	10
Cushion stiffness (N/m)	K_c	70000	82300
Cushion damping (Ns/m)	C_c	150	300
Suspension Spring Stiffness (N/m)	K_{1A}	4900	5300
	K_{1B}	10000	69000
Vertical distance between bump stops (m)	2β	0.075	0.10
Shock absorber angle (radians)	θ	1.1*	1.22**
Shock absorber damping coefficient (Ns/m)	C_{1A}	710	710
	C_{1B}	592	592
Velocity at which transition from C_{1A} to C_{1B} occurs (m/s)	V_s	0.032	0.032
Coulomb friction force (N)	F_{CD}	20	15
Excitation amplitude (m)	z_o	0.0125	0.0125

* Variable angle depending on z_1

** Fixed angle

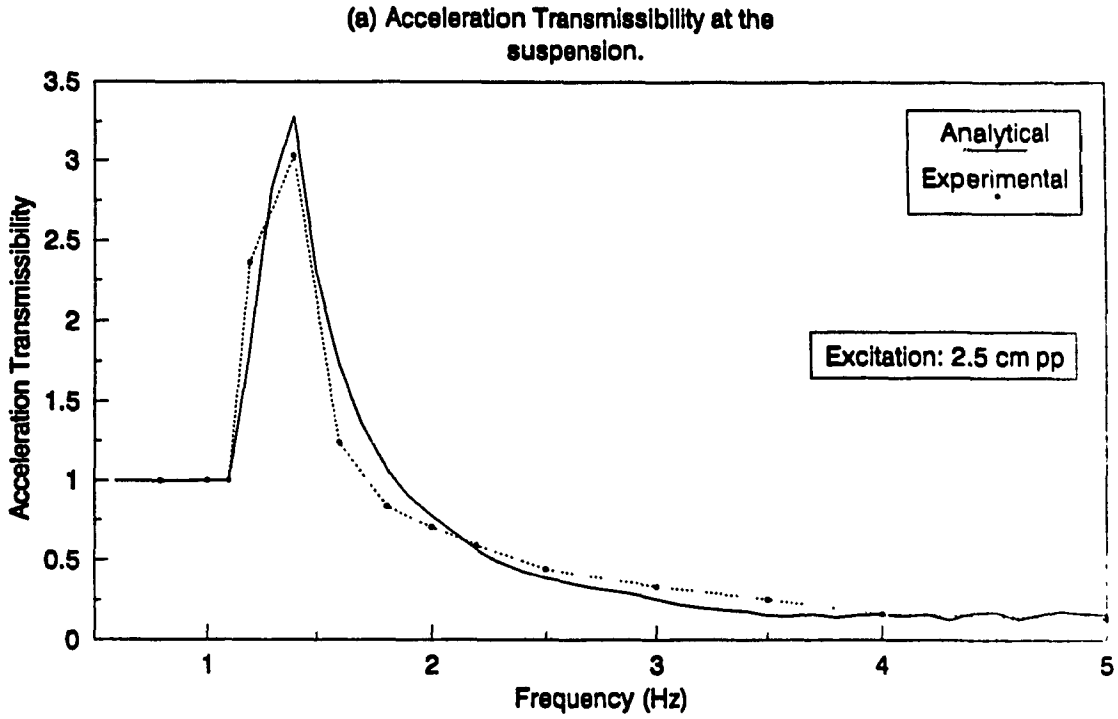

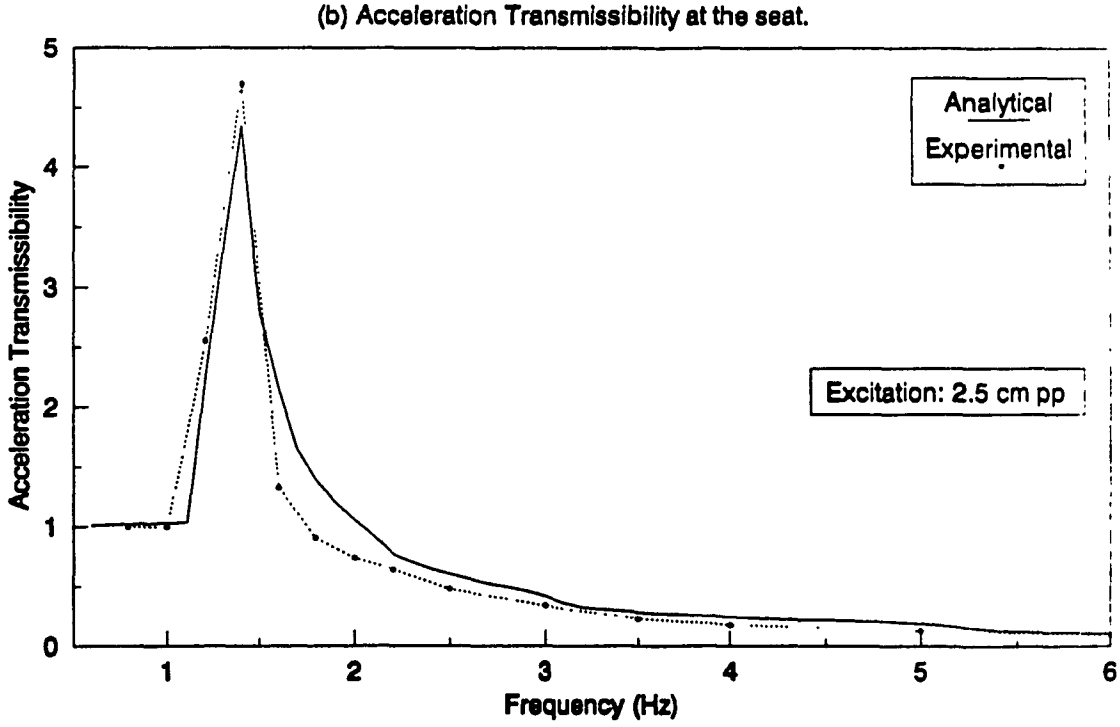

Figure 4.8. Model Verification Using Experimental Results for ISRI Mechanical Seat-Suspension (Shock Absorber Removed): (a) Suspension ($\ddot{z}_1 / \ddot{z}_0$); (b) Seat ($\ddot{z}_2 / \ddot{z}_0$).

extension ends, as shown in Figure 4.9. The peak associated with the extension stop, however, is excessively high as compared to that associated with the compression stop due to rigid bump-stops in extension. A comparison of analytical and experimental acceleration response of the suspension clearly demonstrates a high degree of validation for the analytical model. The peak acceleration, however, is slightly lower than that encountered during experiments.

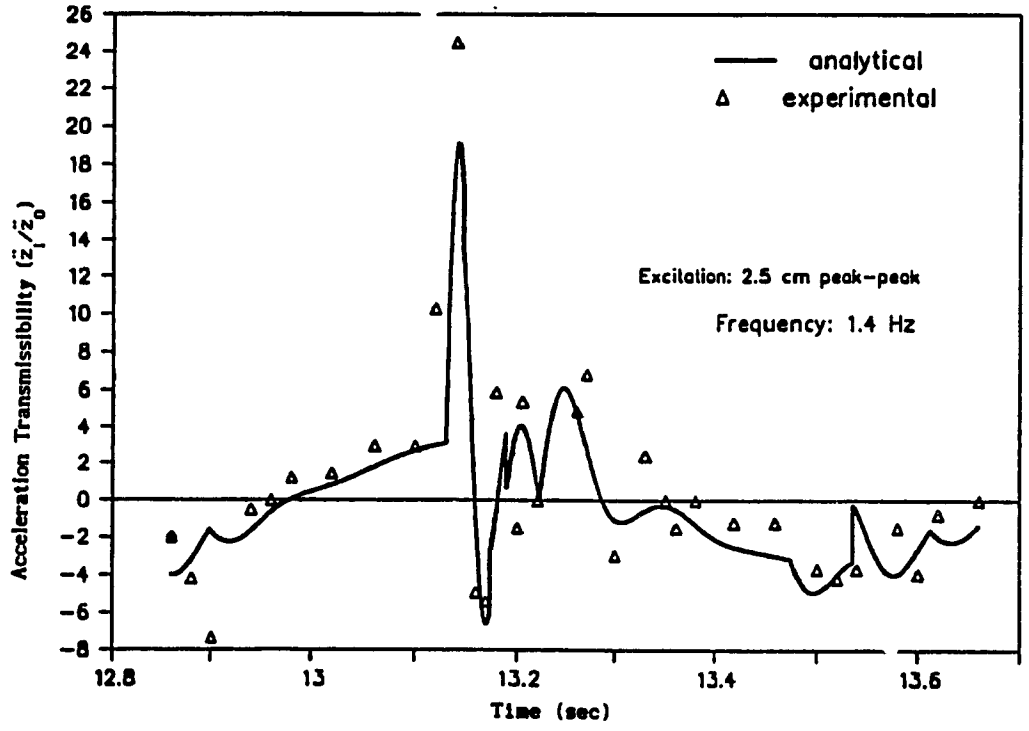

Figure 4.9. Comparison of the Analytical and Experimental Steady State Vibrations of The Suspension Mass at an Excitation Frequency of 1.4 Hz (m_0 = 56.2 kg).

The vibration transmissibility of the damped suspension system, established via numerical integration analysis and laboratory experiments, are presented in Figures 4.10a and 4.10b. The shock absorber parameters are derived from the nonlinear force-velocity characteristics, as discussed in section 2.5.2. The force-velocity characteristics of the shock absorber reveal a high damping coefficient at low velocities due to bleed-orifice. The damping coefficient, however, reduces to a low value due to blow-off at higher velocities. These figures clearly illustrate that the analytical acceleration transmissibility characteristics correlate quite well with those established in the laboratory. The discrepancies at low frequencies below the resonant frequency can be attributed to the limitations of the seat accelerometer and conditioners to measure and to condition low frequency acceleration signals.

4.6.2 Verification of SIFRA Seat-Suspension Model

The analytical model, developed in chapter 2, is further validated against the laboratory results obtained for SIFRA seat-suspension. The acceleration transmissibility that is determined using numerical integration, using the SIFRA model parameters, is compared to that established via laboratory experimentation as shown in Figure 4.11. The experimental results exhibit two peaks, corresponding to 1.4-1.5 Hz and 3.2 Hz, while the computer simulations reveal only one peak corresponding to the natural frequency of the seat suspension (1.4 Hz). Although the acceleration transmissibility around the suspension resonant frequency is quite close to that measured in the laboratory, there exists a discrepancy between the analytical and experimental results around the 3.2 Hz excitation frequency. This is attributed to the clearance between the base plate guides and the suspension base. Relative movement between the base plate and the suspension base is observed around

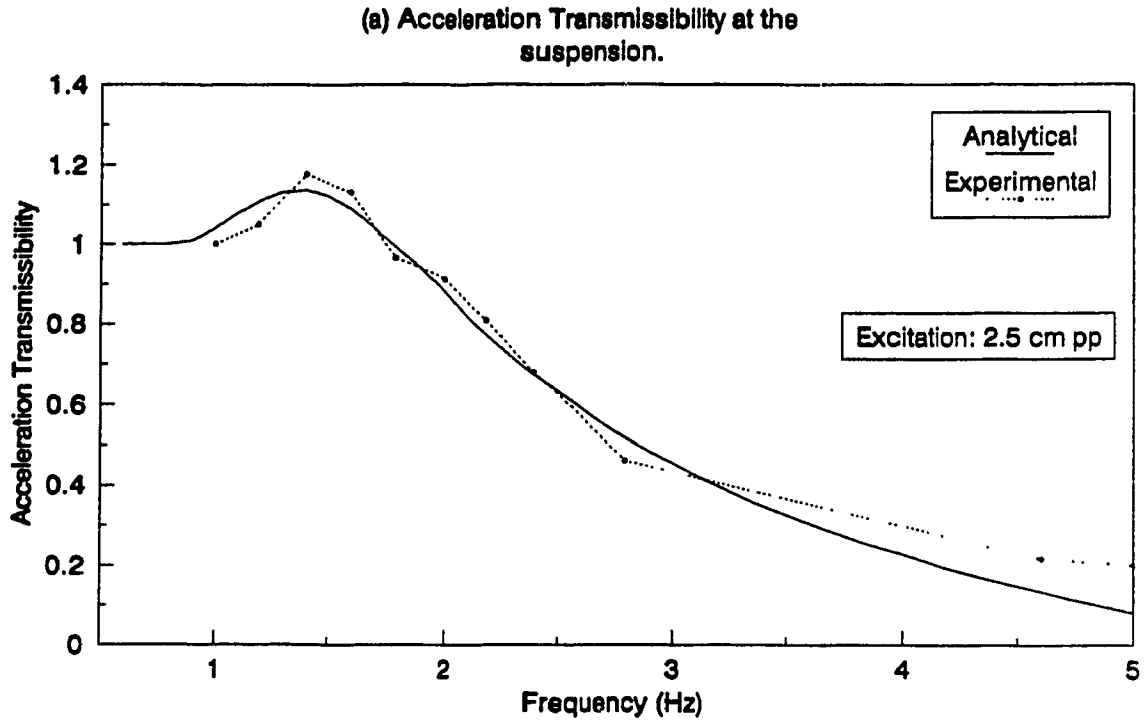

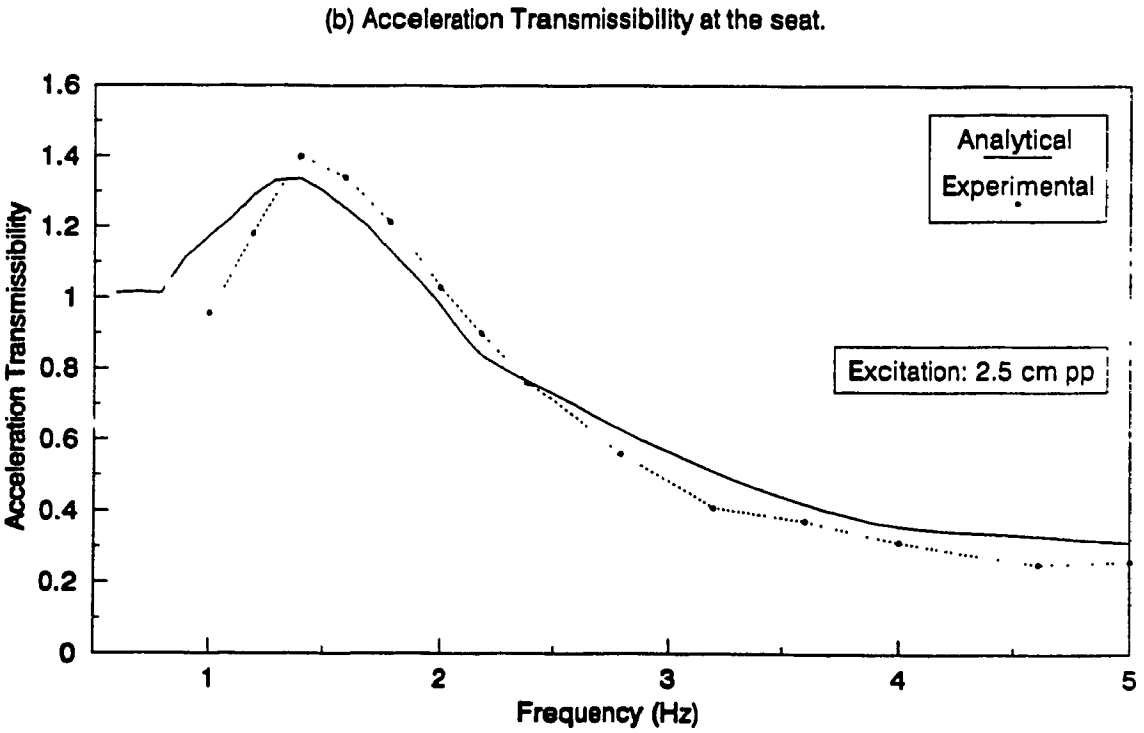

Figure 4.10. Model Verification Using Experimental Results for damped ISRI Mechanical Seat-Suspension (C_{1A}=710 N.s/m, C_{1B}=592 N.s/m): (a) Suspension ($\ddot{z}_1 / \ddot{z}_0$); (b) Seat ($\ddot{z}_2 / \ddot{z}_0$).

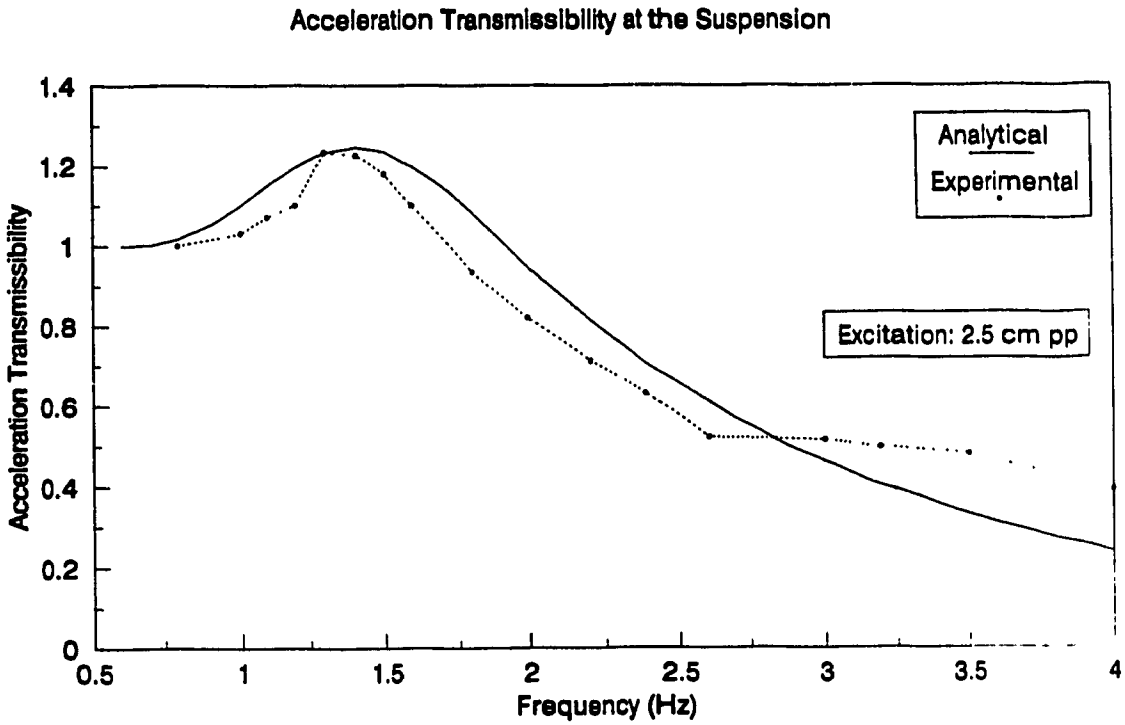

Figure 4.11. Model Verification Using Experimental Results for SIFRA (C_{1A}=710 N.s/m, C_{1B}=592 N.s/m): Suspension, ($\ddot{z}_1 / \ddot{z}_0$).

this excitation frequency. Closer tolerances between the plate and the suspension base can completely eliminate this phenomenon and thus no attempts have been made to further refine the analytical model.

4.7 SUMMARY

In this chapter, instrumentation and test methodology for measuring vibration performance of seat-suspension systems in the laboratory are discussed. Vibration transmissibility characteristics of the selected seat-suspension systems are derived from the laboratory tests using sinusoidal excitations. The nonlinear differential equations of motion for the seat-suspension models are solved using numerical integration algorithm. The analytical results are compared to those established from the laboratory tests in order to validate the analytical model. The comparison demonstrates a high degree of correlation between analytical and experimental data.

CHAPTER 5

RESPONSE EVALUATIONS OF SEAT-SUSPENSION SYSTEMS

5.1 GENERAL

The frequency response characteristics of the nonlinear seat suspension models may be evaluated in the time-domain using numerical integration methods as discussed in chapter 4. Alternatively, frequency response characteristics can be evaluated using the convenient frequency-domain analysis technique. Frequency-domain analysis technique is specifically suited for determination of random response and parametric sensitivity analysis, where many repetitive simulations need to be performed. The frequency-domain analysis technique, however, can only be applied to either linear or linearized system models.

Since the linear systems are easier and more economical to solve than the nonlinear ones, the performance evaluations are effectively achieved by replacing the nonlinear elements by equivalent linear elements. This process of expressing an equivalent linear system is termed as "equivalent linearization." The linearized suspension models can then be conveniently solved in the frequency-domain to determine the frequency as well as random ride response characteristics. Further, the parametric sensitivity analyses of the suspension model can be carried out more effectively using equivalent linear models.

In this chapter, the frequency response characteristics of seat-suspension models are evaluated using numerical integration technique. The nonlinear suspension model is expressed by its linear equivalent, using local equivalent linearization technique based on energy similarity. The effectiveness of the linearization technique is demonstrated by comparing the frequency response characteristics of the linearized model to that of the

frequency response characteristics of the linearized model to that of the nonlinear model. The random ride response of the linearized suspension model is evaluated for random excitations, presented in chapter 3. Figure 5.1 outlines response analyses and evaluations that are discussed in this and the following chapter.

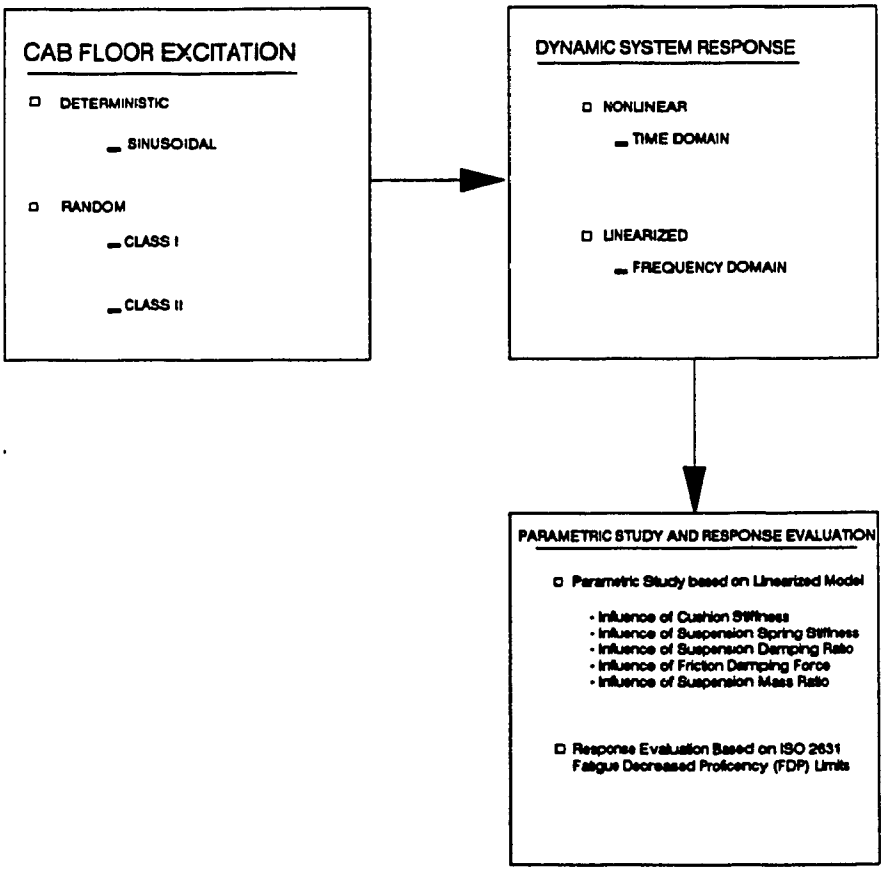

Figure 5.1. Flow Chart for Response Analysis and Performance Evaluations.

5.2 FREQUENCY RESPONSE ANALYSIS OF SEAT-SUSPENSION MODELS

Frequency response characteristics of seat-suspension models are initially evaluated using numerical integration techniques, as discussed in chapter 4. The frequency response characteristics are presented in terms of acceleration transmissibility of the seat. The acceleration transmissibility of the validated seat-suspension models are evaluated for three different human-body models (rigid mass, one- and two-degrees-of-freedom models) to quantify the influence of dynamics of the suspended driver mass on the vibration attenuation performance of the seat-suspension system.

Figures 5.2a and 5.2b present the seat acceleration transmissibilities of the ISRI-mechanical and SIFRA seats, respectively, with three human body models. The peak response of all the models occurs in the 1.3 - 1.4 Hz frequency band and the response characteristics remain almost identical up to excitation frequency of 1.4 Hz, regardless of the type of human body model used. However, in the 2 to 4 Hz, frequency range, where resonant behavior of wheeled off-road vehicles is likely to occur, the seat-suspension with a rigid driver model exhibits 30 to 40 % higher vibration transmissibility than the seat-suspension with one- or two-degrees-of-freedom driver models.

The three- and four-degrees-of-freedom seat-suspension models incorporating one- and two-degrees-of-freedom driver models, respectively, exhibit almost similar seat acceleration transmissibility characteristics up to excitation frequency of 6 Hz. The response ratio of the three-degrees-of-freedom model is slightly lower than that of the four-degrees-of-freedom model. The vibration transmissibility response of the two models, however, differ considerably at excitation frequencies above 6 Hz due to secondary resonances arising from lower and upper body dynamics, as shown in Figure 5.2a. The two-degrees-of-freedom seat-suspension model,

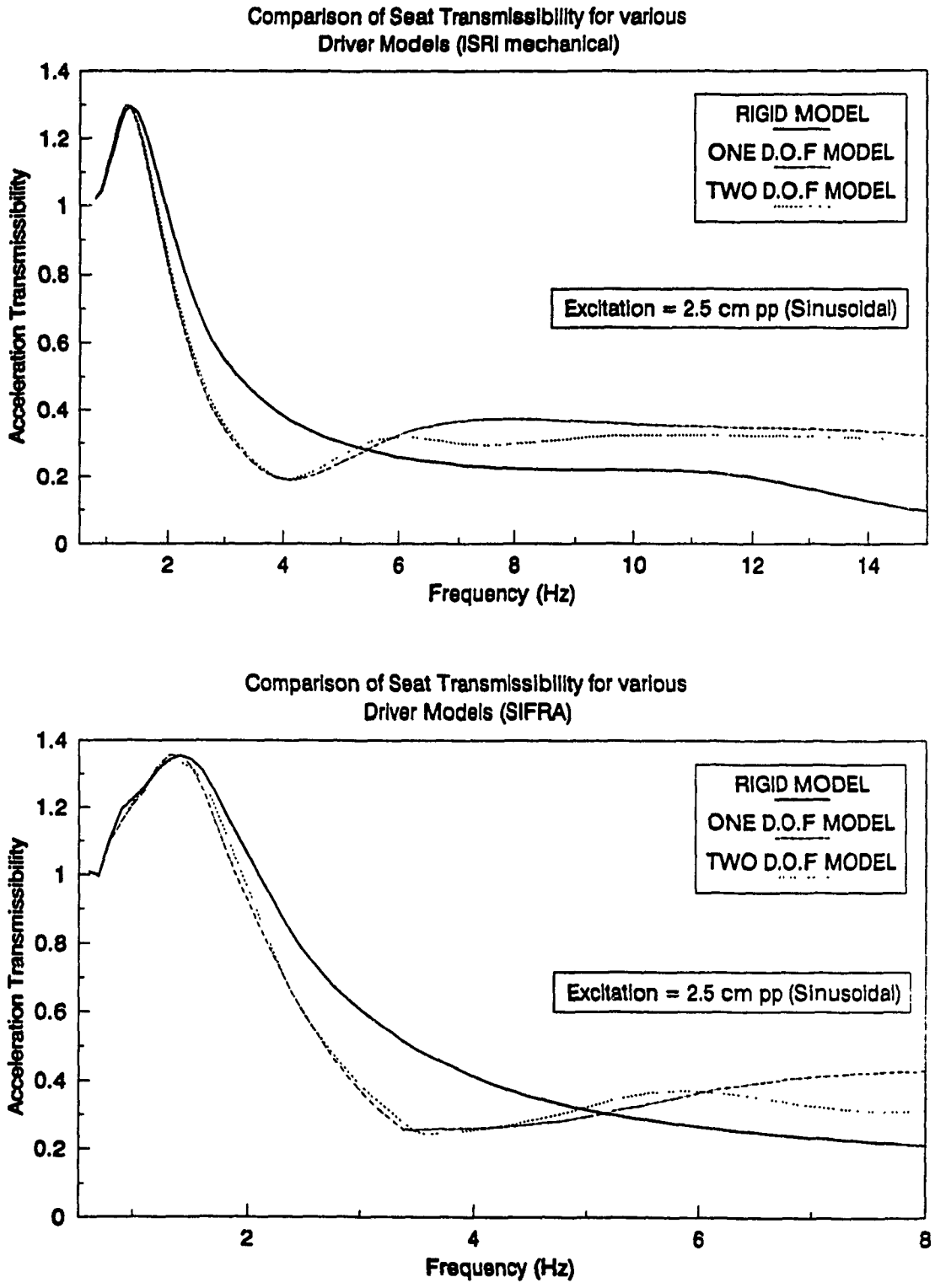

Figure 5.2. Influence of Driver Model on Seat Acceleration Transmissibility.

incorporating the rigid mass driver model, yields lower values of transmissibility ratio at excitation frequencies above 5.5 Hz. A comparison of the response characteristics of the seat-suspension model, incorporating three different human body models, clearly illustrates that human body dynamics contributes considerably to the vibration attenuation performance of a seat-suspension system.

5.3 ANALYSIS IN THE FREQUENCY-DOMAIN

Frequency-domain methods have long been used to analyze linear systems, since the frequency contents of the ride vibration are often of great interest than the time history. In the frequency-domain analysis the time dependent variables are Fourier transformed to frequency dependent variables.

The linear or linearized equations of motion for the seat-suspension models, in general can be expressed in the matrix form:

$$[M]\{\ddot{z}\} + [D]\{\dot{z}\} + [K]\{z\} = [D_f]\{\dot{z}_0\} + [K_f]\{z_0\} \tag{5.1}$$

where [M], [D] and [K] are (n x n) mass, damping and stiffness matrices, respectively. $[D_f]$ and $[K_f]$ are (n x n) forcing damping and stiffness matrices, respectively. $\{z\}$ and $\{z_0\}$ are n x 1 vectors containing response and excitation variables. The differential equations (5.1) are Fourier transformed to yield:

$$\{Z(j\omega)\} = \left[H(j\omega) \right]^{-1} \{Z_0(j\omega)\} \tag{5.2}$$

where $\{Z(j\omega)\}$ and $\{Z_0(j\omega)\}$ are Fourier transforms of vectors containing response and excitation variables, respectively, and $[H(j\omega)]$ is the complex

matrix representing the frequency response function of the linearized seat-suspension model, given by:

$$[H(j\omega)] = \left[-\omega^2 [M] + j\omega [D] + [K] \right]^{-1} \left[j\omega[D_f] + [K_f] \right] \tag{5.3}$$

Determination of the frequency response function $[H(j\omega)]$ thus involves solution of only algebraic equations. The response to random excitations can then be evaluated by characterizing the cab floor excitations in terms of power- and cross-spectral densities (PSD and CSD). For a single input and single output system, the excitation and response power spectral densities are related in the following manner:

$$\Delta_o(j\omega) = h(j\omega)\, h^*(j\omega)\, \Delta_i(j\omega) \tag{5.4}$$

where $\Delta_o(j\omega)$ and $\Delta_i(j\omega)$ are PSD of the response and excitation variables, respectively, $h(j\omega)$ is the frequency response function, and $h^*(j\omega)$ is the complex conjugate of $h(j\omega)$.

The random excitations at the cab floor are classified as class I and class II and are characterized by their acceleration power spectral densities (PSD). The acceleration PSD response of the seat and suspension mass can then be evaluated using the following relationship:

$$\left\{ S_o(j\omega) \right\} = \left[H(j\omega) \right]^2 S_i(j\omega) \tag{5.5}$$

where $\{ S_o(j\omega) \}$ is a vector containing PSD of acceleration response of the seat and the suspension mass, and $S_i(j\omega)$ is the input acceleration PSD.

The frequency-domain simulation technique is computationally much simpler and reduces simulation time considerably as compared to the time domain analysis. However, the frequency-domain method is limited only to linear and linearized system models. The nonlinear differential equations characterizing the dynamics of seat-suspension system thus need to be linearized.

5.4 DEVELOPMENT OF LINEAR EQUIVALENT SEAT-SUSPENSION MODELS

The study of nonlinear suspension models is considerably more complex than that of the linear models, which can be attributed to the fact that the superposition principle is not valid for nonlinear systems. The preliminary designs and performance evaluations of a nonlinear suspension model are therefore often performed assuming linear spring and damping elements. Such a methodology may be considered adequate for systems operating in linear range (small disturbance), where the associated effects of nonlinear elements are of second order. The nonlinear seat-suspension systems do not operate in the linear range and thus can not be accurately analyzed through such linear analytical tools. Alternatively, nonlinear analytical tools may be employed to simulate the nonlinear seat-suspension models. The usual approach is to replace the nonlinear element by the equivalent linear element, whose gain is a function of the nonlinear characteristics. A number of such approximation techniques have been developed to analyze nonlinear systems [56,57].

The equivalent linearization techniques have been widely used to determine the response of stochastically excited nonlinear dynamic systems. These techniques have been reviewed by various researchers [36, 56, 58, 59] to date, with regard to their applicability to specific problems in dynamics,

computational efficiency and degree of accuracy to represent the dynamic quantities of interest.

Equivalent linearization techniques invariably compute equivalent values of viscous damping and stiffness coefficients as functions of response characteristics and type of nonlinearity such that the response behavior of the linear system does not deviate significantly from that of the original nonlinear system. Studies by Scanlan [60] showed that often critical effects of nonlinear damping mechanisms are not accurately characterized by the global linear constants, determined from the linearization theory. It has been established that nonlinear stiffness and damping mechanisms, encountered in vehicle suspensions, in general should be expressed by local equivalent constants, where each local constant is considered valid in a narrow frequency band centered around a selected (local) excitation frequency.

The frequency-domain linearization technique, developed by Thompson [61], has been extended to carry out random response analysis of nonlinear systems using a discrete harmonic linearization technique. The discrete harmonic linearization technique, based on balancing either the average force or the average energy dissipated per cycle has been applied to simulate nonlinear damping mechanisms, such as Coulomb and velocity square dampers. These nonlinear damping mechanisms are represented by an array of local equivalent viscous damping coefficients, where each local constant is determined as a function of local excitation frequency, excitation amplitude and properties of the nonlinearity. Although the discrete harmonic linearization technique provides an effective and convenient tool to evaluate random response of nonlinearly damped mechanical systems, the treatment of nonlinear springs and variable damping due to shock absorber has not been addressed. The discrete harmonic linearization technique has been generalized by Su [62] to simulate

the random response of nonlinear air springs and variable damping, using the principle of energy similarity. The discrete harmonic linearization technique is further generalized to simulate clearance springs. The technique, based on the principle of energy similarity, is applied to formulate locally equivalent linear models of the seat-suspension incorporating variable damper, Coulomb friction and clearance spring.

5.4.1 Computation of Equivalent Linear Coefficients

It has been established that an equivalent viscous damping coefficient of a nonlinear damping element can be obtained by equating the dissipated energy per cycle due to the nonlinear dissipative element to that of an equivalent viscous damper [63]. A conservative restoring element, however, does not dissipate energy, it rather stores or releases the energy during a vibration cycle. The work done by a conservative element during one vibration cycle to the system is equal to the work done by the system into this restoring element, and hence the net work done by the restoring element is zero. The total amount of energy possessed by a conservative element in one complete cycle, however, can be measured by summing the absolute values of both the stored and released energies. A dynamic element, whether dissipative or conservative, linear or nonlinear, can thus be characterized in terms of its possessed energy. In case of a dissipative element, however, the possessed energy is simply the energy dissipated in a cycle.

Assuming harmonic motion across a nonlinear dynamic element, the nonlinear force, $f(z,\dot{z},t)$, due to the nonlinear element can be approximated by the local equivalent stiffness and damping coefficients, where each local coefficient is valid in the vicinity of a selected excitation frequency and excitation amplitude. The nonlinear force can thus be approximated as:

$$f(x,\dot{x},t) = C_{eq}(\omega_k,X)\ \dot{x}(t) + K_{eq}(\omega_k,X)\ x(t)\ ,\quad k = 1,\quad n \tag{5.6}$$

where x(t) is the harmonic motion across the element at discrete excitation frequency ω_k, given by:

$$x(t) = X \sin(\omega_k t) \tag{5.7}$$

X is the amplitude of displacement across the element and n is the total number of excitation frequencies. $C_{eq}(\omega_k,X)$ and $K_{eq}(\omega_k,X)$ are the local equivalent damping and stiffness coefficients, respectively, corresponding to discrete excitation frequency, ω_k, and the relative displacement response, X.

The local equivalent coefficients are established by equating the possessed energy of the nonlinear element to that of an equivalent linear element of the same nature, at a discrete excitation frequency such that each local coefficient is valid in the vicinity of a selected excitation frequency and response amplitude.

Seat-suspension models, presented in section 2.5.2, exhibit suspension nonlinearities due to shock absorber, coulomb friction, and clearance spring. These suspension nonlinearities are expressed by their local equivalent stiffness and damping coefficients, using the generalized discrete harmonic linearization technique. Detailed methodology associated with the derivation of local equivalent coefficients is presented below.

Shock absorber damping: Shock absorbers, employed in seat-suspension systems, exhibit variable damping characteristics associated with bleed- and blow-off control. Force-velocity characteristics of a typical shock absorber, employed in ISRI-mechanical seat-suspensions, are presented in Figure 5.3.

The shock absorber provides high damping constant (C_{1A}), corresponding to bleed-control at low position velocity, and low damping constant (C_{1B}) due to blow-off control at high piston velocity. The transition from high to low damping constant occurs at a velocity V_s. Assuming symmetric characteristics, the nonlinear damping force due to the shock absorber can be expressed as:

$$F_d(x_1,\dot{x}_1,t)= \begin{cases} C_{1A}\,\dot{x}_1\ ; & \text{if } |\dot{x}_1| \le V_s \\ C_{1A}\,V_s\,\mathrm{sgn}(\dot{x}_1) + C_{1B}(\dot{x}_1 - V_s\,\mathrm{sgn}(\dot{x}_1)); & \text{if } |\dot{x}_1| > V_s \end{cases} \tag{5.8a}$$

where the sgn function assumes a value either +1 or -1 to ensure the phase relationship between damping force and velocity. The local equivalent constants corresponding to the nonlinear damping force are evaluated using the principle of energy similarity. The nonlinear damping force can then be represented as:

$$F_d(x_1,\dot{x}_1,t) \cong C_{sh}(\omega_k,X_1)\,\dot{x}_1 \tag{5.8b}$$

where $C_{sh}(\omega_k,X_1)$ is the local damping constant, derived as a function of the excitation frequency, ω_k, and the response amplitude, X_1. The local constant is derived based on balancing the energy dissipated per cycle by the nonlinear damper to that of a linear damper. Assuming harmonic excitation and response

$$x(t) = X \sin(\omega_k t) \tag{5.9}$$

the energy dissipated per cycle, ΔE_{sh}, by the nonlinear damper can be derived from:

$$\Delta E_{sh} = \int_0^{\tau} F_d(x_1,\dot{x}_1,t)\ \dot{x}_1\ dt \tag{5.10}$$

where τ is period of oscillation. The energy dissipated per cycle by the nonlinear damper can be derived by considering a velocity cycle shown in Figure 5.3.

$$\Delta E_{sh} = 4\left[\int_0^{t_1} C_{1A}\dot{x}_1^2 dt + \int_{t_1}^{\pi/2\omega}(C_{1A}V_s + C_{1B}(\dot{x}_1 - V_s))\ \dot{x}_1\ dt\right] \tag{5.11}$$

where t_1 is the time at which piston velocity approaches V_s, given by

$$t_1 = \frac{1}{\omega_k}\ \cos^{-1}\left(\frac{V_s}{\omega_k X_1}\right) \tag{5.12}$$

The solution of Equation (5.11) yields the energy dissipated per cycle by:

$$\Delta E_{sh} = \begin{cases} \pi C_{1A}\omega_k X_1^2 & ;\ \omega_k X_1 \le V_s \\ \pi C_{1A}\omega_k X_1^2 - (C_{1A}-C_{1B})\ \omega_k X_1^2\ (\sin 2\omega_k t_1 - 2\omega_k t_1) & ;\ \omega_k X_1 > V_s \end{cases} \tag{5.13}$$

The local equivalent damping coefficient is then obtained by equating (5.13) to the energy dissipated by a viscous damper, $\Delta E = \pi C_{sh}(\omega_k,X_1)\omega_k X_1^2$:

$$C_{sh}(\omega_k, X_1) = \begin{cases} C_{1A} & ; \ \omega_k X_1 \leq V_s \\ C_{1A} + \dfrac{C_{1B} - C_{1A}}{\pi} (\sin 2\omega_k t_1 - 2\omega_k t_1) & ; \ \omega_k X_1 > V_s \end{cases} \tag{5.14}$$

Coulomb damping: The energy dissipated by the Coulomb damping of the shock absorber and linkage mechanism is proportional to the vibration amplitude. When the amplitude and frequency of excitation are low, the resultant inertia force is less than the friction force of the isolator. The isolator then functions as a rigid connection and offers no resilience. However, as the inertia force exceeds the static friction force, the coulomb damper provides a constant force independent of the response velocity except for the sign. Assuming ideal characteristics and a small viscous band around the discontinuity at zero velocity, as shown in Figure 5.4, the nonlinear friction force can be expressed as [63]:

$$F_f = \begin{cases} F_{CD} \left| \dfrac{\dot{x}_1}{V_b} \right| \text{sgn}(\dot{x}_1) & ; \quad |\dot{x}_1| \leq V_b \\ F_{CD} \text{sgn}(\dot{x}_1) & ; \quad |\dot{x}_1| > V_b \end{cases} \tag{5.15}$$

where V_b is the small value of velocity around zero to represent the viscous band. Assuming harmonic response, the energy dissipated by the Coulomb damper is obtained as [63]:

$$\Delta E_{CD} = 4 F_f X_1 \tag{5.16}$$

The local equivalent damping coefficient due to the Coulomb damping is

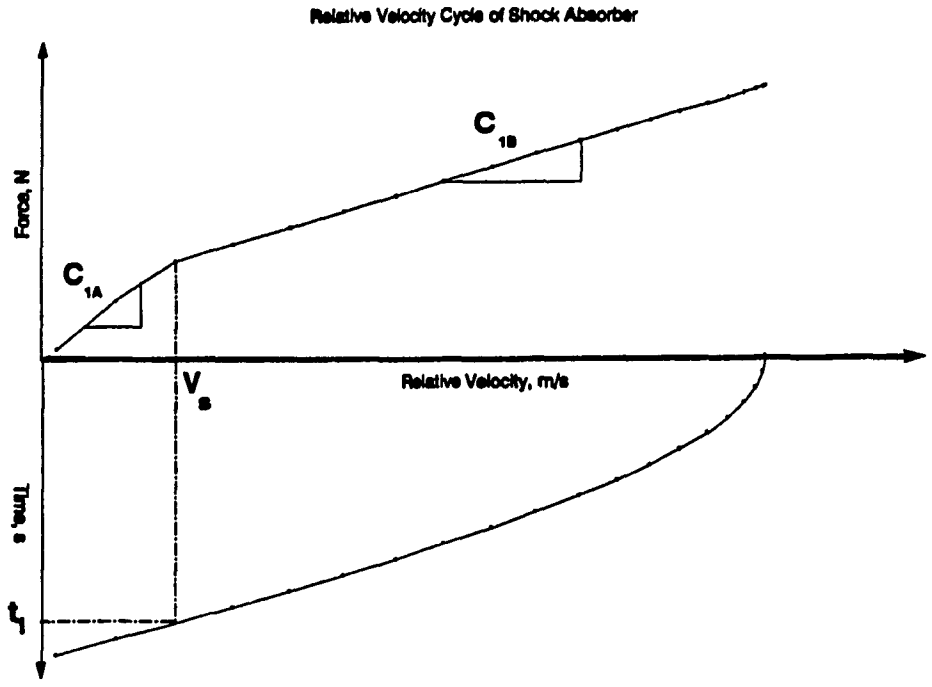

Figure 5.3. Relative Velocity Cycle of Shock Absorber.

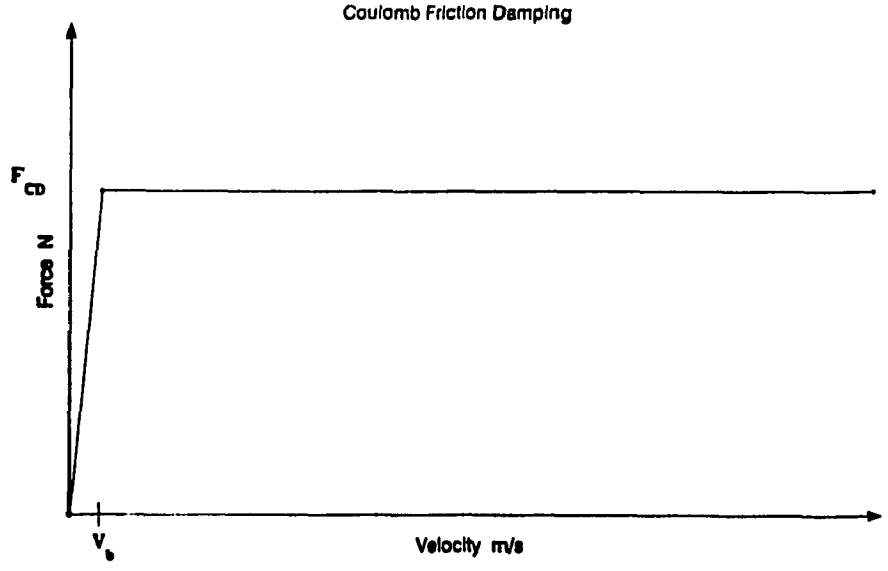

Figure 5.4. Force-Velocity Characteristics of an Ideal Coulomb Friction Damping.

then evaluated by equating Equation (5.16) to the energy dissipated by a linear damper:

$$C_{CD}(\omega_k, X_1) = \frac{4\ F_f}{\pi\ \omega_k X_1} \tag{5.17}$$

The local equivalent damping coefficient due to the nonlinear Coulomb damper and the shock absorber, can then be expressed as the linear sum of their local equivalent damping coefficients:

$$C_{eq}\ (\omega_k, X_1) = C_{sh}\ (\omega_k, X_1) + C_{CD}\ (\omega_k, X_1) \tag{5.18}$$

Bump Stops: Seat-suspension systems are invariably equipped with compression and extension bump-stops to limit the excessive travel of the suspension mass. The bump stops may be either rigid or compliant. Compliant bump stops, however, are highly desirable in view of excessive dynamic deflections of the low natural frequency suspension. Figure 5.5 illustrates the typical force-deflection characteristics of the suspension springs. The force-deflection characteristics reveal low stiffness coefficient due to the primary suspension spring, when the displacement amplitude is with in the maximum permissible travel. The spring rate, however, increases considerably due to the bump stops, when the suspension deflection exceeds the maximum permissible travel. Assuming symmetric characteristics, the nonlinear restoring force due to suspension springs can be expressed as:

$$F_K(x_1) = \begin{cases} K_{1A} x_1 & ; \quad |x_1| \le \beta \\ K_{1A}\beta\ \mathrm{sgn}(x_1) + K_{1B}(x_1 - \beta\,\mathrm{sgn}(x_1)) & ; \quad |x_1| > \beta \end{cases} \tag{5.19}$$

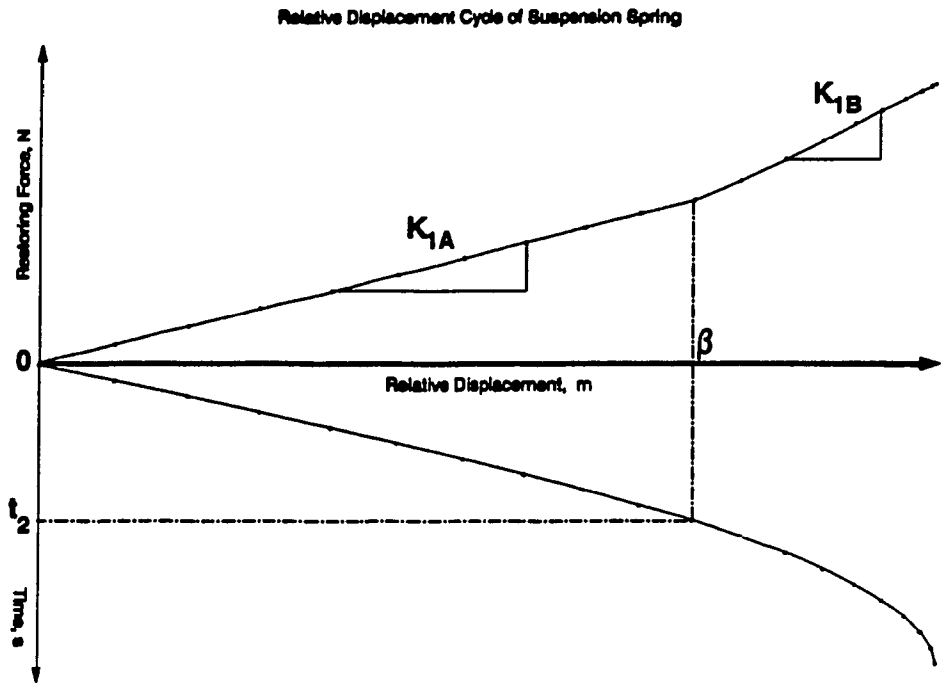

Figure 5.5. Relative Displacement Cycle of Suspension Spring.

where K_{1A} is the suspension stiffness coefficient when the deflection is within the permissible suspension travel, K_{1B} is the spring-rate when deflection exceeds the permissible suspension travel, and β is half the value of maximum permissible travel.

The total energy due to a nonlinear spring in a cycle, which is the sum of absolute values of energy stored and released during each cycle can be evaluated as:

$$\Delta E_K(\omega_k, x_1) = 4 \int_0^{X_1} F_K(x_1) dx_1 \qquad (5.20)$$

From Equations (5.19) and (5.20), the processed energy per cycle may be expressed as:

$$\Delta E_K = 4 \left[\int_0^{t_2} (K_{1A} x_1) \dot{x}_1 dt + \int_{t_2}^{\tau/4} \{K_{1A} \beta + K_{1B}(x_1 - \beta)\} \dot{x}_1 dt \right] \tag{5.21}$$

where t_2 is the time at which suspension deflection approaches the permissible travel, β, given by:

$$t_2 = \frac{1}{\omega_k} \sin^{-1} \left(\left| \frac{\beta}{X_1} \right| \right) \tag{5.22}$$

The solution of Equation (5.21) yields the following expression for energy processed by the nonlinear spring in a cycle:

$$\Delta E_K = \begin{cases} 2 K_{1A} X_1^2 & ; |X_1| \leq \beta \\ 2(K_{1A} - K_{1B}) \left[\beta^2 + 2\beta(X_1 - \beta) \right] + 2K_{1B} X_1^2 & ; |X_1| > \beta \end{cases} \tag{5.23}$$

The local equivalent linear stiffness coefficient at an excitation frequency, ω_k, is then obtained by equating the value of processed energy to that of a linear spring, which yields:

$$K_{eq}(\omega_k, X_1) = \begin{cases} K_{1A} & ; |X_1| \leq \beta \\ (K_{1A} - K_{1B}) \dfrac{\beta^2}{X_1^2} + 2(K_{1A} - K_{1B})(X_1 - \beta) \dfrac{\beta}{X_1^2} + K_{1B} & ; |X_1| > \beta \end{cases} \tag{5.24}$$

The nonlinearities within the seat-suspension models are thus expressed by an array of linear equivalent models as functions of discrete excitation frequency, excitation amplitude, response amplitude and the type of nonlinearity. An iterative algorithm is developed to compute the local coefficients for deterministic excitations. This algorithm is summarized as follows:

(i) The equivalent viscous damping and equivalent stiffness coefficients of the suspension model $C_{eq}(\omega_k, X_1)$ and $K_{eq}(\omega_k, X_1)$, are initially assumed as C^o_{eq} and K^o_{eq} at an excitation frequency ω_k.

(ii) The linearized equations of motion are then Fourier transformed to yield the frequency response matrix, using Equation (5.3).

(iii) The amplitude of relative displacement and velocity response across the isolator are then computed for a sinusoidal excitation $Z_0(\omega_k)$. The equivalent viscous damping, C^1_{eq}, and stiffness, K^1_{eq}, coefficients are then computed using Equations (5.18) and (5.24). The magnitudes of errors between the assumed and computed values are then evaluated as:

$$\varepsilon_D = \left|C^1_{eq}(\omega_k, X_1) - C^0_{eq}(\omega_k, X_1)\right|$$
$$\varepsilon_K = \left|K^1_{eq}(\omega_k, X_1) - K^0_{eq}(\omega_k, X_1)\right| \qquad (5.25)$$

If the maximum of ε_K or ε_D exceeds a specified tolerance, the assumed values of local coefficients are updated and the iterative procedure is repeated until convergence is achieved.

5.5 VERIFICATION OF LINEARIZED MODELS - HARMONIC EXCITATION

The nonlinear seat-suspension models are locally linearized using the harmonic linearization technique and the response characteristics are evaluated for sinusoidal base excitations. The response characteristics of the linearized ISRI and SIFRA seat-suspension models are presented in terms of acceleration transmissibilities and compared to those established via numerical integration. The seat-suspension models with only rigid mass representation of the driver are simulated using the model parameters, derived from static and dynamic tests performed in the laboratory.

Figures 5.6 and 5.7 illustrate a comparison of acceleration transmissibility characteristics of the locally linearized ISRI and SIFRA seat-suspension models, respectively, with those of the nonlinear suspension models. These figures clearly demonstrate the effectiveness of local equivalent linearization technique for constant amplitude harmonic excitations. The comparison reveals errors of small magnitudes only at higher excitation frequencies.

The local equivalent linearization technique provides the local damping and stiffness coefficients using the principle of energy similarity. The peak damping and stiffness forces due to the local damping and stiffness constants, however, differ from that of the nonlinear elements. The error due to the forces due to nonlinear and linearized elements can be established as:

$$\mathcal{E}_D = F_d(x_1, \dot{x}_1, t) - C_{eq}(\omega_k, X_1)\dot{x}_1$$

$$\mathcal{E}_K = F_K(x_1, t) - K_{eq}(\omega_k, X_1)x_1 \qquad (5.26)$$

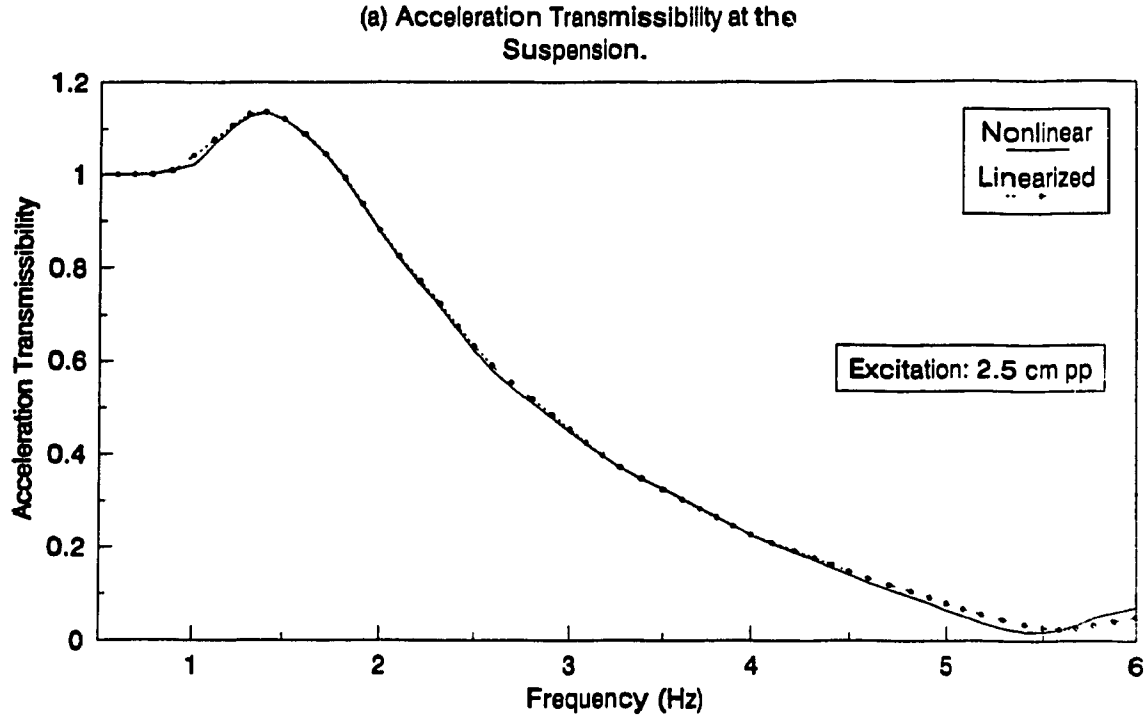

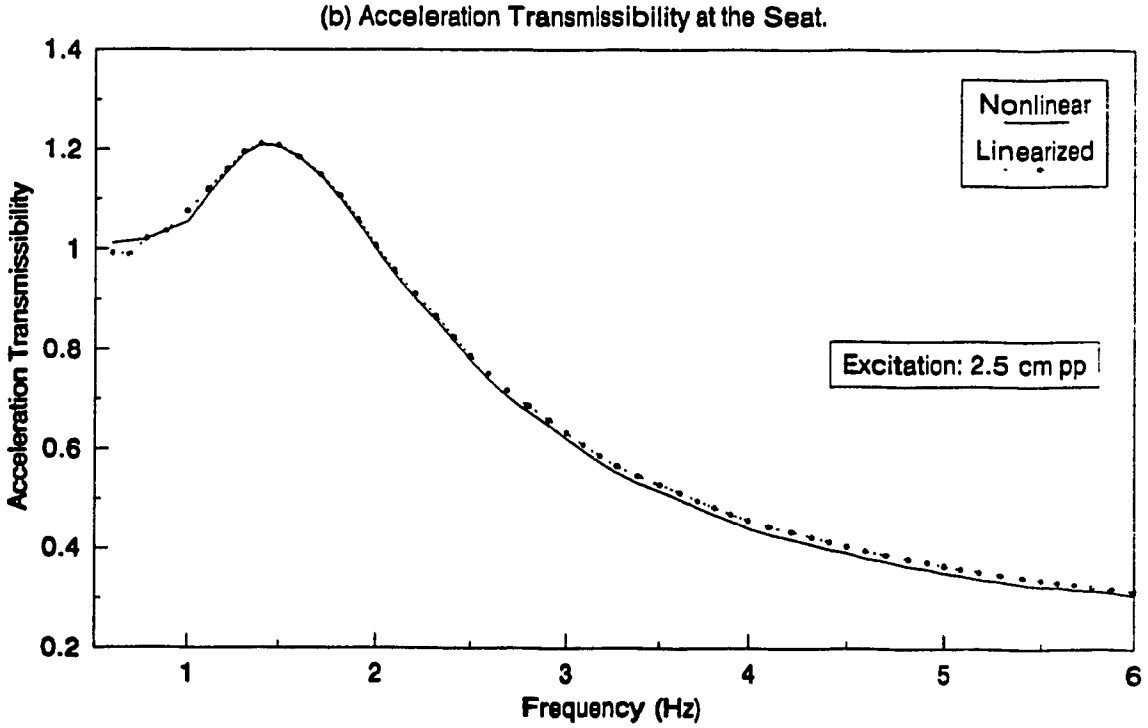

Figure 5.6. Comparison of Response Characteristics of Linearized Model with those of the Nonlinear Model (ISRI: Under-the-Seat Suspension).

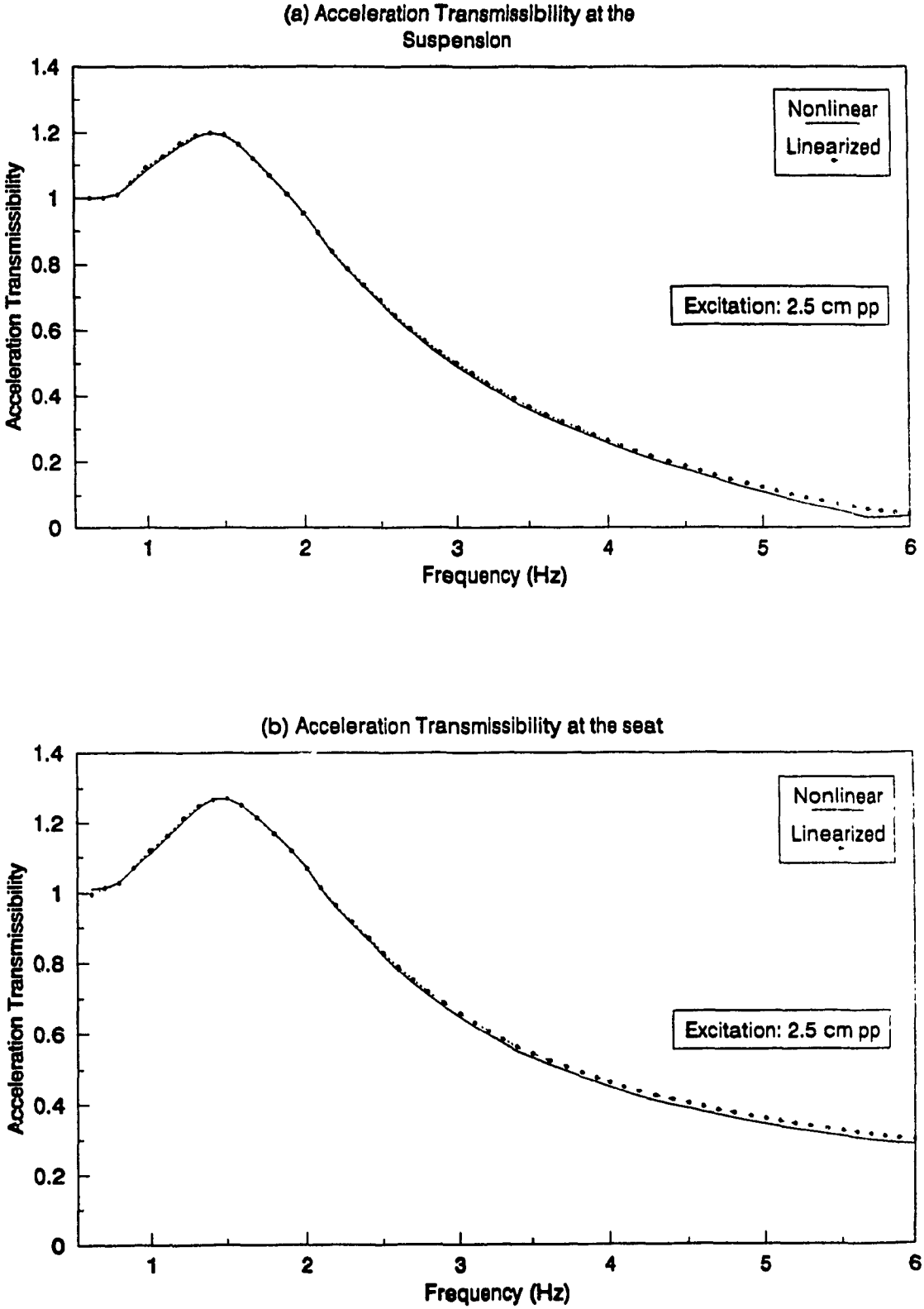

Figure 5.7. Comparison of Response Characteristics of Linearized Model with those of the Nonlinear Model (SIFRA: Behind-the-Seat Suspension).

where $\mathcal{E}_D$ and $\mathcal{E}_K$ are errors between the nonlinear and linearized damping and stiffness forces, respectively. The error between the nonlinear damping forces due to shock absorber and Coulomb damper, and the linearized damping force can be derived from Equations (2.1),(5.8) and (5.15). Assuming small viscous band around the discontinuity in friction force, for low piston velocity ($|\dot{x}_1| < V_b$), the error is obtained as:

$$\mathcal{E}_D = 0 \qquad ; \quad \text{for } |\dot{x}_1| < V_b \tag{5.27}$$

As the piston velocity exceeds the velocity associated with the viscous band (V_b), the error is caused by the linearized friction force only. The error in peak damping force can thus be expressed as:

$$\mathcal{E}_D = F_f \left(1 - \frac{4}{\pi}\right) \qquad ; \quad V_b \le \omega_k X_1 \le V_s \tag{5.28}$$

As the piston velocity exceeds the transition velocity of the shock absorber (V_s), the total error in damping forces is the sum of the errors caused by the linearized Coulomb and shock absorber damping forces. The error in damping force is then obtained as:

$$\mathcal{E}_D = \left[F_{CD} + C_{1A} V_s \, \mathrm{sgn}(\dot{x}_1) + C_{1B}\{\dot{x}_1 - V_s \mathrm{sgn}(\dot{x}_1)\}\right] \tag{5.29}$$

$$- \left[\frac{4F_{CD}}{\pi\omega X_1} + C_{1A} + \frac{C_{1B} - C_{1A}}{\pi}\left(2\omega t_1 - \sin(2\omega t_1)\right)\right] \dot{x}_1; \quad |\omega X_1| > V_s$$

Equation (5.29) reveals that the magnitude of error is dependent upon C_{1A}, C_{1B}, V_s and $\dot{x}_1$. However, as the relative velocity approaches a value considerably larger than V_s, the Equation (5.29) can be simplified to yield an

approximate expression for error in the peak damping force:

$$\mathcal{E}_D = F_f \left(1 - \frac{4}{\pi}\right) + (C_{1B} - C_{1A}) \frac{(2 - \pi)}{\pi} V_s \qquad (5.30)$$

The peak error is thus related to C_{1A}, C_{1B}, V_s, and magnitude of friction force F_f. Equation (5.30) further reveals that error due to Coulomb damping is negative, while the error due to shock absorber damping force is positive. The magnitude of error between nonlinear and linearized damping forces are illustrated in Figures 5.8a and 5.8b. Figure 5.8a shows the error for total damping forces, while Figure 5.8b presents the error in the damping forces due to the shock absorber alone.

The local equivalent linearization technique, estimates the stiffness coefficients due to nonlinear springs, using the principle of energy similarity. An error in representing the nonlinear stiffness by a linearized stiffness is thus caused in a manner similar to the damping mechanism. The error in nonlinear and linear stiffness forces can be derived using Equations (5.19) and (5.24). It can be seen that the magnitude of error remains zero as long as the relative displacement of the suspension mass with respect to the base does not exceed the permissible travel (β):

$$\mathcal{E}_K = 0 \; ; \qquad |X_1| \leq \beta \qquad (5.31)$$

However, as the relative displacement exceeds the permissible travel, a contact with the bump stops is encountered. For this case the error between the nonlinear and linear forces is then obtained as:

$$\mathcal{E}_K = \left[K_{1A}\beta\,\mathrm{sgn}(X_1) + K_{1B}(X_1 - \beta\,\mathrm{sgn}(X_1)) \right] - \left[(K_{1A} - K_{1B})\frac{\beta^2}{X_1^2} + 2(K_{1A} - K_{1B})(X_1 - \beta)\frac{\beta}{X_1^2} + K_{1B} \right] X_1 \; ; \quad |X_1| \geq \beta \tag{5.32}$$

Equation (5.32) is further simplified and the error function is expressed as:

$$\mathcal{E}_D = (K_{1A} - K_{1B})\,\beta \left(\frac{\beta}{X_1} - 1 \right) ; \quad |X_1| \geq \beta \tag{5.33}$$

A comparison of the linearized and the nonlinear restoring forces, presented in Figure 5.9, clearly illustrate that the error tends to increase only when the suspension deflection exceeds the permissible travel.

The vibration attenuation performance of a nonlinear suspension system is dependent on the magnitude of excitation, as demonstrated by the experimental transmissibility characteristics of the seat-suspension systems, shown in Figures 4.3 to 4.7. This dependency of vibration attenuation performance is investigated by studying the frequency response characteristics of the linearized ISRI mechanical seat-suspension model for varying amplitudes of sinusoidal excitations (i.e. 1.25 cm pp, 2.5 cm pp, and 3.75 cm pp). Figures 5.10a and 5.10b illustrate the acceleration transmissibility characteristics at the suspension mass and at the driver mass, respectively. These figures show similar characteristics as those illustrated in the experimental results. An increase in excitation amplitude yields an increase in acceleration transmissibilities, and a reduction in the resonant frequency of the suspension system.

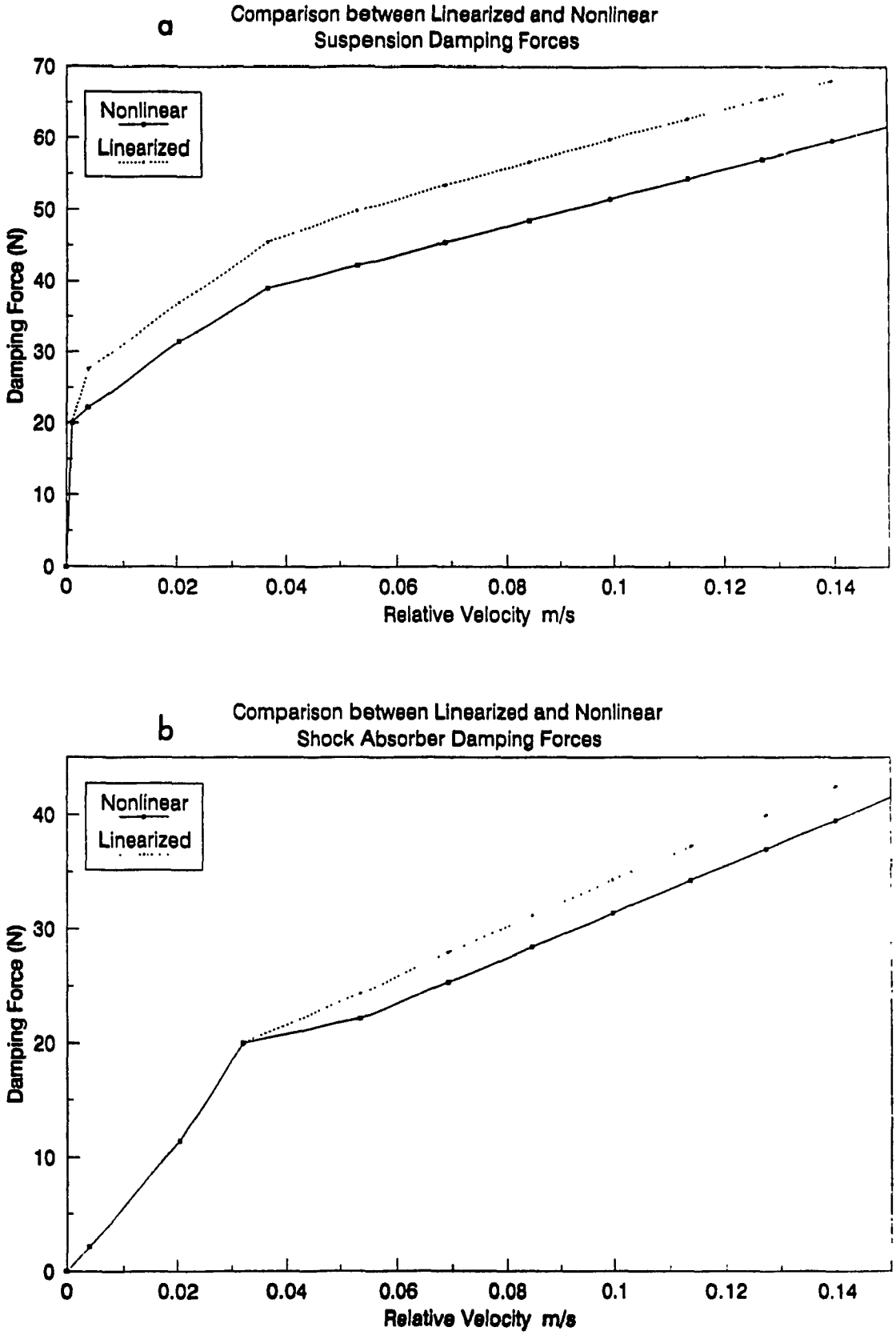

Figure 5.8. Comparison of Linearized and Nonlinear Damping Forces: (a) Total Damping, (b) Shock Absorber Damping.

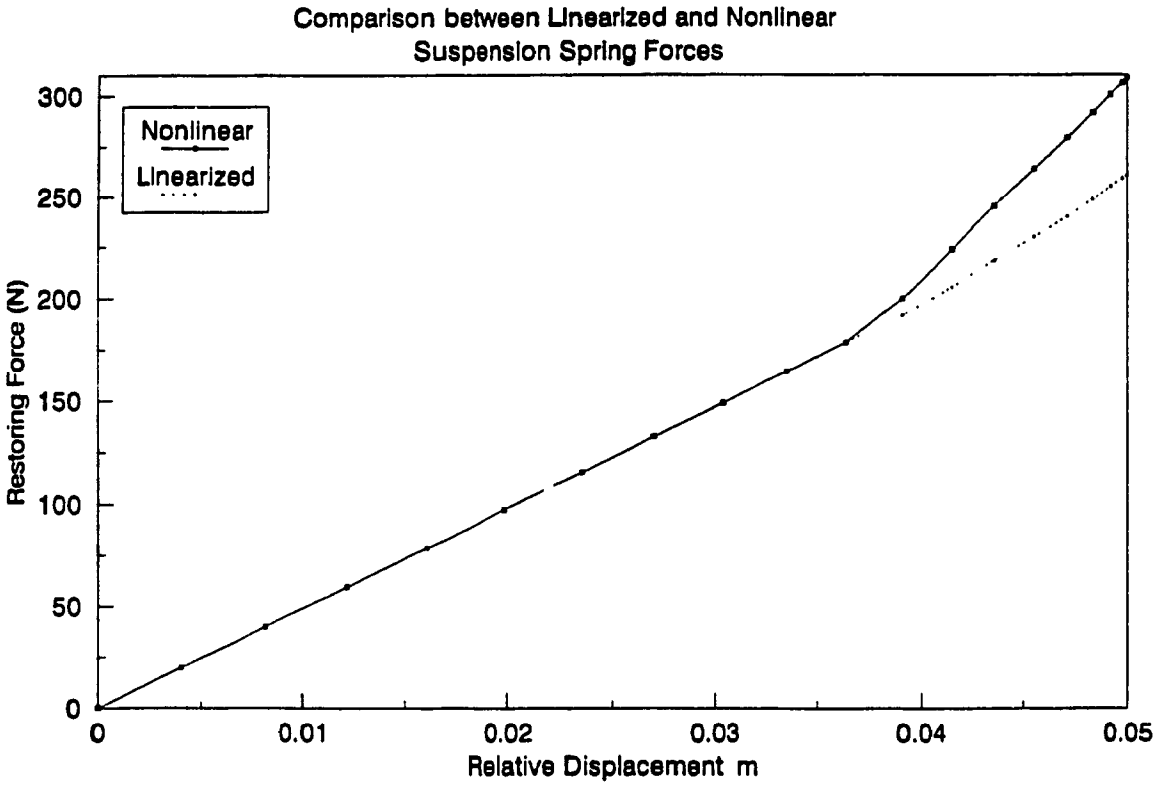

Figure 5.9. Comparison of Linearized and Nonlinear Restoring Forces.

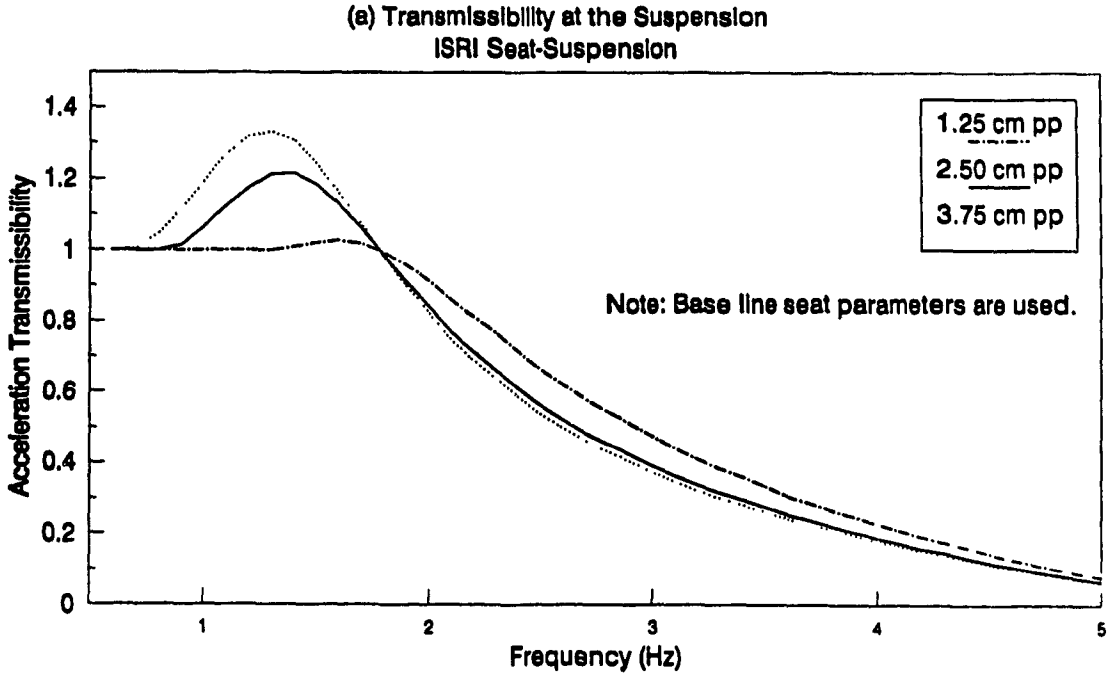

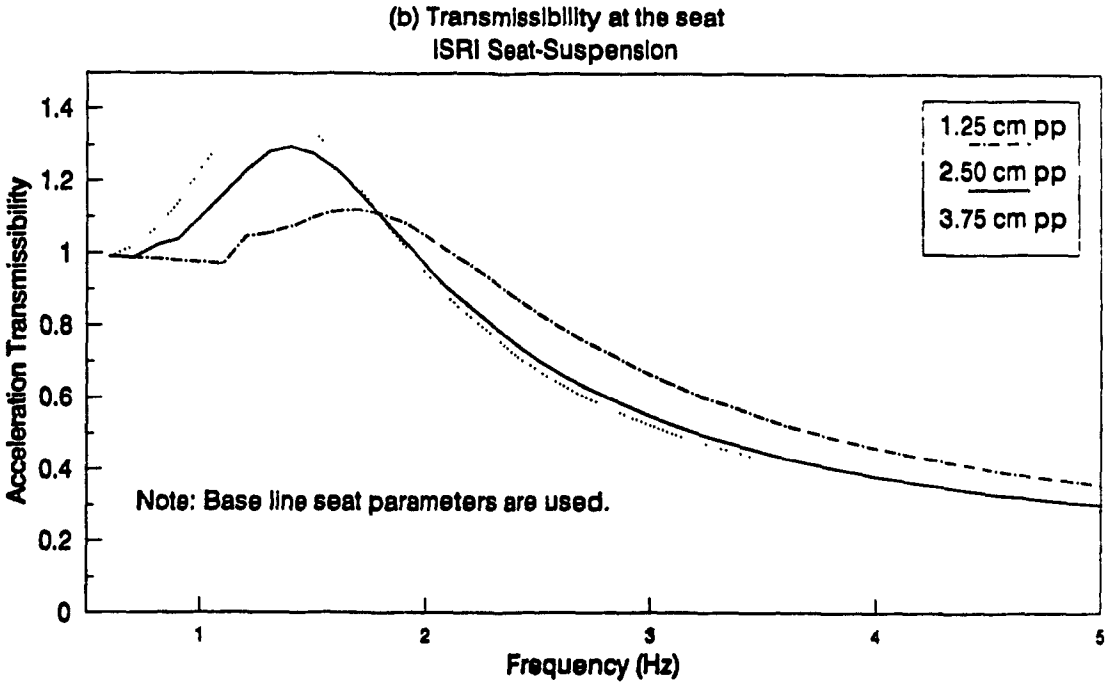

Figure 5.10. Influence of Excitation Amplitude Z_0 on the Seat Acceleration Transmissibility:(a) Suspension; (b) Seat.

5.6 RANDOM RESPONSE ANALYSIS

Ride vibration of an off-road vehicle is random in-nature, often expressed by its power spectral density (PSD). The seat-suspension system is represented by its complex frequency response function, which is used as a transfer function operating on the random vibrations of the cab floor to derive the vibration response spectrum of the seat. Linear analytical models of dynamic systems are conveniently expressed by their frequency response function in order to carry out random response analysis. Nonlinear analytical models of dynamic systems, however, are described by the frequency response functions of their linear equivalent models such that convenient linear analytical tools may be applied to evaluate their response.

5.6.1. Discrete Harmonic Linearization

Discrete harmonic linearization technique can be applied to express the nonlinear vehicle model by an array of local equivalent linear models, where each linear model describes the nonlinear model's behavior in the vicinity of a discrete frequency. Complex frequency response of the local equivalent model can thus be generated to be used as the transfer function operating on the random cab vibrations. Determination of local equivalent constants, however, requires prior knowledge of relative displacement response across the nonlinear elements corresponding to a selected excitation frequency as illustrated in Equations (5.14), (5.17), and (5.24). Since the relative displacement response is dependent upon the excitation amplitude, the random cab floor excitation is represented by an equivalent deterministic excitation to estimate the excitation amplitude. The iterative algorithm, presented in section 5.4.1, is then used to compute the relative displacement response and thus the local equivalent coefficients. The response evaluations are then

performed using the true acceleration PSD instead of the deterministic representation of random excitations.

The iterative methodology initially assumes the values of local equivalent constants to formulate an initial linear model at a pre-selected excitation frequency. The random cab vibration spectrum is discretized to yield the excitation amplitude corresponding to the selected excitation frequency. An excitation amplitude vector is estimated from the power spectral density of the cab vibration, in the following manner:

$$A(\omega_k) = \Psi \left[\int_{\omega_k-\Delta\omega/2}^{\omega_k+\Delta\omega/2} S_1(\omega)\, d\omega \right]^{\frac{1}{2}} \tag{5.34}$$

where $A(\omega_k)$ is the amplitude of acceleration excitation corresponding to excitation frequency ω_k, $S_1(\omega)$ is the PSD of acceleration of the cab floor, $\Delta\omega$ is a small frequency band around the center frequency ω_k, and Ψ is a constant. An acceleration time history is then synthesized using sine series approximation:

$$\ddot{z}_0(t) = \sum_{k=1}^{N} A(\omega_k)\, \mathrm{Sin}(\omega_k t + \varphi_k) \tag{5.35}$$

where N is total number of discretized excitation frequencies, and φ_k is the randomly distributed phase angle. The synthesized time history, estimated from Equation (5.35), is expressed by its acceleration PSD using Fast Fourier Transform [64], and compared to the true cab floor acceleration PSD as, shown

in Figure 5.11. The figure clearly illustrates that the excitation amplitude can be effectively estimated using the sine-series approximation.

The assumed linear system can thus be solved to compute the relative displacement response using the estimated excitation amplitude, $A(\omega_k)$. Equations (5.14), (5.17) and, (5.24) are then solved to determine the local equivalent damping and stiffness constants corresponding to excitation frequency, ω_k.

The spectral density of response acceleration is then computed using the following expression:

$$S_o(j\omega_k) = H(j\omega_k, X(\omega_k)) \quad S_i(j\omega_k) \quad H^{*T}(j\omega_k, X(\omega_k)) \tag{5.36}$$

where $H(j\omega_k, X(\omega_k))$ is the complex frequency response function corresponding to excitation frequency ω_k and amplitude response $X(\omega_k)$, $S_o(j\omega_k)$ is the response acceleration PSD, 'T' designates the transpose and $H^*(j\omega_k, X(\omega_k))$ is the complex conjugate of the frequency response function.

The relative displacement response spectrum is also computed as:

$$S_{rd}(j\omega_k) = \left| \frac{H_{rd}(j\omega_k, X(\omega_k))}{\omega_k^2} \right|^2 S_i(j\omega_k) \tag{5.37}$$

where $S_{rd}(j\omega_k)$ is the relative displacement response spectrum, and $H_{rd}(j\omega_k, X(\omega_k))$ is the relative displacement frequency response function of the seat-suspension. Equations (5.36) and (5.37) clearly illustrate that the random response of seat-suspension models is evaluated for PSD of the acceleration encountered at the cab floor, while a deterministic excitation is

assumed only to determine the frequency response function of the system, as shown in Figure 5.12.

5.6.2. Random Response of Seat-Suspension Models

Random response of the seat-suspension models are evaluated using the local equivalent linearization technique, described in section 5.5.1. Figures 5.13a and 5.13b illustrate the PSD of acceleration response of the driver mass for ISRI and SIFRA seats, subjected to class I and class II cab floor excitations, respectively. The driver is represented as a rigid mass in these analyses. The magnitude of vibration transmitted at the driver-seat interface of ISRI and SIFRA seat-suspensions, respectively, is 53% and 45% of the excitation amplitude of Class I vehicles around the vehicle resonant frequency (3.2 Hz). In the case of Class II vehicle excitations, the magnitudes of vibration transmitted at the driver-seat interface around the vehicle resonant frequency range (2.6 Hz), are reduced by 37% and 25% for the ISRI and SIFRA seat-suspensions, respectively.

The response acceleration PSD at the driver-seat interface are considerably smaller than the cab floor acceleration, excitation for Class I and Class II in the 2.6-3.8 Hz and 2.3-3.2 Hz frequency ranges. The magnitude of transmitted acceleration, however, exceeds the excitation levels slightly in the extremities of these frequency ranges. This is attributed to the suspension lock-up due to extremely small levels of excitation in the extremities.

The PSD of relative displacement response of the seat mass with respect to the cab floor for Class I and Class II cab floor excitations are presented in Figures 5.14a and 5.14b, respectively. The figures illustrate that the relative displacement response of ISRI seat-suspension is higher than that of

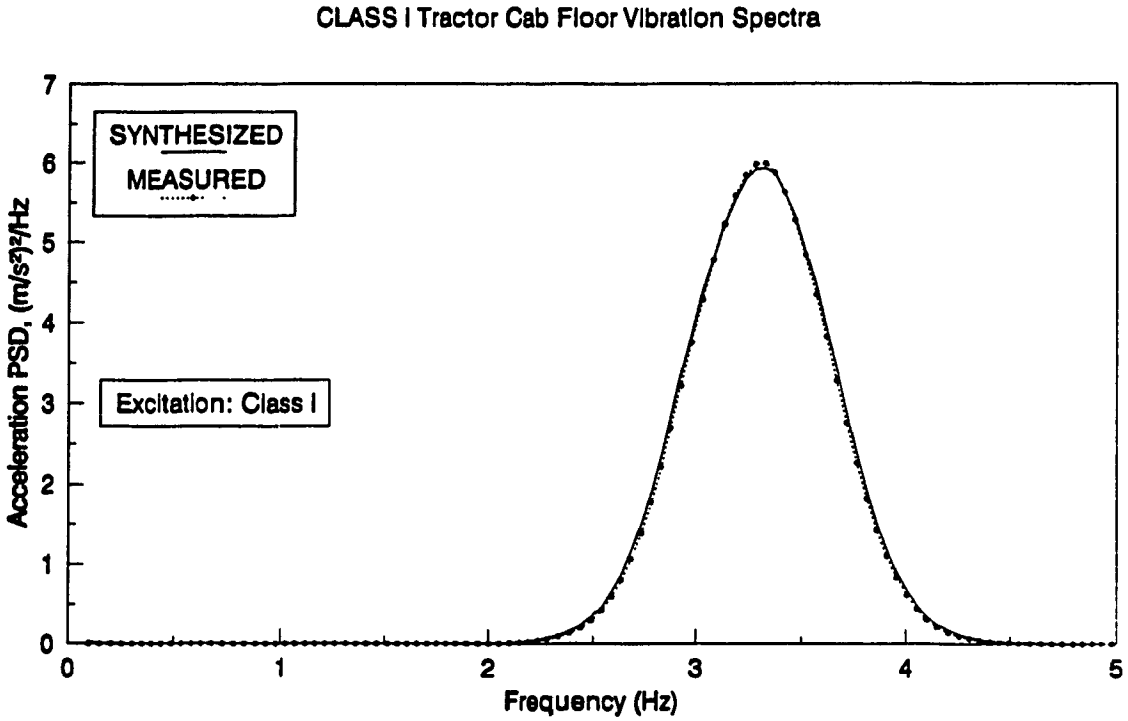

Figure 5.11. Verification of FFT Generated Spectra with Given Vibration Spectra at the Cab Floor.

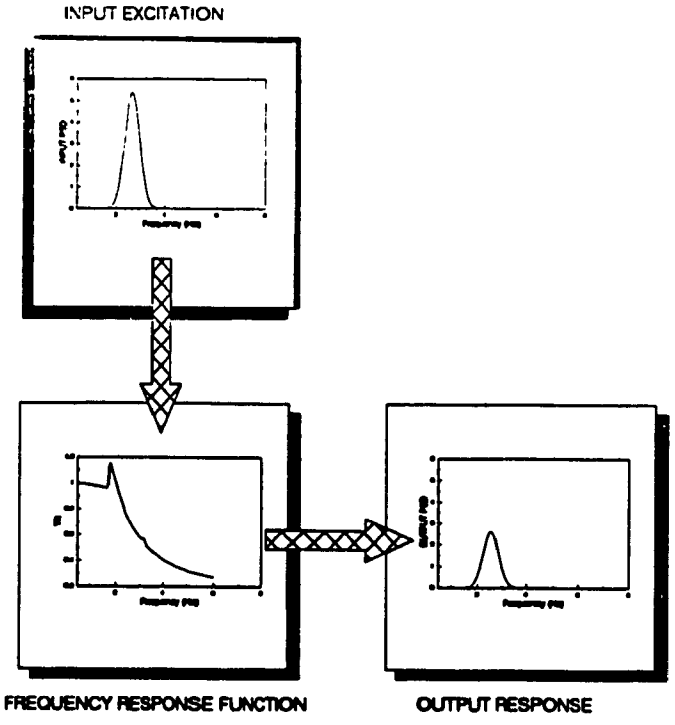

Figure 5.12. Random Response Evaluation of a Seat-Suspension Model.

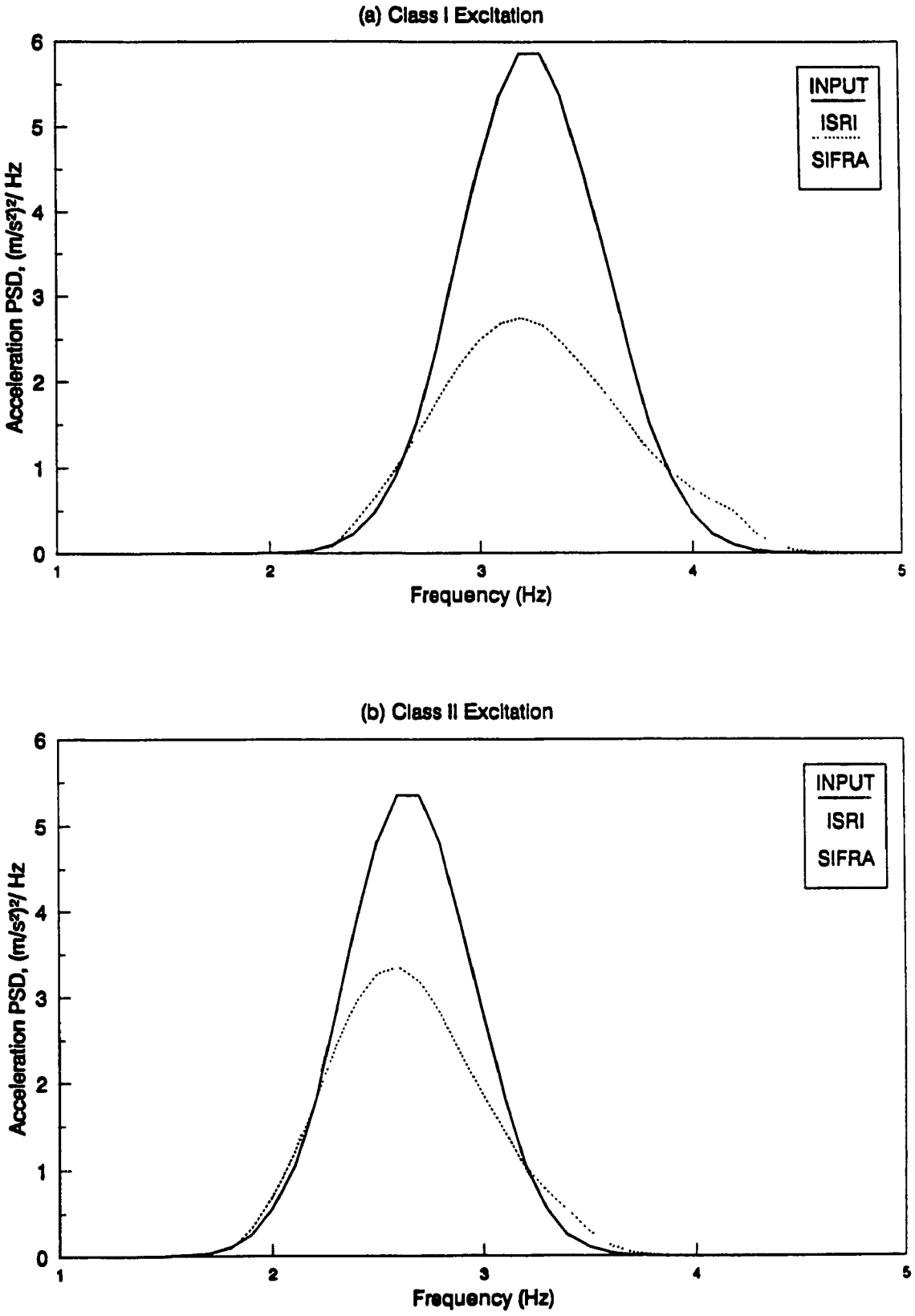

Figure 5.13. PSD of Acceleration Response at the Seat due to: (a) Class I; (b) Class II Cab Floor Excitations.

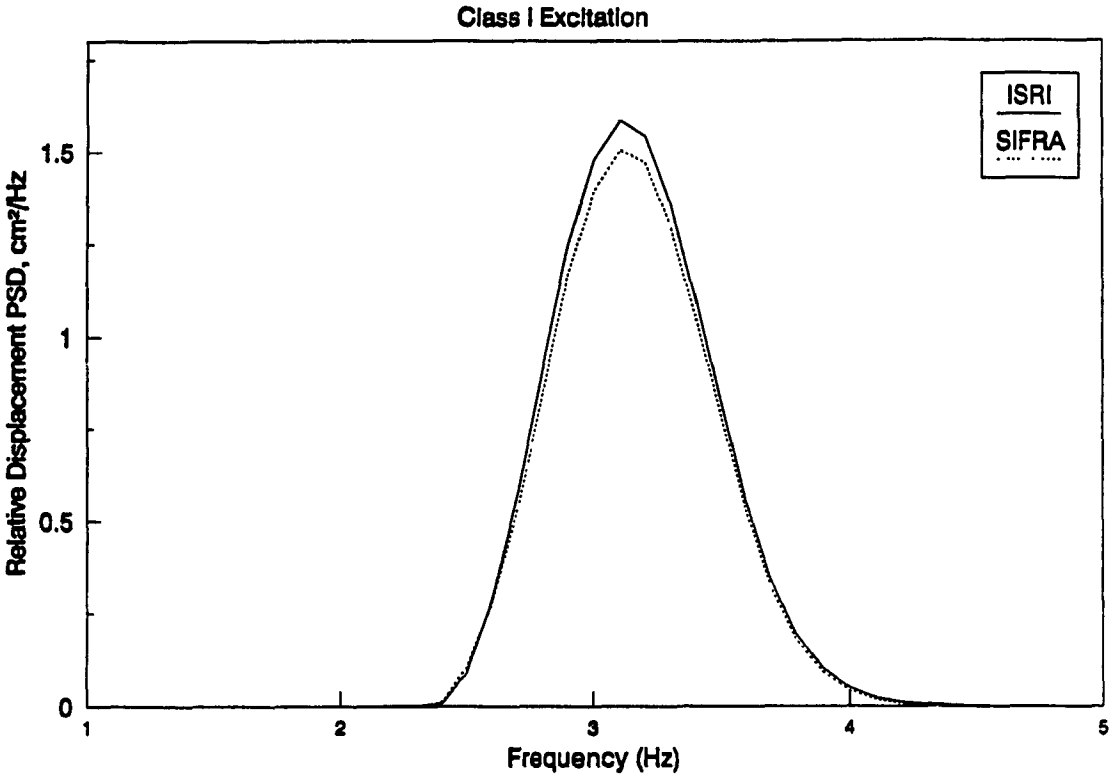

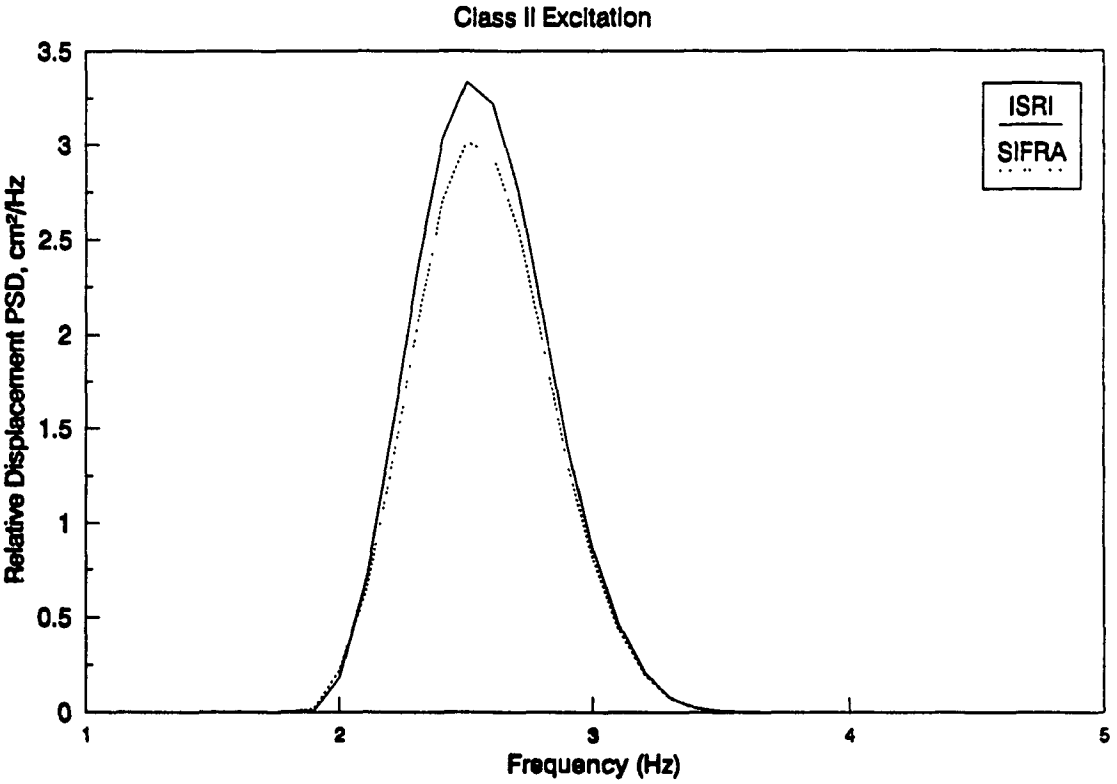

Figure 5.14. PSD of Relative Displacement Response of the Seat due to: (a) Class I; (b) Class II Cab Floor Excitations.

the SIFRA seat-suspension by 5 to 10%, for both Class I and Class II excitations.

The random ride response of two-, three- and four-degrees-of-freedom driver-seat-suspension models is further evaluated to illustrate the influence of human body dynamics on the total ride performance. Figures 5.15a and 5.15b present a comparison of the ride response at the driver-seat interface of rigid, one- and two-degrees-of-freedom driver models, for cab floor excitations arising from Class I and Class II vehicles, respectively. Figures 5.15a and 5.15b clearly illustrate that human body dynamics contributes considerably to the improvement of ride performance of seat-suspension. The one- and two-degrees-of-freedom human body models yield almost identical ride response, while the rigid mass driver model provide a very conservative estimate of the ride response. This is due to the viscoelastic property of the lumped mass human body model. Furthermore, the amplification of vibration levels in the extremities of the frequency ranges described above is considerably suppressed by the human body dynamics. The PSD of relative displacement response of the seated mass with respect to the the cab floor also reduces reasonably when the human body dynamics is taken into consideration, as shown in Figures 5.16a and 5.16b.

5.7 SUMMARY

In this chapter, simulation methods used to predict the dynamic performance of the seat suspension models, both in the time- and frequency-domains are discussed. A local equivalent linearization algorithm is employed to express the nonlinear force-deflection characteristics of bump stops, and force-velocity characteristics of dual-phase shock absorber by an array of local equivalent spring and damping constants. The effectiveness of

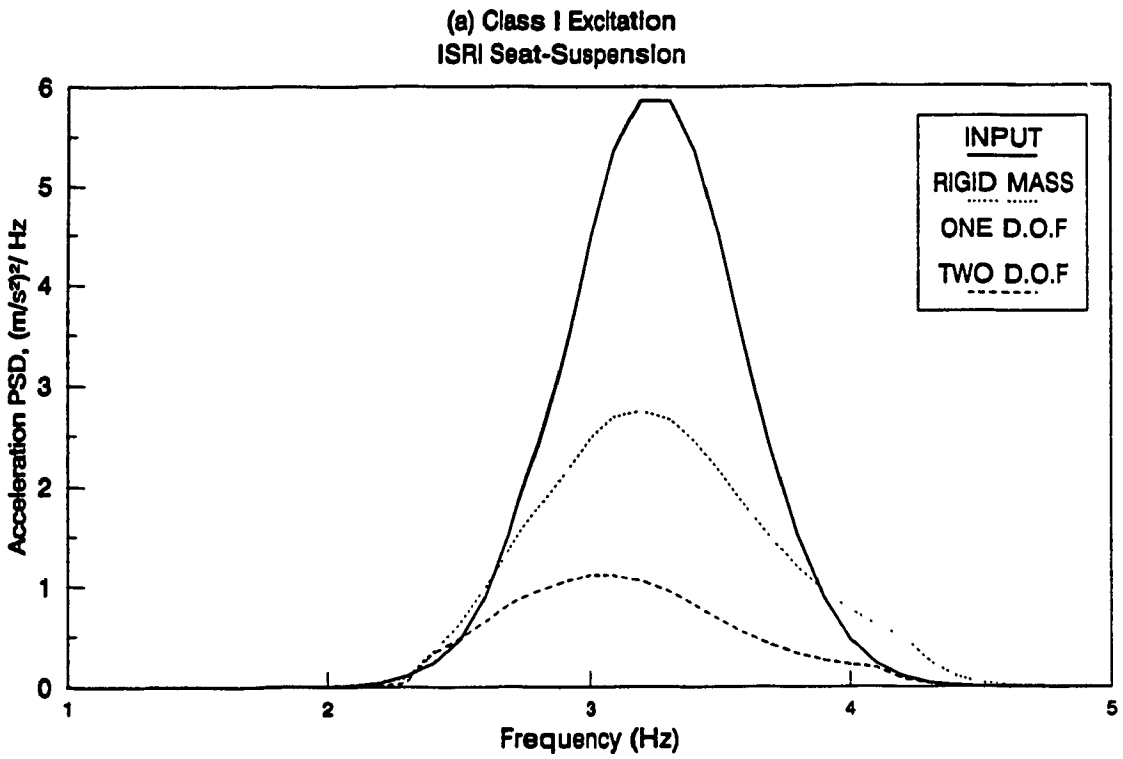

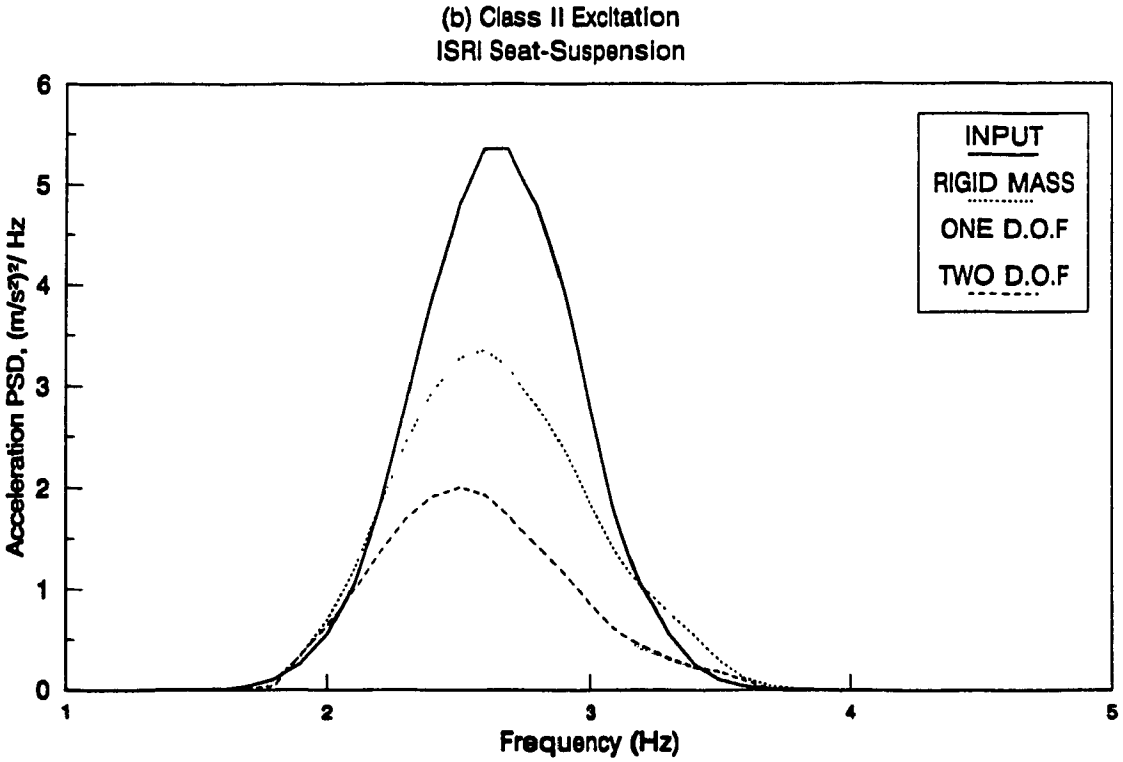

Figure 5.15. Influence of Driver Models on the PSD of Acceleration Response at the seat, due to: (a) Class I; (b) Class II Cab Floor Excitations.

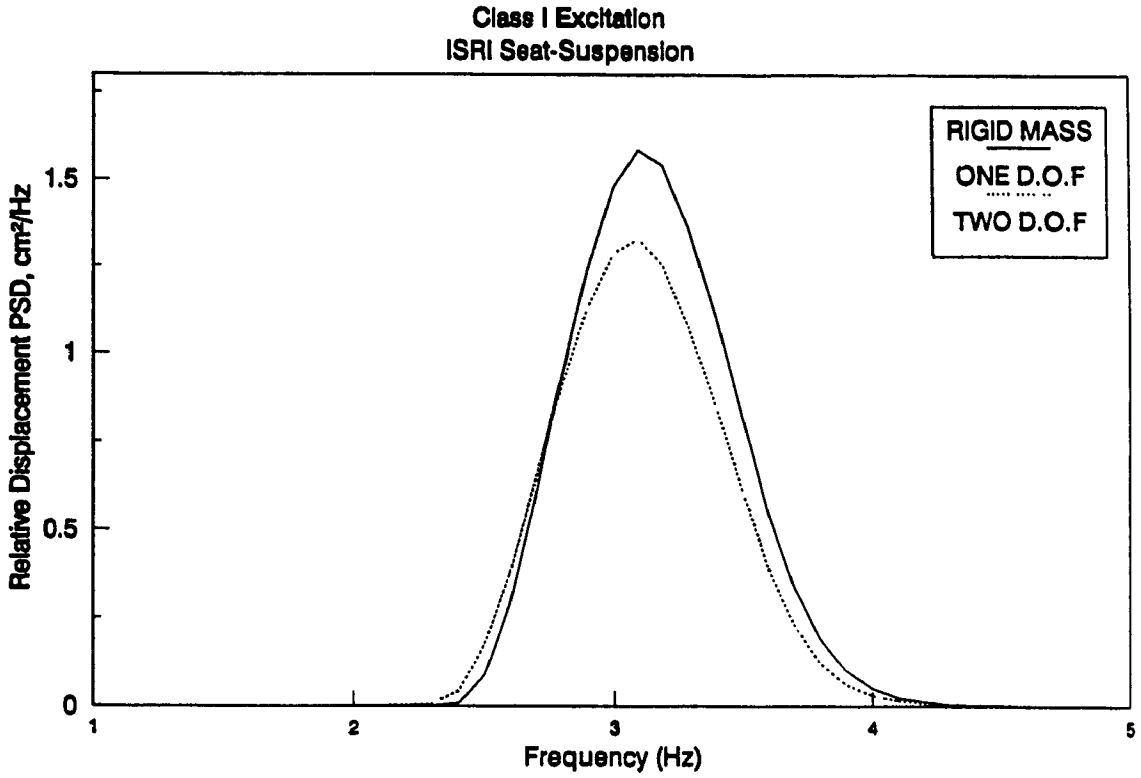

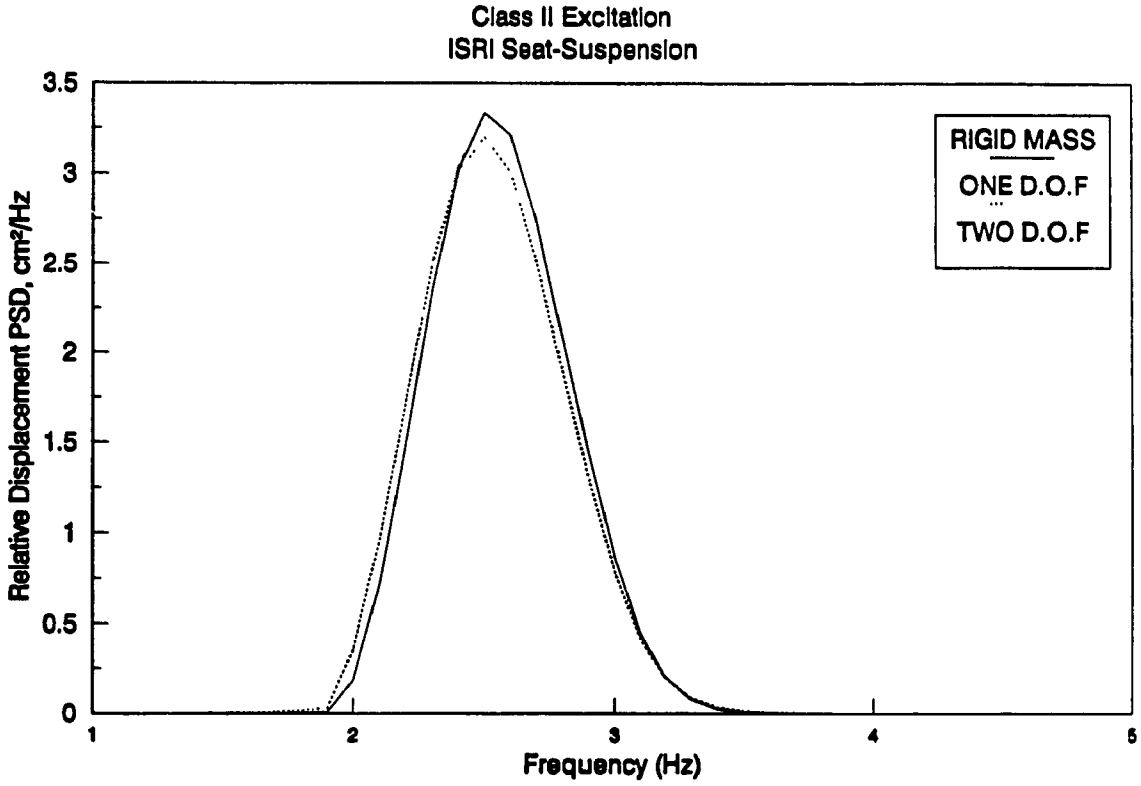

Figure 5.16. Influence of Driver Models on the PSD of Relative Displacement Response of the seat, due to: (a)Class I; (b) Class II Cab Floor Excitations.

this algorithm is verified by comparing the response characteristics of the linearized models to the respective nonlinear models subjected to sinusoidal excitations. The response characteristics of the driver-seat-suspension models are then investigated for stochastic cab floor vibrations described by their acceleration and relative displacement PSD. The ride performance of seat-suspension models is discussed to highlight the contribution of the human body models.

CHAPTER 6

PARAMETRIC STUDY AND PERFORMANCE EVALUATIONS

6.1 GENERAL

Off-road terrain irregularities transmit high amplitude ride vibration at low frequencies through the soft tires. Most off-road wheeled vehicles exhibit resonant behavior at frequencies as low as 2.6 Hz in the vertical mode, 1.5 to 3.5 Hz in the longitudinal and pitch modes, and around 1 Hz in the lateral and roll modes. Such low frequency and high amplitude ride vibrations can be attenuated by employing adequately damped low natural frequency suspension systems. Low natural frequency seat-suspension, however, provides vibration attenuation at an expense of excessive static and dynamic motion of the driver resulting in leg-pumping, inefficient driver-vehicle interactions and poor mobility. Soft suspension also cause inadequate seated height resulting in poor peripheral vision. Adequate suspension damping is further required to isolate the driver from repetitive jolts transmitted from the off-road terrains.

The effectiveness of a seat-suspension system for off-road vehicles is thus strongly related to the static and dynamic characteristics of its components such as cushion, suspension springs, shock absorber, suspension mass, Coulomb damping, and bump stops. A parametric study is thus undertaken to establish the sensitivity of suspension performance to variations in parameters of its components. The parametric sensitivity analysis can then provide a guideline to select design parameters that would yield near optimal ride at the driver-seat interface.

Parametric sensitivity analyses and performance evaluations necessitate

selection of a performance index. The performance index based on either the peak value of the steady-state response or the response spectra over a frequency range of interest, may be selected. A performance index based on the response spectra over a specified frequency range is preferred when performance evaluations are to be carried out in relation to the ISO specified fatigue decreased proficiency limits [23]. Peak values of the steady-state response to harmonic excitations may be considered to investigate the influence of suspension parameters on the vibration attenuation performance of the seat-suspension systems.

In this chapter, three performance indices are described to carry out parametric sensitivity analyses and to assess the suspension performance. The ride performance characteristics of seat-suspension systems are finally assessed using the fatigue decreased proficiency limits proposed in ISO-2631 [23].

6.2 SELECTION OF PERFORMANCE INDICES

The primary objective of the parametric sensitivity analysis is to determine suspension parameters that would yield maximum driver comfort. Although the driver comfort is related to many subjective as well as objective design and operational factors, such as placement of controls, noise, temperature, vision, etc., the driver's comfort related to vibration environment of the vehicle alone is addressed in this study. The driver's comfort related to vibration environment of the vehicle, however, needs to be defined in a quantitative manner in terms of measurable performance indices. The performance indices for vertical seat-suspension systems may be derived based on the consideration of human response to low frequency whole-body

vibrations. The three performance indices, selected to assess the seat-suspension systems are as follows:

(i) Acceleration transmissibility of seat-suspension system, specifically corresponding to resonant frequencies of the seat suspension and the vehicle.

(ii) PSD of acceleration response of the driver in the low frequency range to assess the suspension performance in attenuating terrain induced random vibrations.

(iii) PSD of relative displacement of the driver mass with respect to the cab floor to assess the seat-suspension capabilities in maintaining driver's proficiency to perform various tasks.

6.3 PARAMETRIC SENSITIVITY ANALYSES OF THE SEAT-SUSPENSION MODELS

Sensitivity of the suspension performance indices to variations in a single parameter at a time is investigated in order to determine the near optimal parameters. Specifically, the influence of cushion stiffness, suspension stiffness, suspension damping ratio, Coulomb friction, and suspension mass on the dynamic performance of the seat-suspensions are investigated. The variations are performed about the baseline values of SIFRA and ISRI seat-suspensions listed in Table 4.2. For the purpose of parametric sensitivity analyses, the nonlinear damping characteristics of the shock absorber are expressed by the following damping parameters:

$$\delta_{1A} = \frac{C_{1A}}{2\left(K_{1A}(m_0+m_s)\right)^{\frac{1}{2}}}$$

$$\delta_{1B} = \frac{C_{1B}}{2\left(K_{1A}(m_0+m_s)\right)^{\frac{1}{2}}} \qquad (6.1)$$

where δ_{1A} and δ_{1B} are damping parameters corresponding to bleed- and blow-off damping, respectively. Equations of motion for the seat-suspension models are solved using the local equivalent linearization technique and the response characteristics are presented in terms of the three selected performance criteria. The parametric sensitivity analyses are initially performed on the seat-suspension model with rigid mass representation of the driver, for both ISRI and SIFRA seat-suspension systems. Table 6.1 presents the range of various parameter values used in this parametric study classified as, A, B, C, and D. In order to investigate the effect of human body dynamics, the parametric sensitivity analyses are performed on the ISRI seat-suspension model incorporating one- and two-degrees-of-freedom driver models. The variations in parameter values are with respect to the base line parameters classified as high, base, and low values, as presented in Table 6.2.

The acceleration transmissibility values at the seat's and vehicle's resonant frequencies, and PSD of acceleration and relative displacement responses at the vehicle's resonant frequency are summarized in Tables 6.3 and 6.4. The influence of various suspension parameters on the performance of the seat-suspension systems using rigid mass, one degree-of-freedom, and two degrees-of-freedom driver models are discussed in the following subsections.

6.3.1 Influence of Cushion Stiffness

Figures 6.1a and 6.1b present the influence of cushion stiffness on the acceleration transmissibility of the driver mass of ISRI and SIFRA seats, respectively. The figures reveal that a stiffer cushion tends to reduce the resonant acceleration transmissibility, while the influence on acceleration transmissibility around the vehicle's resonant frequency (2.6 Hz) is

Table 6.1

Parameter Values of ISRI and SIFRA Seat-Suspension Models,

(Rigid Mass Driver Model).

PARAMETER	SEAT TYPE	PARAMETER VALUES A	B	C	D
CUSHION STIFFNESS, K_c (kN/m)	ISRI	80.0	70.0*	50.0	30.0
	SIFRA	90.0	82.3	60.0	40.0
SUSPENSION STIFFNESS, K_{1A} (kN/m)	ISRI	6.0	5.5	4.9	4.0
	SIFRA	6.0	5.3	4.5	4.0
SUSPENSION DAMPING RATIO, δ_{1A}	ISRI	0.40	0.48	0.60	0.70
	SIFRA	0.50	0.60	0.70	0.80
SUSPENSION DAMPING RATIO, δ_{1B}	ISRI	0.40	0.30	0.20	0.10
	SIFRA	0.60	0.50	0.30	0.10
TRANSITION VELOCITY, V_s (m/s)	ISRI	0.016	0.032	0.096	0.192
	SIFRA	0.016	0.032	0.096	0.192
COULOMB DAMPING FORCE, F_{CD} (N)	ISRI	40.0	30.0	20.0	10.0
	SIFRA	35.0	25.0	15.0	5.0
MASS RATIO, μ (m_s/m_o)	ISRI	0.35	0.27	0.20	0.15
	SIFRA	0.25	0.18	0.15	0.10

* Underlined values refer to baseline parameters

Table 6.2

Parameter Values of ISRI Seat-Suspension Model,

(One and Two D.O.F Driver Models).

PARAMETER	PARAMETER VALUES LOW	BASE*	HIGH
CUSHION STIFFNESS, K_c (kN/m)	50.0	70.0	80.0
SUSPENSION STIFFNESS, K_{1A} (kN/m)	4.0	4.9	6.0
SUSPENSION DAMPING RATIO, δ_{1A}	0.40	0.48	0.6
SUSPENSION DAMPING RATIO, δ_{1B}	0.30	0.40	0.50
TRANSITION VELOCITY, V_s (m/s)	0.016	0.032	0.092
COULOMB DAMPING FORCE, F_{CD} (N)	10.0	20.0	30.0
MASS RATIO, μ	0.20	0.27	0.35

* Refers to baseline values

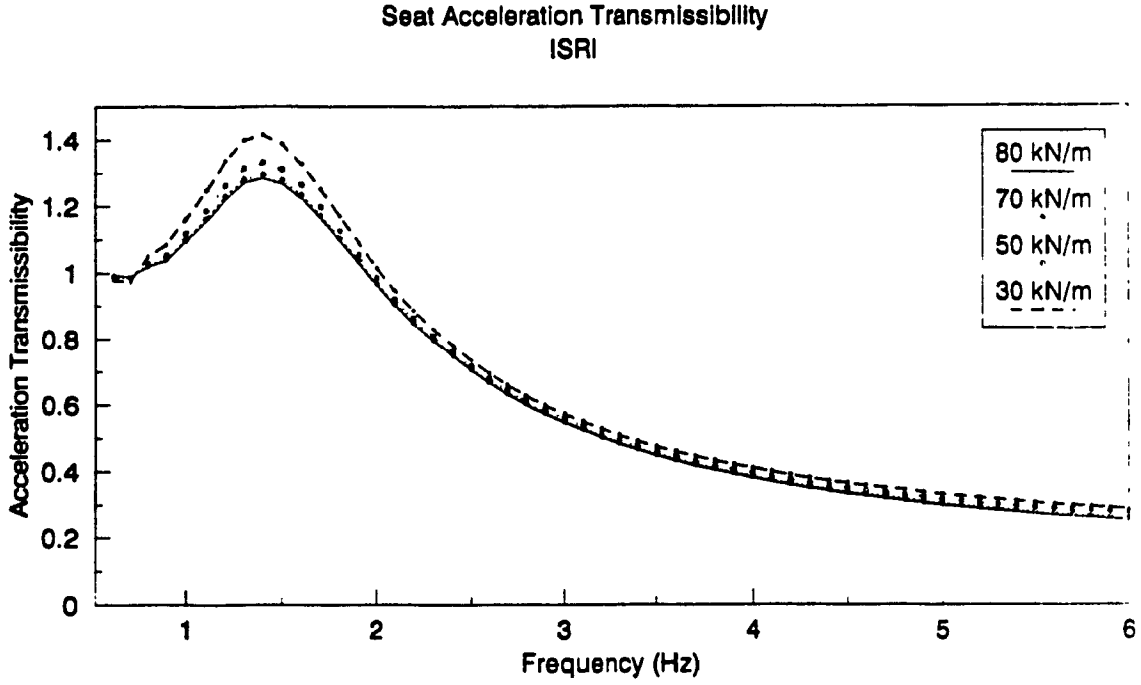

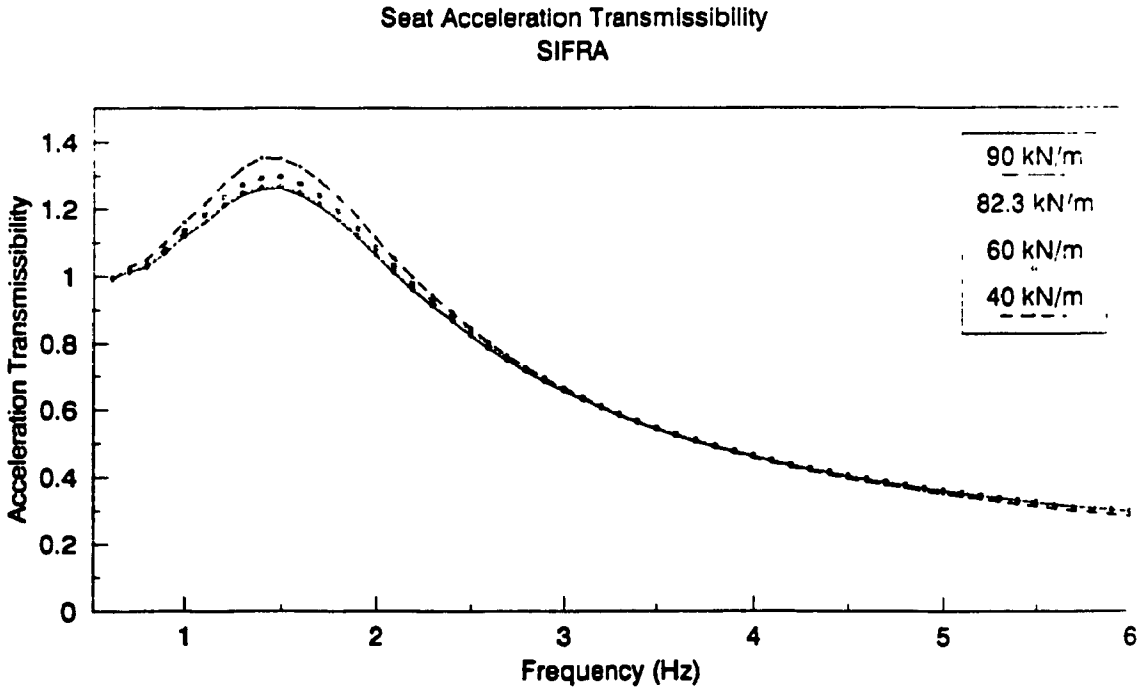

Figure 6.1. Influence of Cushion Stiffness on the Acceleration Transmissibility of the Seat: (a) ISRI, and (b) SIFRA.

insignificant. Very stiff cushions, however, encourage slouched posture and thus result in driver discomfort at the tuberosities. On the other hand, soft cushions tend to push the femur bone upward leading to increased pressure and possibly pain and discomfort at the hip joint. Softer cushions also tend to reduce the resonant frequency of the seat-suspension, from 1.5 Hz to 1.4 Hz, with a significant increase in the acceleration transmissibility of the driver mass. In view of the driver comfort and acceleration transmissibility, it is desirable to select a cushion that is neither too hard nor too soft.

Ride vibrations encountered at the cab floor dominate in the frequency band, centered around the resonant frequency of the vehicle. Class I and Class II vehicles exhibit resonant behavior around 3.25 and 2.6 Hz, respectively. Influence of cushion stiffness on the vibration attenuation performance of the seat-suspension, subjected to random ride excitations of a Class II vehicle, is investigated using the local equivalent linearization technique presented in section 5.6. The sensitivity of acceleration PSD response of ISRI and SIFRA seats, subjected to these cab floor vibrations, to variations in cushion stiffness are presented in Figures 6.2a and 6.2b, respectively. The figures clearly illustrate that softer cushions tend to increase the acceleration response of the driver mass significantly in the frequency range 2.0 - 3.5 Hz. The acceleration PSD specifically increases in the frequency band centered around 2.6 Hz. Soft cushions also yield large dynamic deflections of the driver mass with respect to the cab floor, as illustrated by the relative displacement PSD response shown in Figures 6.3a and 6.3b.

Parametric studies conducted using ISRI seat-suspension model with one- and two-degrees-of-freedom driver models, show similar influence of the

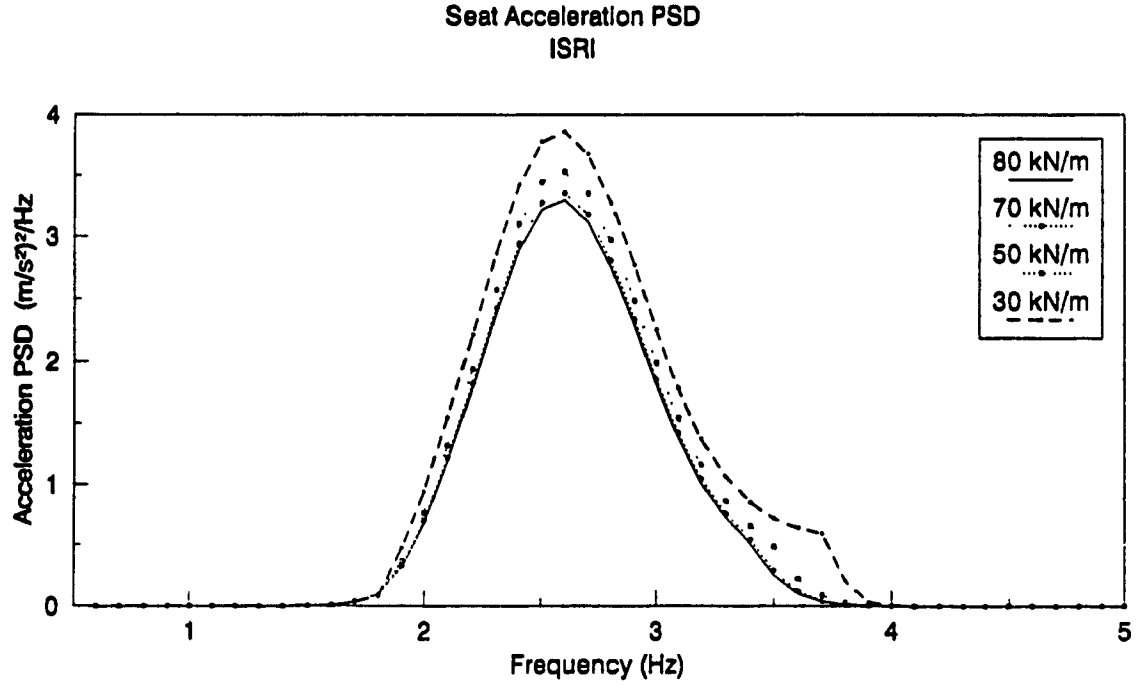

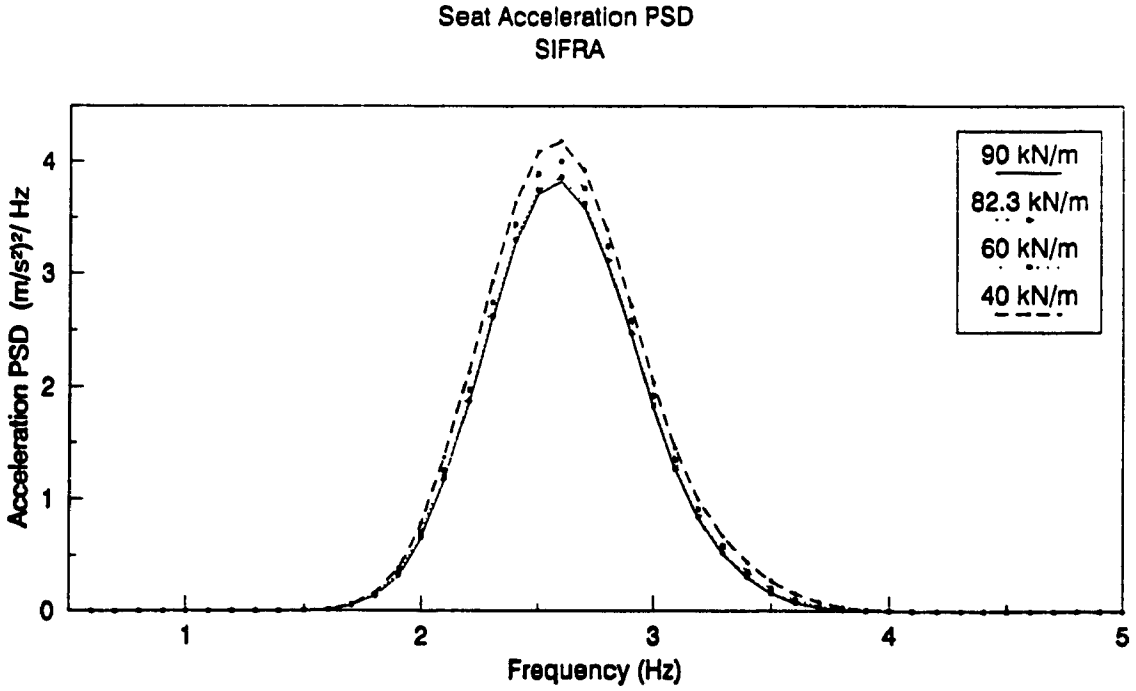

Figure 6.2. Influence of Cushion Stiffness on the PSD of Acceleration Response at the Seat: (a) ISRI, (b) SIFRA.

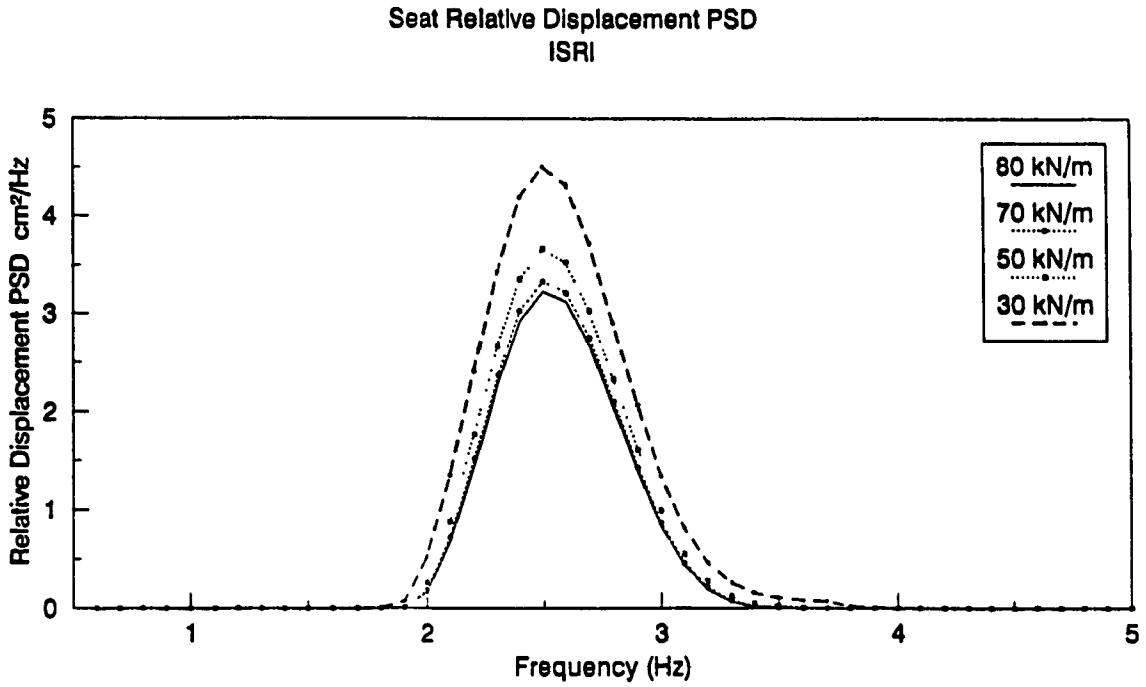

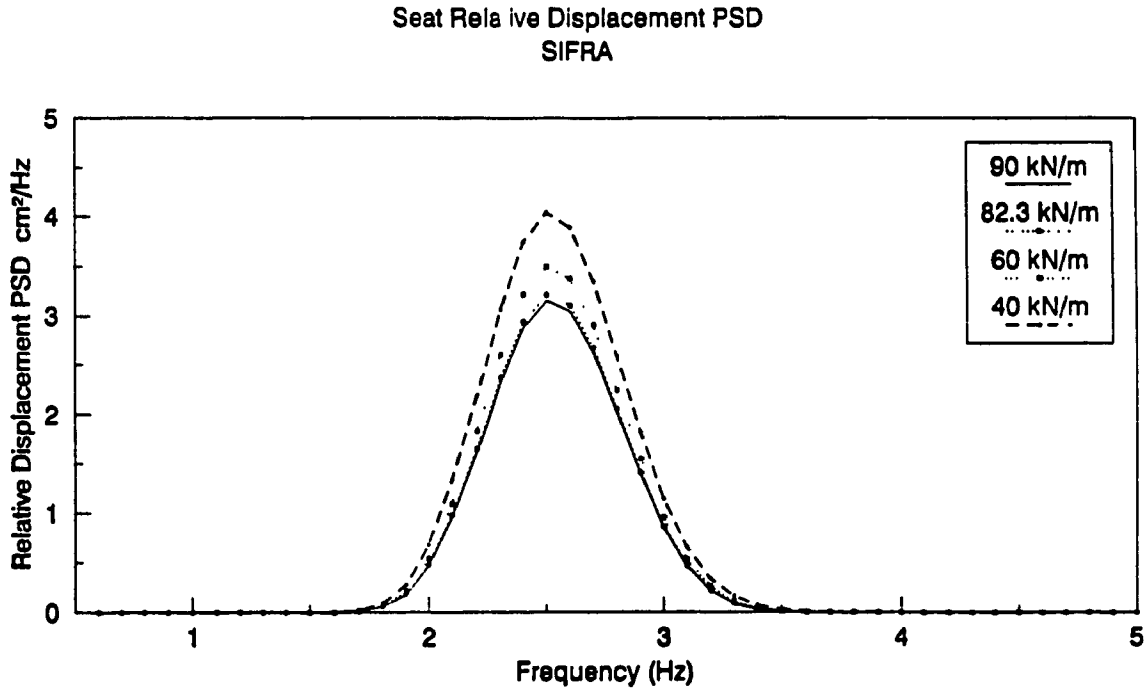

Figure 6.3. Influence of Cushion Stiffness on the PSD of Relative Displacement Response of the Seat: (a) ISRI, (b) SIFRA.

cushion stiffness. Figures 6.4 to 6.6 present the influence of cushion stiffness on the seat transmissibility, acceleration PSD, and relative displacement PSD characteristics, respectively.

Figures 6.1 to 6.6 demonstrate that firm cushions can improve suspension performance by reducing the resonant transmissibility of the seat, transmitted vibration around the vehicle's resonant frequency, and relative motion of the driver with respect to the cab floor. The slouched posture, encouraged by too stiff cushions, however, can be avoided by integrating an adjustable lumbar support within the back-rest.

6.3.2 Influence of Suspension Spring

The ride performance of a seat-suspension system is strongly influenced by its spring rate. An increase in suspension spring rate yields increased natural frequency and reduced damping factor. The resonant acceleration transmissibility of both the seats thus increases, when suspension spring rate is increased, as shown in Figures 6.7a and 6.7b. Stiffer suspension further yields high acceleration transmissibility corresponding to excitation frequencies in the vicinity of vehicle's resonant frequency. The ride performance of seat-suspension systems is thus deteriorated, when subjected to random excitations at the cab floor as demonstrated in Figures 6.8a and 6.8b. The acceleration PSD of the driver mass increases considerably corresponding to vehicle's resonant frequency, 2.6 Hz, when the suspension spring rate is increased. Although, the stiffer suspension yields lower relative displacement response of the driver's mass, with respect to the cab floor, at low excitation frequencies, the relative displacement response at vehicle's

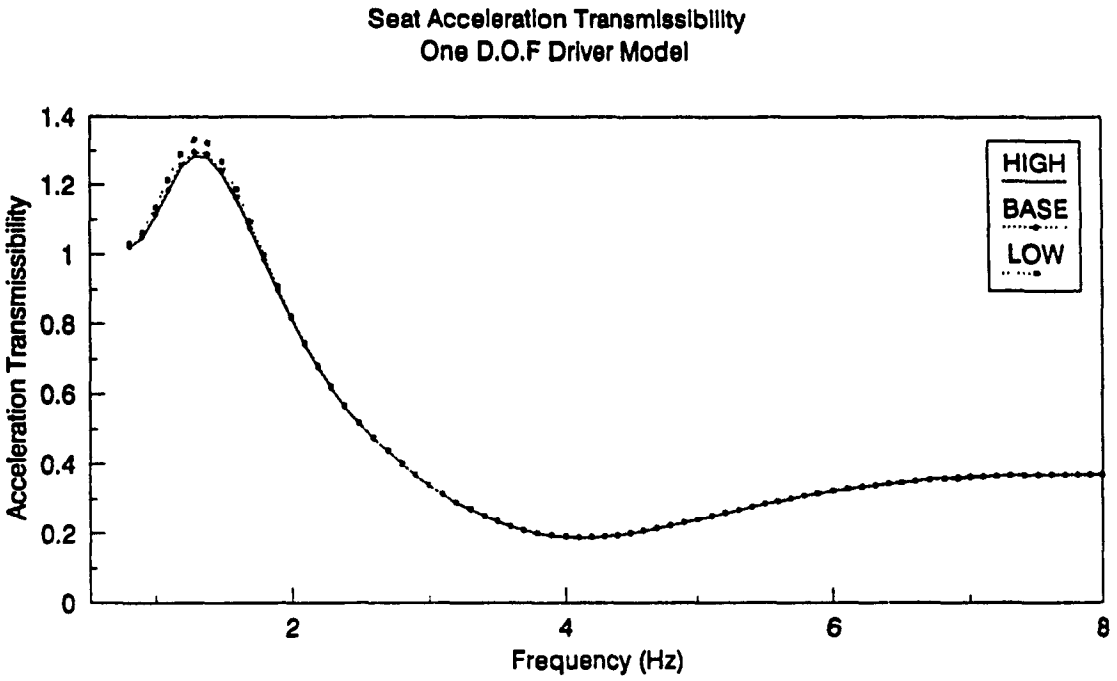

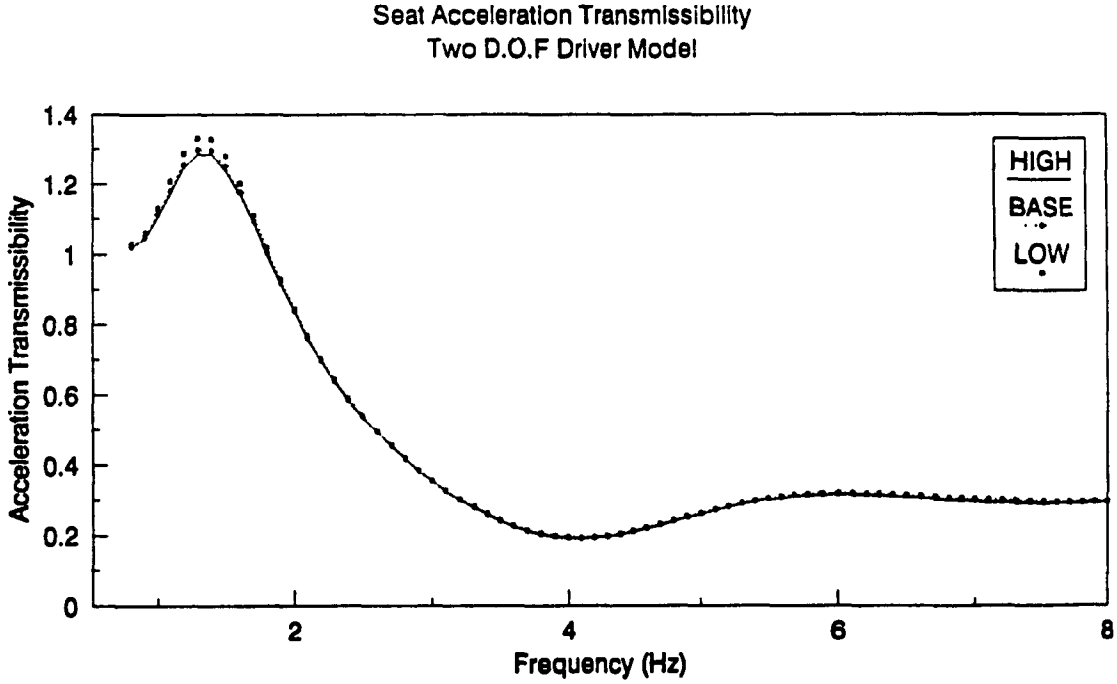

Figure 6.4. Influence of Cushion Stiffness on the Acceleration Transmissibility of the Seat Using (a) One D.O.F; (b) Two D.O.F Driver Model.

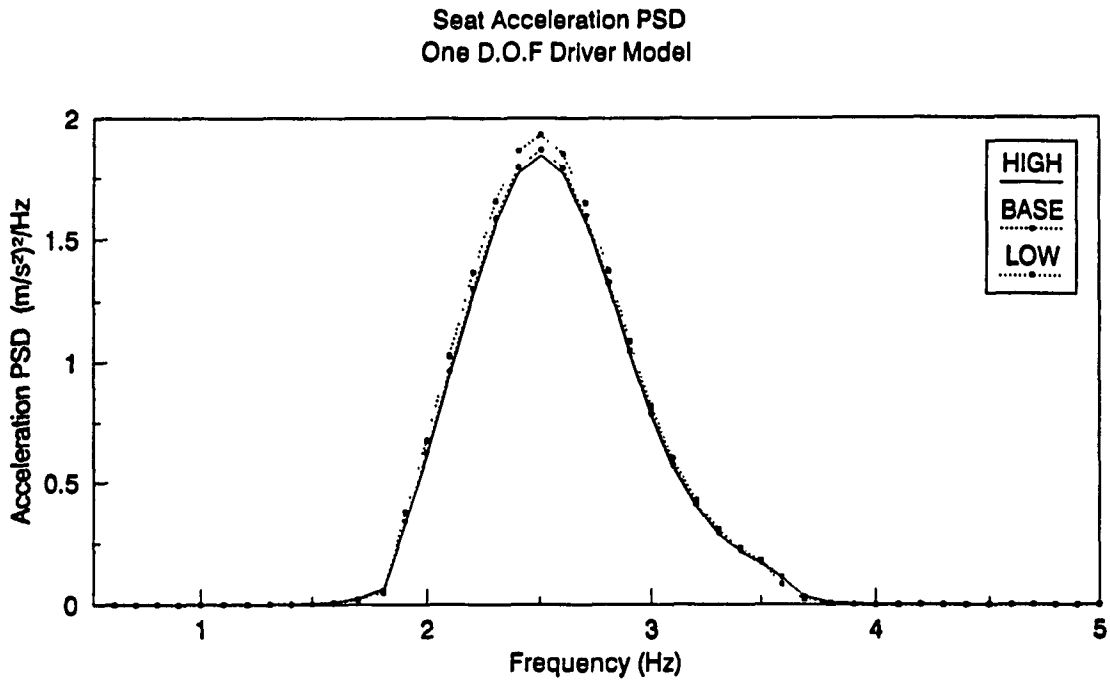

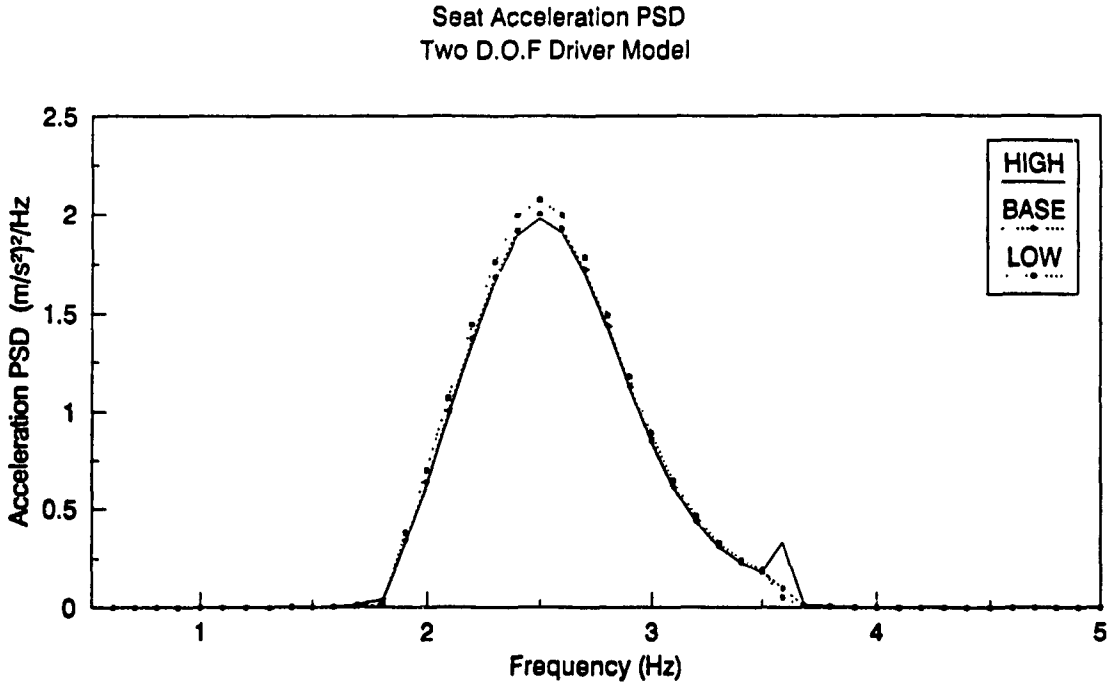

Figure 6.5. Influence of Cushion Stiffness on the PSD of Acceleration Response at the Seat Using (a) One D.O.F; (b) Two D.O.F Driver Models.

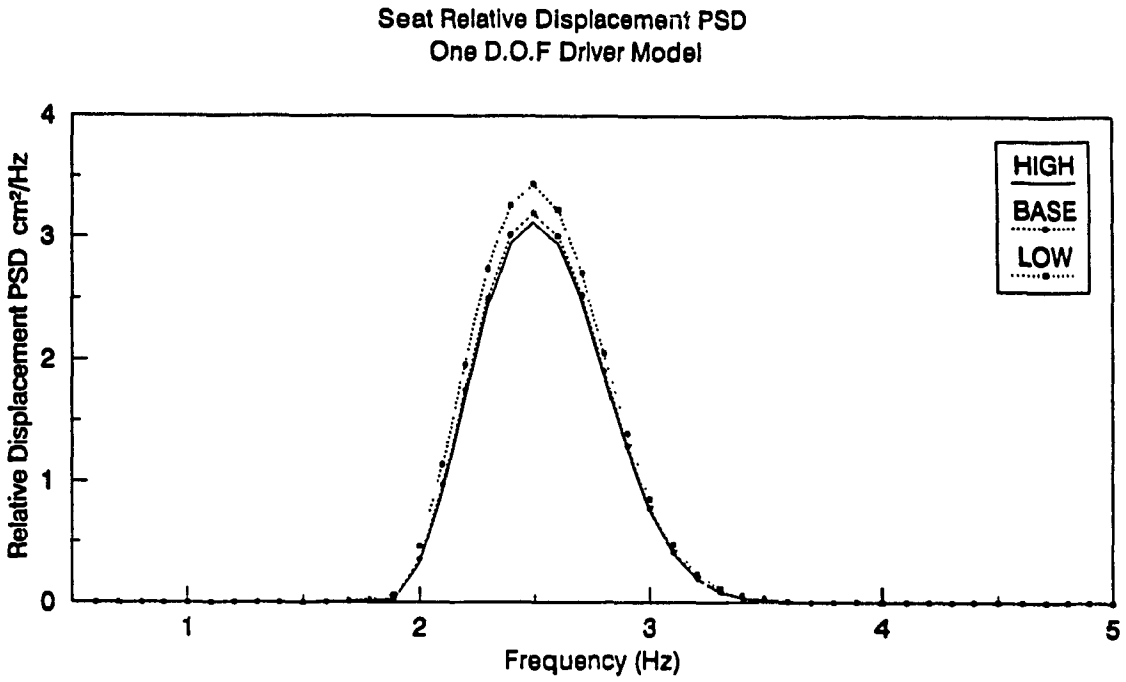

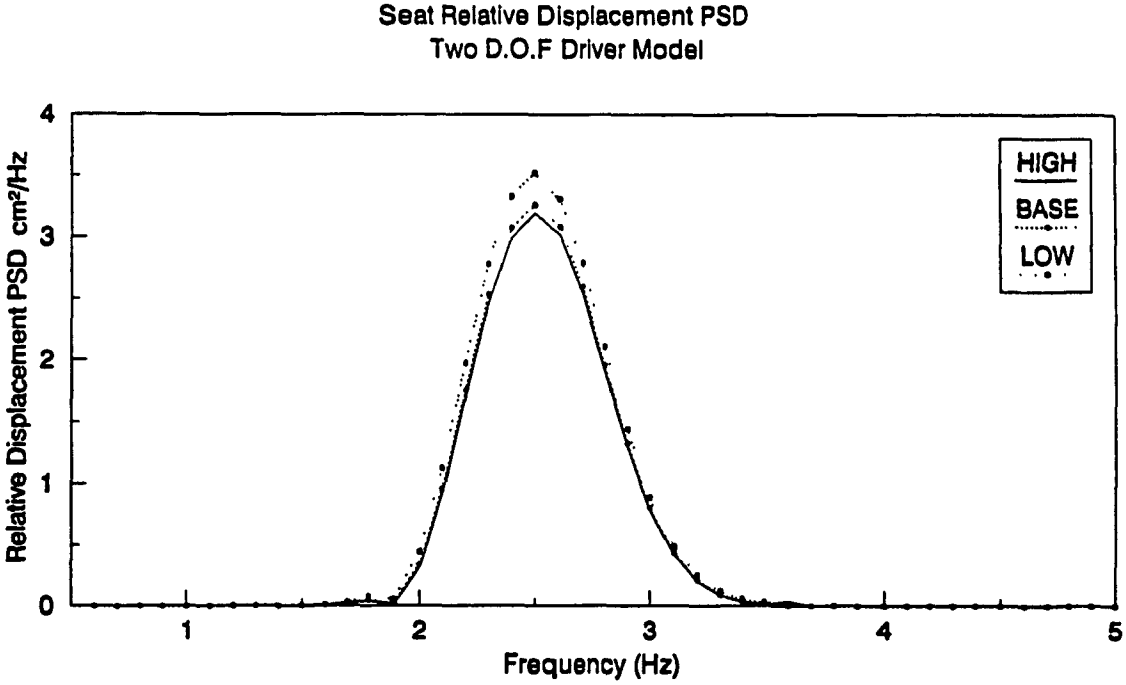

Figure 6.6. Influence of Cushion Stiffness on the PSD of Relative Displacement Response of the Seat Using (a) One D.O.F; (b) Two D.O.F Driver Models.

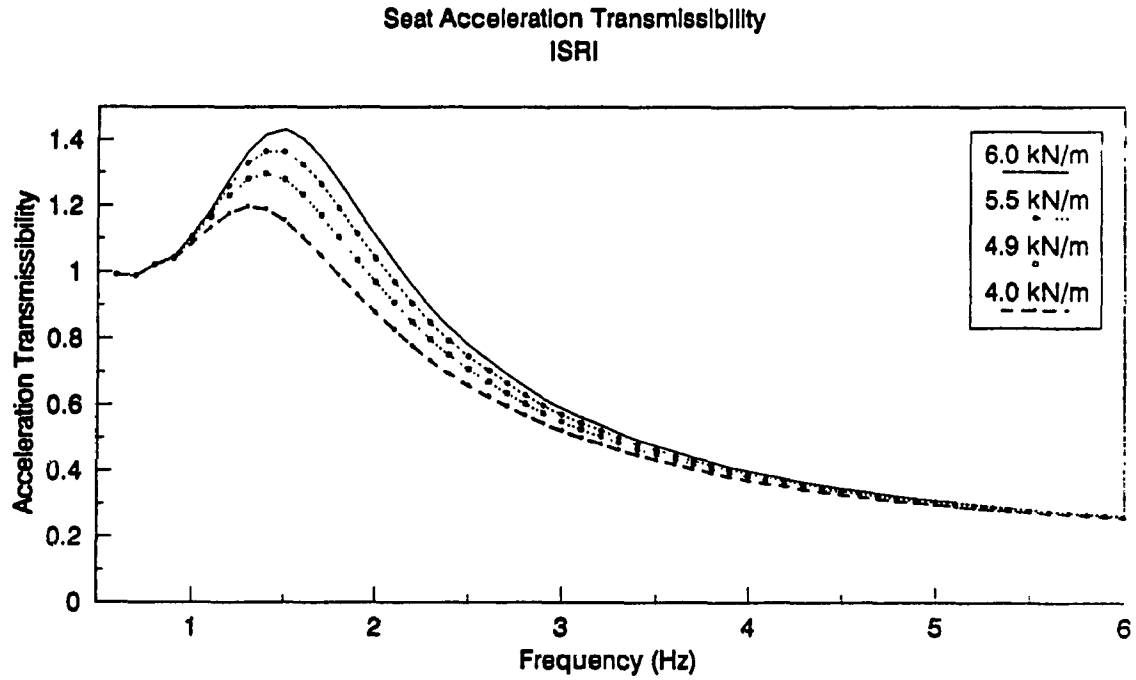

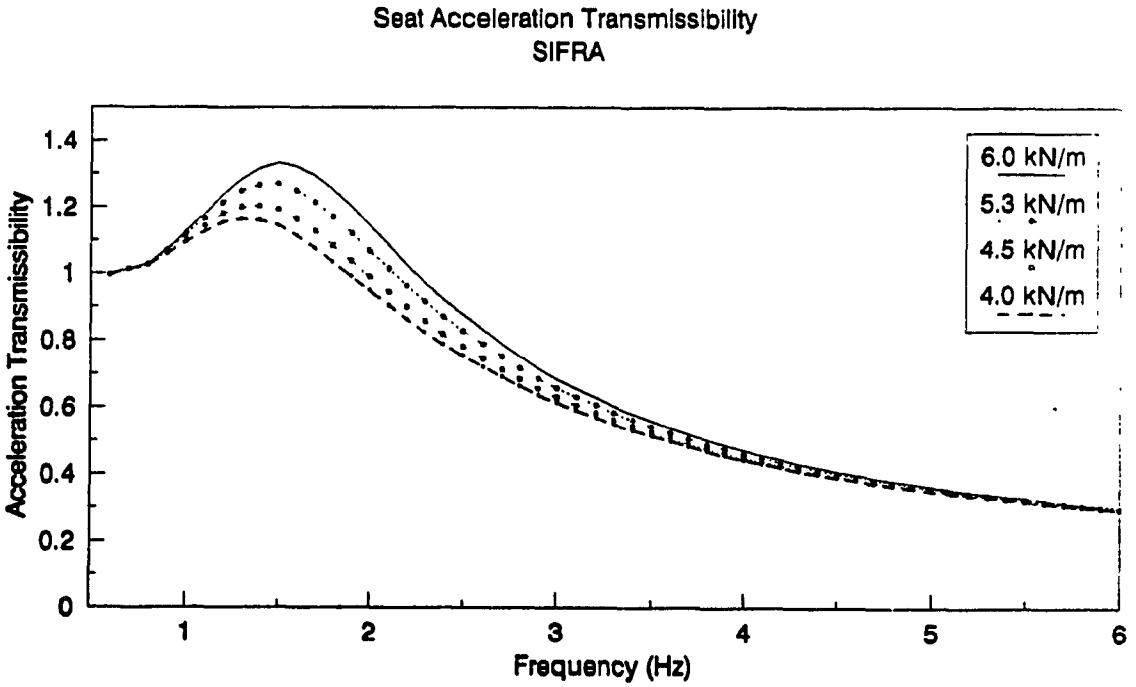

Figure 6.7. Influence of Suspension Spring Rate on the Acceleration Transmissibility of the Seat: (a) ISRI, and (b) SIFRA.

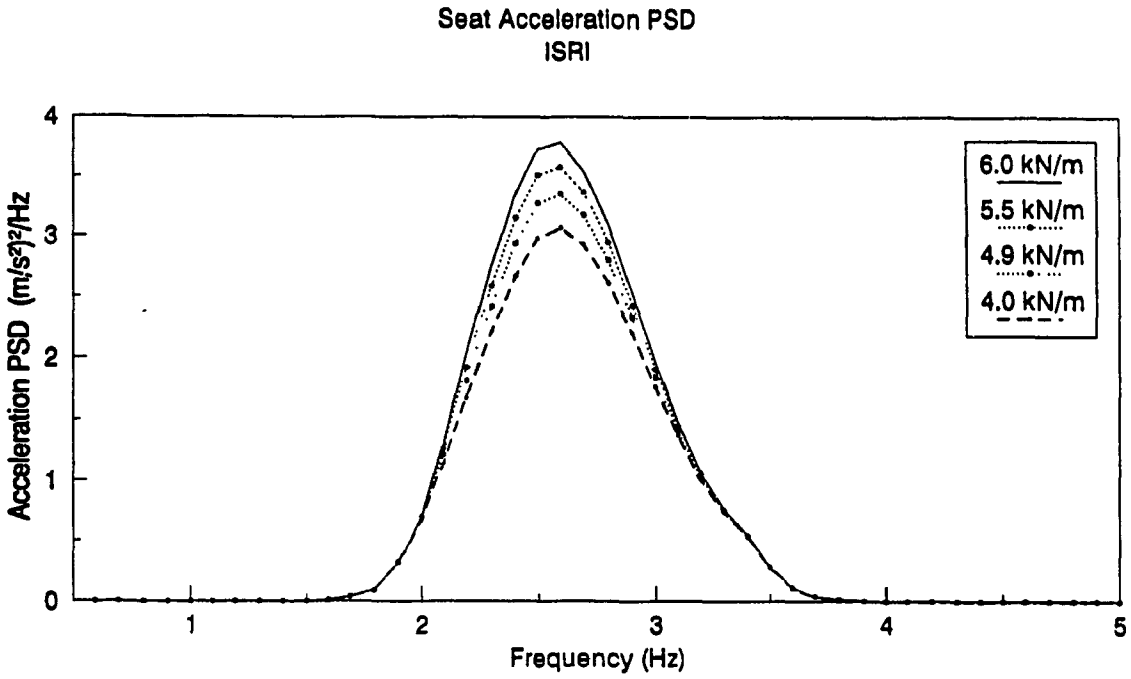

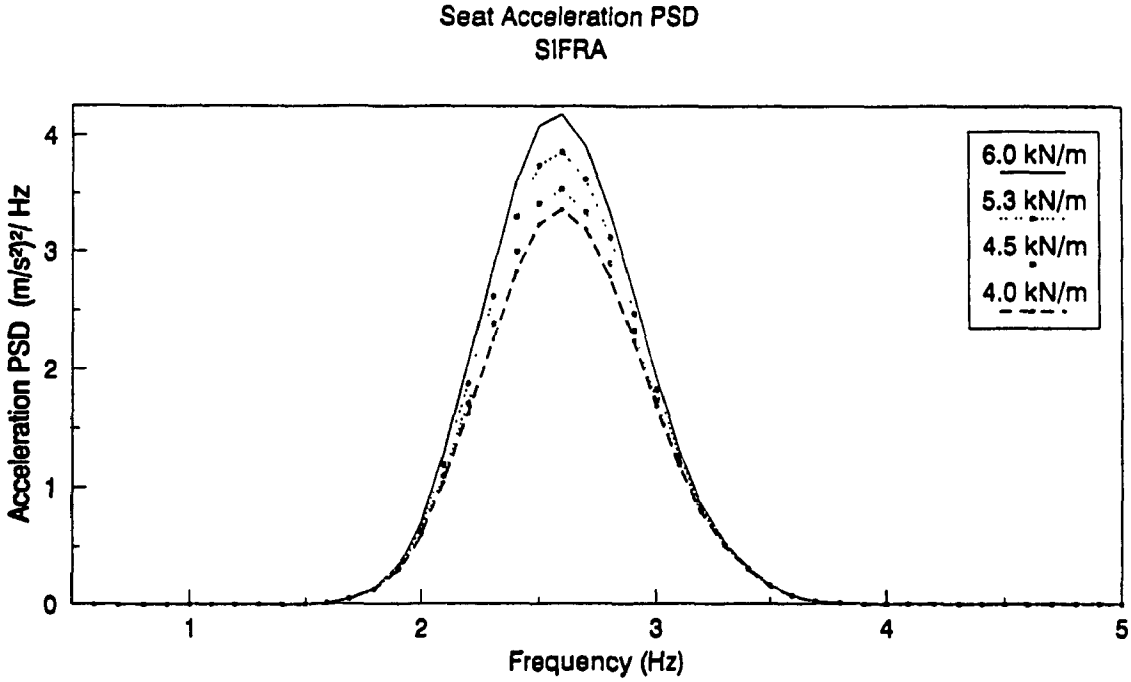

Figure 6.8. Influence of Suspension Spring Rate on the PSD of Acceleration Response at the Seat: (a) ISRI, (b) SIFRA.

resonant frequency increases with an increase in the spring rate as shown in Figures 6.9a and 6.9b.

Parametric studies conducted using ISRI seat-suspension model with one- and two-degrees-of-freedom driver models, show similar influence of the suspension spring stiffness. Figures 6.10 to 6.12 present the acceleration transmissibility, acceleration PSD, and relative displacement PSD characteristics, respectively, of the seat-suspension models incorporating dynamic human body models.

The influence of suspension spring rate on the performance characteristics can be further described in view of variation in driver's weight. A variation in driver weight alters the seat's natural frequency, and its transmissibility characteristics. It is thus extremely vital to design height/weight adjustment mechanism independent of the suspension spring rate. The spring rates must be selected such that the values of resonant acceleration transmissibility and relative displacement are within acceptable values. The resonant acceleration transmissibility less than 1.25 may be considered excellent for off-road vehicle seat-suspension systems.

6.3.3. Influence of Shock Absorber Damping Parameters

An important factor in vibration isolation is the amount of damping present in the isolator and its influence on the vibration isolation performance. In this study, the damping due to suspension shock absorber is described by two damping parameters, δ_{1A} and δ_{1B}, corresponding to bleed- and blow-off damping, as expressed in Equation (6.1). The damping parameter, δ_{1A}, during the bleed-cycle is often considerably larger than δ_{1B}.

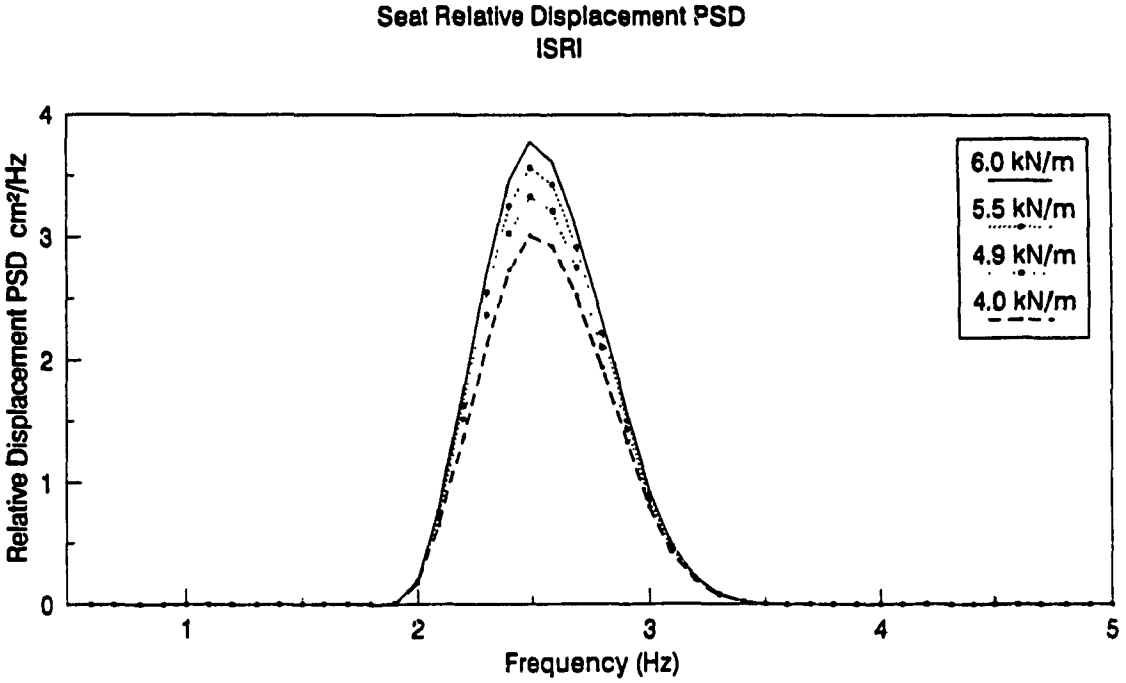

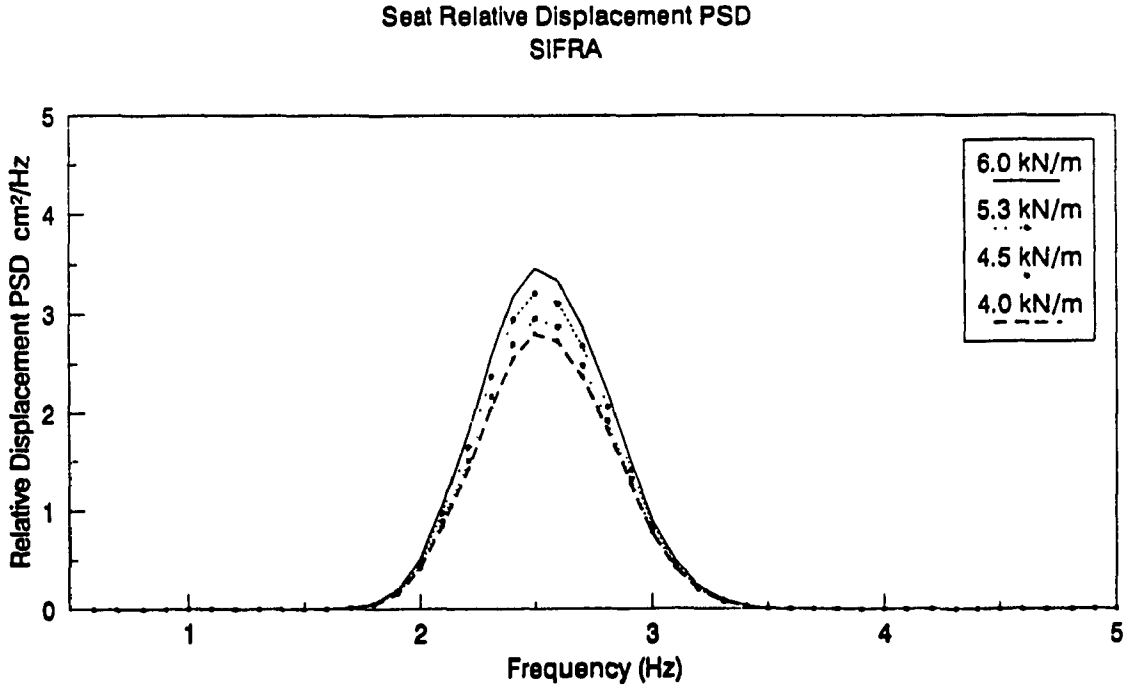

Figure 6.9. Influence of Suspension Spring Rate on the PSD of Relative Displacement Response of the Seat: (a) ISRI, (b) SIFRA.

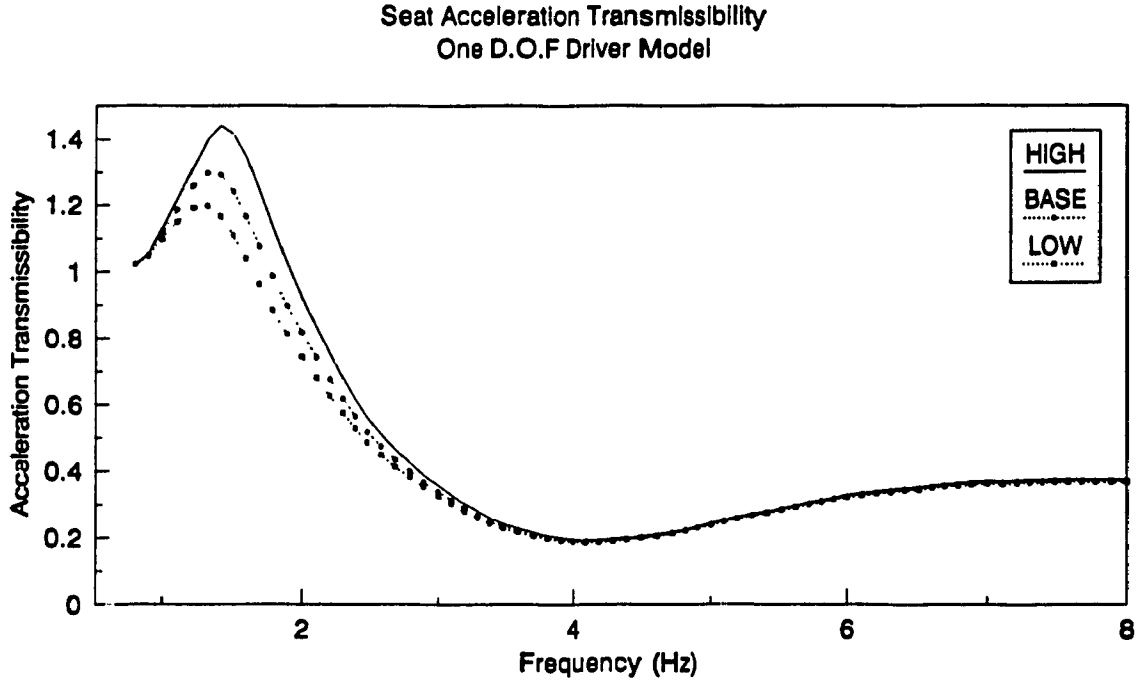

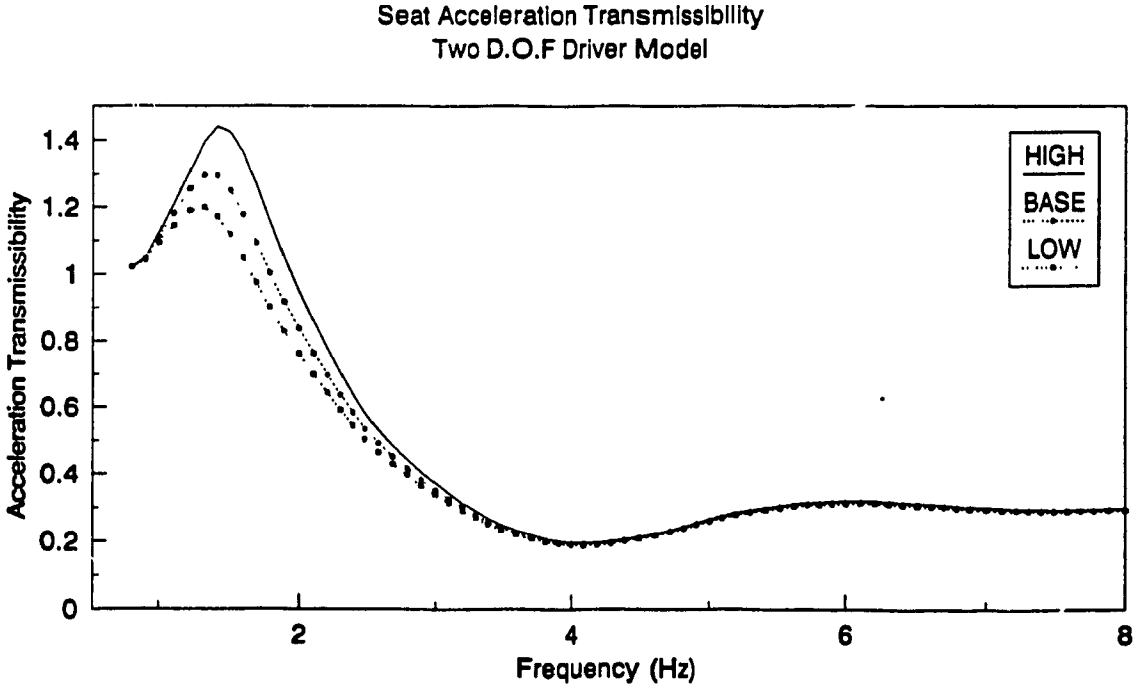

Figure 6.10. Influence of Suspension Spring Rate on the Acceleration Transmissibility of the Seat Using (a) One D.O.F; (b) Two D.O.F Driver Model.

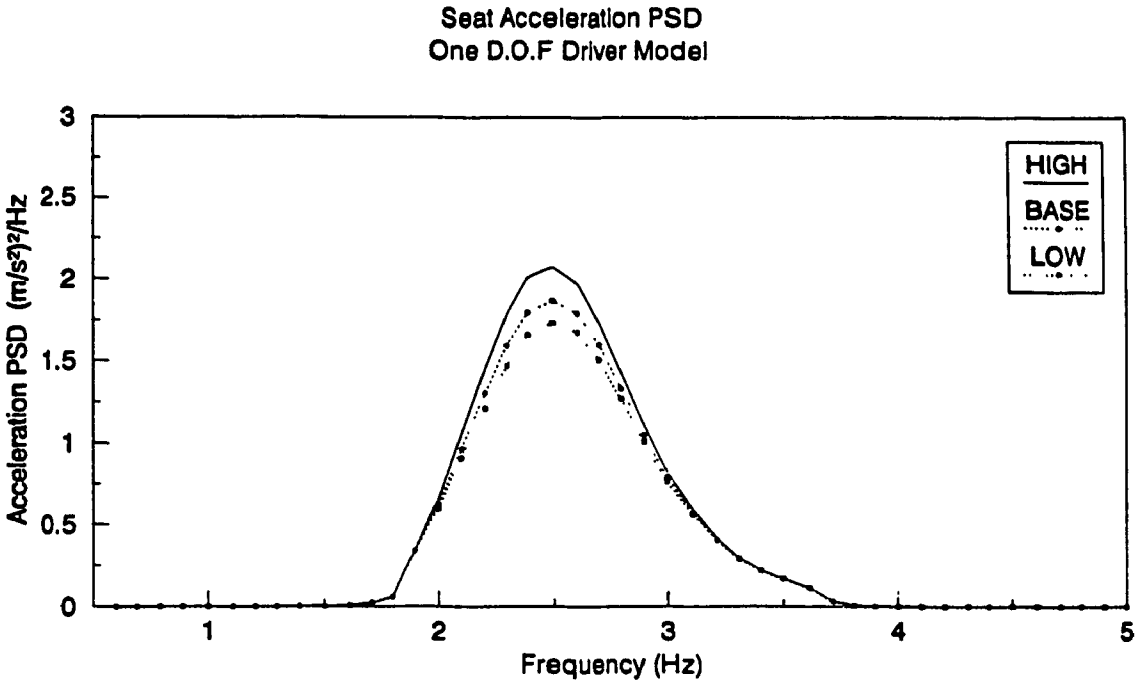

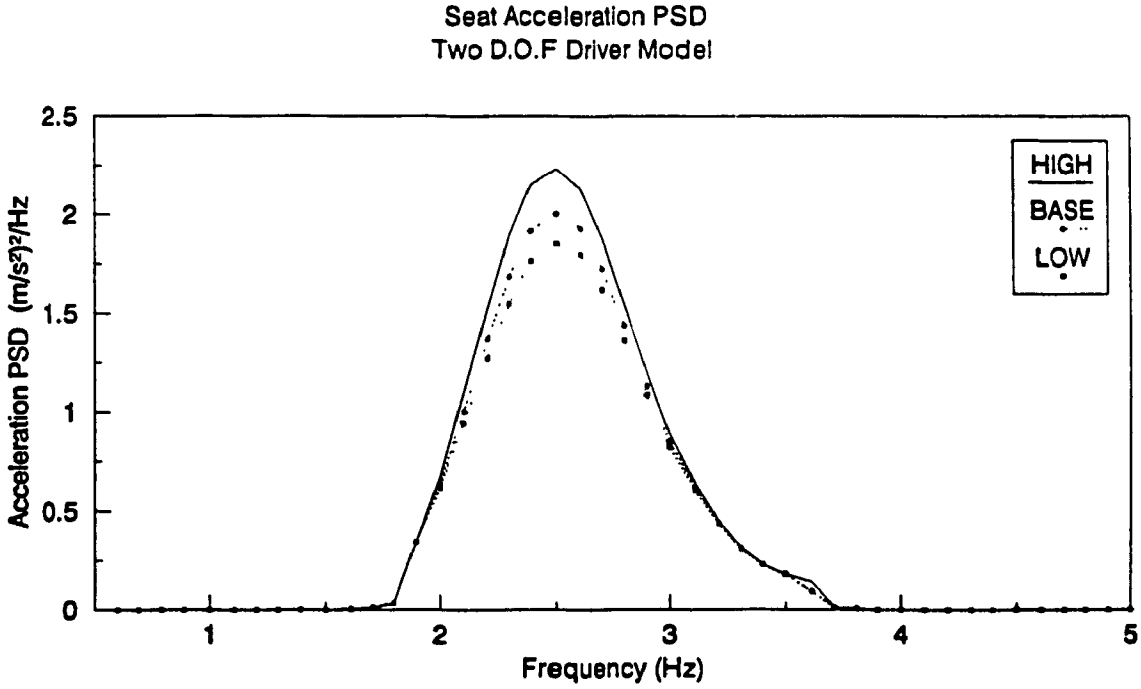

Figure 6.11. Influence of Suspension Spring Rate on the PSD of Acceleration Response at the Seat Using (a) One D.O.F; (b) Two D.O.F Driver Models.

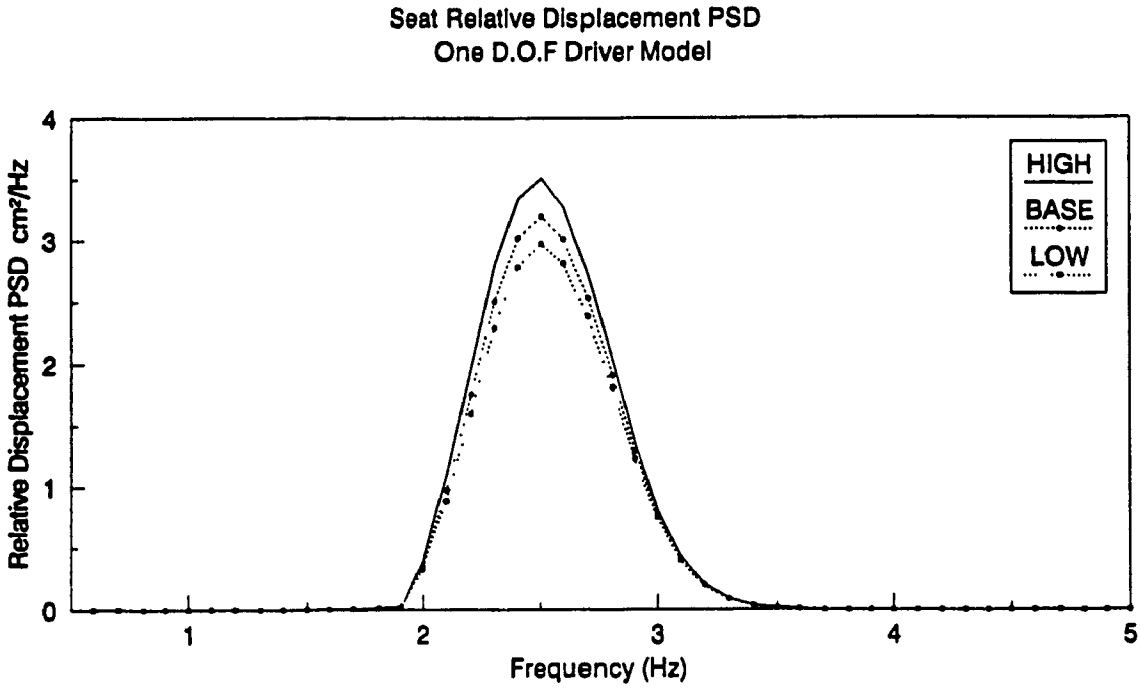

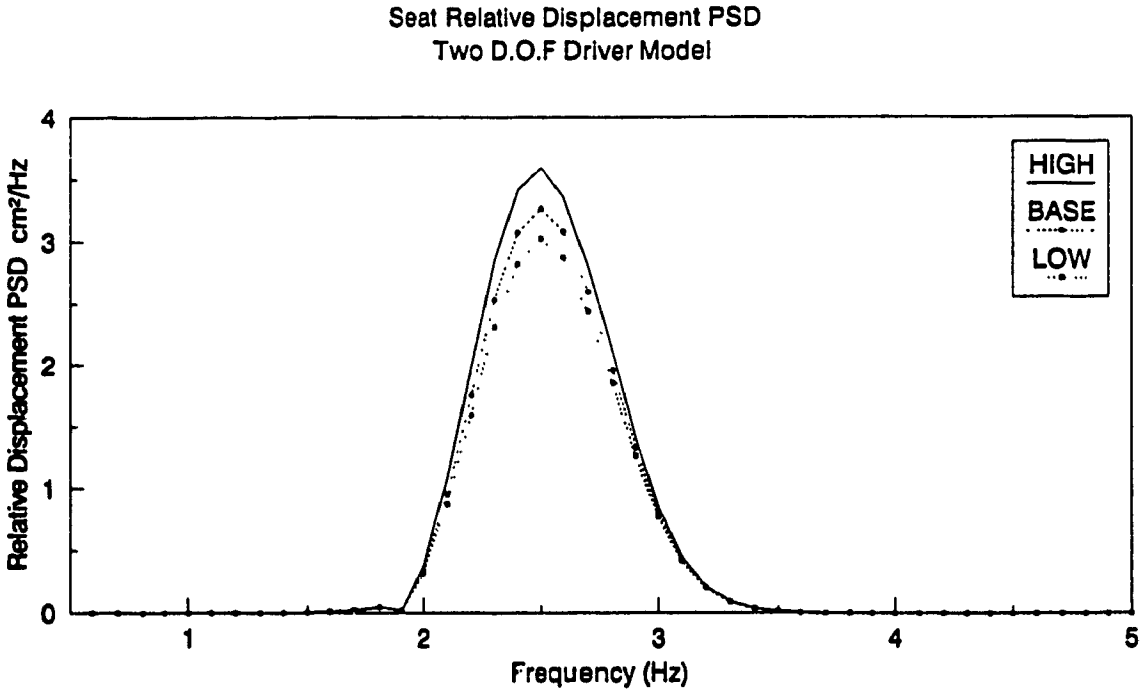

Figure 6.12. Influence of Suspension Spring Rate on the PSD of Relative Displacement Response of the Seat Using (a) One D.O.F; (b) Two D.O.F Driver Models.

Variations in either one of the damping parameters will affect the vibration transmission performance quite considerably, as shown in Figures 6.13a and 6.13b. An increase in the damping parameter, δ_{1A}, suppresses the resonant transmissibility response along with an increase in the acceleration transmissibility response corresponding to vehicle's resonant frequency. The acceleration PSD response, around the vehicle's resonant frequency, decreases for lower values of δ_{1A} and PSD of the corresponding relative displacement of the driver mass increases, as shown in Figures 6.14 and 6.15. The variations in damping parameters affect the transmissibility and random response characteristics of seat-suspension models with one- and two-degrees-of-freedom driver models, in a very similar manner, as illustrated in Figures 6.16 to 6.18.

Variations in the damping parameter, δ_{1B}, also exhibit similar effects on the vibration isolation performance of the seat-suspension. Changes in δ_{1B}, however, yield variations of considerable magnitude in the seat transmissibility, when compared to those caused by changes in δ_{1A}, as illustrated in Figures 6.19a and 6.19b. A reduction in δ_{1B} yields poor transmissibility at the seat's resonant frequency and superior acceleration transmissibility at the vehicle's resonant frequency. A lower value of δ_{1B}, thus, leads to considerably lower acceleration PSD and larger relative displacement PSD of the driver mass, as illustrated in Figures 6.20 and 6.21. The variations in δ_{1B} exhibit more influence on the SIFRA seat response, when compared to that on the ISRI seat.

Figures 6.22 to 6.24 present the acceleration transmissibility, acceleration PSD and relative displacement PSD, respectively, for three- and four-degrees-of-freedom ISRI seat-suspension model incorporating one- and

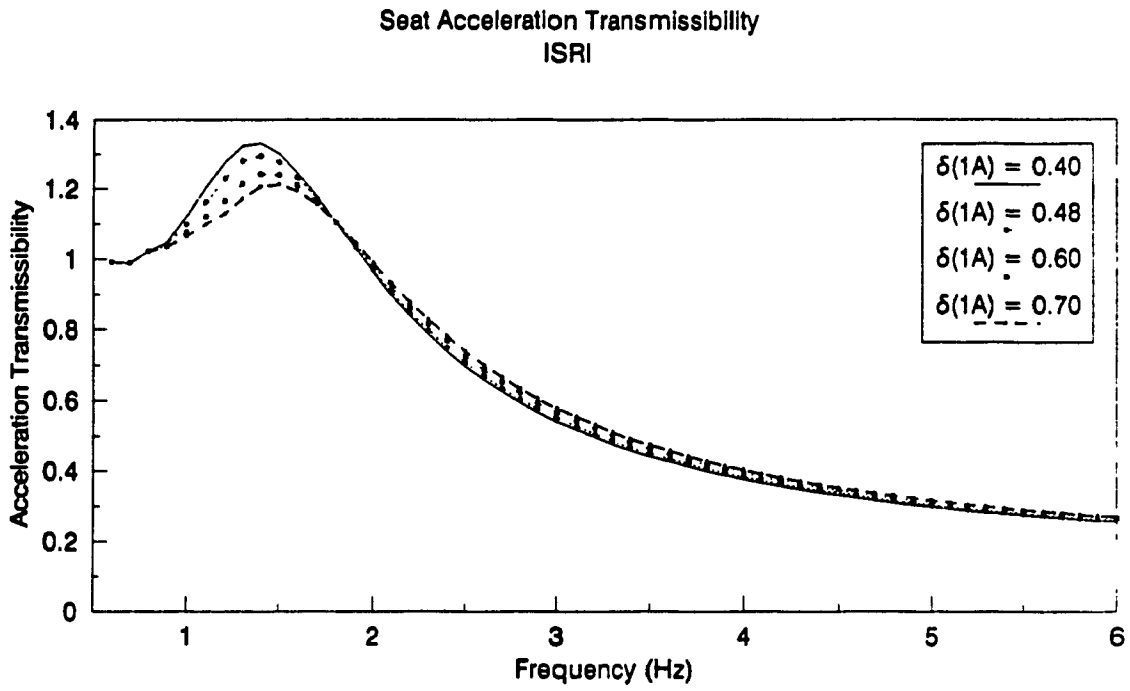

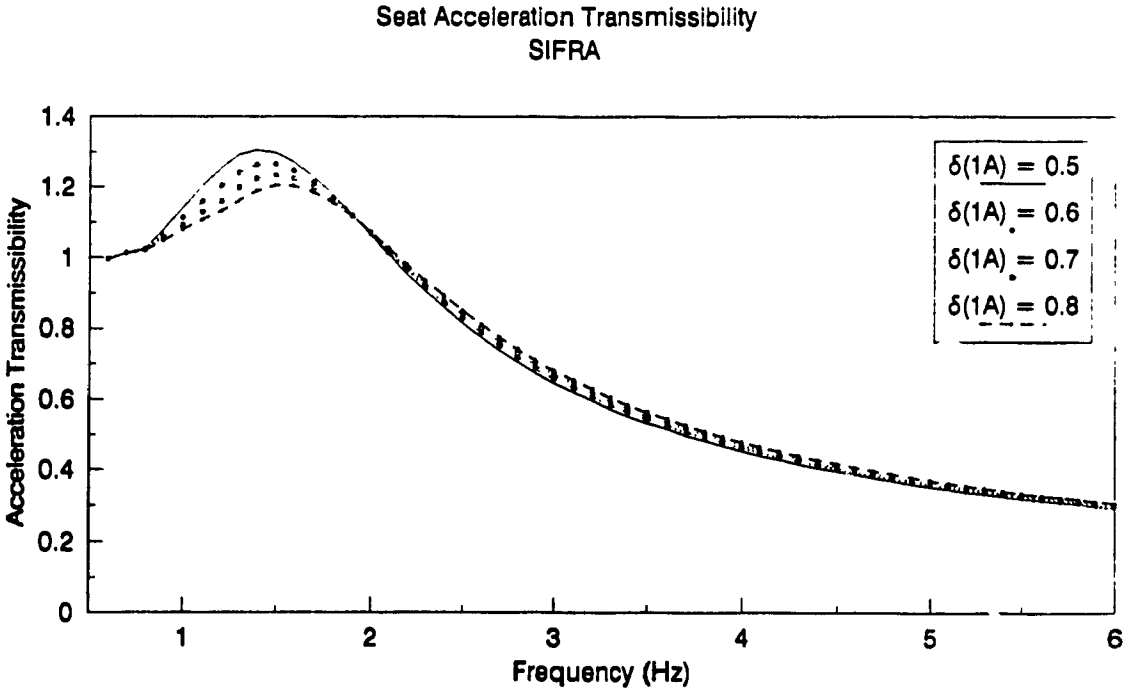

Figure 6.13. Influence of Shock Absorber Bleed-Off Damping, (δ_{1A}) on the Acceleration Transmissibility of the Seat: (a) ISRI, (b) SIFRA.

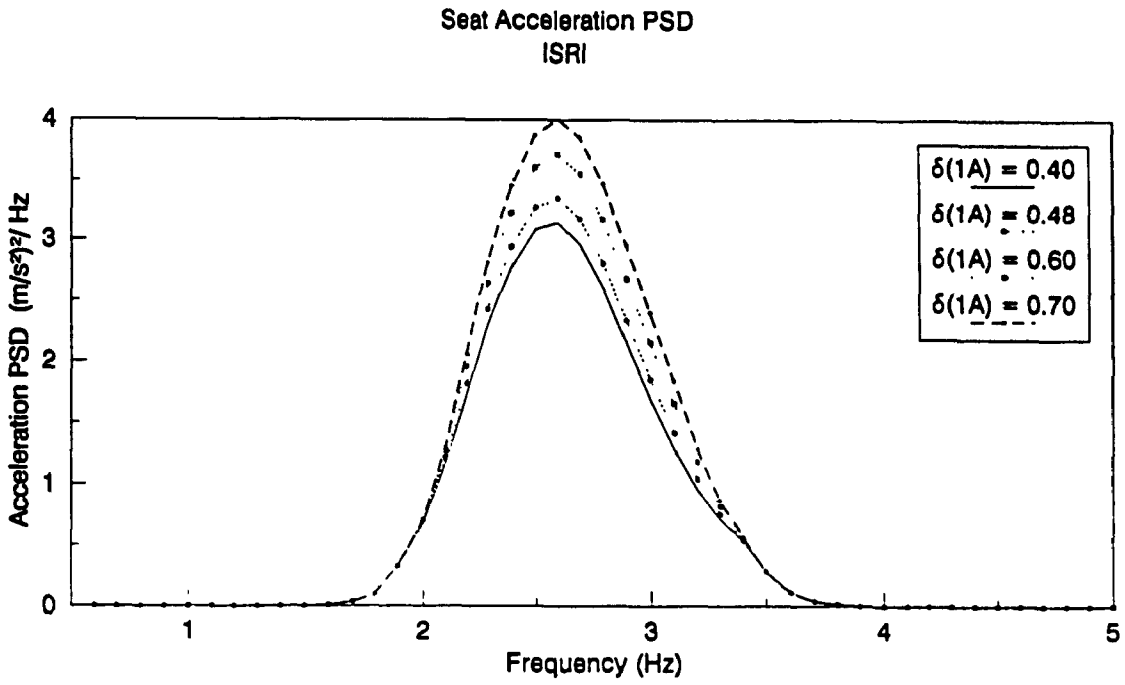

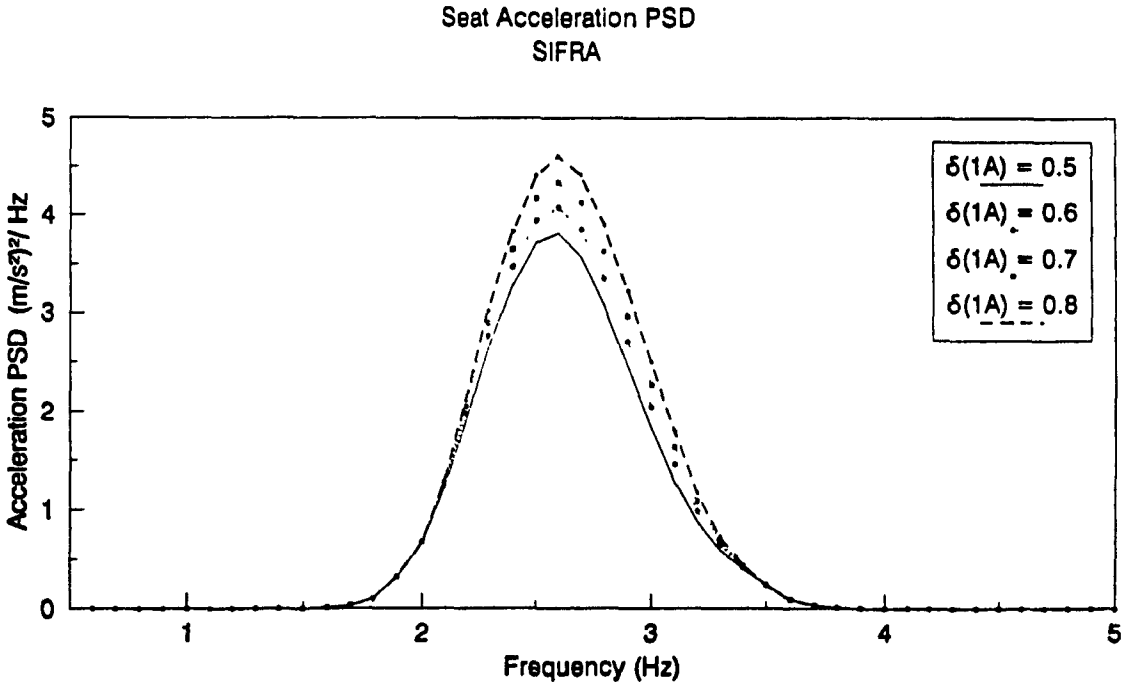

Figure 6.14. Influence of Shock Absorber Bleed-Off Damping, (δ_{1A}) on the PSD of Acceleration Response at the Seat: (a) ISRI, (b) SIFRA.

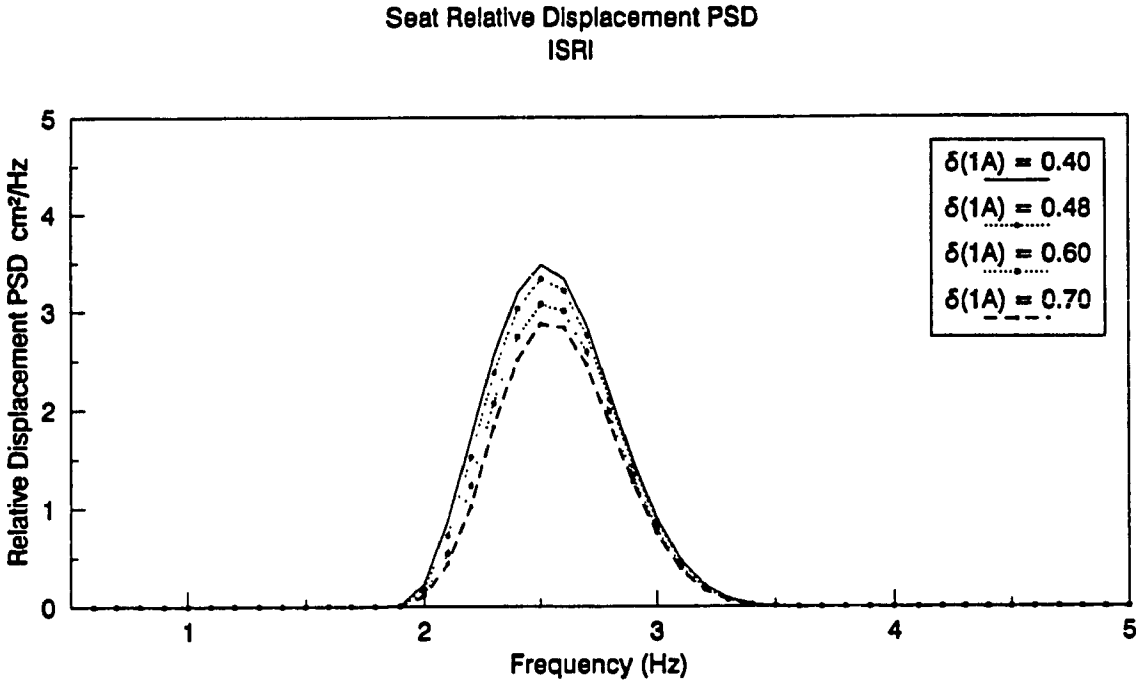

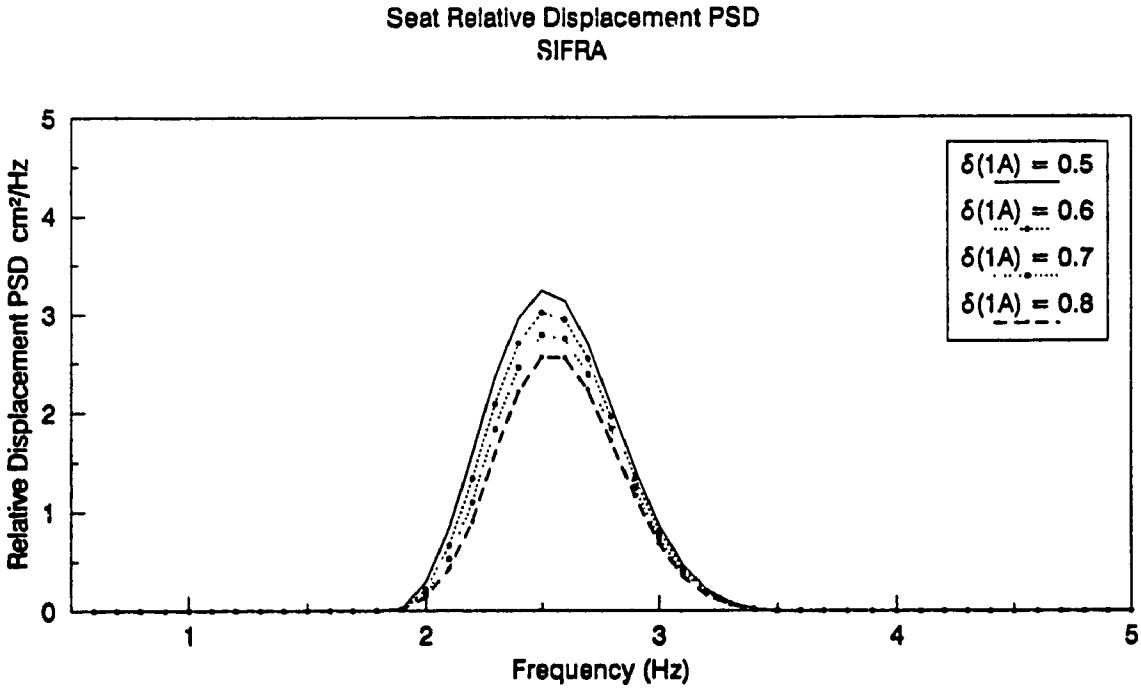

Figure 6.15. Influence of Shock Absorber Bleed-Off Damping, (δ_{1A}) on the PSD of Relative Displacement Response of the Seat: (a) ISRI, (b) SIFRA.

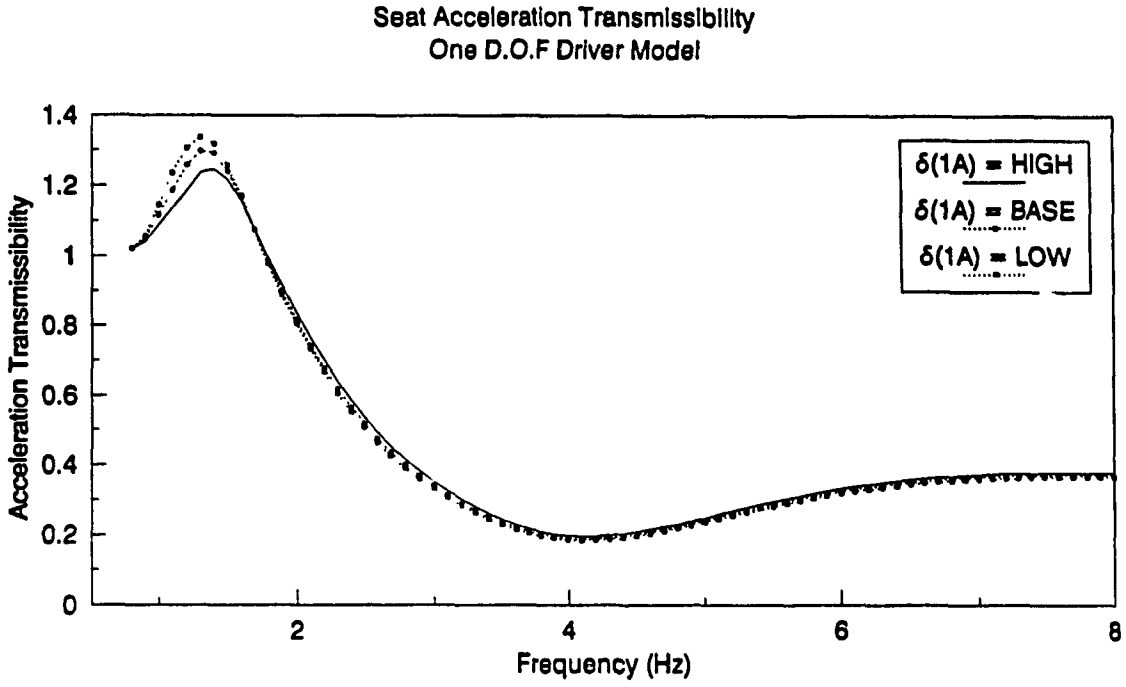

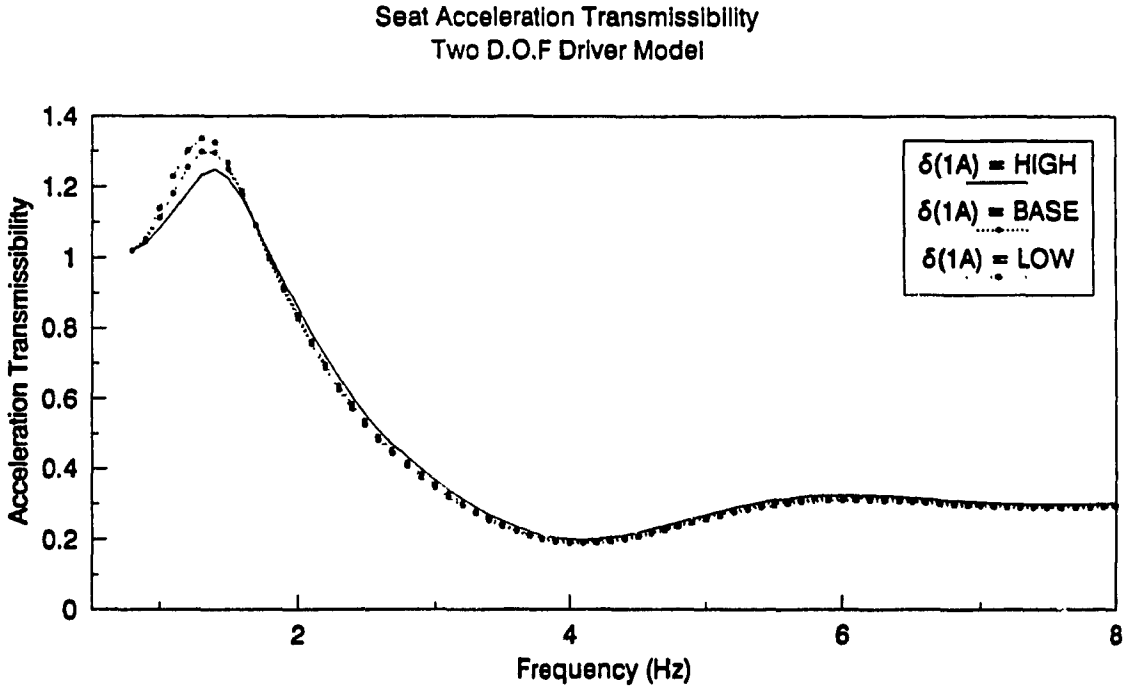

Figure 6.16. Influence of Shock absorber Bleed-Off Damping, (δ_{1A}) on the Acceleration Transmissibility of the Seat Using (a) One D.O.F; (b) Two D.O.F Driver Model.

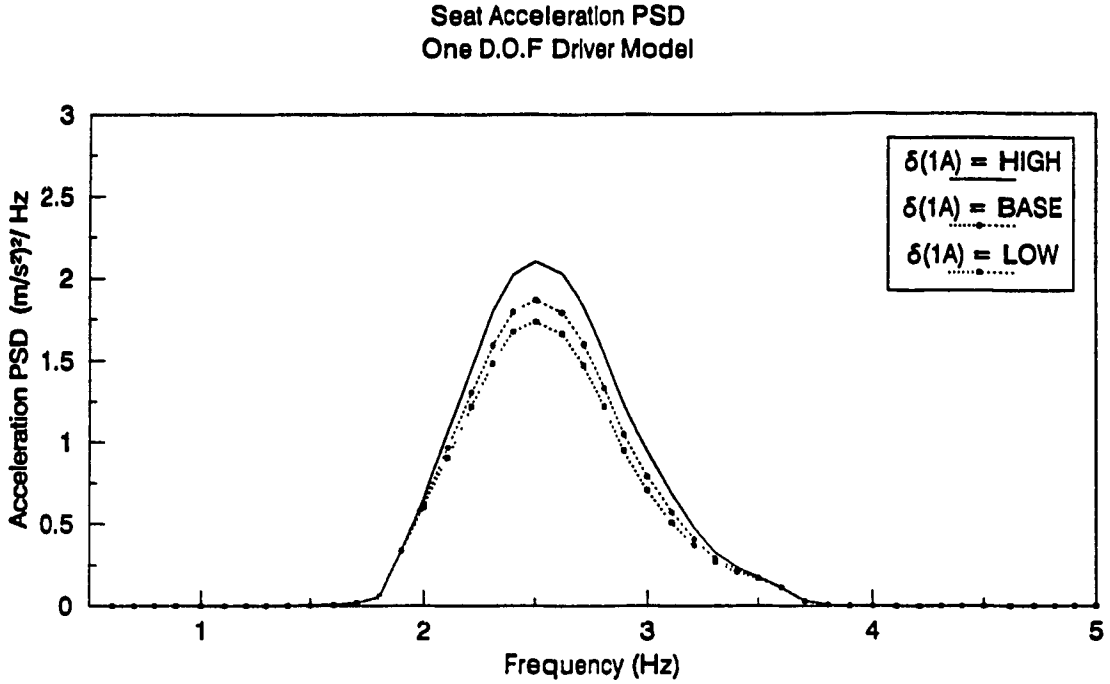

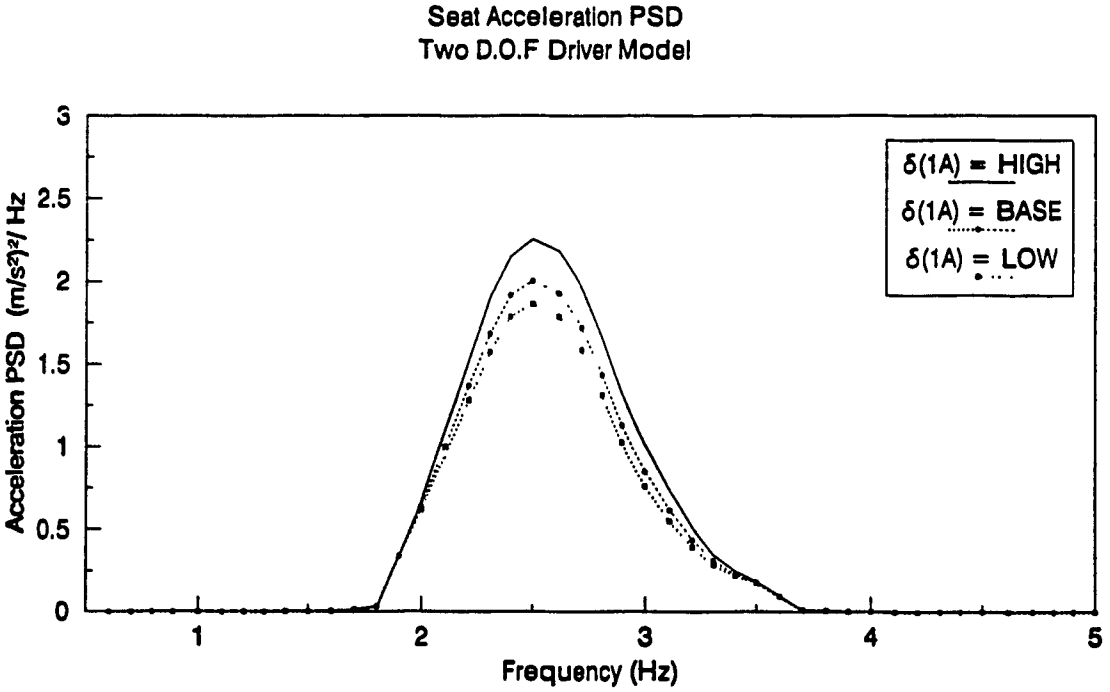

Figure 6.17. Influence of Shock Absorber Bleed-Off Damping, (δ_{1A}) on the PSD of Acceleration Response at the Seat Using (a) One D.O.F; (b) Two D.O.F Driver Models.

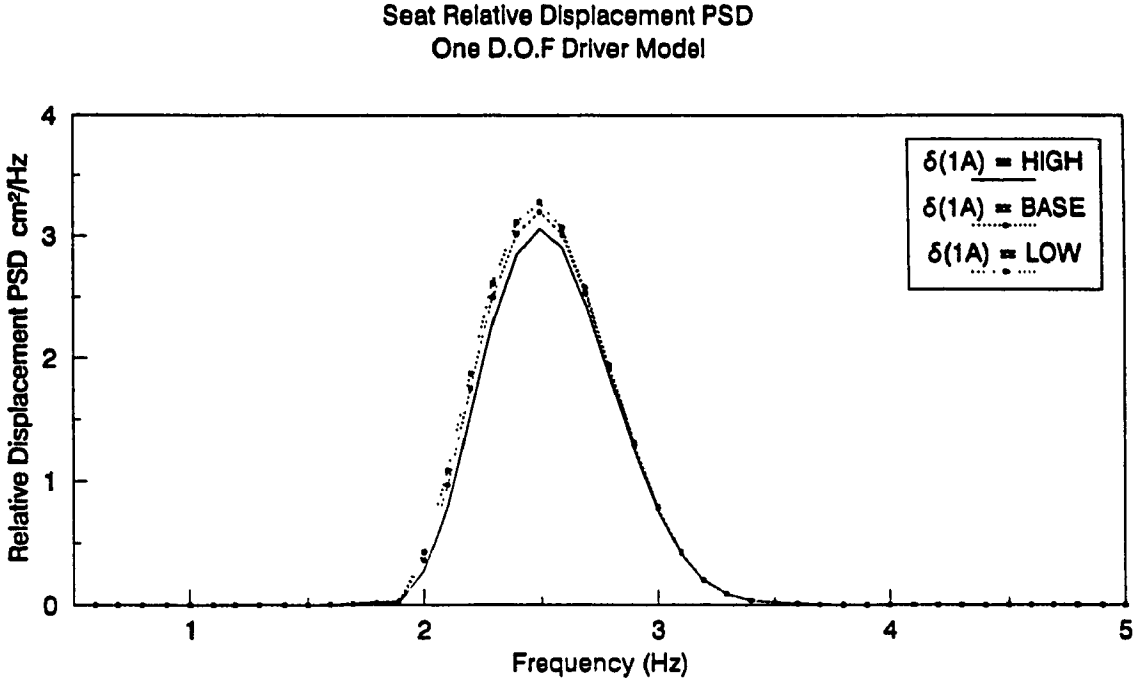

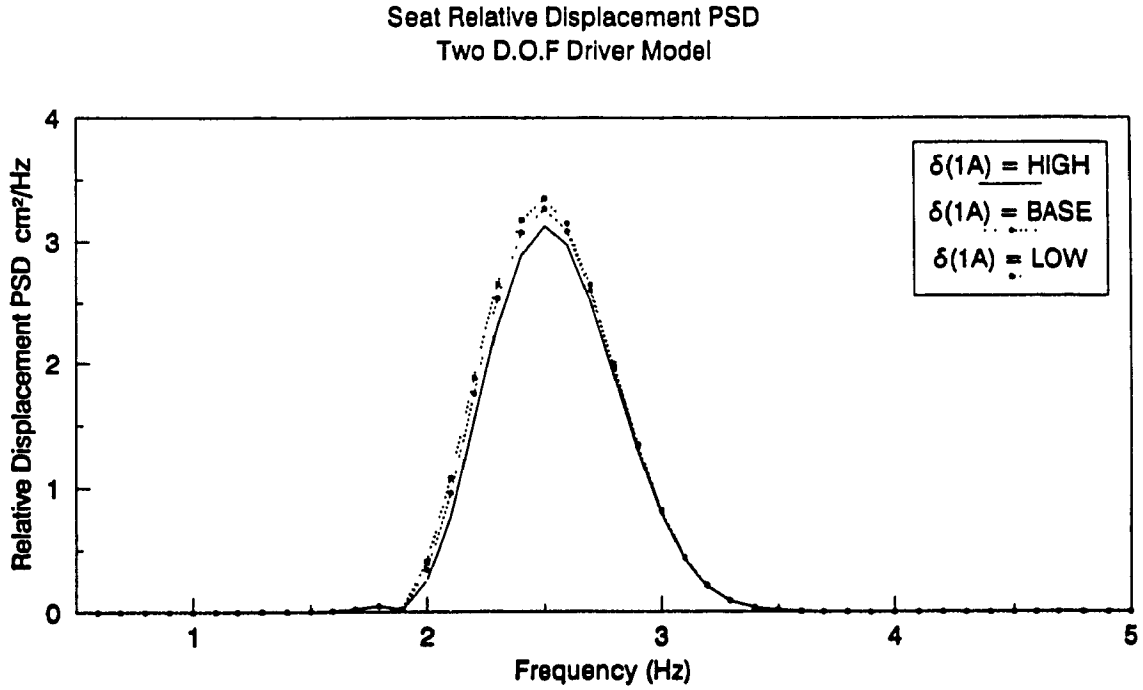

Figure 6.18. Influence of Shock Absorber Bleed-Off Damping (δ_{1A}) on the PSD of Relative Displacement Response of the Seat Using (a) One D.O.F; (b) Two D.O.F Driver Models.

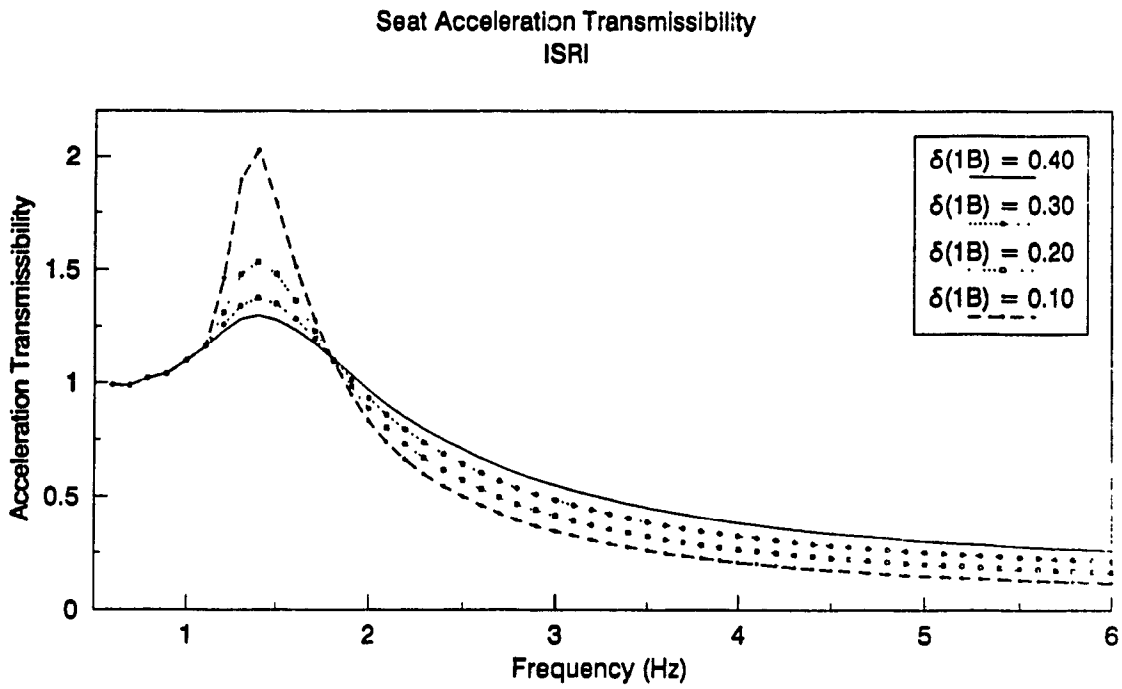

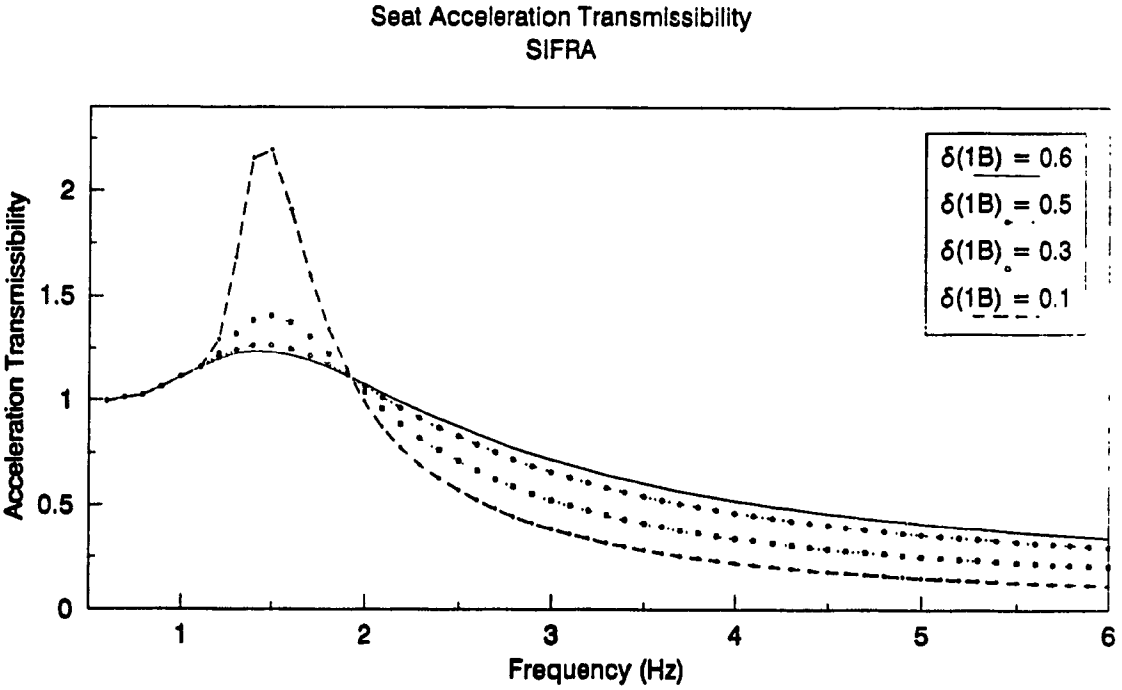

Figure 6.19. Influence of Shock Absorber Blow-Off Damping, (δ_{1B}) on the Acceleration Transmissibility of the Seat: (a) ISRI, (b) SIFRA.

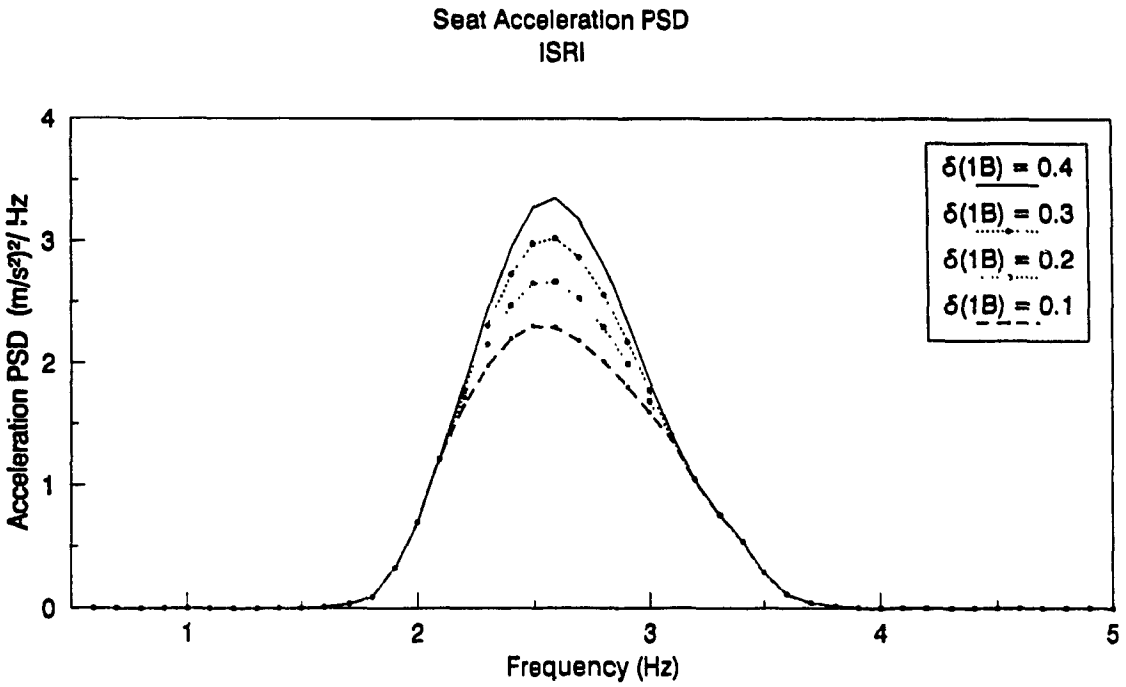

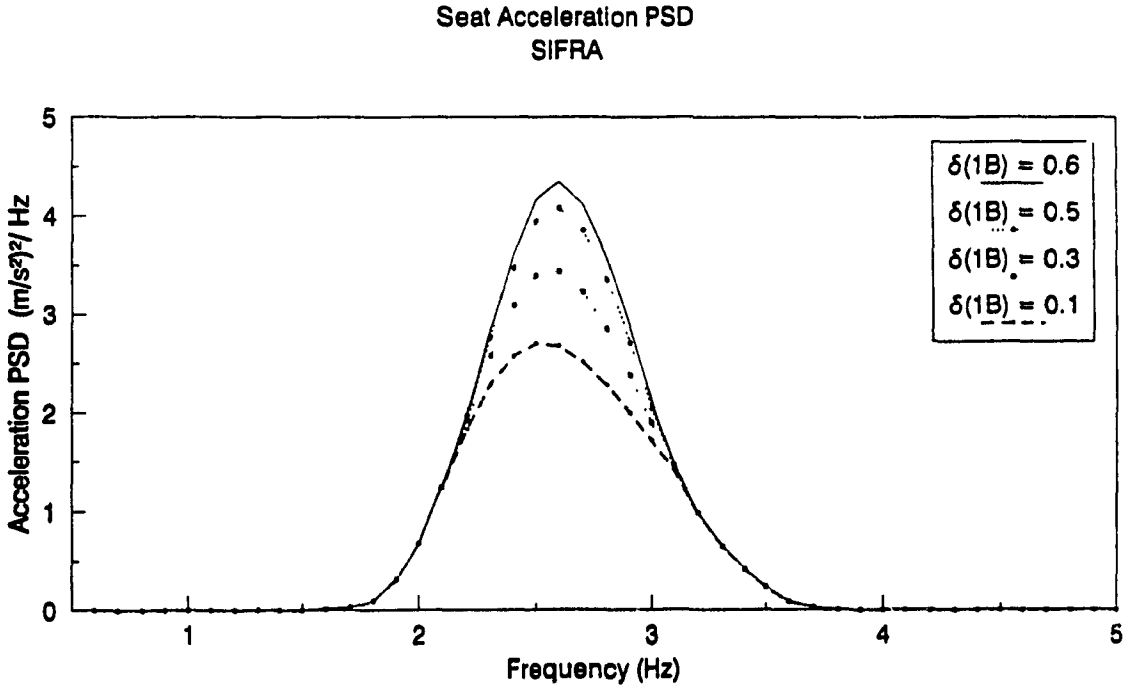

Figure 6.20. Influence of Shock Absorber Blow-Off Damping, (δ_{1B}) on the PSD of Acceleration Response at the Seat: (a) ISRI, (b) SIFRA.

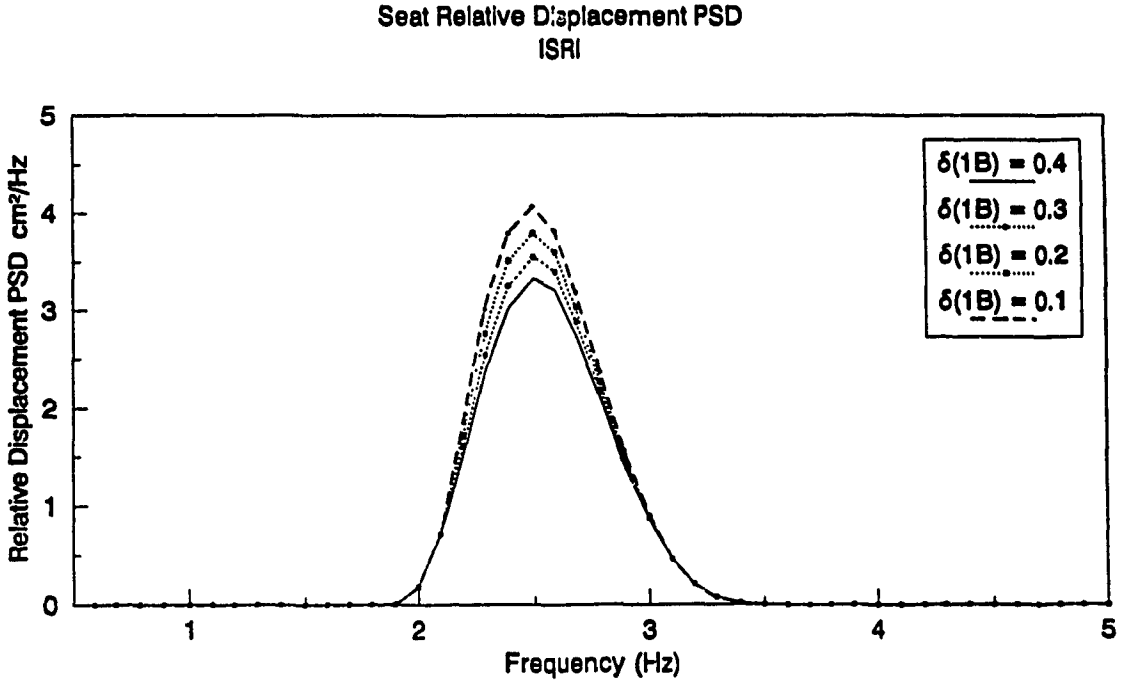

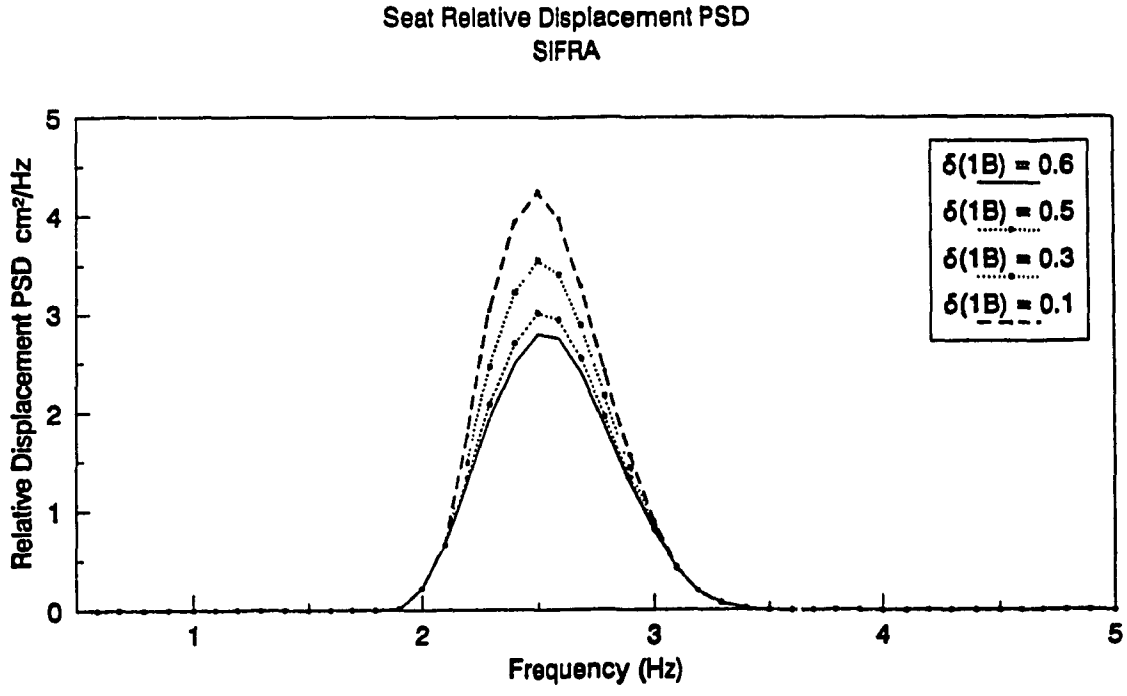

Figure 6.21. Influence of Shock Absorber Blow-Off Damping, (δ_{1B}) on the PSD of Relative Displacement Response of the Seat: (a) ISRI, (b) SIFRA.

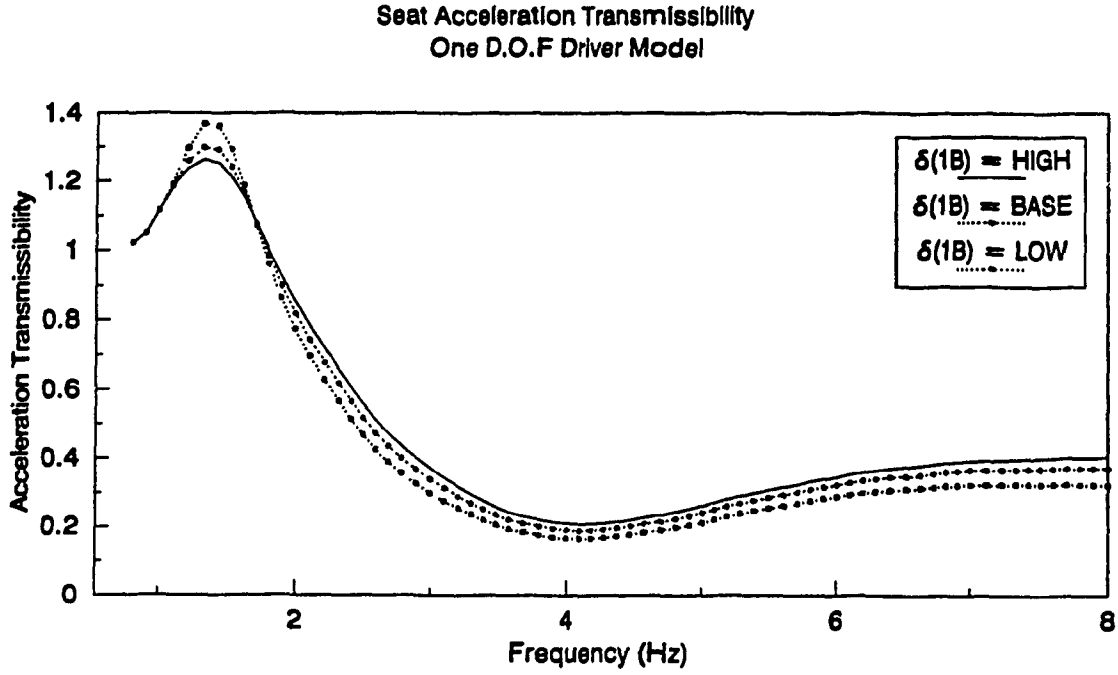

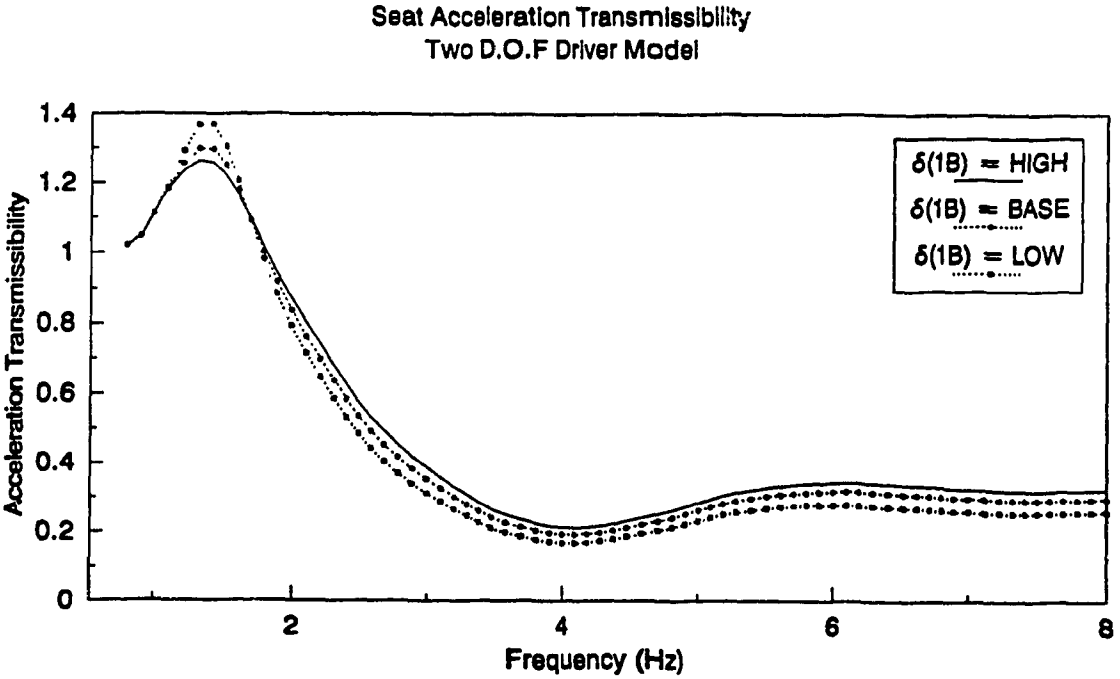

Figure 6.22. Influence of Shock absorber Blow-Off Damping, (δ_{1B}) on the Acceleration Transmissibility of the Seat Using (a) One D.O.F; (b) Two D.O.F Driver Model.

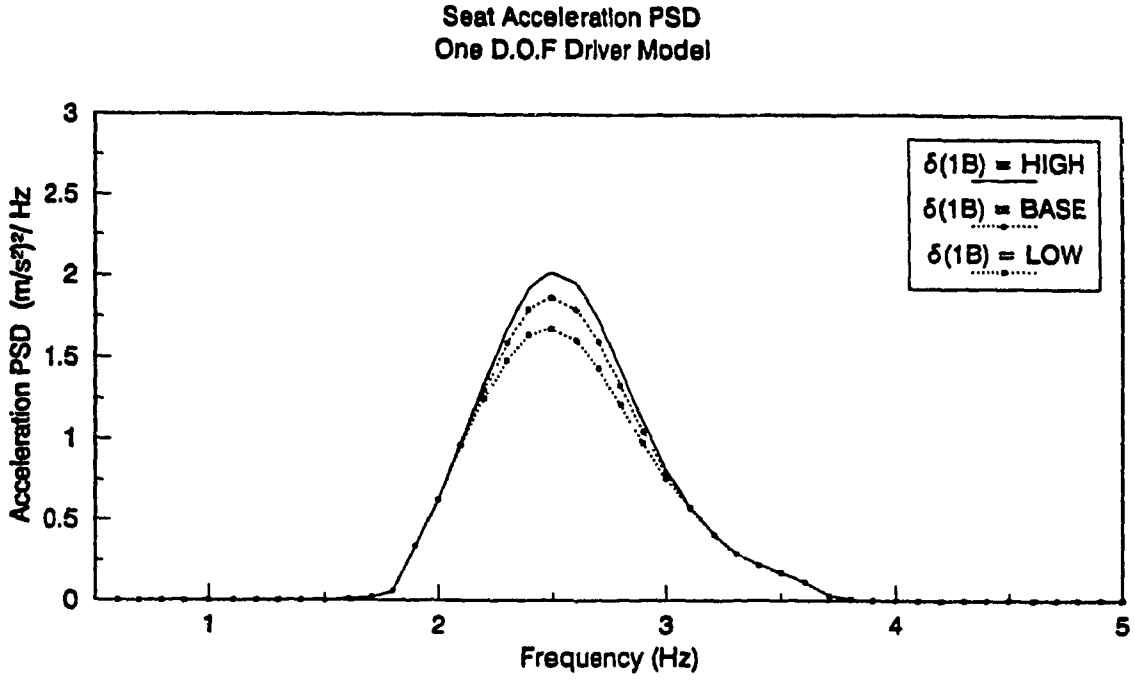

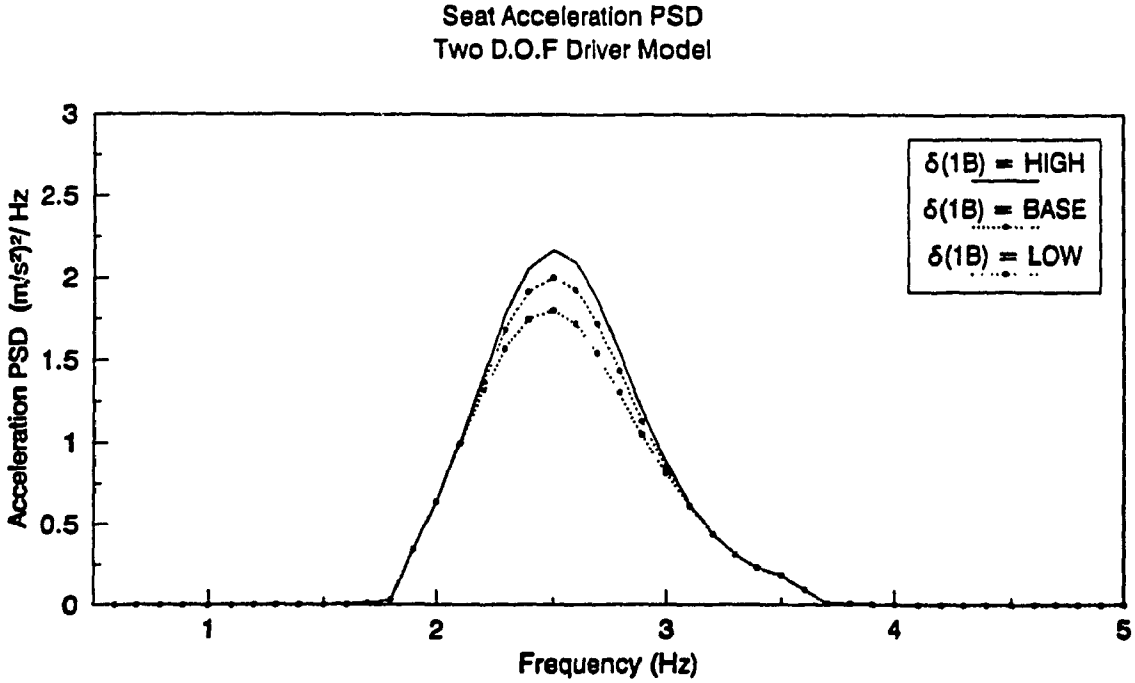

Figure 6.23. Influence of Shock Absorber Blow-Off Damping, (δ_{1B}) on the PSD of Acceleration Response at the Seat Using (a) One D.O.F; (b) Two D.O.F Driver Models.

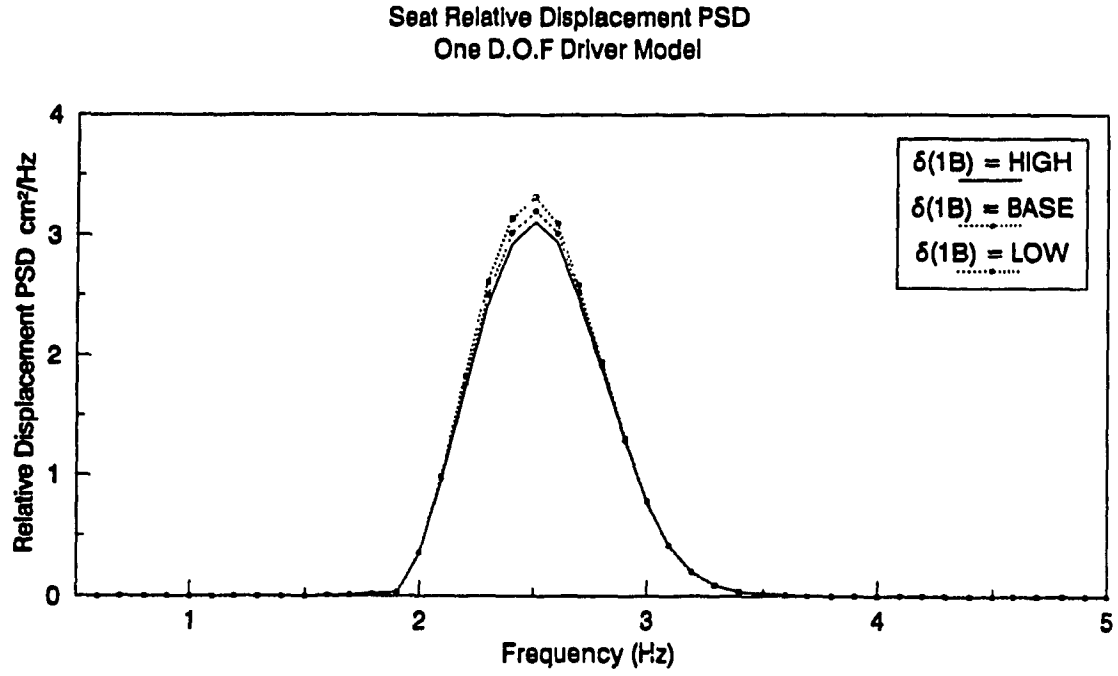

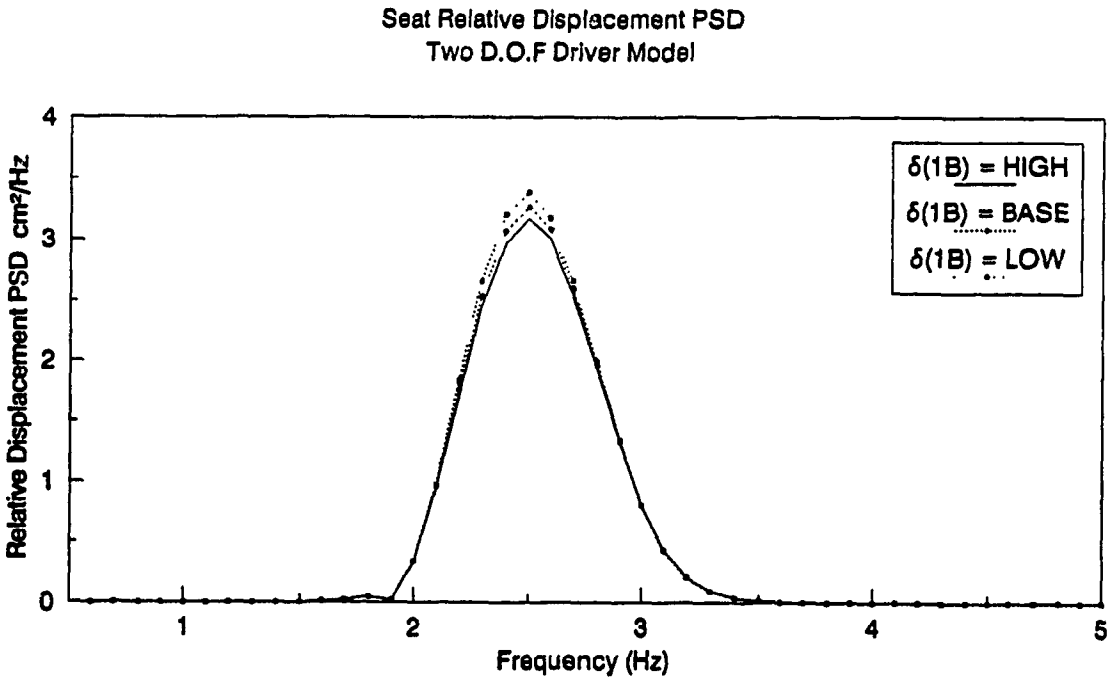

Figure 6.24. Influence of Shock Absorber Blow-Off Damping (δ_{1B}) on the PSD of Relative Displacement Response of the Seat Using (a) One D.O.F; (b) Two D.O.F Driver Models.

two-degrees-of-freedom human body models. An increase in δ_{1B} yields lower resonant transmissibility and relative displacement PSD response, while the acceleration PSD response increases. The variation in response characteristics due to variations in δ_{1B}, however, are relatively small, when compared to those of the two-degrees-of-freedom seat-suspension models.

Apart from the damping parameters, the performance characteristics of the seat-suspension system are influenced by the transition velocity, V_s, as shown in Figures 6.25a and 6.25b. An increase in V_s, suppresses the seat resonant transmissibility response along with an increase in the acceleration response corresponding to the vehicle's resonant frequency around 2.6 Hz, due to extended duration of the bleed-off damping. This is further evidenced by the increased acceleration PSD response with an increase in V_s, as shown in Figures 6.26a and 6.26b. The PSD of relative displacement response of the driver mass, however, decreases with an increase in V_s, as shown in Figures 6.27a and 6.27b. The transition velocity, V_s, therefore is selected to achieve a compromise between the acceleration PSD and the relative displacement PSD responses.

Figure 6.28 presents the influence of V_s on the acceleration transmissibility response of the three- and four-degrees-of-freedom seat-suspension models. An increase in V_s tends to slightly reduce the resonant transmissibility and slightly increase the acceleration transmissibility near the vehicle's resonant frequency. A slight increase in acceleration response at vehicle's resonant frequency is further demonstrated by the acceleration PSD response presented in Figure 6.29. The PSD of the corresponding relative displacement response, however, decreases slightly with increase in V_s, as shown in Figure 6.30.

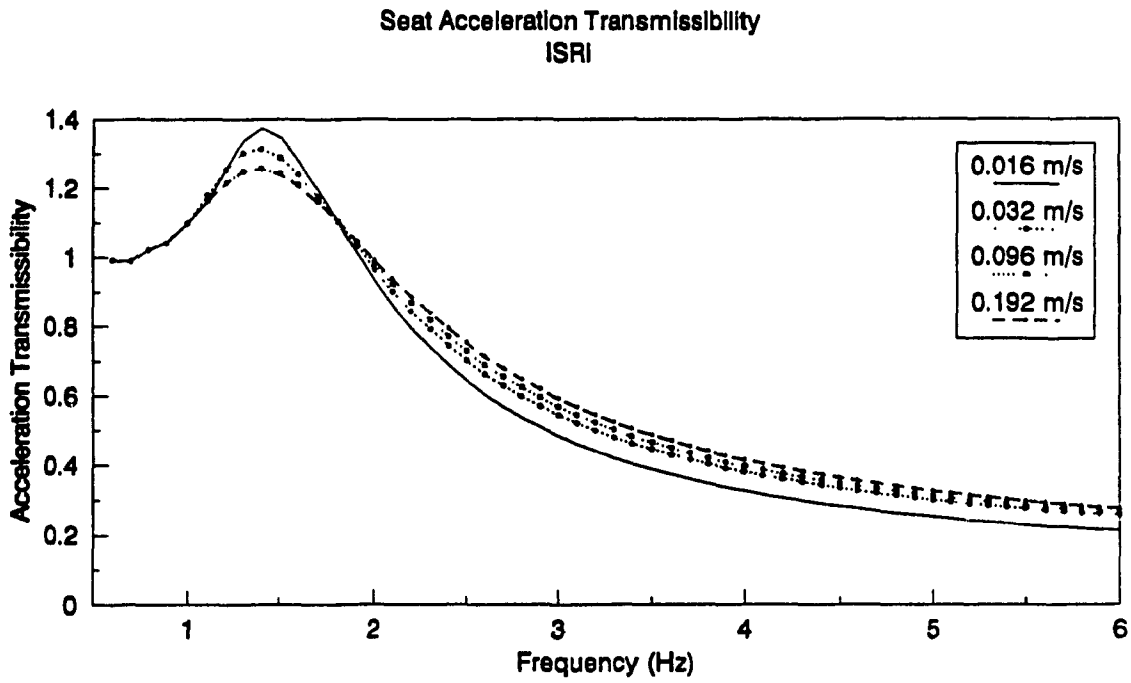

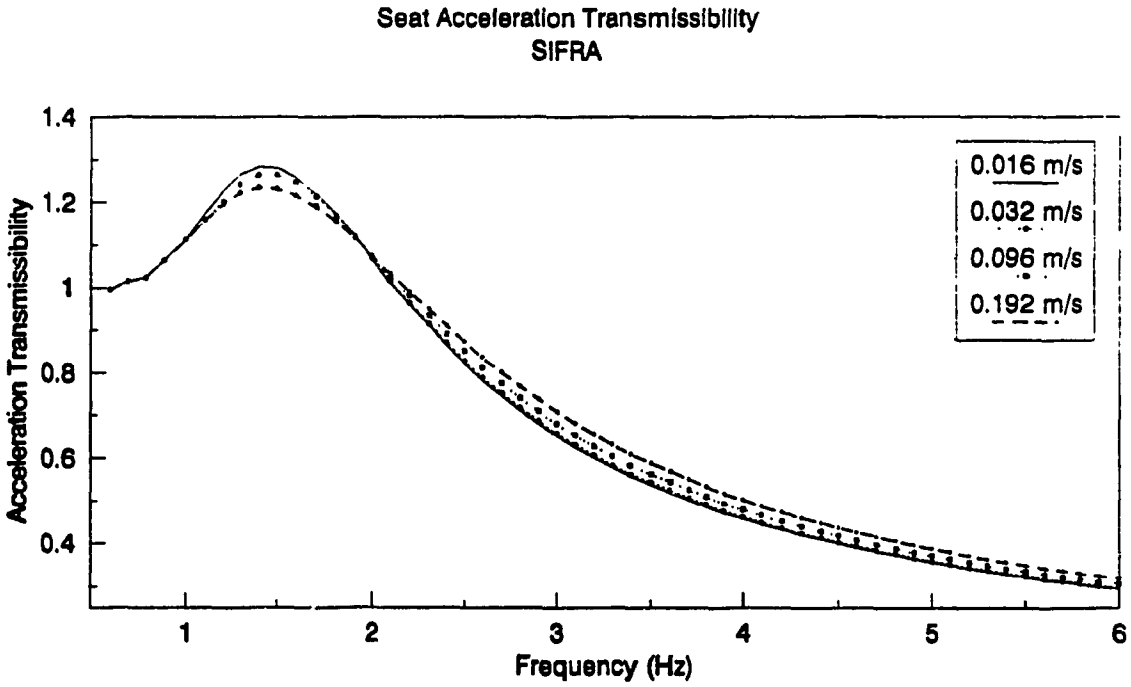

Figure 6.25. Influence of Shock Absorber Preset Velocity, (V_s) on the Acceleration Transmissibility of the Seat: (a) ISRI, (b) SIFRA.

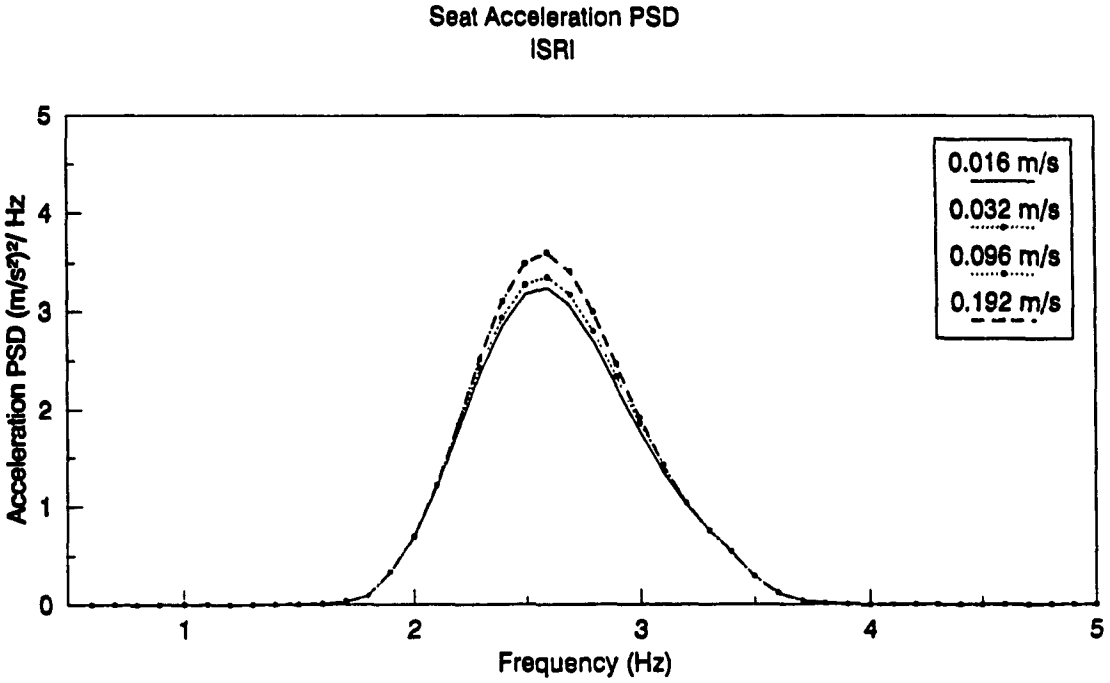

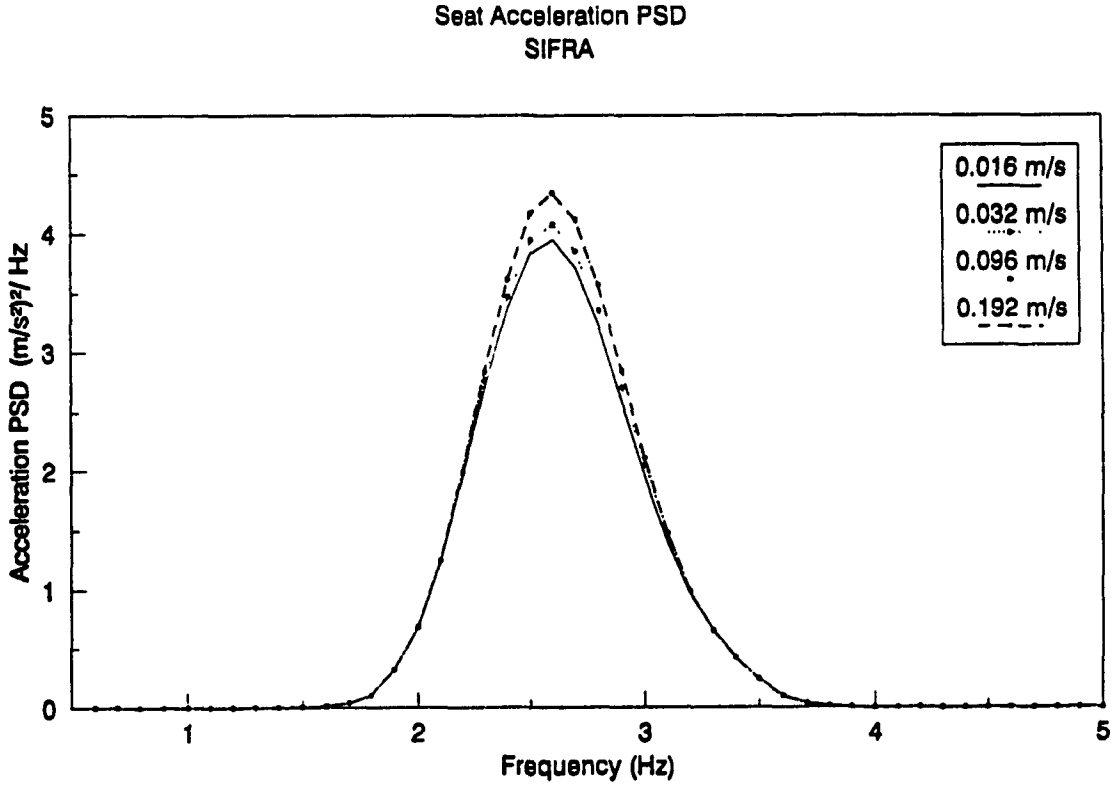

Figure 6.26. Influence of Shock Absorber Preset Velocity, (V_s) on the PSD of Acceleration Response at the Seat: (a) ISRI, (b) SIFRA.

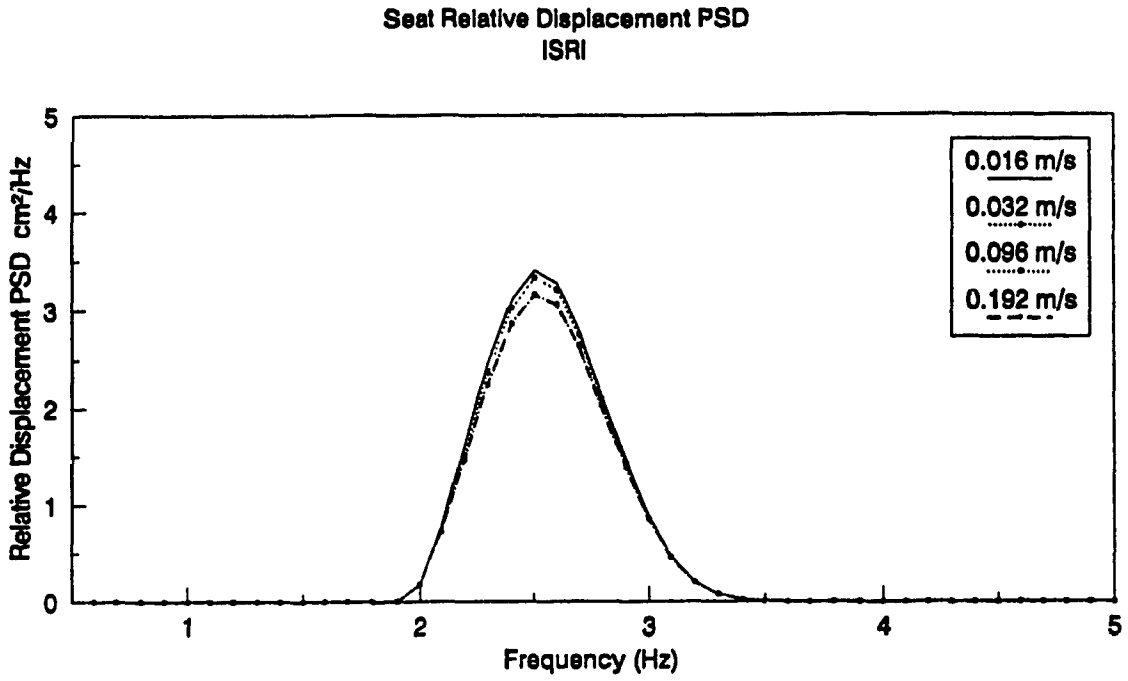

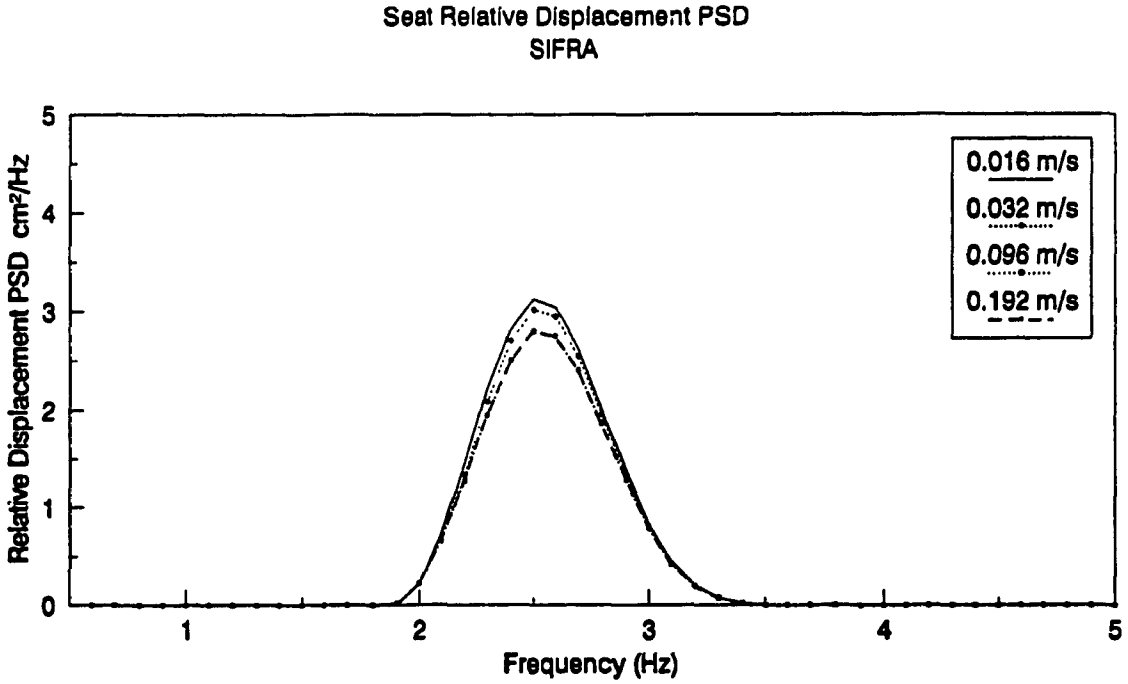

Figure 6.27. Influence of Shock Absorber Preset Velocity, (V_s) on the PSD of Relative Displacement Response of the Seat: (a) ISRI, (b) SIFRA.

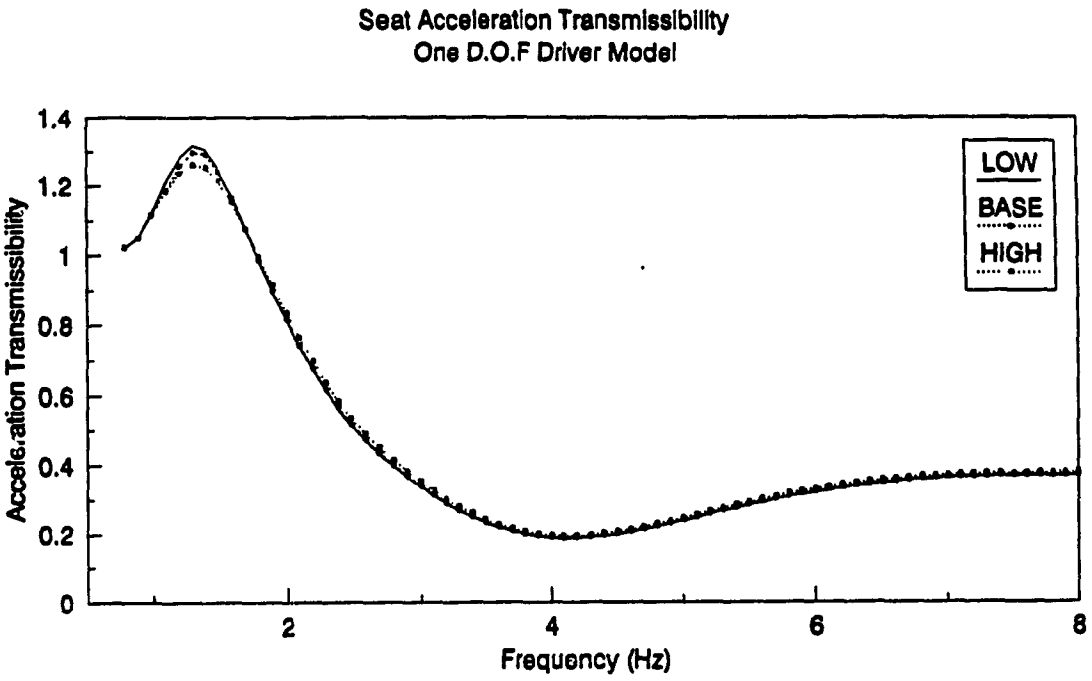

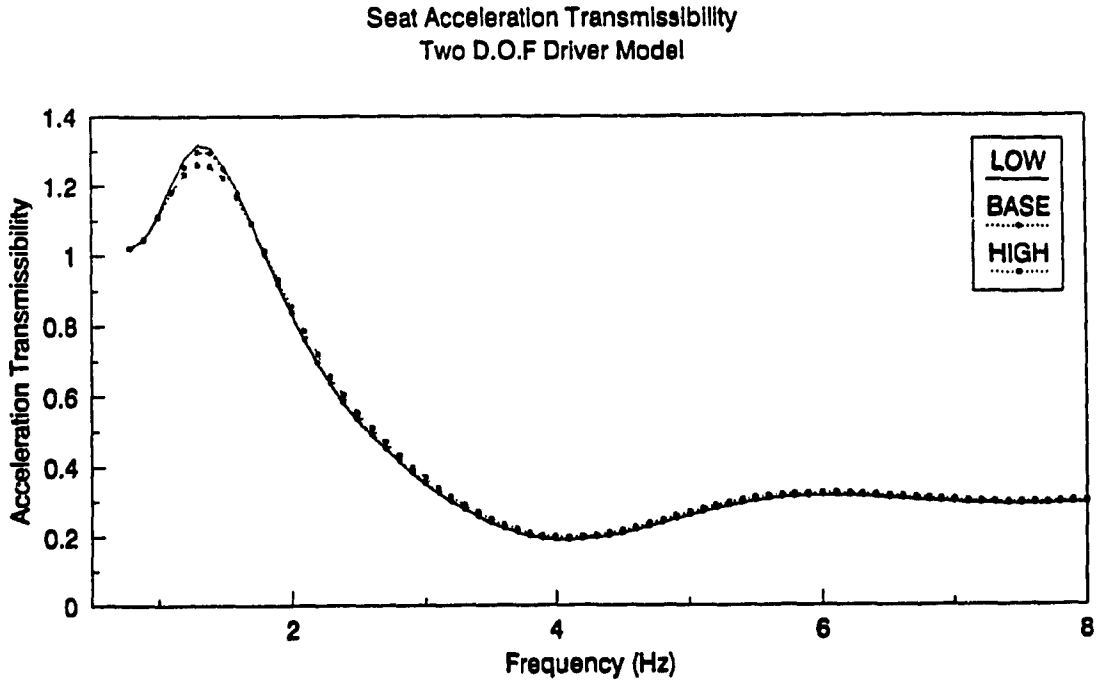

Figure 6.28. Influence of Shock absorber Preset Velocity, (V_s) on the Acceleration Transmissibility of the Seat Using (a) One D.O.F; (b) Two D.O.F Driver Model.

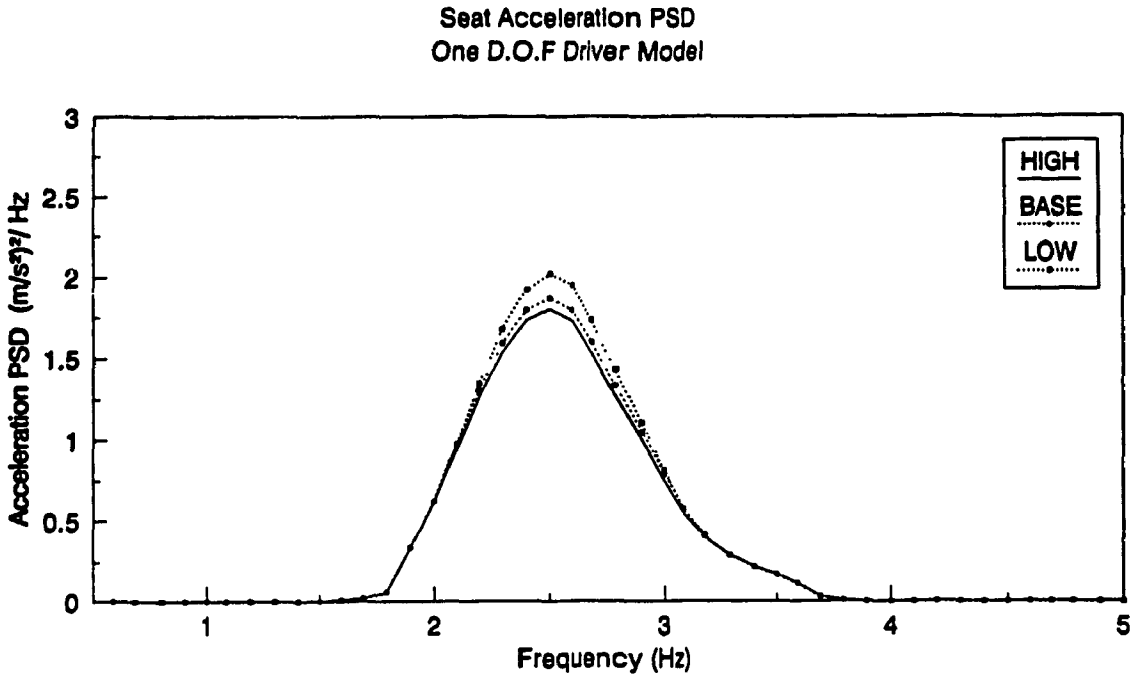

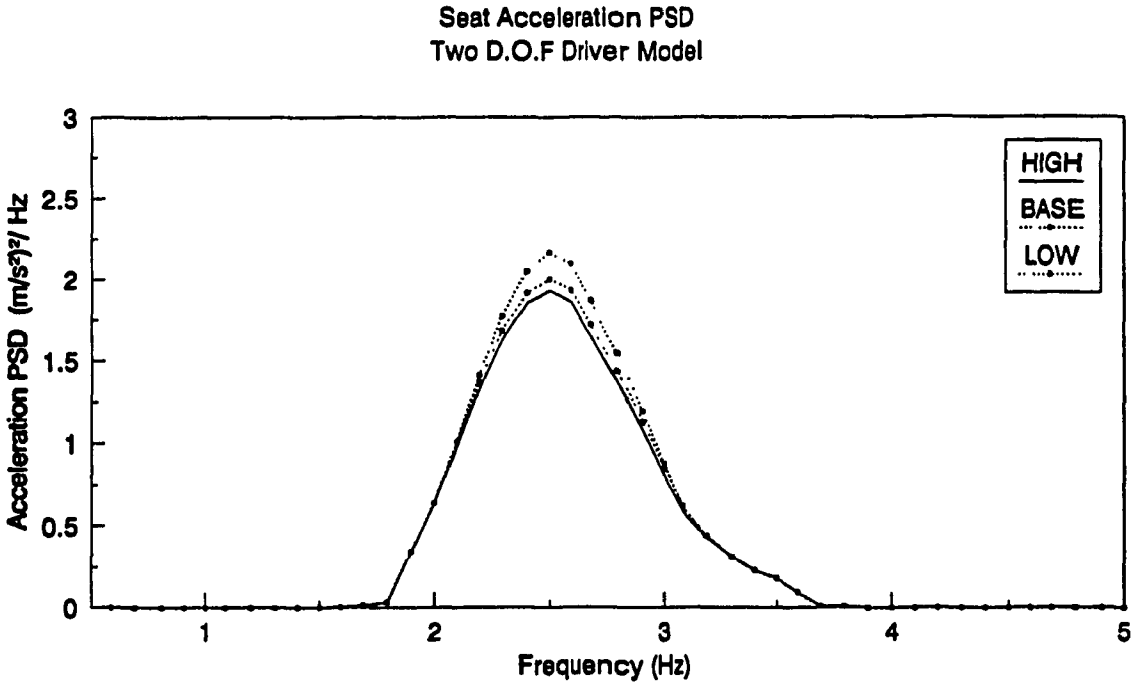

Figure 6.29. Influence of Shock Absorber Preset Velocity, (V_s) on the PSD of Acceleration Response at the Seat Using (a) One D.O.F; (b) Two D.O.F Driver Models.

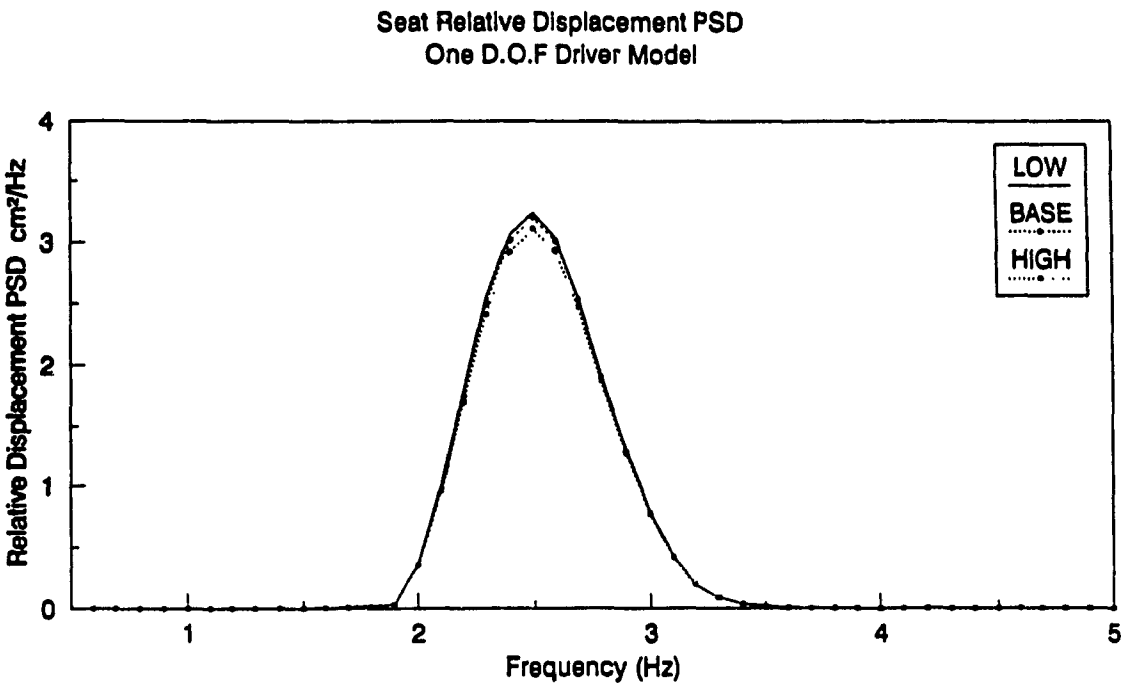

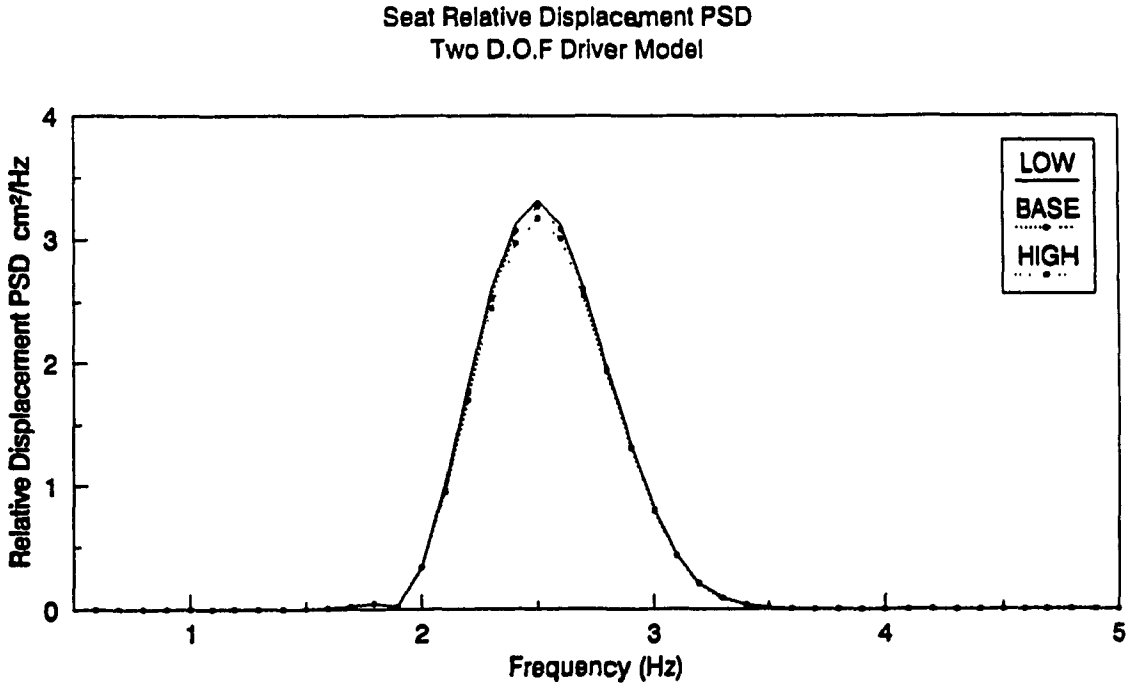

Figure 6.30. Influence of Shock Absorber Preset Velocity (V_s) on the PSD of Relative Displacement Response of the Seat Using (a) One D.O.F; (b) Two D.O.F Driver Models.

6.3.4 Influence of Coulomb Damping Force

The Coulomb friction force due to rollers, linkages, height control mechanisms, and shock absorber seal affects the suspension performance considerably. A high value of Coulomb friction yields locked suspension at low excitation frequencies, limits the effective suspension travel, and suppresses the resonant transmissibility, as illustrated in Figures 6.31a and 6.31b. The acceleration transmissibility at the vehicle's resonant frequency, however, increases due to increased damping caused by high Coulomb friction force. A low value of Coulomb friction force results in high resonant acceleration transmissibility, lower damped resonant frequency and improved vibration isolation around the vehicle's resonance. In view of the vibration attenuation performance, a medium high value of coulomb friction may be selected.

The acceleration PSD of the driver mass of the seat-suspension system, subjected to random cab floor ride vibrations, also increases considerably with an increase in Coulomb friction force, as illustrated in Figures 6.32a and 6.32b. The corresponding PSD of relative displacement PSD of the driver mass, however, decreases with an increase in Coulomb friction force, as shown in Figures 6.33a and 6.33b. Figures 6.34 to 6.36 present the acceleration transmissibility, acceleration PSD and relative displacement PSD, respectively, of the seat with one- and two-degrees-of-freedom driver models. The response characteristics demonstrate similar effect as that of Coulomb friction force.

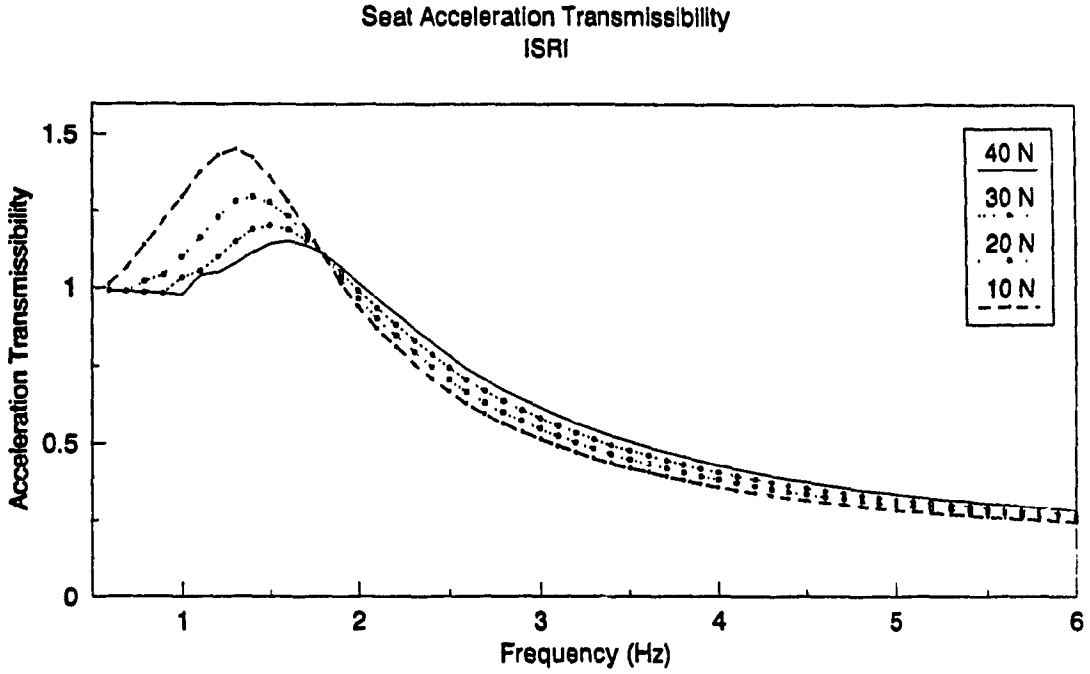

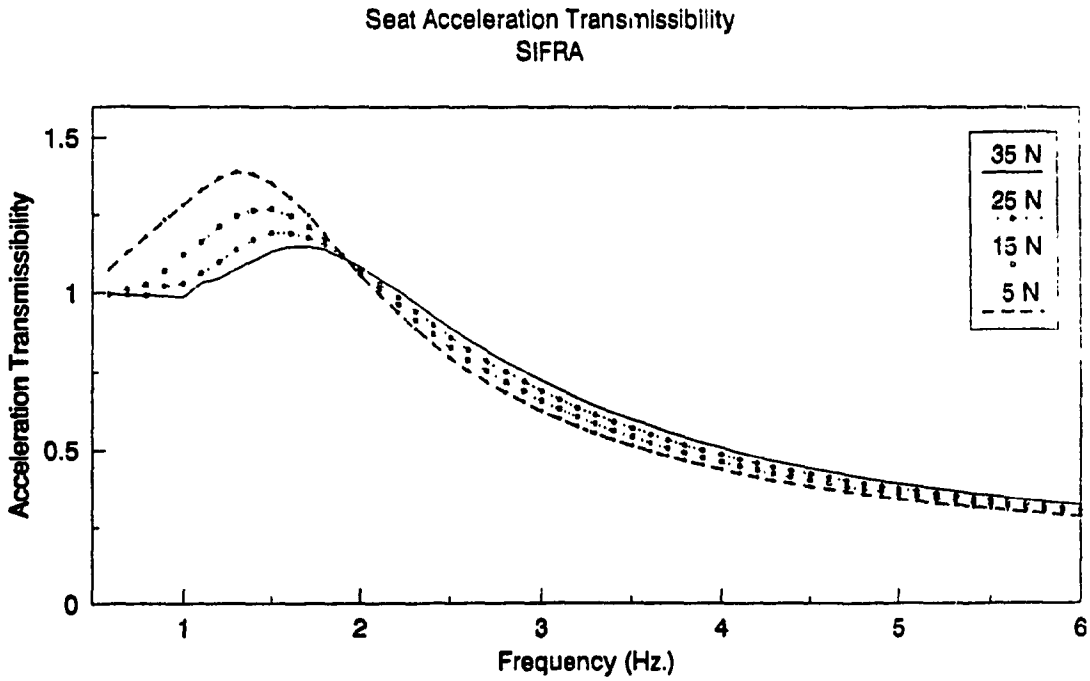

Figure 6.31. Influence of Coulomb Friction Damping on the Acceleration Transmissibility of the Seat: (a) ISRI, (b) SIFRA.

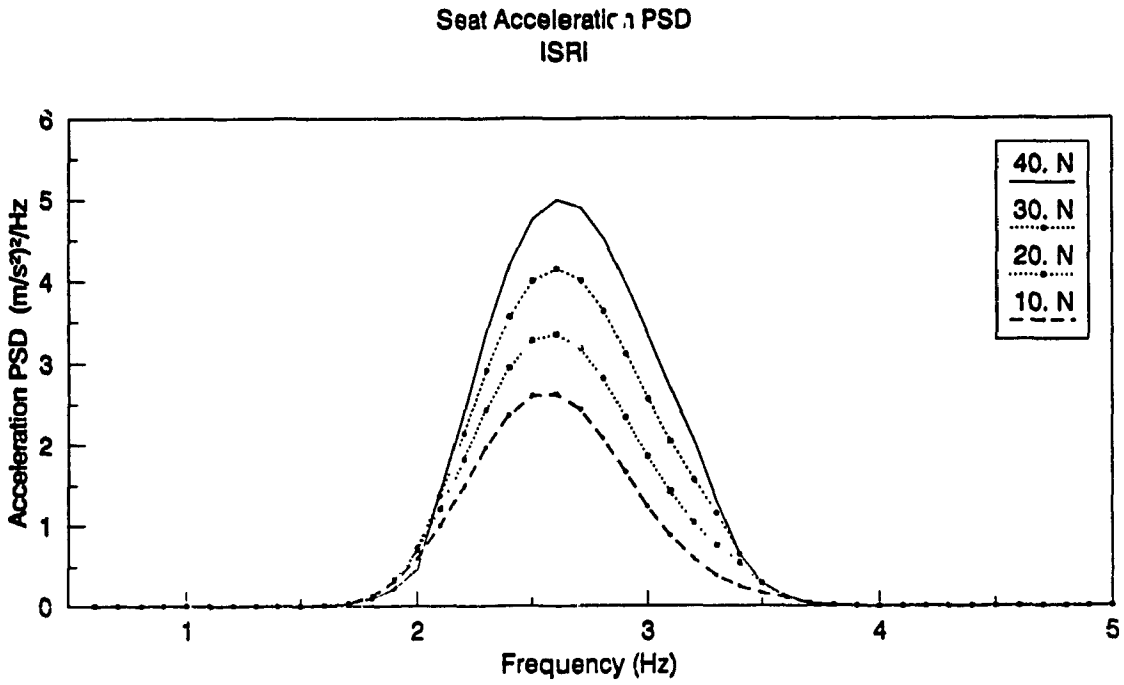

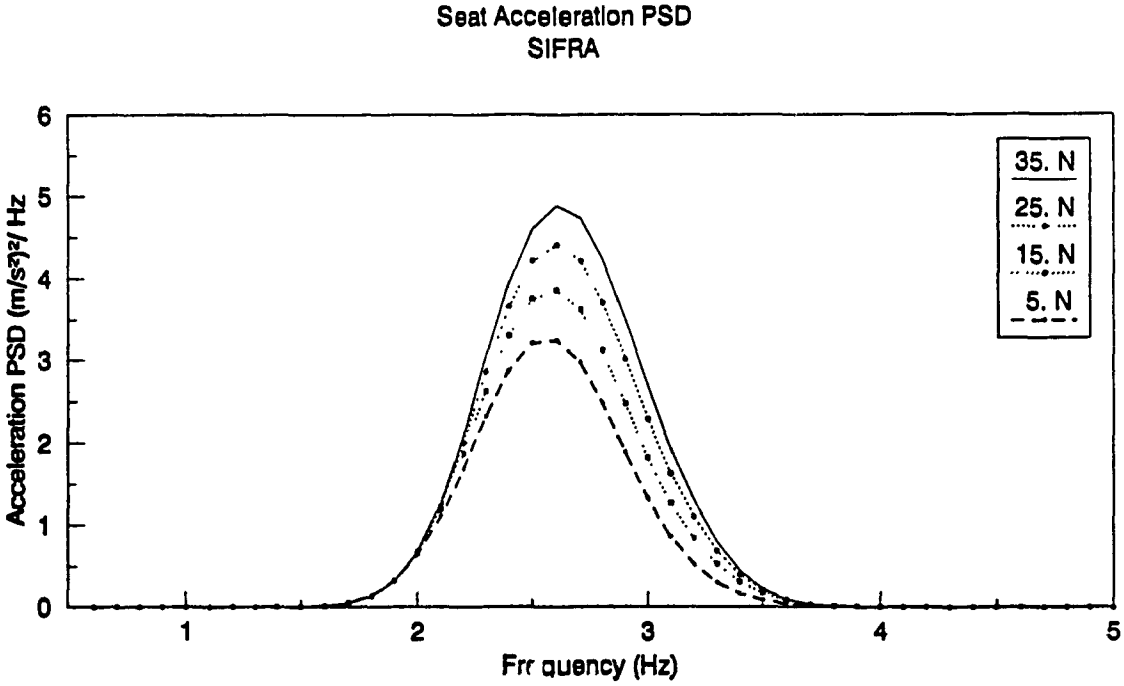

Figure 6.32. Influence of Coulomb Friction Damping on the PSD of Acceleration Response at the Seat: (a) ISRI, (b) SIFRA.

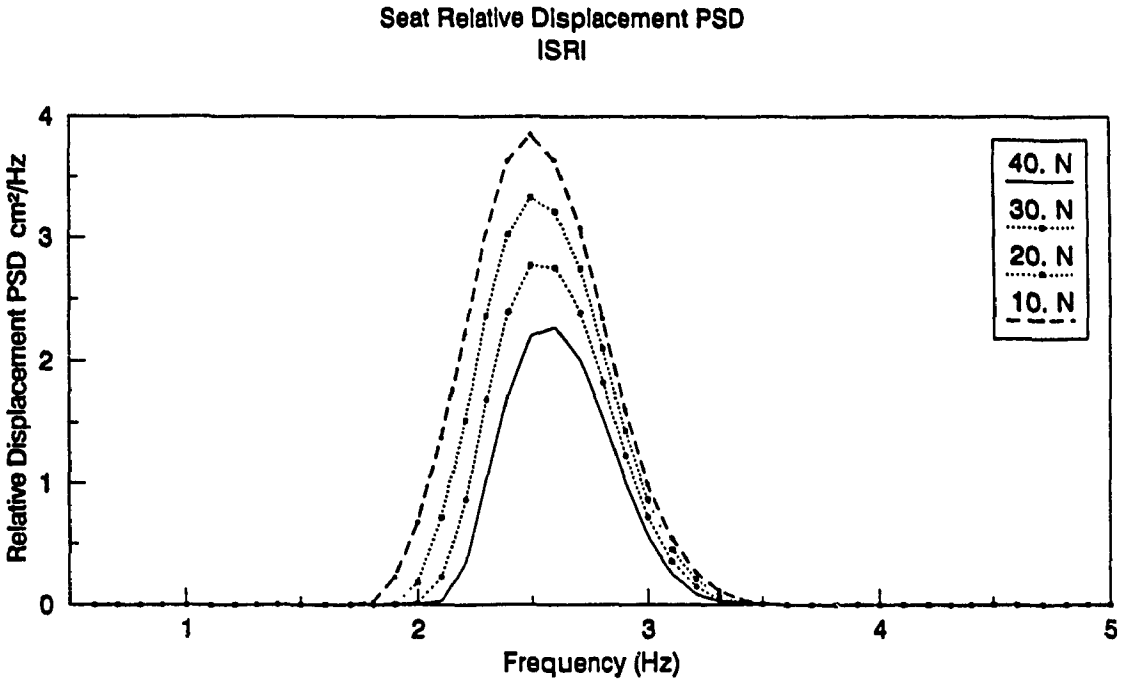

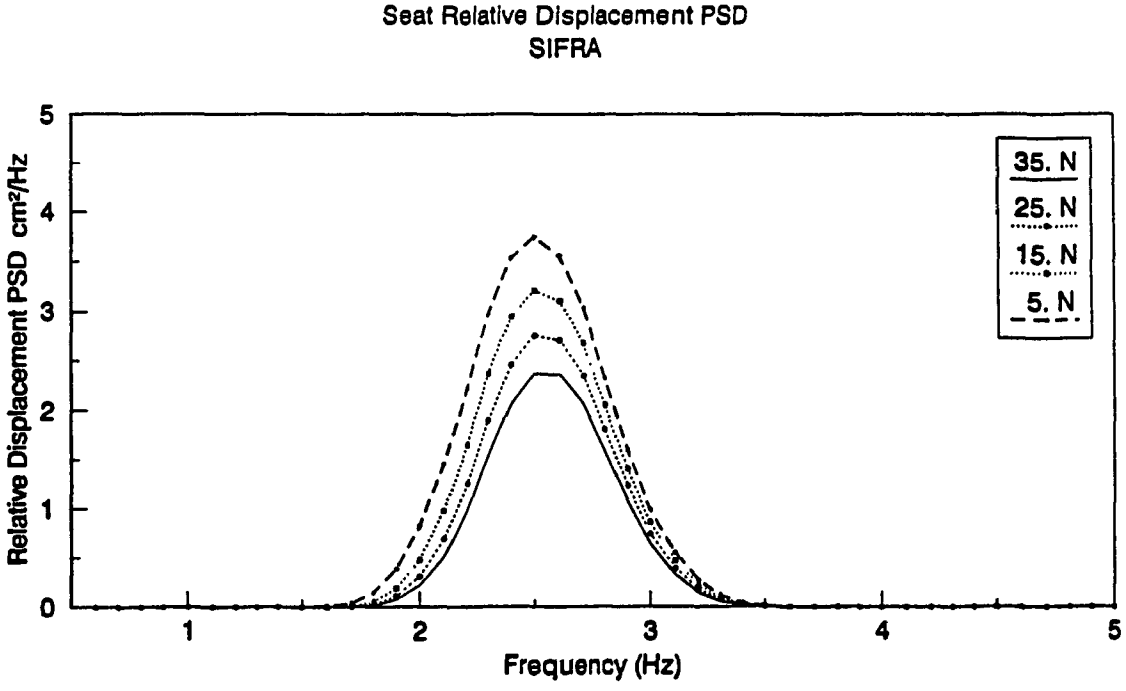

Figure 6.33. Influence of Coulomb Friction Damping on the PSD of Relative Displacement Response of the Seat: (a) ISRI, (b) SIFRA.

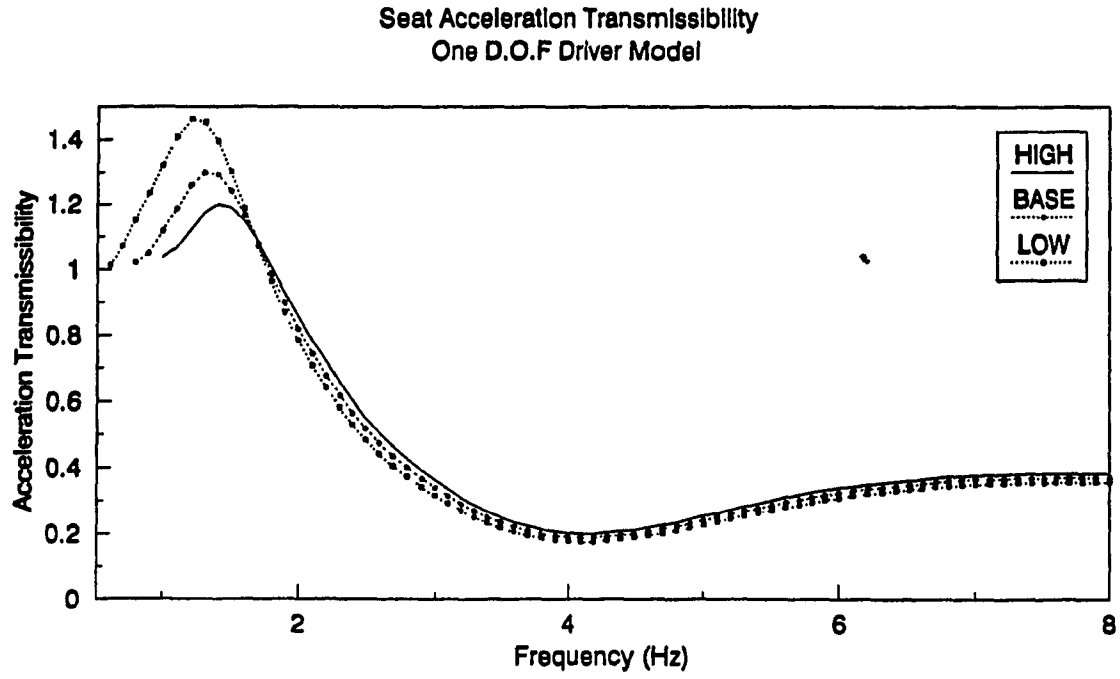

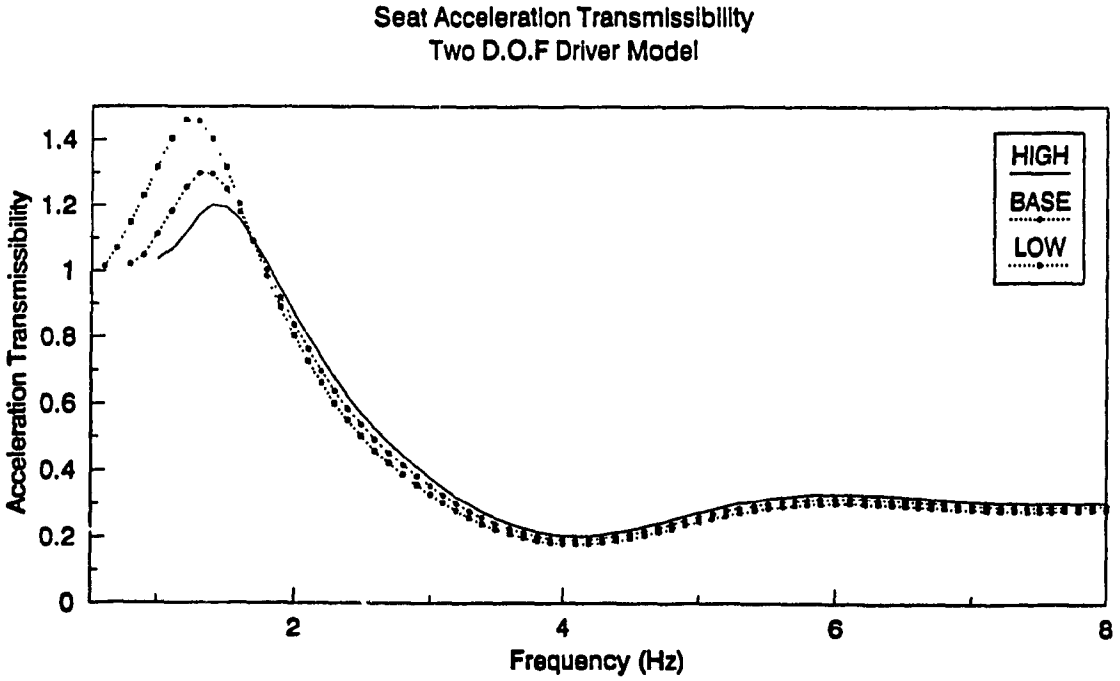

Figure 6.34. Influence of Coulomb Friction Damping on the Acceleration Transmissibility of the Seat Using (a) One D.O.F; (b) Two D.O.F Driver Model.

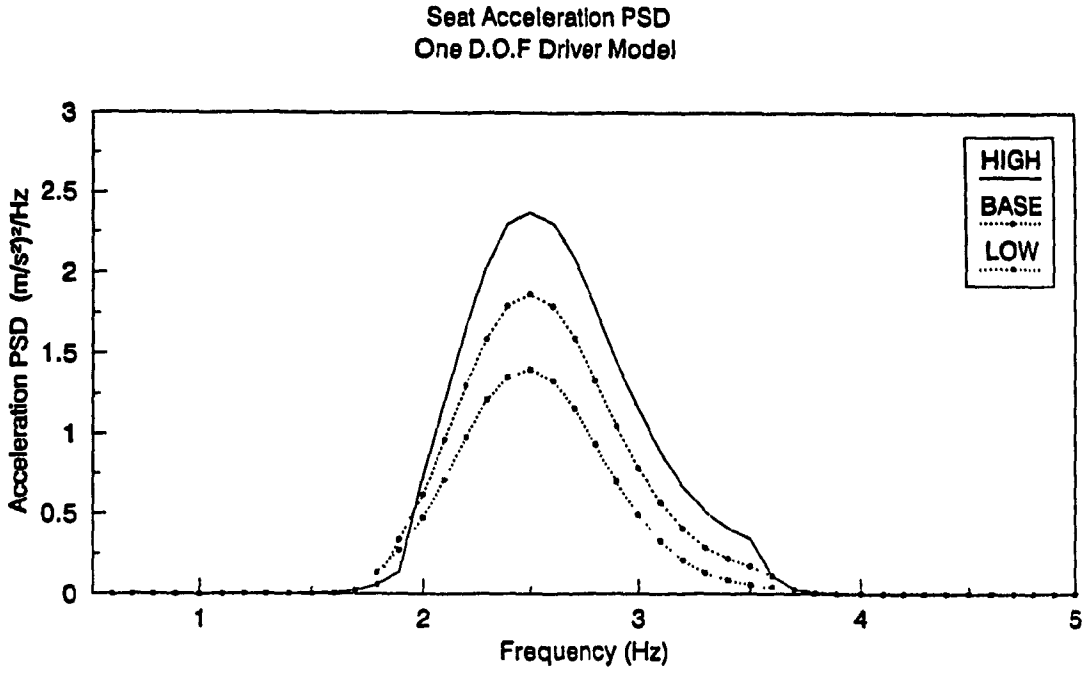

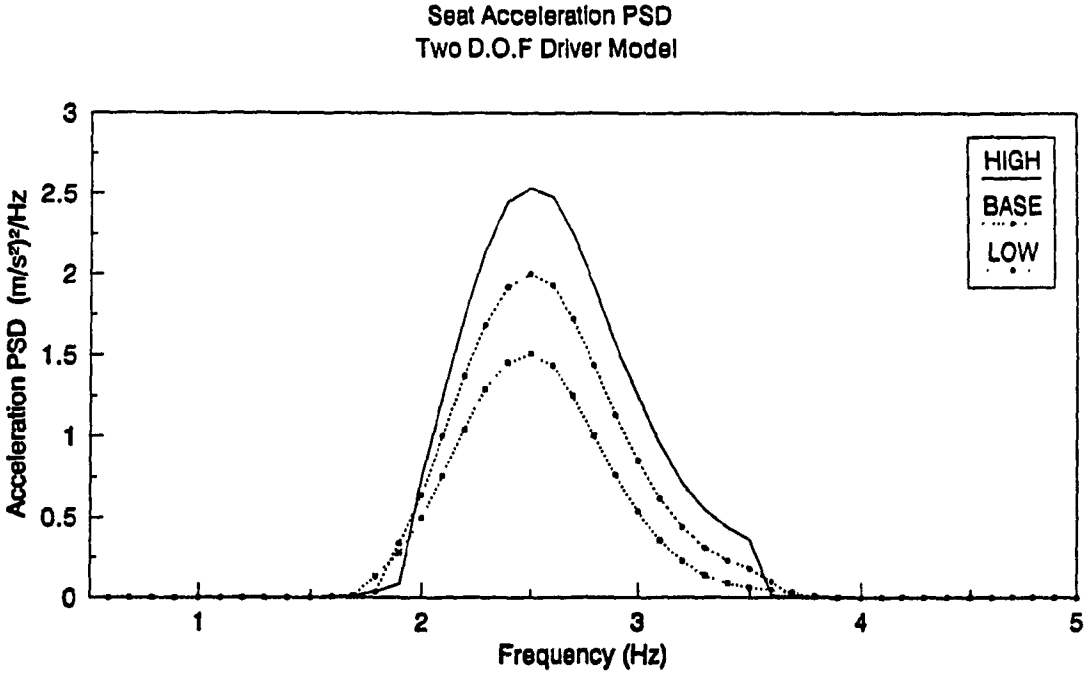

Figure 6.35. Influence of Coulomb Friction Damping on the PSD of Acceleration Response at the Seat Using (a) One D.O.F; (b) Two D.O.F Driver Models.

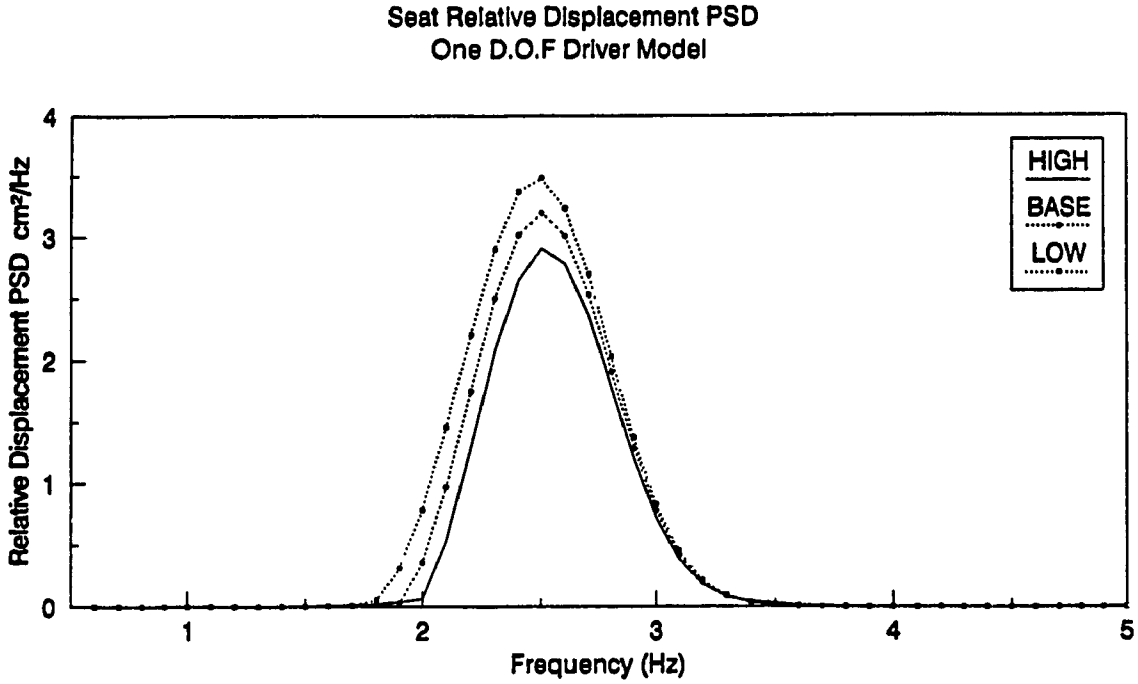

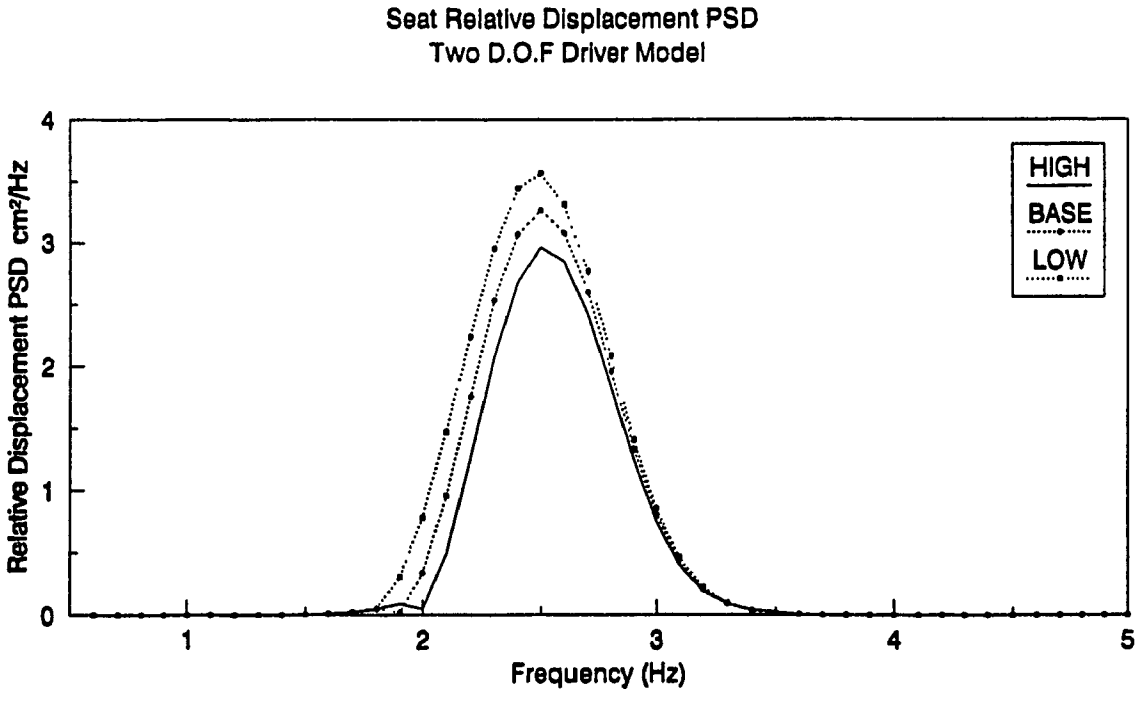

Figure 6.36. Influence of Coulomb Friction Damping on the PSD of Relative Displacement Response of the Seat Using (a) One D.O.F; (b) Two D.O.F Driver Models.

6.3.5 Influence of Suspension Mass

Figures 6.37a and 6.37b illustrate the influence of suspension mass ratio, ($\mu = m_s/m_0$), on the acceleration transmissibility characteristics of ISRI and SIFRA seats, respectively. An increase in the suspension mass yields lower resonant frequency of the seat-suspension system and larger resonant acceleration transmissibility, since the system becomes less damped with an increase in the suspension mass, as illustrated in Equation (6.1). The increase in acceleration transmissibility at the seat resonant frequency, however, is only minimal. The acceleration transmissibility corresponding to vehicle's resonant frequency, reduces considerably with an increase in the suspension mass. The improved vibration isolation is attributed to lower resonant frequency and decreased damping factor caused by the heavier suspension.

The acceleration PSD of the driver mass for the seat-suspension model, subjected to random cab floor excitation, also decreased considerably, as shown in Figure 6.38a and 6.38b. The influence of suspension mass on the relative displacement response of the driver mass is quite insignificant as seen in Figure 6.39. A considerable improvement in ride performance can thus be realized by increasing the suspension mass. A large mass ratio, however, may result in a bulky seat isolator.

Similar parametric sensitivity analyses performed on the ISRI seat-suspension model with one- and two-degrees-of-freedom driver models, show similar influence of the suspension mass, as in the case of the rigid mass model discussed above. An increase in the suspension mass leads to slightly lower resonant frequencies and slightly reduces the acceleration transmissibility in the frequency range 1.5 to 4.0 Hz, as shown in

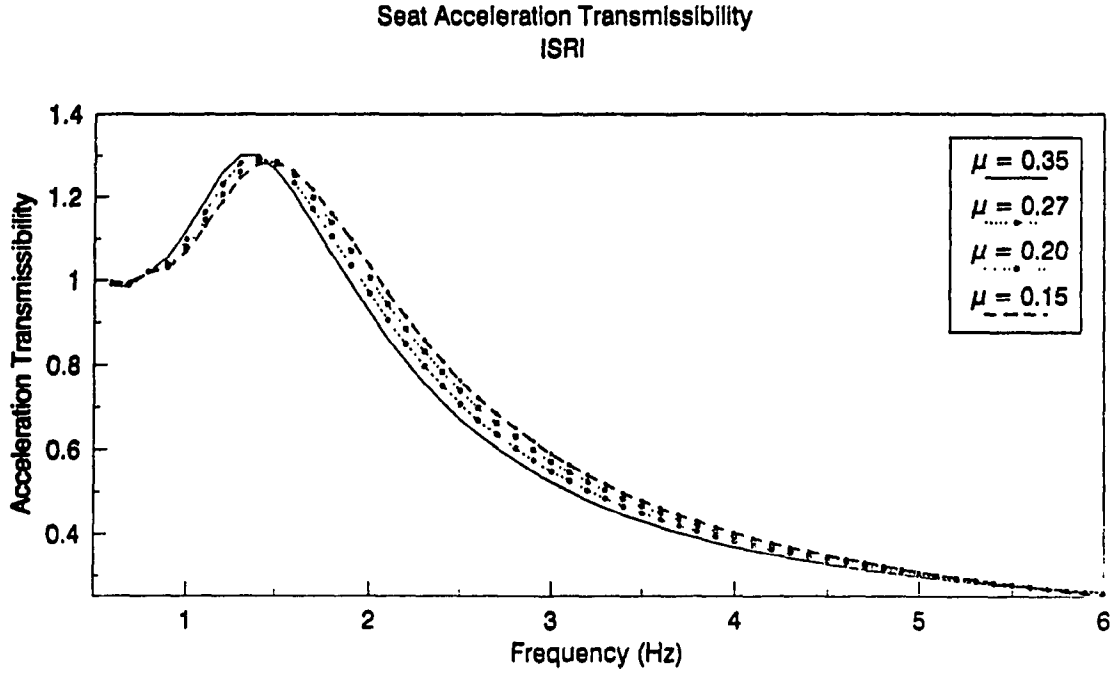

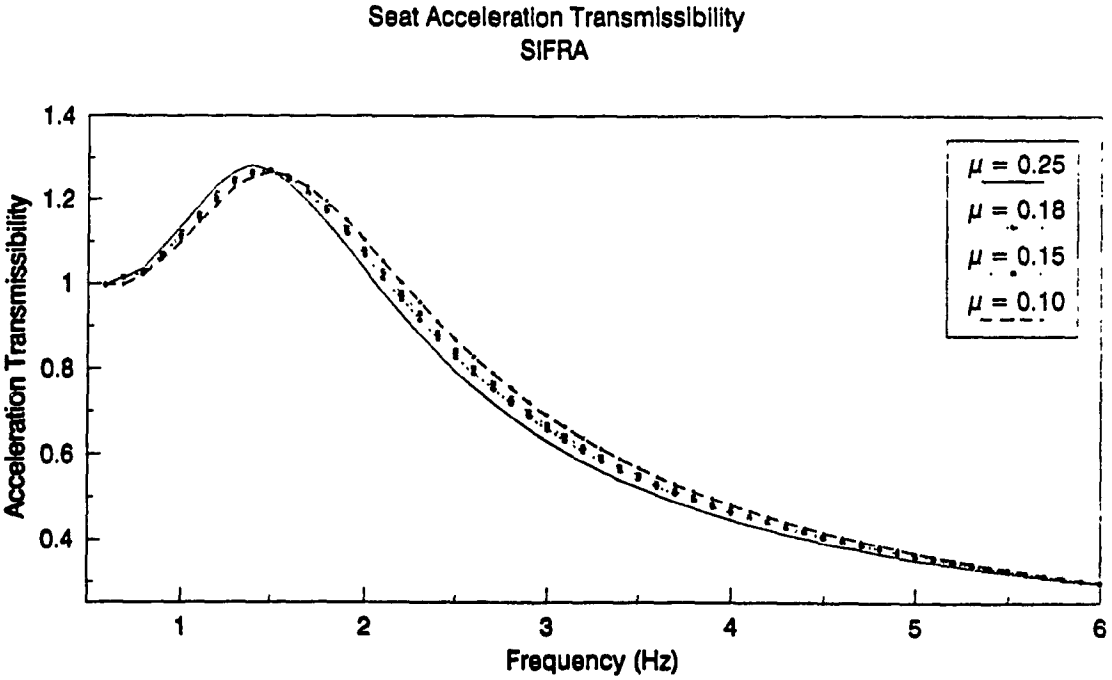

Figure 6.37. Influence of Suspension Mass Ratio, (μ) on the Acceleration Transmissibility of the Seat: (a) ISRI, (b) SIFRA.

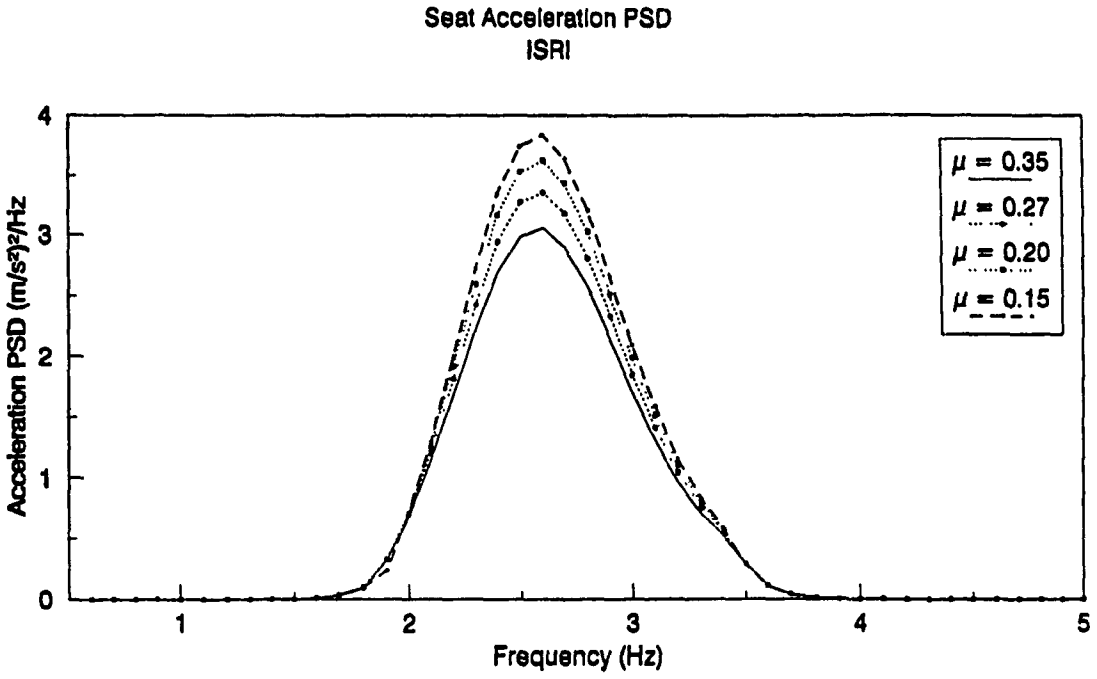

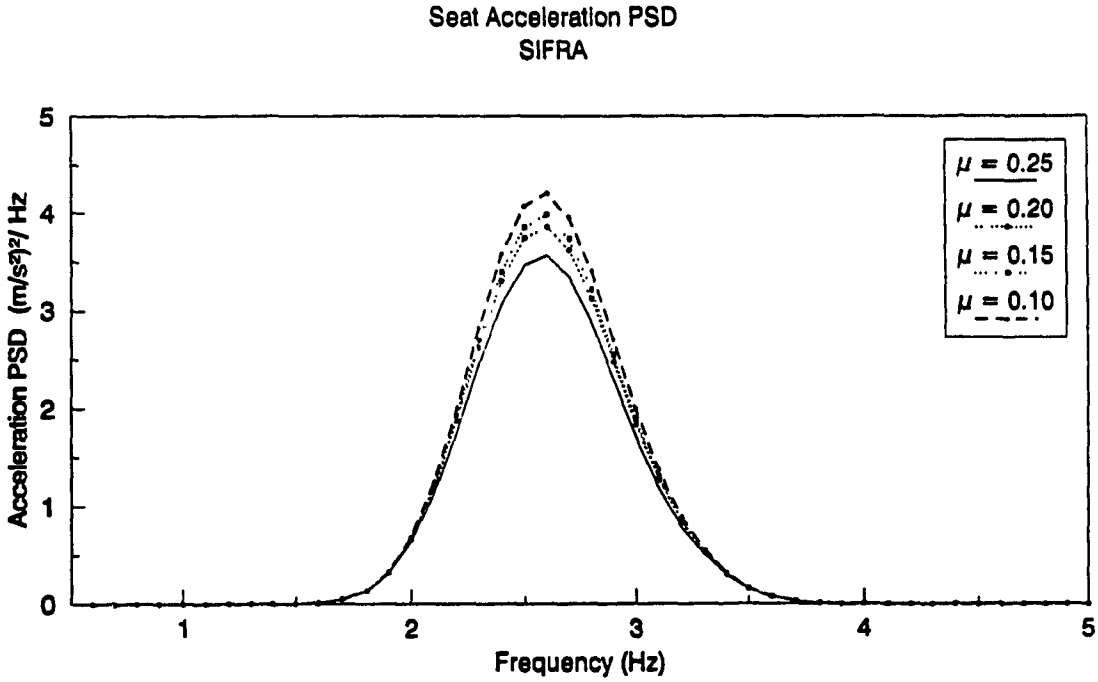

Figure 6.38. Influence of Suspension Mass Ratio, (μ) on the PSD of Acceleration Response at the Seat: (a) ISRI, (b) SIFRA.

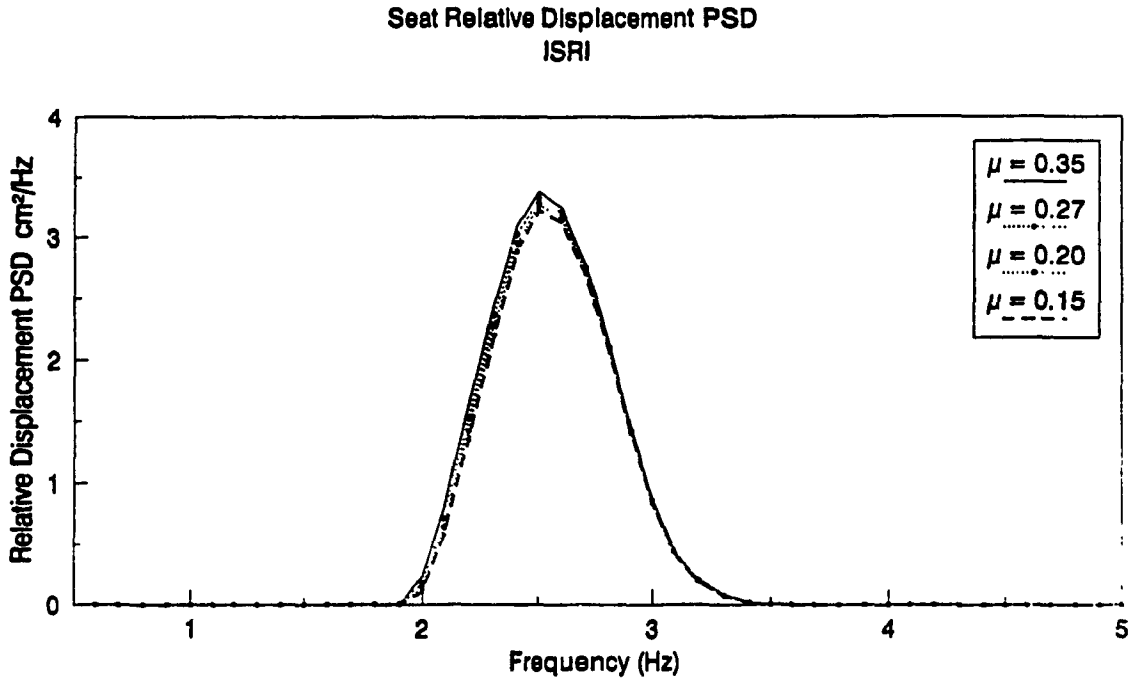

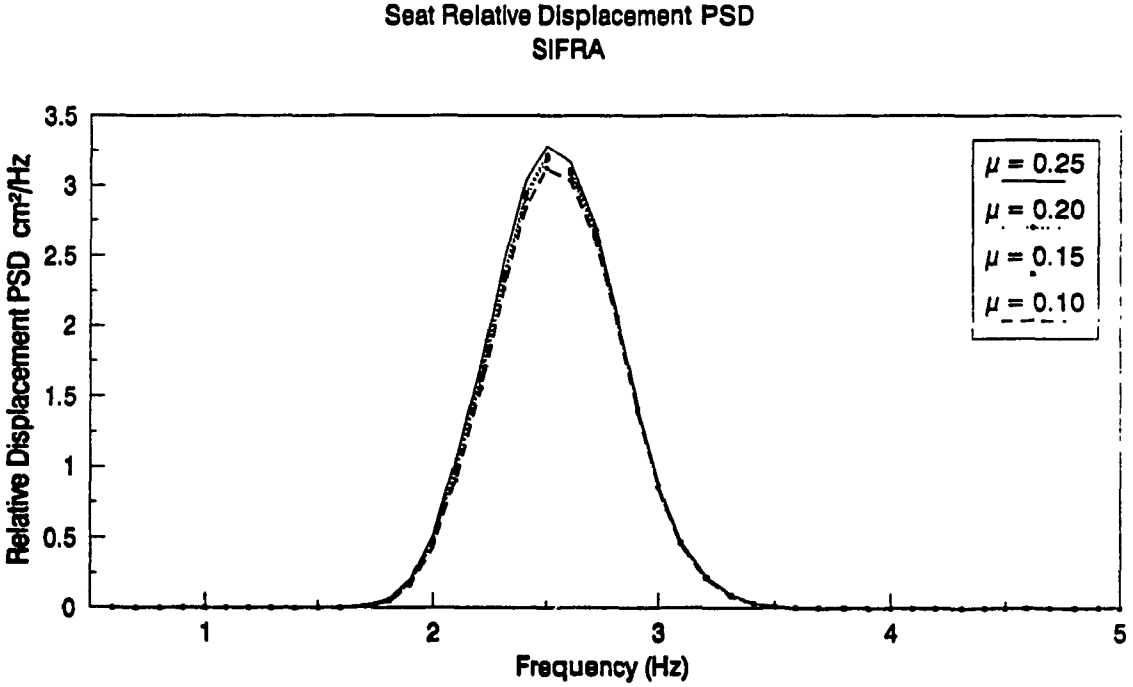

Figure 6.39. Influence of Suspension Mass Ratio, (μ) on the PSD of Relative Displacement Response of the Seat: (a) ISRI, (b) SIFRA.

Figures 6.40a and 6.40b. The acceleration transmissibility response of the ISRI seat increases slightly in the frequency range 4 Hz to 6 Hz, and decreases at frequencies above 6 Hz, due to the human body dynamics. An increase in μ value thus tends to reduce the PSD of the acceleration response with only minimal influence on the relative displacement PSD response, as shown in Figures 6.41 and 6.42.

6.4 RIDE ASSESSMENT OF SEAT-SUSPENSION MODELS

Various methods of rating the severity of exposure to whole-body vibrations and defining limits of exposure have been developed in the past for specific applications. These methods are based on experimental research and have been applied to predict the discomfort, annoyance, health risks, interference with activities and motion sickness associated with the WBV measured in a wide range of environments. Griffin [18] has presented description of these methods applied to all types of vibrations: multiple-axis and multiple-input motions which are steady-state, random or transient. Whole-body vibrations recorded on forestry vehicles contain peak acceleration levels whose intensities vary depending upon the type of tire-terrain interactions occurring during vehicle operations. From measurements carried out on skidders it is reported that the crest factor (CF), ratio of weighted peak to weighted root-mean square 'a_{rms}' acceleration, could typically vary over the range 5-12.5 for vertical vibrations [24].

Although, the various subjective and objective studies conducted during the past two-decades clearly show number of discrepancies concerning methods of measurement and assessment, the boundaries proposed by the ISO-2631 [23]

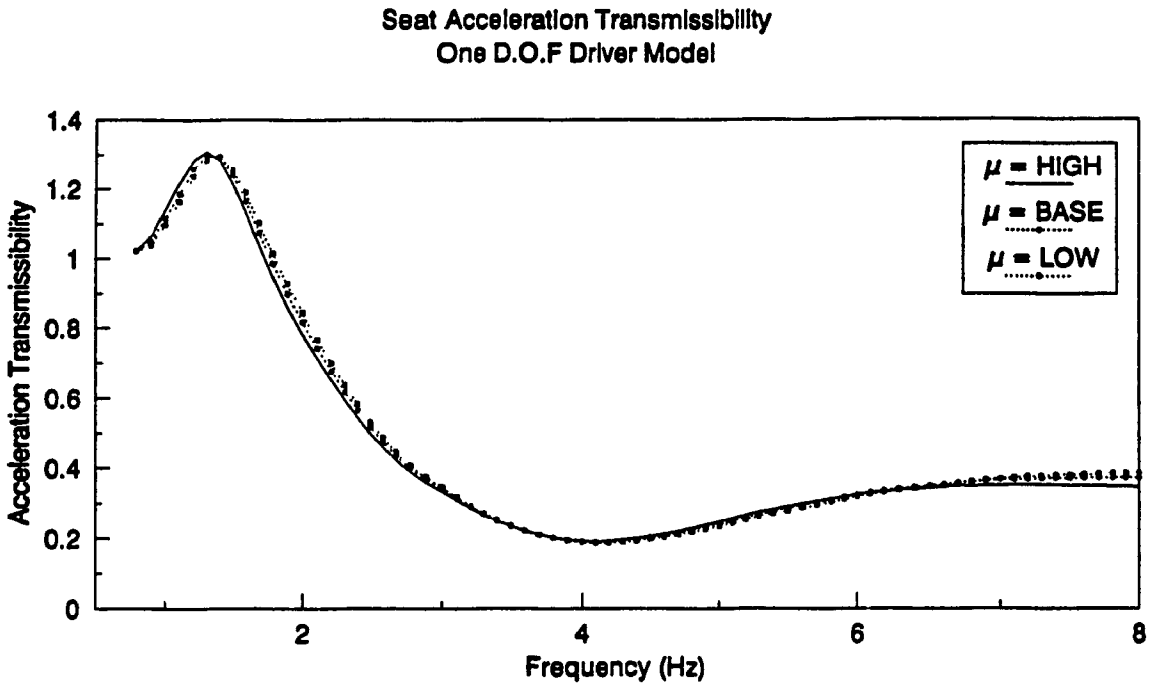

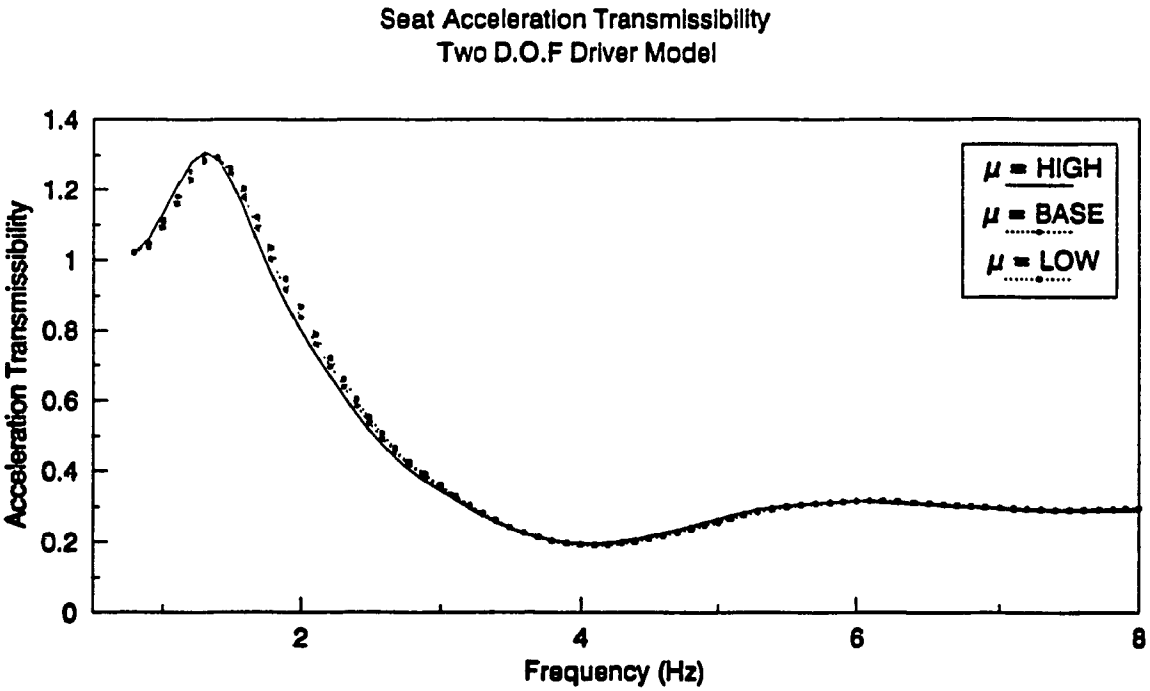

Figure 6.40. Influence of Suspension Mass Ratio, (μ) on the Acceleration Transmissibility of the Seat Using (a) One D.O.F; (b) Two D.O.F Driver Model.

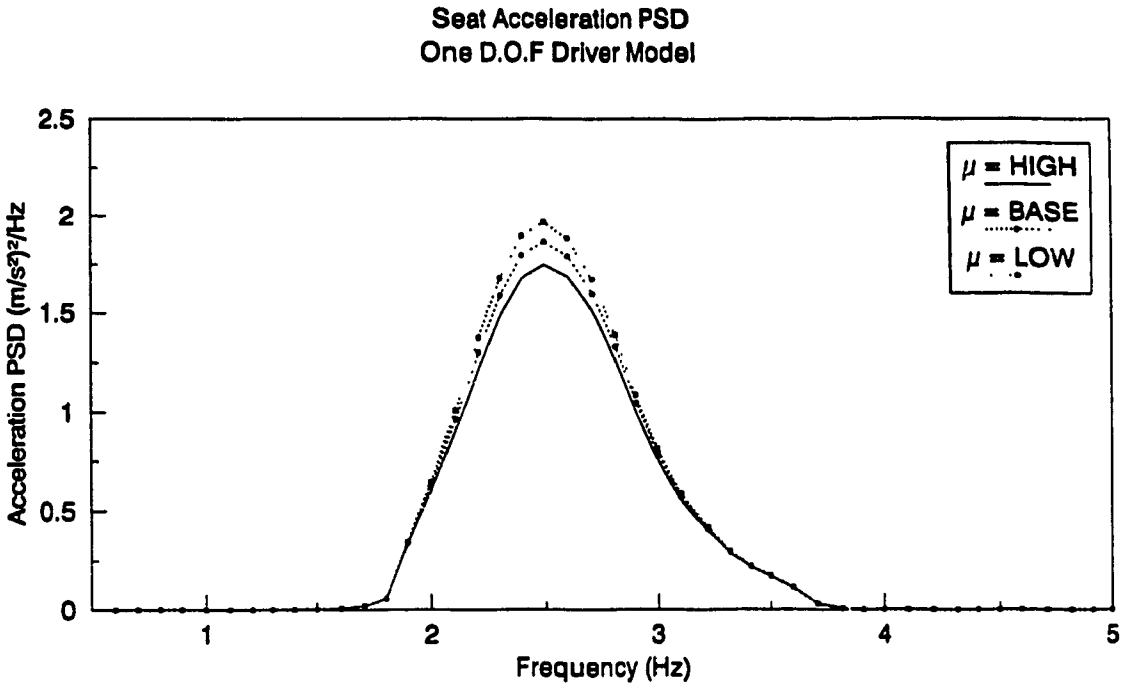

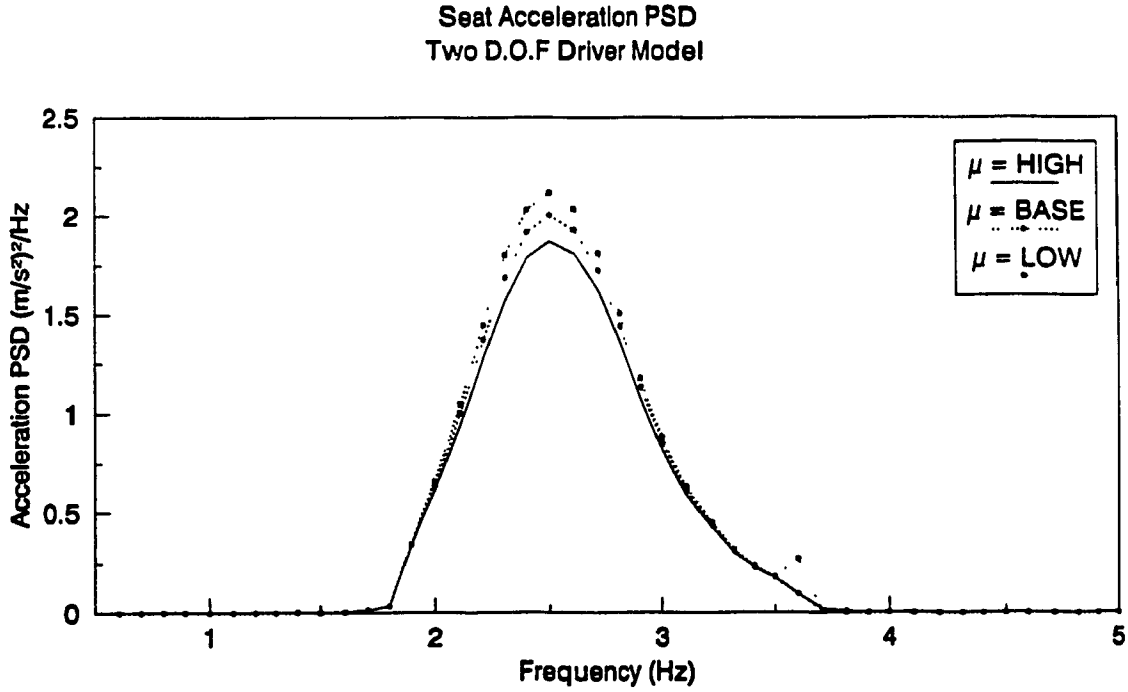

Figure 6.41. Influence of Suspension Mass Ratio, (μ) on the PSD of Acceleration Response at the Seat Using (a) One D.O.F; (b) Two D.O.F Driver Models.

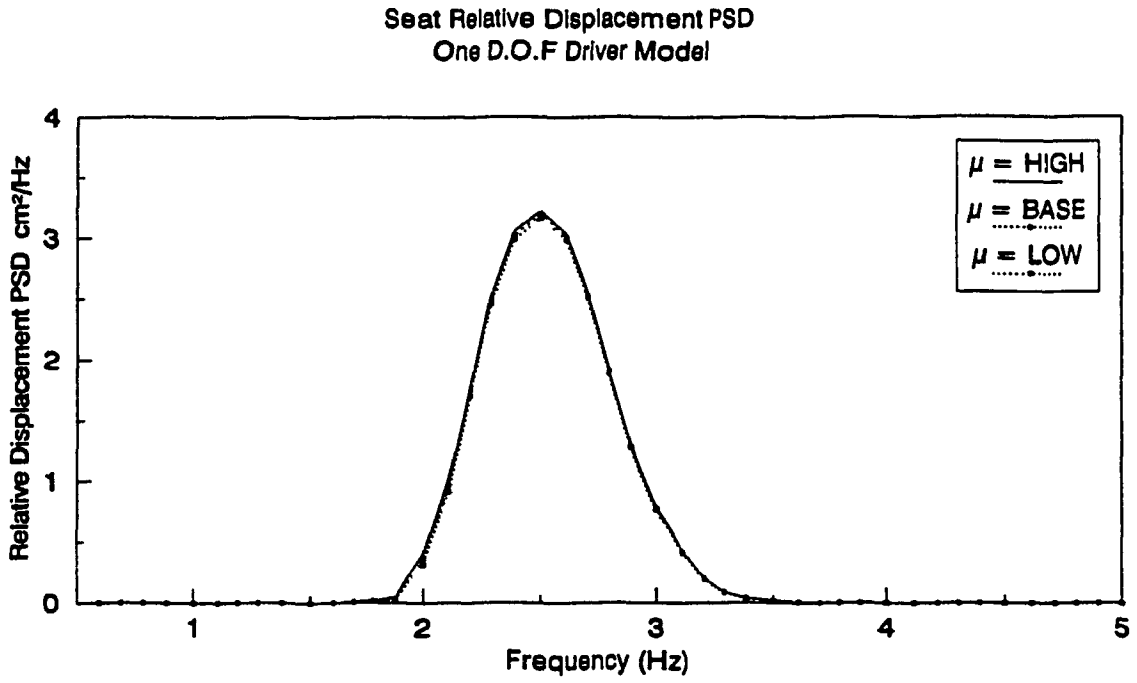

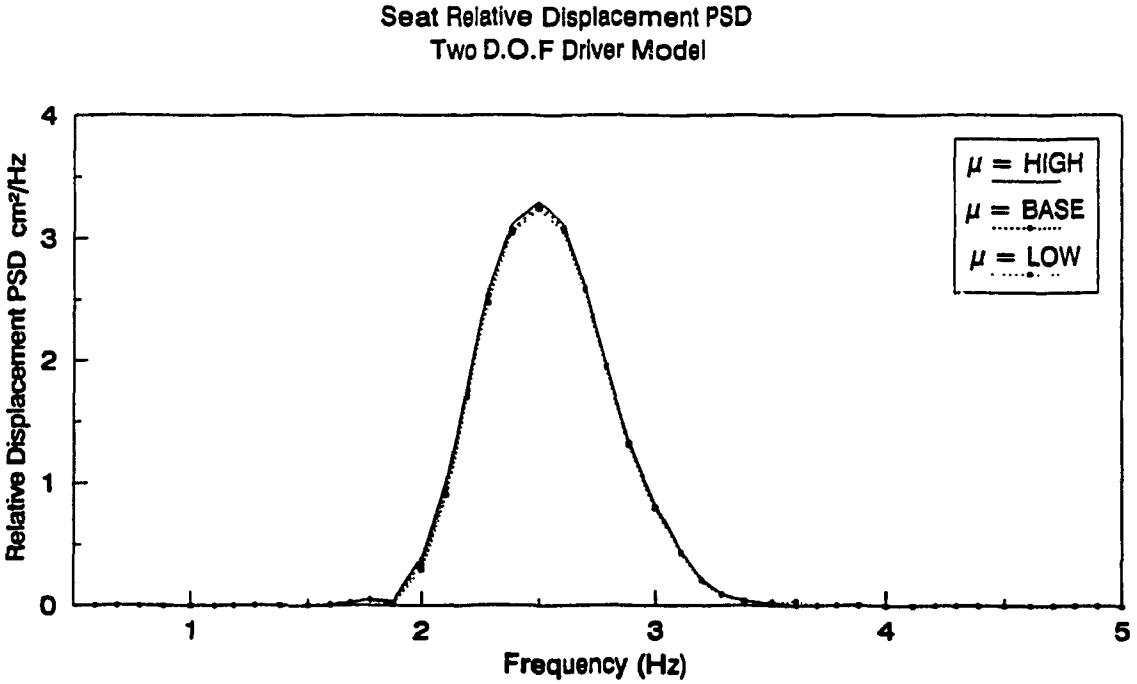

Figure 6.42. Influence of Suspension Mass Ratio, (μ) on the PSD of Relative Displacement Response of the Seat Using (a) One D.O.F; (b) Two D.O.F Driver Models.

have been the most widely used technique to assess the effects of low frequency WBV. The ISO-2631 boundaries, however, are limited to WBV with crest factor smaller than 6. In view of the lack of another universally accepted standard, the relative performance of the seat models are carried out using the fatigue decreased proficiency limits proposed by the ISO-2631.

The ISO recommended limits based on $\frac{1}{3}$ octave frequency bands are given in terms of the root mean squared (rms) accelerations. The rms acceleration limits have also been expressed in terms of equivalent acceleration PSD limits to facilitate the ride assessment using the acceleration PSD data [36].

6.4.1. Performance Evaluation of Seat-Suspension Models

The ride performance characteristics of the seat-suspension models, subjected to Class I and Class II cab floor excitations, are assessed, using the equivalent acceleration PSD limits of the ISO-2631 limits recommended for preservation of working efficiency. The acceleration PSD of the seat mass for the baseline ISRI and SIFRA seat suspension systems are compared to the ISO proposed fatigue decreased proficiency limits for 1.0, 2.5 and 4.0 hours exposure limits, shown in Figures 6.43a and 6.43b. The results clearly reveal that seats do not provide satisfactory ride for even 1 hour exposure, when subjected to Class I vehicle excitation. The acceleration PSD of the ISRI seat, however, is lower than that of the SIFRA seat, as shown in Figure 6.43a. The ISRI seat, however, provides a satisfactory ride for 1 hour exposure for class II vehicles, while the ride response of the SIFRA seat slightly exceeds the 1 hour exposure limit, as shown in Figure 6.43b.

The acceleration PSD of the driver mass exhibits peak response near the vehicle's resonant frequency (2.6 Hz). Further assessment of the

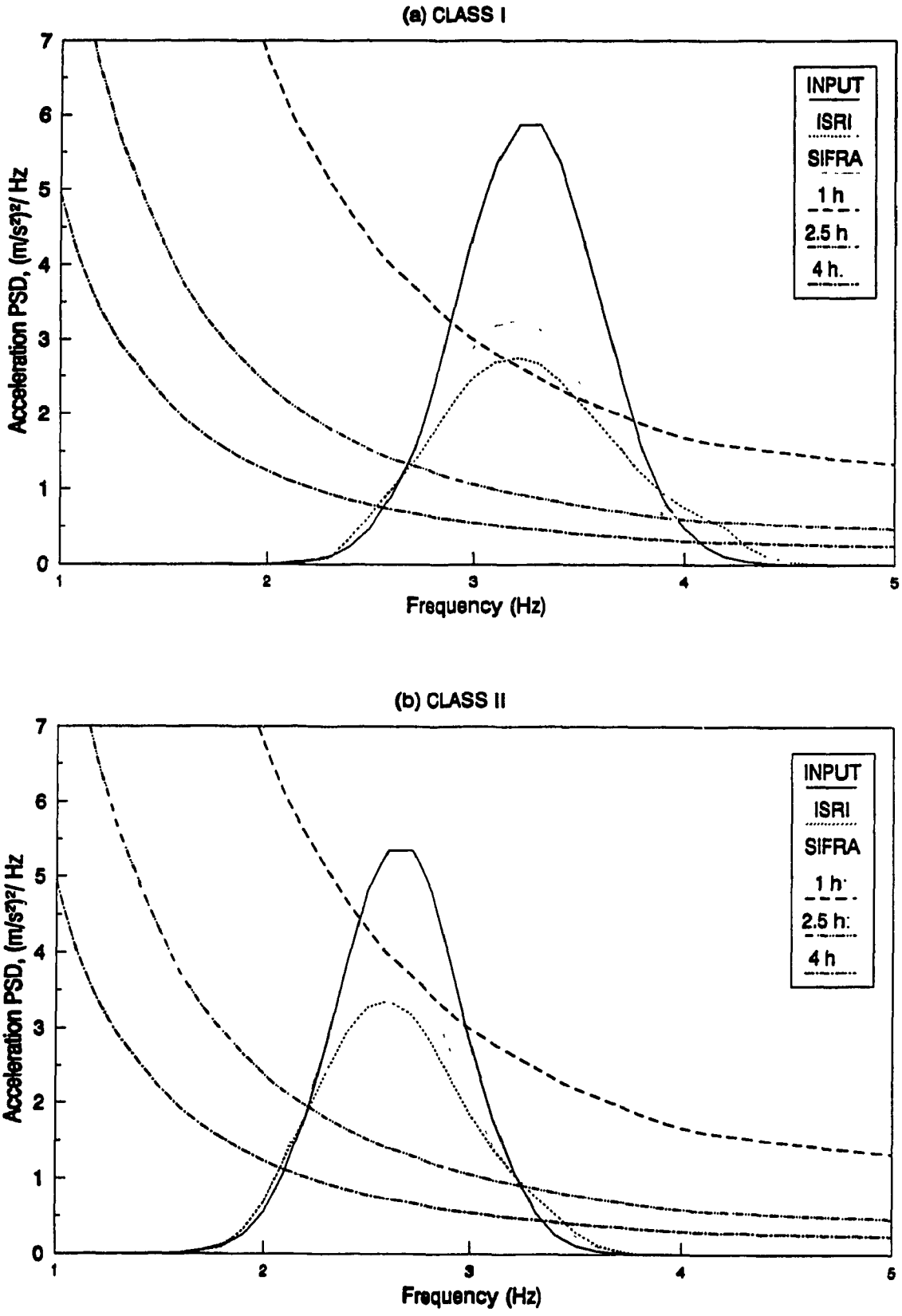

Figure 6.43. Ride Evaluation Based on ISO Fatigue Decreased Proficiency Limits: (a) Class I; (b) Class II Cab Floor Excitation.

seat-suspension performance are thus carried out by comparing response characteristics at 2.6 Hz to the ISO proposed limits at the same frequency. Figures 6.44 and 6.45 present the influence of suspension parameters on the acceleration PSD response at 2.6 Hz, and the corresponding limits for 1.0, 2.5, and 4.0 hours exposure. The legends A, B, C, and D refer to the set of parameter values listed in Table 6.1. Figures 6.44 and 6.45 illustrate the following:

- An increase in cushion stiffness yields improved ride and both the seats with a stiffer cushion provide satisfactory ride for 1 hour exposure.
- A reduction in suspension spring-rate tends to improve the ride quality considerably.
- A reduction in magnitude of Coulomb friction offers considerably superior ride performance.
- The ride performance of both seats improve with an increase in the suspension mass ratio.
- A shock absorber with high value of δ_{1A}, and lower values of δ_{1B} and V_s can provide considerable improvement in ride performance of seat-suspension systems.

From Figures 6.44 and 6.45, it is evident that the damping parameters (both δ_{1A} and δ_{1B}) and the Coulomb friction influence more the ride performance, while the cushion stiffness, the suspension stiffness, the transition velocity, and the mass ratio have significant but relatively less influence on the over all ride performance of the seat-suspension systems.

The dynamics associated with the human driver also contribute to the seat-suspension performance and thus the overall ride quality. In order to illustrate the contribution made by the human body driver, the ride performance of seat-suspension systems with one- and two-degrees-of-freedom human body models is further assessed with reference to the ISO fatigue

Table 6.3a

Influence of Seat-Suspension Parameters on the Seat Acceleration Transmissibility, at the Seat's Resonant Frequency (ISRI and SIFRA, Rigid Mass Driver Models).

Parameter	Seat Type	PARAMETER VALUES			
		A	B	C	D
		Peak Transmissibility Ratio (Frequency)			
CUSHION STIFFNESS (K_C)	ISRI	1.285 (1.4)	1.296 (1.4)	1.331 (1.4)	1.417 (1.4)
	SIFRA	1.263 (1.5)	1.269 (1.5)	1.298 (1.5)	1.353 (1.4)
SUSPENSION STIFFNESS (K_{1A})	ISRI	1.430 (1.5)	1.364 (1.4)	1.296 (1.4)	1.198 (1.3)
	SIFRA	1.332 (1.5)	1.269 (1.5)	1.202 (1.4)	1.165 (1.3)
SUSPENSION DAMPING RATIO (δ_{1A})	ISRI	1.331 (1.4)	1.296 (1.4)	1.243 (1.4)	1.214 (1.5)
	SIFRA	1.305 (1.4)	1.264 (1.5)	1.234 (1.5)	1.206 (1.5)
SUSPENSION DAMPING RATIO (δ_{1B})	ISRI	1.296 (1.4)	1.374 (1.4)	1.532 (1.4)	2.028 (1.4)
	SIFRA	1.234 (1.4)	1.264 (1.5)	1.406 (1.5)	2.198 (1.5)
TRANSITION VELOCITY (V_S)	ISRI	1.314 (1.4)	1.296 (1.4)	1.258 (1.4)	1.258 (1.4)
	SIFRA	1.283 (1.4)	1.264 (1.5)	1.234 (1.5)	1.234 (1.5)
COULOMB DAMPING FORCE (F_{CD})	ISRI	1.151 (1.6)	1.202 (1.5)	1.296 (1.4)	1.453 (1.3)
	SIFRA	1.149 (1.7)	1.194 (1.5)	1.267 (1.5)	1.391 (1.3)
MASS RATIO (μ)	ISRI	1.300 (1.4)	1.296 (1.4)	1.288 (1.4)	1.285 (1.5)
	SIFRA	1.280 (1.4)	1.269 (1.5)	1.268 (1.5)	1.266 (1.5)

Table 6.3b

Influence of Seat-Suspension Parameters on the Seat Acceleration Transmissibility, at the Vehicle's Resonant Frequency (ISRI and SIFRA, Rigid Mass Driver Models).

PARAMETER	SEAT TYPE	PARAMETER VALUE			
		A	B	C	D
		TRANSMISSIBILITY RATIO @ 2.6 Hz			
CUSHION STIFFNESS (K_C)	ISRI	0.665	0.669	0.679	0.695
	SIFRA	0.786	0.788	0.797	0.806
SUSPENSION STIFFNESS (K_{1A})	ISRI	0.733	0.702	0.669	0.626
	SIFRA	0.830	0.788	0.746	0.722
SUSPENSION DAMPING RATIO (δ_{1A})	ISRI	0.658	0.669	0.687	0.701
	SIFRA	0.775	0.788	0.801	0.813
SUSPENSION DAMPING RATIO (δ_{1B})	ISRI	0.669	0.604	0.532	0.461
	SIFRA	0.838	0.788	0.664	0.523
TRANSITION VELOCITY (V_s)	ISRI	0.664	0.669	0.690	0.715
	SIFRA	0.781	0.788	0.811	0.836
COULOMB DAMPING FORCE (F_{CD})	ISRI	0.745	0.707	0.669	0.631
	SIFRA	0.852	0.820	0.788	0.755
MASS RATIO (μ)	ISRI	0.635	0.669	0.699	0.722
	SIFRA	0.754	0.788	0.802	0.828

Table 6.3c

Influence of Seat-Suspension Parameters on the PSD of Acceleration Response of seat, at the Vehicle's Resonant Frequency (ISRI and SIFRA, Rigid Mass Driver Models).

PARAMETER	SEAT TYPE	PARAMETER VALUES							
		A	B	C	D	A	B	C	D
		ACCELERATION PSD, $(m/s^2)^2/Hz$				REL. DISPLACEMENT PSD, cm^2/Hz			
CUSHION STIFFNESS (K_2)	ISRI	3.296	3.354	3.528	3.860	3.233	3.332	3.666	4.505
	SIFRA	3.820	3.857	4.000	4.185	3.149	3.213	3.500	4.045
SUSPENSION STIFFNESS (K_{1A})	ISRI	3.785	3.575	3.354	3.074	3.772	3.564	3.332	3.018
	SIFRA	4.184	3.857	3.537	3.363	3.462	3.214	2.954	2.804
SUSPENSION DAMPING RATIO (δ_{1A})	ISRI	3.147	3.354	3.715	4.011	3.476	3.332	3.081	2.877
	SIFRA	3.818	4.078	4.342	4.609	3.240	3.015	2.787	2.560
SUSPENSION DAMPING RATIO (δ_{1B})	ISRI	3.354	3.027	2.668	2.294	3.332	3.555	3.805	4.073
	SIFRA	4.343	4.078	3.439	2.703	2.799	3.015	3.558	4.245
TRANSITION VELOCITY (V_s)	ISRI	3.246	3.354	3.606	3.606	3.407	3.332	3.164	3.164
	SIFRA	3.950	4.078	4.343	4.343	3.125	3.015	2.799	2.799
COULOMB DAMPING FORCE (F_{CD})	ISRI	4.995	4.151	3.354	2.626	2.277	2.780	3.332	3.844
	SIFRA	4.877	4.404	3.857	3.243	2.369	2.755	3.214	3.746
MASS RATIO (μ)	ISRI	3.057	3.353	3.620	3.836	3.385	3.332	3.278	3.229
	SIFRA	3.562	3.857	3.979	4.207	3.282	3.210	3.180	3.120

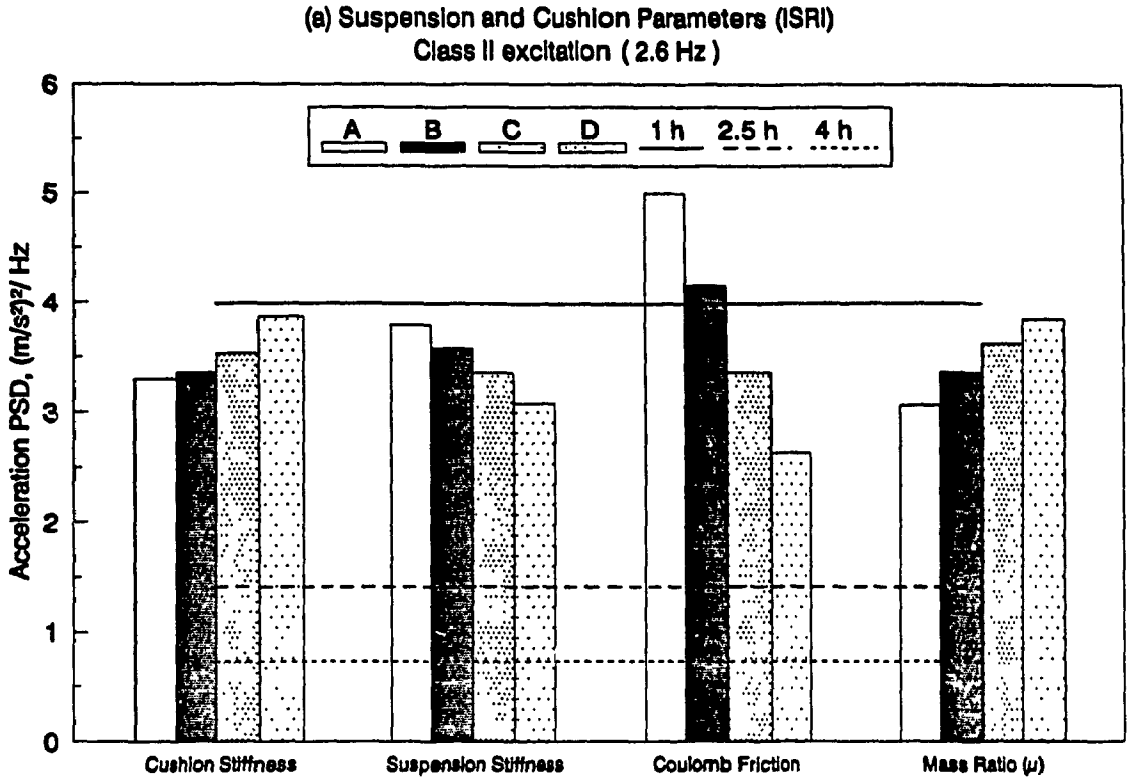

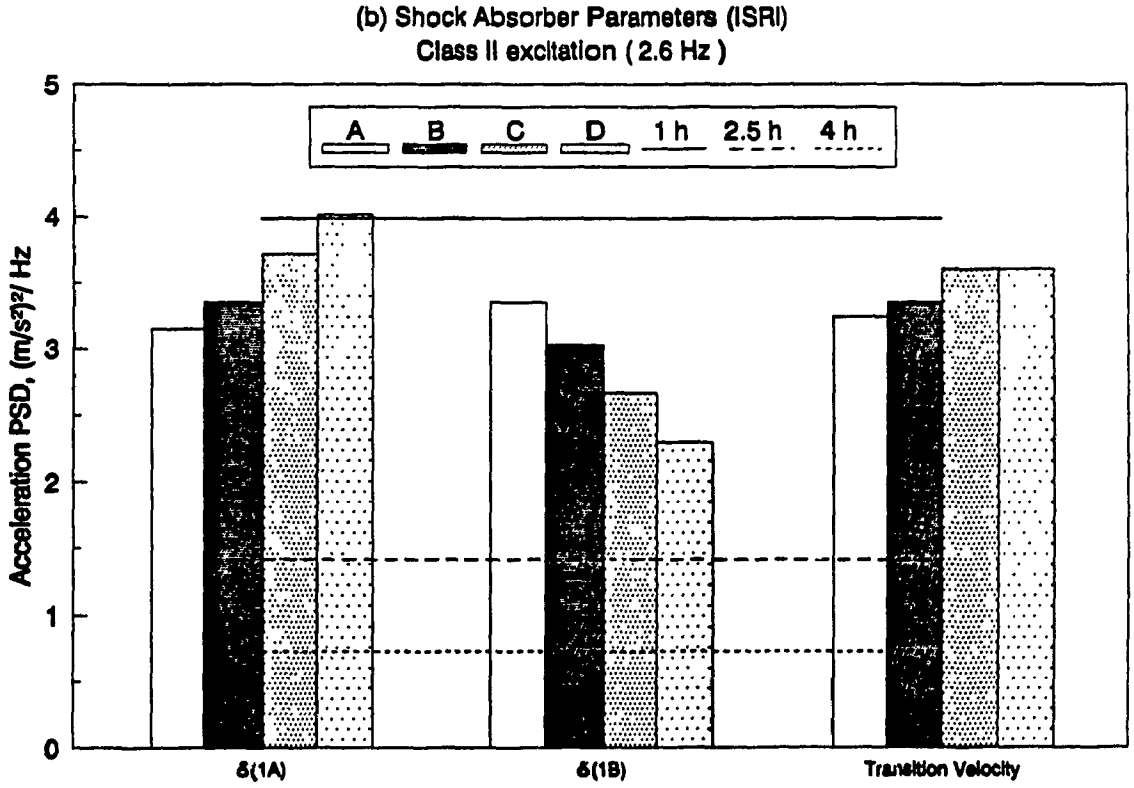

Figure 6.44. Influence of Seat-Suspension Parameters (ISRI) on the PSD of Seat Acceleration at the Vehicle's Resonant Frequency: (a) Suspension and Cushion; (b) Shock Absorber Parameters.

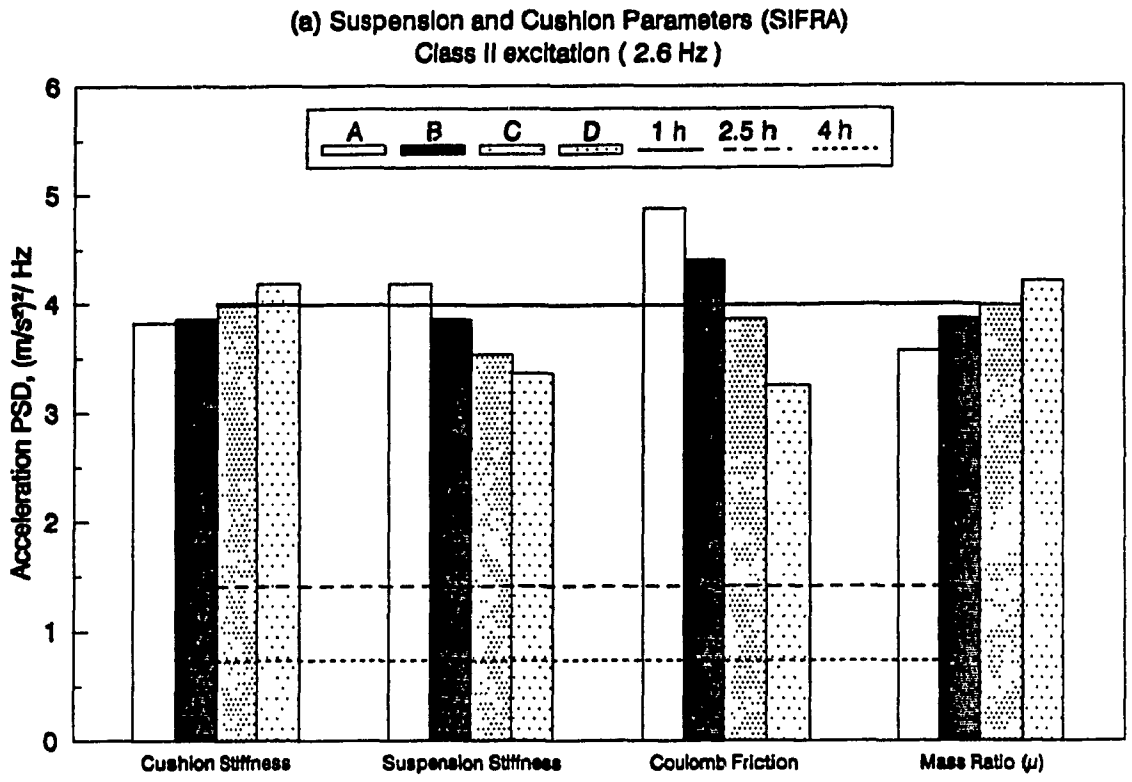

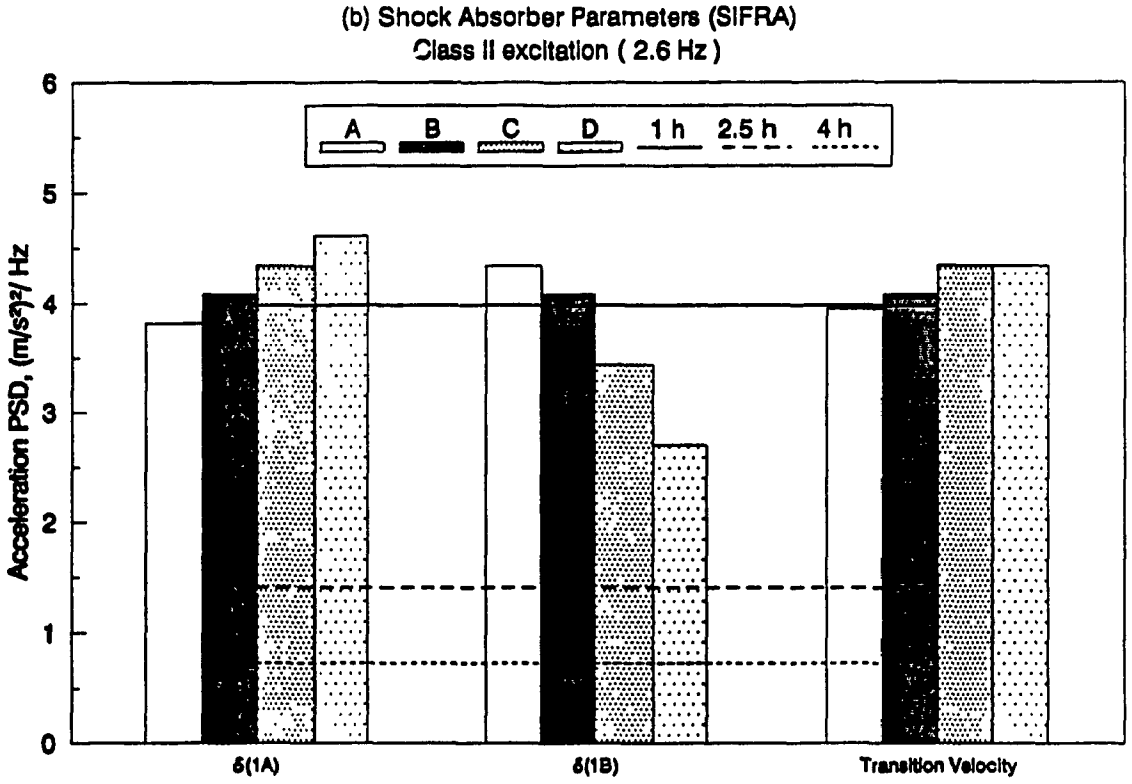

Figure 6.45. Influence of Seat-Suspension Parameters (SIFRA) on the PSD of Seat Acceleration at the Vehicle's Resonant Frequency: (a) Suspension and Cushion; (b) Shock Absorber Parameters.

decreased proficiency limits. Figures 6.46a and 6.46b present the acceleration PSD of the three- and four-degrees-of-freedom seat-suspension models for excitations arising from Class I and Class II vehicles. A comparison of Figures 6.43 and 6.46 clearly illustrates the influence of the human driver model to the total ride performance of the seat-suspension systems.

Both the ride models provide satisfactory ride for 2.5 h exposure, particularly, when subjected to Class I excitations, as shown Figure 6.46a. The ride response slightly exceeds the 2.5 h exposure limit, when subjected to Class II vehicle excitation. The influence of seat parameters on the ride performance of these models, based on Class II cab floor excitations, are assessed using the ISO fatigue decreased proficiency limits for 1.0, 2.5, and 4.0 hours exposure at 2.6 Hz, as shown in Figures 6.47 and 6.48. It should be noted, the legends LOW, BASE, and HIGH refer to the parameter values listed in Table 6.2. Figures 6.47 and 6.48 illustrate the following:

- Softer cushions deteriorate the ride performance of the driver-seat-suspension systems.
- An increase in stiffness of ISRI cushions, however, yields only slight improvement in vehicle ride.
- Softer suspension spring yields considerable improvement in absolute acceleration response at the driver-seat interface. Too soft a suspension, however, deteriorates the ride performance of the driver-seat-suspension systems due to excessive static and dynamic deflections.
- A low Value of Coulomb friction force provides a considerable improvement in ride performance. The ride performance of the three-degrees-of-freedom driver-seat-suspension model with low friction is within the 2.5 hours exposure limit.
- An increase in suspension mass ratio provides considerable improvement in the ride performance of driver-seat-suspension models.

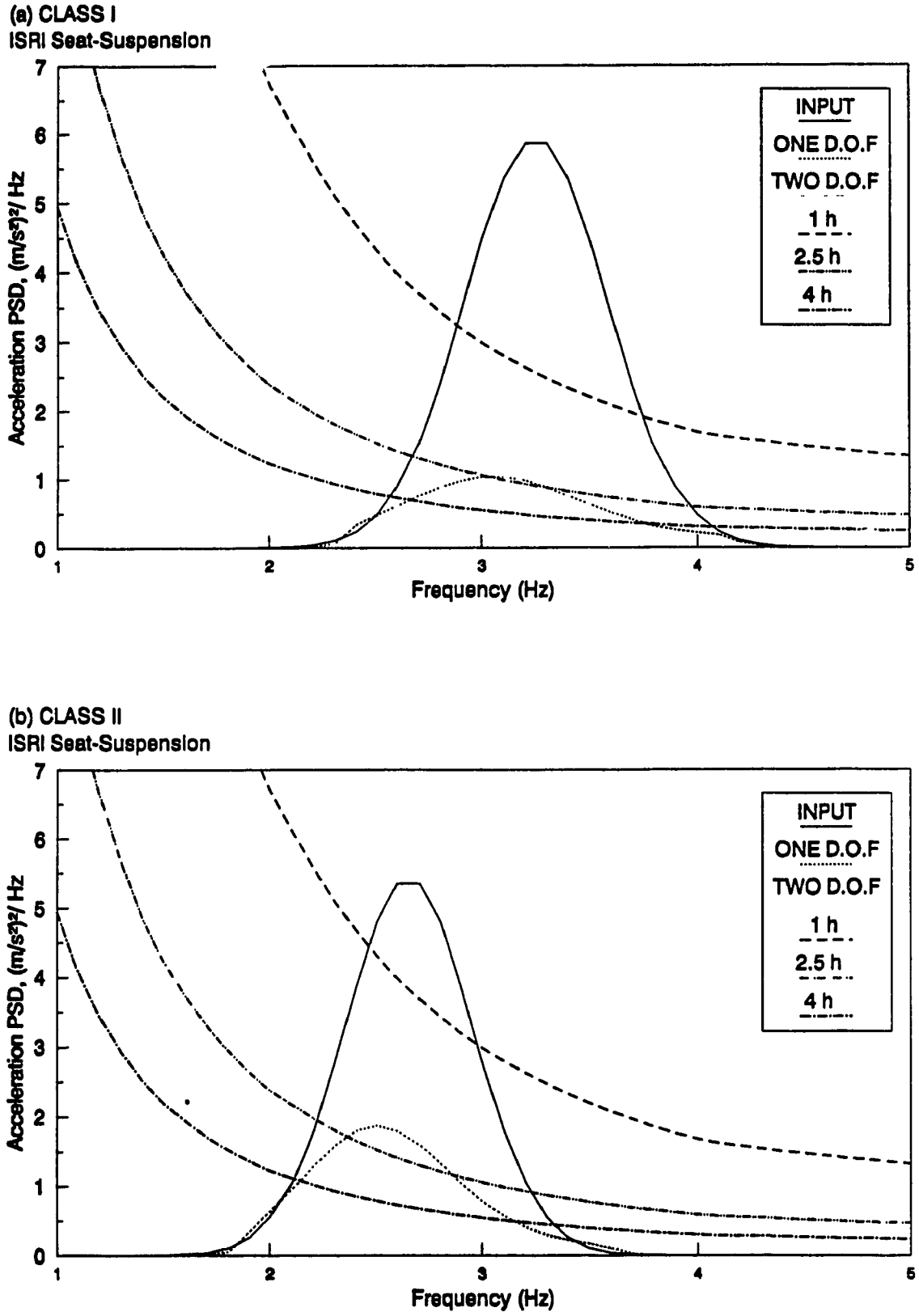

Figure 6.46. Ride Evaluation Based on ISO Fatigue Decreased Proficiency Limits for Seats Incorporating Driver Models: (a) Class I; (b) Class II Cab Floor Excitation.

Table 6.4a

Influence of Seat-Suspension Parameters on the Seat Acceleration Transmissibility, at the Seat's Resonant Frequency (ISRI: One and Two D.O.F. Driver Models).

PARAMETER	TYPE OF THE DRIVER MODEL (D.O.F.)	PARAMETER VALUES		
		LOW	BASE	HIGH
		PEAK TRANSMISSIBILITY RATIO (FREQ)		
CUSHION STIFFNESS (K_c)	ONE	1.333 (1.3)	1.298 (1.3)	1.287 (1.3)
	TWO	1.332 (1.3)	1.297 (1.3)	1.286 (1.3)
SUSPENSION STIFFNESS (K_{1A})	ONE	1.197 (1.3)	1.298 (1.3)	1.440 (1.4)
	TWO	1.199 (1.3)	1.297 (1.3)	1.440 (1.4)
SUSPENSION DAMPING RATIO (δ_{1A})	ONE	1.337 (1.3)	1.298 (1.3)	1.247 (1.4)
	TWO	1.337 (1.3)	1.297 (1.3)	1.249 (1.4)
SUSPENSION DAMPING RATIO (δ_{1B})	ONE	1.369 (1.3)	1.298 (1.3)	1.262 (1.3)
	TWO	1.369 (1.4)	1.297 (1.3)	1.261 (1.3)
TRANSITION VELOCITY (V_s)	ONE	1.317 (1.3)	1.298 (1.3)	1.262 (1.3)
	TWO	1.316 (1.3)	1.297 (1.3)	1.261 (1.3)
COULOMB DAMPING FORCE (F_{CD})	ONE	1.463 (1.2)	1.298 (1.3)	1.200 (1.4)
	TWO	1.460 (1.2)	1.297 (1.3)	1.200 (1.4)
MASS RATIO (μ)	ONE	1.293 (1.4)	1.298 (1.3)	1.308 (1.3)
	TWO	1.292 (1.4)	1.297 (1.3)	1.308 (1.3)

Table 6.4b

Influence of Seat-Suspension Parameters on the Seat Acceleration Transmissibility, at the Vehicle's Resonant Frequency (ISRI: One and Two D.O.F. Driver Models).

PARAMETER	TYPE OF THE DRIVER MODEL (D.O.F.)	PARAMETER VALUES		
		LOW	BASE	HIGH
		TRANSMISSIBILITY RATIO		
CUSHION STIFFNESS (K_c)	ONE	0.477	0.473	0.472
	TWO	0.496	0.492	0.490
SUSPENSION STIFFNESS (K_{1A})	ONE	0.448	0.473	0.509
	TWO	0.466	0.492	0.530
SUSPENSION DAMPING RATIO (δ_{1A})	ONE	0.463	0.473	0.490
	TWO	0.482	0.492	0.510
SUSPENSION DAMPING RATIO (δ_{1B})	ONE	0.426	0.473	0.511
	TWO	0.443	0.492	0.532
TRANSITION VELOCITY (V_s)	ONE	0.469	0.473	0.490
	TWO	0.487	0.492	0.510
COULOMB DAMPING FORCE (F_{CD})	ONE	0.442	0.473	0.503
	TWO	0.460	0.492	0.523
MASS RATIO (μ)	ONE	0.486	0.473	0.458
	TWO	0.506	0.492	0.475

Table 6.4c

Influence of Seat-Suspension Parameters on the PSD Acceleration response at the Seat, at the Vehicle's Resonant Frequency (ISRI: One and Two D.O.F. Driver Models).

PARAMETER	TYPE OF THE DRIVER MODEL (D.O.F.)	PARAMETER VALUES					
		LOW	BASE	HIGH	LOW	BASE	HIGH
		ACCELERATION PSD $((m/s^2)^2/Hz)$			REL. DISPLACEMENT PSD (cm^2/Hz)		
CUSHION STIFFNESS (K_C)	ONE	1.932	1.869	1.846	3.441	3.202	3.130
	TWO	2.075	2.003	1.978	3.518	3.266	3.190
SUSPENSION STIFFNESS (K_{1A})	ONE	1.733	1.869	2.076	2.975	3.202	3.508
	TWO	1.852	2.003	2.232	3.025	3.266	3.593
SUSPENSION DAMPING RATIO (δ_{1A})	ONE	1.737	1.869	2.104	3.280	3.202	3.065
	TWO	1.864	2.003	2.251	3.349	3.266	3.122
SUSPENSION DAMPING RATIO (δ_{1B})	ONE	1.680	1.869	2.021	3.314	3.202	3.113
	TWO	1.800	2.003	2.167	3.387	3.266	3.170
TRANSITION VELOCITY (V_S)	ONE	1.800	1.869	2.021	3.243	3.202	3.113
	TWO	1.931	2.003	2.167	3.309	3.266	3.171
COULOMB DAMPING FORCE (F_{CD})	ONE	1.402	1.869	2.376	3.489	3.202	2.914
	TWO	1.510	2.003	2.535	3.567	3.266	2.962
MASS RATIO (μ)	ONE	1.887	1.794	1.687	3.174	3.202	3.232
	TWO	2.119	2.003	1.870	3.240	3.266	3.294

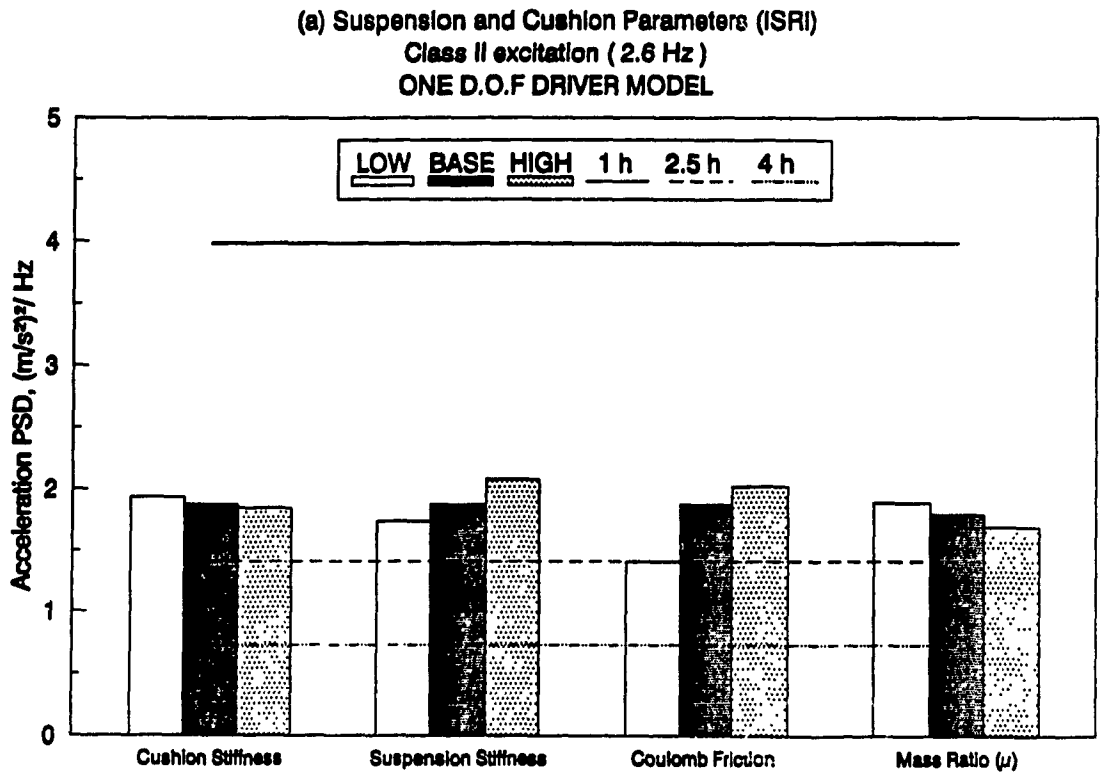

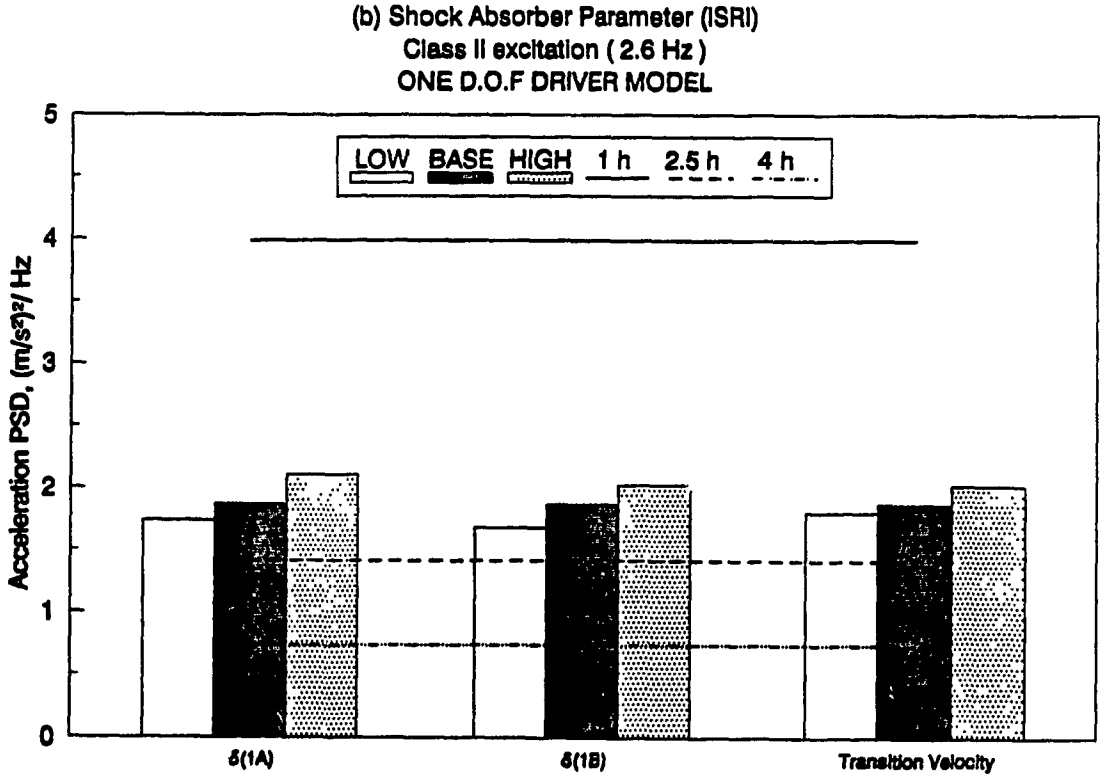

Figure 6.47. Influence of Seat-Suspension Parameters (Three D.O.F. Model) on the PSD of Seat Acceleration at the Vehicle's Resonant Frequency: (a) Suspension and Cushion; (b) Shock Absorber Parameters.

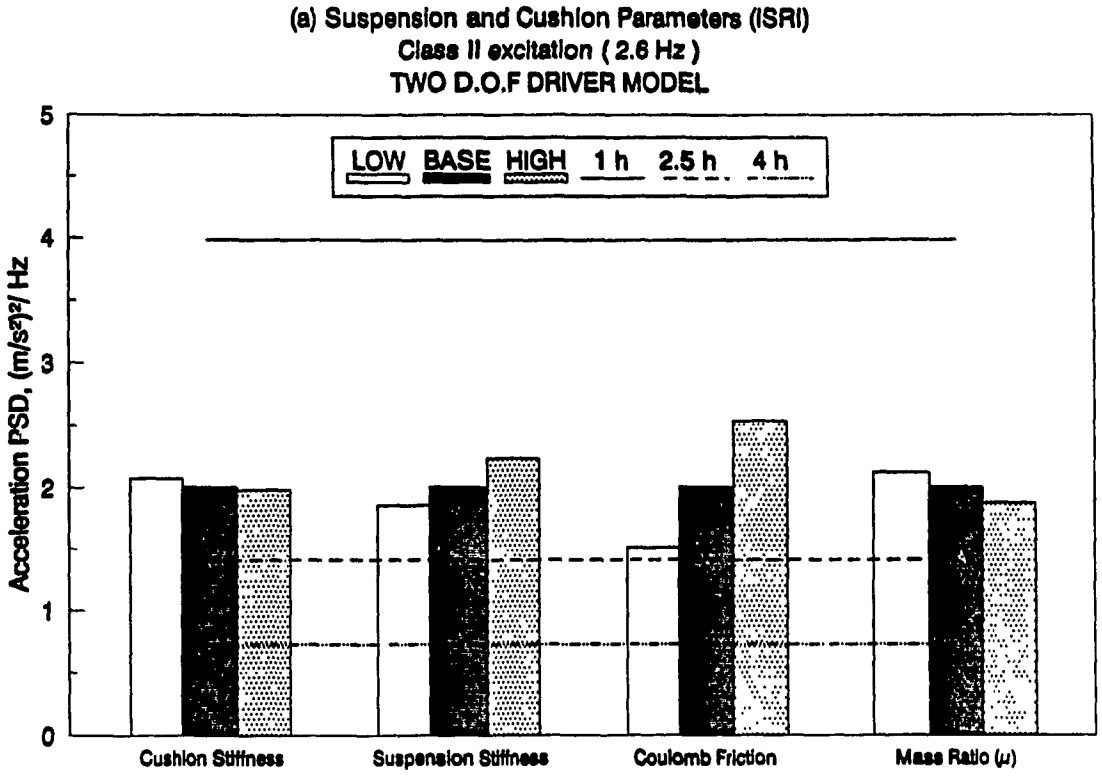

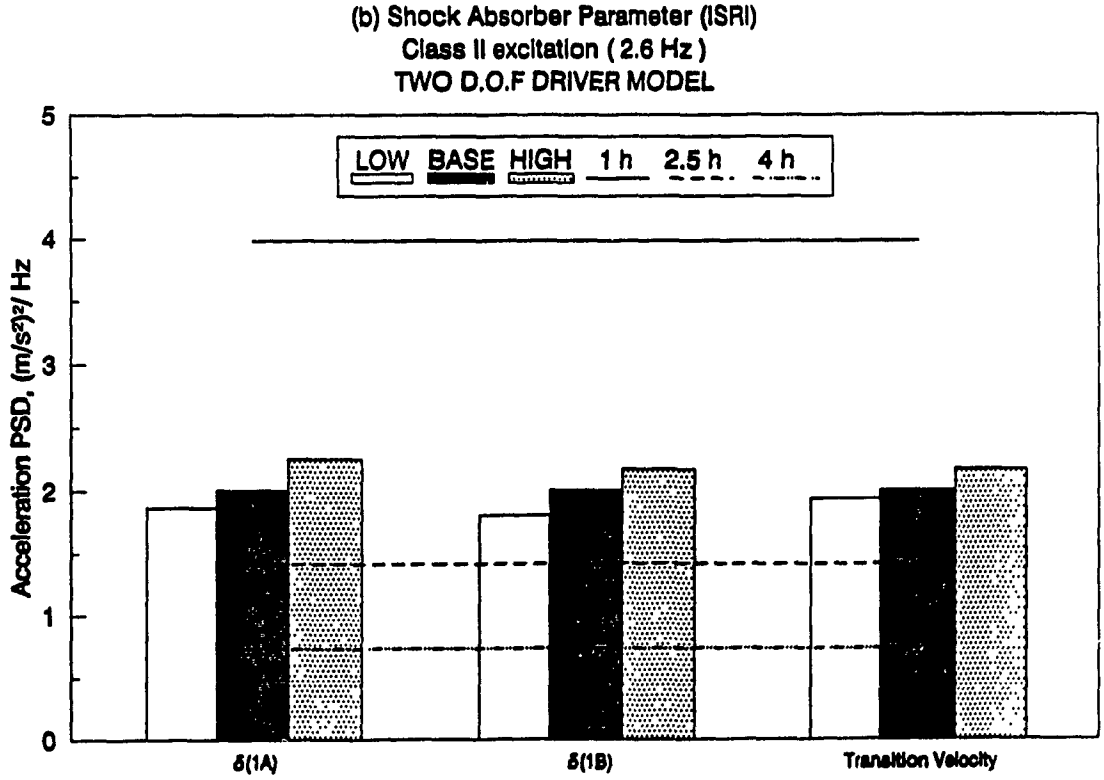

Figure 6.48. Influence of Seat-Suspension Parameters (Four D.O.F. Model) on the PSD of Seat Acceleration at the Vehicle's Resonant Frequency: (a) Suspension and Cushion; (b) Shock Absorber Parameters.

. Lower values of damping parameters, δ_{1A}, δ_{1B}, and transition velocity, V_s, provide improved ride quality.

6.5 SUMMARY

Parametric sensitivity analyses of the seat-suspension models incorporating rigid mass, one- and two-degrees-of-freedom driver models are carried out based on class II cab floor excitations. Three performance indices based on deterministic and random response characteristics are selected to investigate the influence of various parameters on the ride performance of the driver seat-suspension models. The acceleration and relative displacement PSD's, and transmissibility characteristics at the vehicle's resonant frequency (2.6 Hz) are considered as measures of the ride performance. The parametric sensitivity analyses illustrated that appropriate selection of cushion stiffness, suspension stiffness, Coulomb friction and shock absorber parameters can provide considerable improvement in the ride performance.

The acceleration PSD response of the driver-seat-suspension models are assessed using the ISO-2631 fatigue decreased proficiency limits and it is concluded that the human body dynamics contributes significantly to the overall ride performance.

CHAPTER 7

CONCLUSIONS AND RECOMMENDATIONS FOR FUTURE WORK

7.1 HIGHLIGHTS OF THE INVESTIGATION

In this thesis, passive seat-suspension systems are investigated, experimentally and analytically, to achieve improved ride quality of off-road vehicles. The major highlights of the thesis include:

- Development of a seat-suspension selection criteria based on vibration requirements and ergonomic considerations, and review of various suspension designs.
- Development of a general two-degrees-of-freedom model incorporating nonlinearities due to suspension geometry, bump stops, Coulomb friction and shock absorber, and to characterize the dynamics of the entire ensemble of seat-suspension systems for off-road vehicles.
- Identification of model parameters through static and dynamic testing of suspension components.
- Study of seated human body models to investigate their contributions to the total ride dynamics of driver-seat-suspension models.
- Laboratory testing of various seat-suspension systems and validation of analytical models.
- Development of three- and four-degrees-of-freedom analytical models of the driver-seat-suspension system to investigate the influence of driver dynamics on the ride performance.
- Implementation of the energy based local equivalent linearization technique to characterize nonlinear force-displacement behavior of bump stops and force-velocity behavior of dual phase shock absorber as

an array of local equivalent spring and damping constants.

- Determination of vibration transmissibility characteristics and parametric sensitivity analyses of driver-seat-suspension models.
- Random response analysis of driver-seat-suspension models and ride assessment with reference to the ISO proposed fatigue decreased proficiency limits.

7.2 CONCLUSIONS

The following conclusions are drawn from the experimental and analytical studies conducted in this investigation.

- Human body is most sensitive to vertical whole-body vibrations in the frequency range 1-8 Hz, and wheeled off-road vehicle vibrations dominate in the same frequency range.
- Only secondary vehicle suspensions, such as seat- and cab-suspension offer potentials to attenuate the high amplitude and low frequency whole-body vibrations.
- The off-road vehicle seat-suspension systems can be characterized by a general two-degrees-of-freedom dynamic model incorporating geometric nonlinearities and suspension nonlinearities due to bump stops, Coulomb friction and shock absorber.
- Impedance characteristics of a seated driver reveals peaks in frequency ranges 4-6 Hz and 7-11 Hz, respectively, due to resonance of lower and upper bodies. The dynamics of the human body can be thus characterized by either one- or two-degrees-of-freedom dynamic models.
- Laboratory testing of seat-suspension systems revealed that nominal value of the resonant frequency of most seat-suspensions lie in the

range 1.25-1.6 Hz. The natural frequency can be lowered by adjusting the suspension for a soft-ride.

- The acceleration transmissibility characteristics, measured in the laboratory revealed strong dependence on the selected ride position, amplitude of excitation, static and dynamic characteristics of the cushion, bump stops, and shock absorber geometry.
- Soft cushion, employed in the ISRI mechanical seat, result in amplification of the acceleration response of the suspension mass corresponding to the suspension resonant frequency. The acceleration response at the driver-seat interface, thus, increases due to soft cushion. The stiff cushion, employed in SIFRA seat, attenuates the acceleration of the suspension mass at low excitation levels leading to further reduction in transmitted vibration at the driver-seat interface. It is thus concluded that firm cushions provide better vibration isolation characteristics. The slouched posture encouraged by firm cushions, however, can be prevented by integrating adjustable lumbar supports.
- A soft pneumatic seat-suspension yields high transmissibility at its resonant frequency and extremely superior vibration attenuation performance around the vehicle resonant frequency (2.6 Hz). The soft pneumatic seat-suspension, however, causes excessive static and dynamic relative deflections.
- High damping of shock absorbers, employed in mechanical seat-suspensions (ISRI and SIFRA) suppress the resonant peak effectively but yields higher values of transmissibility ratio around 2.6 Hz. These suspensions perhaps offer a good compromise in

providing low resonant transmissibility and slightly higher values corresponding to the vehicle's resonant frequency.

- The experimental acceleration transmissibility data correlated reasonably well with the results obtained from computer simulation of the nonlinear seat-suspension model.
- Computer simulation of the driver-seat-suspension, models revealed that the driver dynamics contributes considerably to the overall performance.
- Local equivalent linearization technique based on the principle of energy similarity, is applied to study the frequency response characteristics of the seat-suspension models subjected to deterministic and stochastic excitations. A comparison of response characteristics of linearized and nonlinear models revealed that the linearization technique can predict the nonlinear system's response quite accurately and requires considerably less computer time.
- The parametric sensitivity analyses performed on seat-suspension and driver-seat-suspension models revealed that soft suspension springs provide improved ride quality. The spring-rate, however, needs to be tuned as a function of the dominant excitation frequency in order to avoid bottoming caused by excessive relative motion.
- Shock absorbers must be selected to achieve a compromise between the magnitudes of acceleration transmissibility corresponding to the suspension and vehicle's resonant frequencies.
- An increase in suspension mass ratio yields improved vibration isolation performance.

- High friction damping degrades the vibration attenuation property of the seat-suspension for low frequency and low amplitude excitations. The magnitude of vibration transmitted around the vehicle's resonant frequency also increases due to high friction. Moderate friction damping is recommended to suppress the acceleration levels transmitted at the seat resonant frequency.
- It is concluded that the seat-suspension models provide 43-53%, and 25-37% vibration reduction when subjected to Class I and Class II cab floor excitations, respectively. The seats, in general, provide a satisfactory ride for 1 hour exposure for Class II vehicles.
- The parametric studies conducted on the seat-suspension models illustrate that the ride performance characteristics can be improved by changing the suspension parameters.

7.3 RECOMMENDATIONS FOR FURTHER INVESTIGATION

The experimental and analytical studies performed in this investigation focus on the dynamic performance of driver seat-suspension system alone, assuming standardized random and constant amplitude sinusoidal excitations at the cab floor. The ride perceived by the driver is a function of the terrain roughness, vehicle dynamics, driver enclosure, and seat location with in the vehicle. Therefore, studies incorporating a full scale vehicle model are recommended in order to study the performance characteristics of the seat-suspension system in a realistic environment of multiple axes vibration. Such a study may be vital to study the suspension performance under shock excitations encountered during off-road operations.

The limits defined in the ISO-2631 are applicable only to motions with crest factor less than 6. The off-road vehicle vibrations that may impair health or cause severe discomfort exhibit high crest factors. Alternative measures are therefore needed to assess the ride quality of driver-seat-suspension system in an off-road vehicle. The assessment method, based on fourth power of acceleration, may be explored to assess such off-road vehicle vibrations.

Development of nonlinear human body models that could closely approximate the impedance characteristics of human body to a wider range of frequencies is recommended for more realistic assessment of seat-suspension performance on the vibration levels of specific parts, specifically the abdomen and the spinal column.

Studies on kinematic and dynamic characteristics of various seat-suspension linkages need to be undertaken to select optimal linkage mechanism and to evaluate pitching motions caused by the linkage.

The choice of optimal seat-suspension parameters for passive isolators involves a compromise among the relative displacement, acceleration response corresponding to suspension natural frequency, and acceleration response corresponding to vehicle resonant frequency. It is therefore desirable to formulate a multi-variable constrained nonlinear optimization problem to achieve optimal parameters that will maximize the ride performance of the seat-suspension.

REFERENCES

1. Ograwa, S. "Study of Riding Quality With New Concept," Japanese Railway Engineering, Vol. 21, No. 1, 1981, pp. 16-22.

2. Rakheja, S. and Sankar, S. "Review of Ride Vibration Standards and Tolerance Criteria," CONCAVE Research Center Report 05-88, August 1988.

3. Sanders, S.M. "Human Factors in Engineering and Design," McGraw Hill, 1987.

4. Gruber, G.J. "Relationship Between Whole-Body Vibration and Morbidity Patterns Among Interstate Truck Drivers," U.S. DHEW/NIOSH Public No.77-167, 1976.

5. Schmitz, M.A. and Simons, A.K. "Man's Response to Low Frequency Vibration," ASME Paper No. 5A-A-200, 1959.

6. Milby, T.H. and Spear, R.C. "Relationship Between Whole-body Vibration and Morbidity Patterns Among Heavy Equipment Operators," U.S. DHEW/NIOSH Public NO.74-131, 1974.

7. Spear, R.C., Keller, C.A., Behrens, V., Hudes, M., and Tarter, D. "Morbidity Patterns Among Heavy Equipment Operators Exposed to Whole-Body Vibration," U.S. DHEW/NIOSH Public No.77-120, 1976.

8. Guignard, J.C. and King, P.F. "Aeromedical Aspects of Vibration and Noise," AGARDograph No. 17, NATO, Technical Editing and Reproduction Ltd, Charlotte St. London, 1972.

9. Jakubowski, R. "General Characteristics of Vibration at Different Work Places in Agriculture and Forestry," Med. Wicj., Vol. 4, 1969, pp. 47-50.

10. Clarsoo, S. "The Effects of Vibration on the Skeleton, Joints and Muscles : A Review of the Literature," Applied Ergonomics, 13, 1982, pp. 251-258.

11. Shoenberger, R.W. "Human Response to Whole-Body Vibration, Perceptual and Motor Skills," Monograph Supplement 1-V34, Missoula, Montana, 1972.

12. Magid, E.B. and Coermann, R.R. "Human Tolerance to Whole-Body Sinusoidal Vibration," Aerospace Medicine, 31, 1960, pp. 915-924.

13. Temple, W.E., Clarke, N.P., Brinkley, J.W., and Mandel, M.J. "Man's Short-Time Tolerance to Sinusoidal Vibration," Aerospace Medicine, 35, 1964, pp. 923-930.

14. Gibbon, J.M. and Boyse, D.S. "Tractor Operators Survey," NIAE Dept. Note, DS/SY/123/1952, July 1971.

15. Hornick, R.J. "Effects of Tractor Driving on Operators," Agric. Engng., Vol. 42, No. 12, 1959, pp. 674-676.

16. Matthews, J. "Ride Comfort for Tractor Operators, *Review of Existing Information*," Journal of Agric. Eng., Vol. 9, No. 1, 1964, pp. 3-31.

17. Müller, E.A. "The Effects of Sinusoidal Vibration on Man in Seating and Standing Positions," Arb. Physiol. Agrew. Ent., Berlin, Vol. 5, 1938, pp. 2712-2727.

18. Griffin, M.J. "Evaluation of Vibration with Respect to Human Response," SAE Paper No. 860047, 1986.

19. Miwa, T. "Evaluation Methods for Vibration Effect: Part 8, The vibration Greatness of Random Waves," Industrial Health, Vol. 7, 1969, pp. 89-115.

20. Oborne, D.J. " Techniques Available for the Assessment of Passenger Comfort," Applied Ergonomics, Vol. 9, No. 1, March 1978, pp. 211-225.

21. Society of Automotive Engineers. "Measurement of Whole-Body Vibration of the Seated Operator of Off-Highway Work Machines," SAE J1013, January 1980.

22. Van Deusen, B.D. "Human Response to Vehicle Vibration," Transaction SAE, Vol. 77, No. 1, 1968, pp. 328-345.

23. International Standard Organization ISO-2631 / 1. "Evaluation of Human Exposure to Whole-Body Vibration," Part 1 : General Requirements, 1985.

24. Boileau, P.E. and *et. al.* "Evaluation of Human Exposure Using Fourth Power Method and Comparison with ISO-2631," Journal of Sound and Vibration, Vol. 129, No. 1, 1989, pp. 143-154.

25. Lee, R.A. and Pradko, F. "Analytical Analysis of Human Vibration," SAE Paper No. 680091, January 1968.

26. Murphy, N.R. "Further Developments in Ride Quality Assessment," ISTVS 8th International Conference, Cambridge, 1984.

27. Verein Deutscher. "Assessing the Effects of Vibration on Human Beings," VDI-2057. Translated and Published by Peter Peregrinus Ltd. Stevenge, Herts, U.K., 1963.

28. Janeway, R.N. "Passenger Vibration Limits," SAE Journal Vol. 77, No. 1, 1968, pp. 346-370.

29. Goldman, D.E. "A Review of Subjective Responses to Vibratory Motion of the Human Body in the Frequency Range 1-70 cps," Naval Med. Res. Institute, Report No. 4, March 1948.

30. Rakheja, S., Sankar, S., and Bhat, R.B. "Ride Vibration Levels at the Driver-Seat Interface," CONCAVE Research Center: Report, November 1987.

31. Claar II, P.W. and Sheth, P. "Off-road Vehicle Ride : Review of Concepts and Design Evaluations With Computer Simulations," SAE Paper No. 801023, 1980.

32. Stikeleather, L.F. "Operator Seats for Agricultural Equipment," ASAE Distinguished Lecture Series, No. 7, 1981.

33. Gillespie, T.D. "Heavy Truck Ride," SAE / SP-85 / 607, 1985.

34. Stikeleather, L.F. and Suggs, C.W. "An Active Suspension System for Off-road Vehicles," Trans. of ASAE, Vol. 13, No. 1, 1970, pp. 99.

35. Young, R.E. and Suggs, C.W. "Seat-Suspension System for Isolation of Roll and Pitch in Off-road Vehicles," Trans. of ASAE, Vol. 16, No. 5, 1973, pp. 876.

36. Rakheja, S. "Computer Aided Dynamic Analysis and Optimal Design of Off-road Tractors," Ph.D. Thesis Concordia University, Montreal, 1983.

37. Coermann, R.R., and Whittwer, A.L. "The Passive Dynamic Mechanical Properties of the Human Abdomen Thorax System and of the Whole-body System," Aerospace Medicine, Vol. 31, No. 6, 1960, pp. 443.

38. Stikeleather, L.F. and Timothy, L.F. "Simulation of Seat Ride Performance by the Mechanical Impedance of the Test Load," SAE Paper No. 891161, 1989, pp. 371-382.

39. Griffin, M.J. "Biodynamic Response to Whole-Body Vibration," Shock and Vibration Digest, Vol. 13, No. 8, August 1981, pp. 3-12.

40 Suggs, C.W., Stikeleather, L.F., Harrison, J.Y., and Young, R.E. "Application of Dynamic Simulator in Seat Testing," Transaction ASAE, Vol. 13, No. 3, 1970, pp. 378-381.

41. Park, W.H. and Wambold, J.C. "A Human Model for Measuring Objective Ride Quality," ASME Paper No. 75-DET-6. Presented at Design Engineering Technical Conference, Washington, D.C., September 17-19 1975.

42. Demic, M. "A Contribution to Identification of a Nonlinear Biodynamic Oscillatory Model of Man," Int. Journal of Vehicle Design, Vol. 10, No. 2, 1989.

43. Patil, M.K. and Palanichamy, M.S. "A Mathematical Modeling of Tractor-Occupant System with A New Seat-Suspension for Minimization of Vibration Response," Applied Math. Modeling, Vol. 12, February 1988.

44. Kyeong, K.UK. "Ride Simulation of Passive, Active and Semi-Active Seat-Suspensions for Off-road Vehicles," Ph.D. Thesis, University of Illinois at Urbana-Champaign, 1981.

45. Fairley, T.E. and Griffin, M.J. "Test Method for The Prediction of Seat Transmissibility," SAE Paper No. 860046, 1986.

46. Ishikawa, F. and Kobayashi, K. "Vibration Measurement and Evaluation of Tractor Seats," In Noise and Vibration in Agriculture and Forestry, Proceedings of the 8th Joint Ergonomics Symposium, Sisloe, Bedford Shire, UK, September 1985.

47. SAE J1384. "Classification of Agricultural Wheeled Tractors for Vibration Tests of Operator seats," SAE Hand Book, 1988, pp. 40.334 - 40.335.

48. SAE J899. "Operator's Seat Dimensions For Off-road Self-Propelled Work Machines," SAE Standard Revised, December 1988.

49. Styner, R.M. and Whyte, R.T. "Design Criteria For Tractor Seats," In Noise and Vibrations in Agriculture and Forestry. Proceedings of the 8th Joint Ergonomics Symposium, Sisole, Bedford Shire, UK, September 1985.

50. Boileau, P.E. and Scory, H. "Les lombalgies chez les conducteurs de débusqueuses: Étude des vibrations appliquées au corps entier dans les chantiers forestiers du Québec," Arch. Mal. Prof., 49 (5):1988, pp. 305-314.

51. Webb, R.D.G. and Hope, P.A. "Ergonomics and Skidder Operations in Northern Ontario: A Perliminary Investigation," Information Report DPC-X-15, Environment Canada, Canadian Forestry Service, 1983.

52. de Longchamp, J.H. "Operator Seat Design Problems in Reference to Theoretical Vibration Isolation and Practical European Recommendations," SAE Paper No. 730824, 1973.

53. Stikeleather, L.F. "Review of Ride Vibration Standards and Tolerance Criteria," Transaction SAE, Vol. 85, 1976, pp. 1460-1467.

54. Suggs, C.W., Abrams, C.F., and Stikeleather,L.F. "Application of A Damped Spring Mass Human Vibration Simulator in Vibration Testing of Vehicle seats," Ergonomics, 12, 1, 1969, pp. 79-90.

55. SAE J1051. "Deflection of Cushion for Off-road Work Machine," SAE Hand Book, 1988, pp. 40.328-40.330.

56. Meirovitch, L. "Elements of Vibrations Analysis," 2nd. ed. New York, McGraw-Hill, 1986.

57. Zwillinger, D. "Hand Book of Differential Equations," Academic Press Inc., San Diego, 1989.

58. Van Vliet, M. "Computer Aided Dynamic Analysis and Design of Off-road Motorcycle Suspensions," Ph.D. Thesis Concordia University, 1983.

59. Baucke, K.E. and Kelly, J.M. "Equivalent Linearizations for Practical Hysterical Systems," Journal of Nonlinear Dynamics, July 1990, pp. 213-229.

60. Scanlan, R.H. "Linear Damping Models and Causality in Vibration," Journal of Sound and Vibration, Vol. 13, 1970, pp. 499-503.

61. Thomson, W.T. "Theory of Vibrations with Applications," 3rd ed. Englewood Cliffs, New Jersey: Prentice Hall, 1988.

62. Su, H., Rakheja, S., and Sankar, T.S. "Response of a Nonlinear Vehicle Suspension With Tunable Shock Absorber to Random Road Excitation," Diagnostic, Vehicle Dynamics and Special Topics, ASME Pub. DE-Vol. 18-5,

12th Biennial ASME Conference on Mechanical Noise and Vibration, Montreal, September 1989, pp. 185-194.

63. Rakheja, S. and Sankar, S. "Local Equivalent Representation of Nonlinear Mechanisms," Eng. Comput., Vol. 3, March 1986, pp. 11-17.

64. Newland, D.E. "An Introduction to Random Vibration and Spectral Analysis," 2nd. ed. London: Longman Group Limited, 1985.